



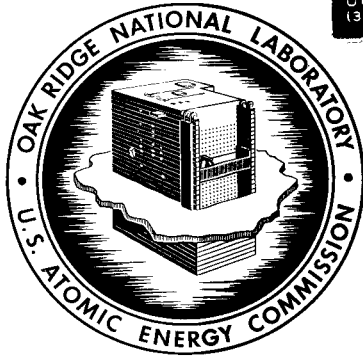
3 4456 0515802 1

cy. 1

ORNL-4637
UC-80 - Reactor Technology

GAS-COOLED REACTOR AND THORIUM UTILIZATION PROGRAMS
SEMIANNUAL PROGRESS REPORT
FOR PERIOD ENDING SEPTEMBER 30, 1970

OAK RIDGE N
CENTRAL
DOCUM
LIBRARY
DO NOT TRANS
If you wish s
document, se
and the libra
UCN-7969
(3 3-67)



OAK RIDGE NATIONAL LABORATORY
operated by
UNION CARBIDE CORPORATION
for the
U.S. ATOMIC ENERGY COMMISSION

Printed in the United States of America. Available from
National Technical Information Service
U.S. Department of Commerce
5285 Port Royal Road, Springfield, Virginia 22151
Price: Printed Copy \$3.00; Microfiche \$0.95

This report was prepared as an account of work sponsored by the United States Government. Neither the United States nor the United States Atomic Energy Commission, nor any of their employees, nor any of their contractors, subcontractors, or their employees, makes any warranty, express or implied, or assumes any legal liability or responsibility for the accuracy, completeness or usefulness of any information, apparatus, product or process disclosed, or represents that its use would not infringe privately owned rights.

ORNL-4637
UC-80 – Reactor Technology

Contract No. W-7405-eng-26

GAS-COOLED REACTOR AND THORIUM UTILIZATION PROGRAMS
SEMIANNUAL PROGRESS REPORT
For Period Ending September 30, 1970

P. R. Kasten, Program Director
J. H. Coobs, Associate Director
A. L. Lotts, Associate Director

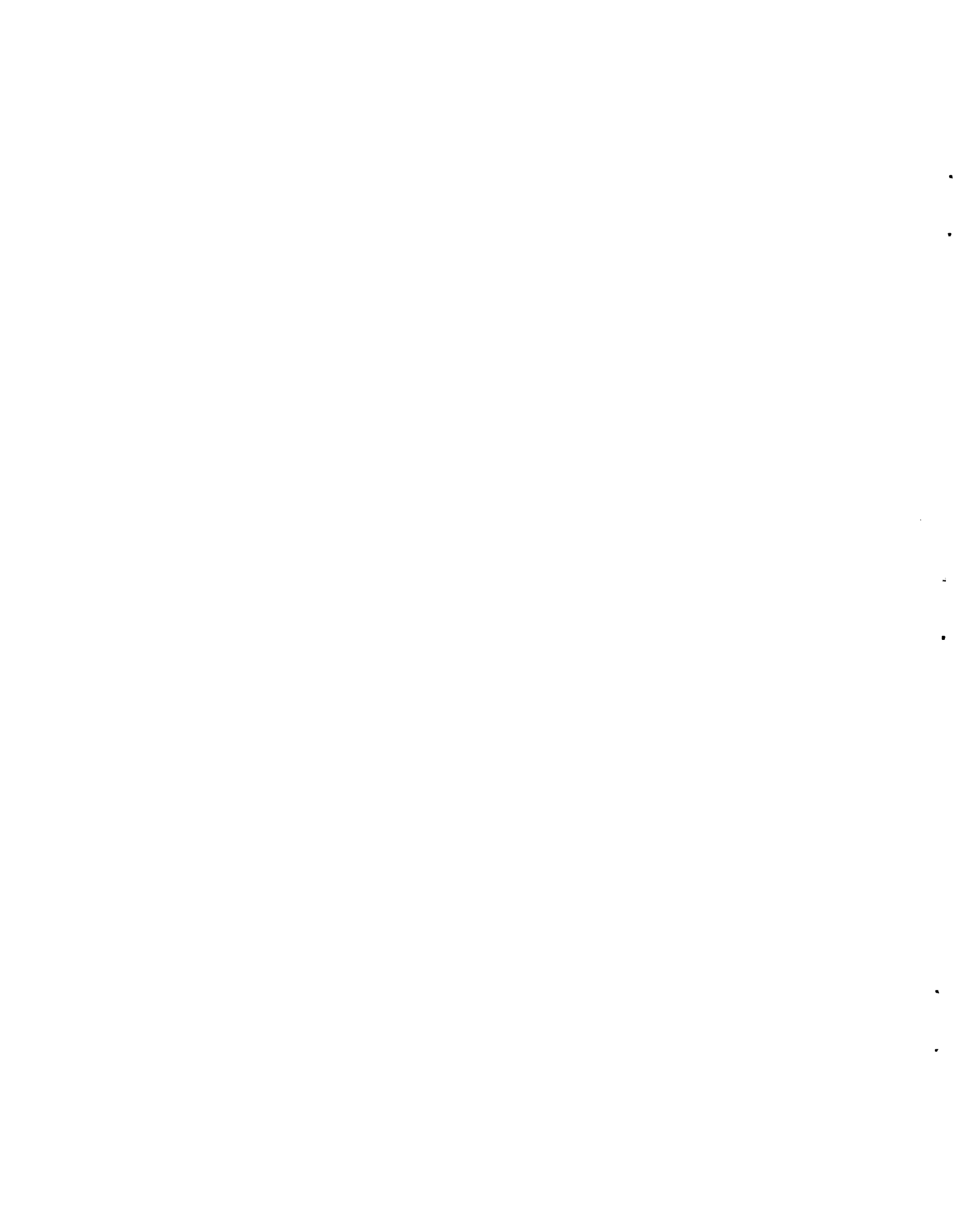
JULY 1971

OAK RIDGE NATIONAL LABORATORY
Oak Ridge, Tennessee
operated by
UNION CARBIDE CORPORATION
for the
U. S. ATOMIC ENERGY COMMISSION

LOCKHEED MARTIN ENERGY RESEARCH LIBRARIES



3 4456 0515802 1

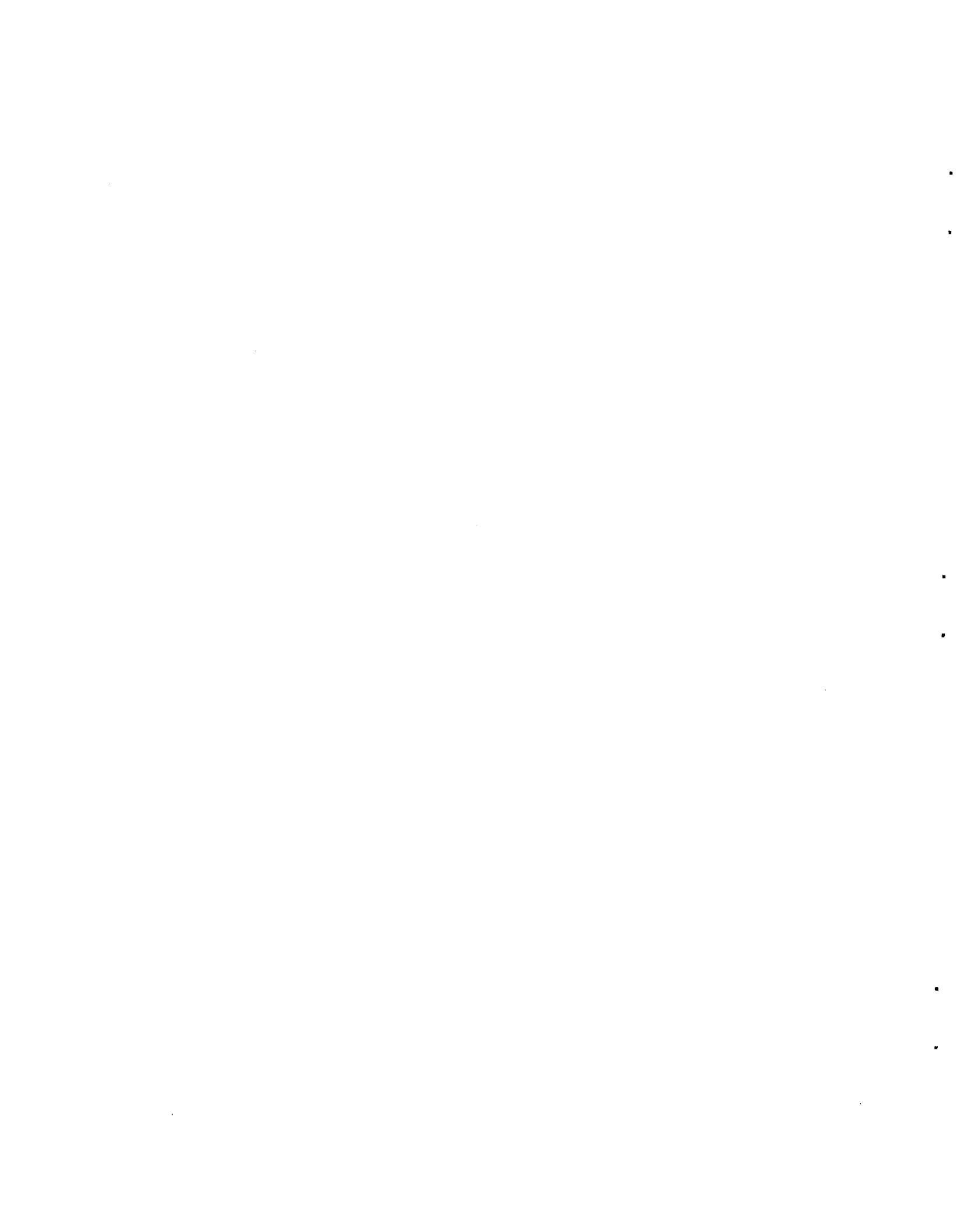


Contents

FOREWORD	vii
SUMMARY	ix
PART I. HIGH-TEMPERATURE GAS-COOLED REACTOR DEVELOPMENT	
INTRODUCTION	1
1. FUEL ELEMENT DEVELOPMENT	3
1.1 Coated Fuel Particles Derived from Carbonized Ion-Exchange Resins	3
1.1.1 Chemistry of ion-exchange resins	4
1.1.2 Carbonization of fueled resin microspheres	6
1.1.3 Irradiation testing	7
1.2 Development of Bonded Beds of Coated Particles for HTGR Fuel Elements	9
1.3 Irradiation Tests on HTGR Fuel Elements	11
1.3.1 HTGR-HFIR target capsules	12
1.3.2 HTGR-HFIR instrumented capsules	13
1.3.3 Irradiation experiments at DFR – Experiment DN-5	23
2. FISSION-PRODUCT RELEASE AND TRANSPORT STUDIES	24
2.1 Fission-Product Release from High-Burnup Coated Fuel Particles by Postirradiation Anneals	24
2.1.1 Fission-product release from coated fuel particles in a bonded bed during postirradiation anneals	24
2.1.2 Diffusion of cesium in pyrolytic-carbon coatings	25
2.1.3 Cesium release through Triso coatings at high temperatures	27
2.1.4 Failure model analysis of irradiated Triso-coated particles	28
2.2 Fission-Product Transport and Deposition	29
3. NUCLEAR SAFETY PROGRAM STUDIES	34
3.1 Fuel Integrity and Fission-Product Release	34
3.2 Studies of Reactions of Graphite with Steam	35
3.3 Fission-Product Behavior in an HTGR Coolant Circuit	35
3.3.1 Experiments on dust behavior	36
3.3.2 Fission-product surveillance program	36

4. CORROSION STUDIES OF WELDS IN ALLOYS FOR ADVANCED STEAM GENERATORS	37
4.1 General Corrosion at 595 and 650°C	37
4.1.1 Studies of similar- and dissimilar-metal weldments	37
4.1.2 Studies on simulated "root-pass" compositions	38
4.2 Preferential Corrosion	39
PART II. GAS-COOLED BREEDER REACTOR DEVELOPMENT	
5. GCBR FUEL STUDIES	40
5.1 Irradiation of GCBR-ORR Capsule 04-P9	40
5.2 F-1 Irradiation Capsules for EBR-II	47
5.2.1 Fuel fabrication	49
5.2.2 Fuel-pin fabrication	49
5.2.3 Capsule fabrication	49
PART III. PRESTRESSED-CONCRETE PRESSURE VESSEL RESEARCH AND DEVELOPMENT	
INTRODUCTION	51
6. CONCRETE MATERIALS INVESTIGATIONS	52
6.1 Triaxial Creep Tests at the University of Texas	52
6.1.1 Data analysis and preparation of reports	52
6.1.2 Conclusions from preliminary evaluation	53
6.1.3 Inspection and evaluation of test specimens	54
6.1.4 Loading of specimens to evaluate the effect of age prior to loading	54
6.1.5 Data collection	56
6.2 Multiaxial Creep Tests at Waterways Experiment Station	56
6.2.1 Unloading procedure	56
6.2.2 Status of testing	56
6.2.3 Testing failures	56
6.3 Moisture-Migration Test at Waterways Experiment Station	56
7. MODEL STUDIES	65
7.1 Structural Behavior of Prestressed-Concrete Reactor Vessels	65
7.1.1 Test vessels with special instrumentation	65
7.1.2 Studies of experimental data	66
7.1.3 Supporting analytical studies	70
7.2 PCRV Thermal-Cylinder Test	70
7.2.1 Instrumentation	74
7.2.2 Preliminary inelastic analysis	75
PART IV. THORIUM UTILIZATION PROGRAM	
8. INTRODUCTION	78
9. HTGR FUEL RECYCLE DEVELOPMENT PROGRAM PLAN	82
9.1 Background	82
9.2 Scope	82

9.3 Organization	82
9.4 Status	84
10. HEAD-END REPROCESSING DEVELOPMENT	85
10.1 Engineering Studies	85
10.2 Head-End Reprocessing Studies with Unirradiated HTGR Fuels	90
10.2.1 Resin-bonded fuel stick from early Fort St. Vrain reactor prototype fuel	90
10.2.2 One-sixth section of a prototype Fort St. Vrain fuel element	92
10.3 Head-End Reprocessing Studies with Irradiated HTGR Fuels – Study of Dragon Compact 8375	94
10.3.1 Crushing studies	94
10.3.2 Breakage during size-reduction studies	94
10.3.3 Release of ^3H and ^{85}Kr	95
10.4 Procurement of Irradiated HTGR Fuels for Head-End Studies	96
10.4.1 ORNL Biso-coated (Th,U)O ₂ sol-gel microsphere compacts	96
10.4.2 ORNL test capsule	96
10.4.3 Recycle test elements	97
11. REFABRICATION DEVELOPMENT	100
11.1 Sol-Gel Studies and Particle Preparation	100
11.1.1 ThO ₂ -UO ₂ microsphere preparation	100
11.1.2 Urania-sol preparation	100
11.1.3 Sphere forming	103
11.2 Fueled-Graphite Fabrication Development	104
11.2.1 RTE fabrication	104
11.2.2 Particle coating	107
11.2.3 Fuel stick fabrication	109
12. FUEL IRRADIATIONS	110
12.1 Capsule Tests	110
12.2 Recycle Test Elements	111
ORGANIZATION CHART	115



Foreword

This is the first combined report of the Gas-Cooled Reactor Program and the Thorium Utilization Program. These programs are being carried out at the Oak Ridge National Laboratory under sponsorship of the U.S. Atomic Energy Commission and concern development of high-temperature gas-cooled reactors (HTGR), fuel-recycle technology for HTGR's, and gas-cooled fast breeder reactors (GCBR). The major effort is in HTGR technology and emphasizes development and demonstration of the technology required for economic fuel recycle, fuel development and associated irradiation testing, fission-product behavior, the strength characteristics of prestressed-concrete reactor vessels (PCRV) and associated materials, and reactor safety. Work in GCBR development emphasizes fuel development and irradiation testing, fission-product behavior in vented fuel elements, and studies of reactor safety and afterheat removal. A close coordination is maintained with Gulf General Atomic (GGA) in the design and development of gas-cooled reactors and in HTGR fuel-recycle development.

Major incentives for developing the HTGR concept are the prospects for economically competitive power production while conserving low-cost uranium ore reserves. The good neutron economy and fuel performance permit high burnup and associated low fuel-cycle costs. The high-temperature capability of the graphite core structure facilitates reactor plant operation at high thermodynamic efficiency, and thus requirements for heat dissipation to the environment are low. Excellent fission-product retention by the coated fuel particles leads to coolant circuits with low radioactivity levels. Further, the high exposures attainable with HTGR fuels permit the development of economic fuel recycling. At the same time, the development of fuel-recycle technology is important to the commercial acceptance of HTGR's as economic power producers.

The fuel-recycle effort is part of the national HTGR fuel-recycle development program being carried out by the USAEC, GGA, and ORNL. The program at ORNL includes development of head-end processing methods for irradiated fuels, production of microspheres containing recycle fuel, microsphere coating technology, recycle-fuel-element fabrication technology, and associated equipment and process development.

HTGR fuel development work at ORNL has largely been concerned with evaluating, understanding, and improving fuel performance. Part of this effort also includes study of the behavior of certain fission products. Coated-particle fuel studies involve irradiation testing, with emphasis on demonstration of satisfactory fuel and materials performance at the required fast-neutron fluences. In these tests, the high flux isotope reactor (HFIR) has proved to be highly useful as an irradiation source. Also, a small effort on reactor core studies is maintained to place the fuel development in proper perspective and to assist in fuel-cycle choices.

During the past few years, a program for prestressed-concrete development was implemented. The effort is based on establishing analytical methods by which reactor vessels and other structures can be designed. This is strongly supported by experimental work to measure properties of concrete, with emphasis on creep and moisture behavior under multiaxial loading. Model studies to test analytical methods and to establish fracture modes are also emphasized. A common set of materials is used throughout the program to provide internal consistency so that all the results can be correlated. Due to funding limitations the program has been restricted, but experiments to measure long-term creep and moisture migration behavior are continuing.

Important development work directly related to the GCR base program is also conducted under the reactor safety program and the fuels and materials development

program. For completeness, some results obtained under these programs are reported here, including work on corrosion of steam generator tube and weld materials by water, and reactor safety studies.

The helium-cooled GCBR offers a high breeding ratio, a doubling time of less than ten years, a core conversion ratio of approximately 1.0, a small reactivity change from loss of coolant, a potentially nonradioactive circuit, and high thermal efficiency. The high core conversion ratio makes possible extended operating periods without refueling and low reactivity swings during fuel exposure. The principal questions concerning the concept center around afterheat removal under all circumstances and the development of a metal-clad ceramic fuel element for operation at relatively high cladding temperatures. The fuel service requirements for this reactor are basically similar to those for the liquid-metal-fueled breeder reactor (LMFBR), and thus the program draws heavily on the development of the latter concept. ORNL fuel work now principally in-

volves irradiation testing of pins. Initial irradiation test results for a vented fuel element are encouraging.

Historically, gas-cooled reactor work at ORNL was first related to the AGR type of reactor, as applied with helium cooling in the experimental gas-cooled reactor (EGCR). Later, emphasis was shifted to include reactors with graphite-moderated fuel of the pebble-bed type. Fuel development for the German AVR reactor was conducted first under terms of the AVR Memorandum of Understanding. This program demonstrated, through irradiation testing, the capability of coated-particle fuels for service in directly cooled nonpurged circuits. Information from AVR operation is provided to ORNL under terms of the AVR Memorandum of Understanding. Similarly, information from the operation of the Dragon Reactor is obtained through the provisions of an exchange agreement. The excellent operating performance of these reactors has provided much valuable experience.

Summary

PART I. HIGH-TEMPERATURE GAS-COOLED REACTOR DEVELOPMENT

1. Fuel Element Development

1.1 Coated fuel particles derived from carbonized ion-exchange resins

Coated particles with kernels made from ion-exchange resins offer attractive alternates to the present reference HTGR fissile fuel particles, which consist of dense UO_2 or UC_2 particles surrounded by two layers of pyrolytic carbon — a thick low-density buffer layer and an outer dense layer. The alternates are low-density particles with a thin buffer layer to protect the outer layer from fission-recoil damage. A column-loading technique for contacting the resin particles with concentrated solutions was developed that gives reproducible loadings of 85 to 90% of the theoretical limit. Differential thermal analysis of fueled sulfonated resins indicated the temperatures at which rapid composition changes occur and therefore the temperatures at which careful control of heating rate is required during carbonization. Fueled particles can also be prepared by using carboxylic cation-exchange resins, which contain no residual sulfur.

The structures of the particles from the two types of resin consist of finely dispersed UOS or UO_2 , respectively, in a glassy carbon matrix. The particles have uranium densities as high as 2 g/cm^3 and a porosity of about 30%. Resin-derived particles with duplex pyrolytic-carbon coatings survived irradiation at 1000°C to a fluence of 6×10^{21} neutrons/cm² ($E > 0.18 \text{ MeV}$) and a burnup of 9% heavy metal.

1.2 Development of bonded beds of coated particles for HTGR fuel elements

Additional work is in progress on the development of bonded beds of coated particles in which materials are

being used that are similar to the Poco graphite filler which showed adequate resistance to irradiation damage in previous experiments. A number of commercially available and less expensive filler materials were characterized, and techniques were developed for injection bonding of particle beds. The optimum workable quantities of filler material in the matrix varied from 27 wt % natural-flake graphite to more than 50 wt % Thermax carbon black. Specimens prepared with these fillers were carbonized by two techniques; they were either confined in a graphite tube or packed in a bed of natural-flake graphite. The first method yielded fuel sticks with consistently higher matrix densities than those packed in natural-flake graphite; however, large fractions of particle coatings were broken. Apparently, confinement in the graphite tube produces high stresses that the outer low-density coatings are too weak to withstand. Several series of bonded fuel sticks containing the experimental filler materials were prepared for irradiation testing in two HFIR capsules. Most of these were carbonized in a packed bed of graphite to avoid broken coatings.

1.3 Irradiation tests on HTGR fuel elements

Two types of irradiation facilities in the HFIR are used to test HTGR fuels. The HT capsules, which are small and uninstrumented, occupy a target position in HFIR and permit rapid attainment of the desired exposure. The HRB capsules are inserted in the removable beryllium reflector region and are relatively large, instrumented, and swept. The fast-neutron flux in HRB positions is about 35% of that in the target capsules.

The fourth HT capsule (HT4) contained 20 specimens of bonded beds, some of which were irradiated at 1060°C and the remainder at 800°C to a maximum fast-neutron fluence of 7.5×10^{21} neutrons/cm² ($E > 0.18 \text{ MeV}$). Examination of this capsule was completed

by metallographic examination of two specimens that were bonded with 15V pitch containing 40 wt % Poco graphite. These specimens survived the exposure without coating failure or debonding.

Capsule HT6 was installed in HFIR on August 28, 1970, to be irradiated for three reactor cycles. The 20 specimens of bonded beds and 22 samples of coated particles were supported in six graphite magazines and will be irradiated at design temperatures of 1070 or 800°C. Four of the samples of coated particles were prepared by coating fueled carbonized-resin kernels, and 16 samples consist of Triso-coated ThC₂ particles supplied by Gulf General Atomic.

Examination of bonded specimens irradiated in capsule HRB1 was completed. The capsule was irradiated for 186 days and attained a maximum fast-neutron fluence of 5.8×10^{21} neutrons/cm². Specimens that received maximum exposure swelled slightly (~1.5%) and were difficult to remove from the graphite sleeve. Specimens bonded with resin containing 15% graphite were severely debonded, while those bonded with Varcum containing 40% Poco graphite filler were intact. The Triso-coated ThO₂ particles performed without failure, while some fracture (5 to 35%) of outer carbon layers on Triso-coated (Th,U)O₂ and UO₂ particles was attributed to the low initial density of the coating and interaction with the nonbonding layer on the coatings. The swelling observed in some specimens was attributed to failure of a large fraction of the coated inert (ZrO₂) particles.

Preparation of specimens and parts for capsule HRB2 is in progress.

2. Fission-Product Release and Transport Studies

2.1 Fission-product release from high-burnup coated fuel particles by postirradiation anneals

Irradiated bonded beds of Biso-coated UO₂ particles were annealed at 1250°C. Cesium release at the end of a 2500-hr anneal was 25%. A diffusion coefficient of 5×10^{-12} cm²/sec was calculated for the pyrolytic-carbon coatings of the particles in the bonded bed. Individual Biso-coated UO₂ particles were annealed at 1400°C. Diffusion coefficients calculated for cesium in the pyrolytic-carbon coating ranged from 2.6×10^{-11} to 1.3×10^{-10} cm²/sec. The cesium release ranged from 0.5 to 17%.

SiC layers in Triso-coated fuel particles broke down at temperatures above 1800°C and released solid fission products. The failure of the SiC may have been due to cracking or, possibly, to porosity. The Walther "Stress-

2" computer code was used to analyze the mode of failure. These calculations showed a high probability of SiC coating failure without simultaneous pyrolytic-carbon coating failure in the Triso-coated particles and indicated a relation between internal fission-gas pressure and failure of the SiC. The results of the calculations compared favorably with experimental data.

2.2 Fission-product transport and deposition

Data obtained from experiments in the fission-product deposition loop on the transport of cesium through graphite evaporators were correlated with an analytical model based on the transverse flow of helium through the graphite. This flow, which results from pressure differentials, provides a mechanism for the observed transport of cesium through the graphite barrier.

3. Nuclear Safety Program Studies

Correlations are being sought between the mechanical properties of particle coatings and the failure of particles when annealed at temperatures above normal operating temperatures. The Walther "Stress-2" code has given calculational results in reasonable agreement with experimental data.

Measurements of the steam-graphite reaction rate for various graphite specimens indicated that the iron content of HTGR graphite should be kept low. In-pile tests performed to date on high-iron-containing graphite indicate that the steam-graphite reaction rate was not influenced significantly by the radiation field.

A small program was initiated for collecting and collating data on fission-product distribution in HTGR coolant circuits through measurements in the Peach Bottom reactor.

4. Corrosion Studies of Welds in Alloys for Advanced Steam Generators

Field corrosion tests of welds in advanced steam generator alloys were run with commercial steam as the corrosion medium. General corrosion is assessed by determining attack rates, characterizing scales, and calculating long-term corrosion from weight-gain data. Susceptibility to preferential corrosion is determined by examining for knife-line attack at weld fusion lines and by conducting U-bend tests.

Inconel 625, Hastelloy X, and IN 102 as both base and filler metals, Incoloy 800 as base metal, and Inconel 82 as filler metal exhibited very good corrosion

resistance at both 595 and 650°C. Welds containing Inconel 600 and austenitic stainless steel exhibited somewhat inferior behavior. No preferential or unusual attack was noted.

PART II. GAS-COOLED BREEDER REACTOR DEVELOPMENT

5. GCBR Fuel Studies

The joint ORNL-GGA irradiation testing program for the evaluation of (U,Pu)O₂-fueled metal-clad fuel pins for the GCBR has progressed from the testing of sealed fuel pins to the testing of vented fuel pins. It has been shown that the fuel-cladding-interacting type of sealed fuel pin works well in thermal-neutron irradiation tests, and it is the current backup concept for the GCBR. The vented fuel pin is the reference GCBR fuel pin because of its better performance potential and the fact that the information being developed in LMFBR fuel-pin-testing programs is directly applicable. The better performance potential is a direct result of the elimination of any large pressure differential across the fuel-pin cladding by adjusting the fuel-pin internal pressure, through the venting system, to match the reactor coolant pressure.

An instrumented thermal-neutron irradiation test of the first GCBR vented fuel pin is being conducted in the ORR poolside facility (capsule C4-P9). This test will provide information on the overall performance of the fuel pin at a heat-generation rate of approximately 16 kW/ft and a maximum temperature of 700°C at the outer surface of the type 316 stainless steel cladding. In addition, the release of fission products to and through the charcoal fission-product trap in the fuel pin is being monitored during the test to obtain data on fission-product release and charcoal trapping efficiency as a function of various operating conditions. The system has operated successfully to a burnup of over 15,000 MWd/MT on the way toward a burnup goal of about 75,000 MWd/MT.

Eight encapsulated fuel pins with type 316 stainless steel cladding (the F-1 series) were prepared for fast-neutron irradiation in the EBR-II. These pins are designed with large plenum volumes and internal charcoal traps to minimize internal pressure buildup due to release of fission gases from the fuel during operation and to simulate the vented type of fuel pin. The pins will operate at a heat-generation rate of approximately 15 kW/ft with cladding midwall temperatures between 590 and 790°C to cover the entire range of temperature of interest for near- and long-term GCBR application. Approval for these tests has been

obtained, and irradiation of the first seven pins is scheduled to begin in November 1970.

PART III. PRESTRESSED-CONCRETE PRESSURE VESSEL RESEARCH AND DEVELOPMENT

6. Concrete Materials Investigations

The investigations on moisture movement in mass concrete and the multiaxial creep studies have progressed in a very satisfactory manner. The moisture migration experiment has been under way for approximately two years, and the data indicate that movement of free water is greatly inhibited under conditions that simulate the thermal environment in a reactor vessel wall. Concrete creep behavior for multiaxial states of stress, two levels of moisture, two aggregate types, and two temperature levels were studied in over 100 specimens.

7. Model Studies

The structural model tests on head-region behavior were extended to obtain additional information on crack initiation and propagation in structures designed to fail in shear under internal pressure loading. Work on the small thermal cylinder test was reactivated, and assembly of the equipment for the experiment is proceeding. The plans call for casting the concrete structure this fiscal year. The instrumentation for this experiment has required considerable development and testing because the projected service conditions are quite demanding.

PART IV. THORIUM UTILIZATION PROGRAM

8. Introduction

The objective of the thorium utilization program at ORNL is the development of the technology required for economic recycle of HTGR fuels. The ORNL program is part of the national HTGR fuel recycle development program, which is sponsored by the USAEC, Gulf General Atomic, and ORNL, to make possible economical utilization of fuel in HTGR's. The program at ORNL includes head-end reprocessing studies, fueled-microsphere production, coating technology, recycle-fuel fabrication, and associated equipment and process development. Related work includes waste treatment and disposal, recycle-fuel irradiations, and conceptual design of a commercial recycle plant. The reference fuel cycle is based on the utilization of

Th- ^{233}U fuel in 1000-MW(e) HTGR's. The reference fuel element is a hexagonal block of graphite containing microspheres coated with pyrolytic carbon and silicon carbide bonded into sticks that fit into fuel holes in the graphite block. Four types of particles are used to permit isolation of spent ^{235}U (which contains ^{236}U) and to lower fabrication costs. The schedule for the HTGR fuel recycle development program requires the design, construction, and installation of a pilot-scale facility by 1976 and obtaining information needed for commercial plant conceptual design by mid-1977.

9. HTGR Fuel Recycle Development Program Plan

The planning of the HTGR fuel recycle development program is being documented in a program plan. The plan states the objectives of the development program, outlines the required activities, and summarizes the current state of recycle-fuel processing and fabrication technology. Further, the plan reflects a progression of work activities that must begin in 1971 and extend into 1981 in order that a commercial recycle plant can be designed, constructed, and placed into operation to realize maximum economy from HTGR fuel recycle.

10. Head-End Reprocessing Development

Head-end methods are being developed for reprocessing HTGR fuels. Both the Fort St. Vrain and 1000-MW(e) reference reactor fuels are included in the development program. Fort St. Vrain fuel sticks contain Triso-coated (i.e., an SiC layer sandwiched between two isotropic carbon layers) (U,Th) C_2 and Th C_2 particles. The SiC coating remains intact during the burning step, and methods are being developed to physically separate the particles. The 1000-MW(e) reference fuel consists of Triso-coated fissile particles ($^{235}\text{UC}_2$) and Biso-coated (i.e., two pyrolytic-carbon layers) fertile ($^{233}\text{U,Th}$) O_2 particles. Burning the Biso-coated (U,Th) C_2 particles in a fluidized bed converts them into a finely divided oxide powder; the ($^{233}\text{U,Th}$) O_2 particles may retain their shape. Methods are being developed to separate the fissile particles, the alumina used in the fluidized-bed burner, and the fertile particles (or residue). Tentatively the aim is to limit the loss of ^{233}U to the ^{235}U stream to about 5% and the inclusion of ^{235}U in the ^{233}U stream to about 10%.

10.1 Engineering studies

Detailed process flowsheets of the head-end and acid-Thorex solvent-extraction steps are being prepared

based on use of the thorium-uranium recycle facility (TURF) to demonstrate prototype hot operations. Major problem areas requiring development are separation of particles from graphite before burning the fuel and from each other on the basis of size difference after burning, development of suitable burners, and development of methods for cleaning up gaseous process wastes.

10.2 Head-end reprocessing studies with unirradiated HTGR fuels

In small-scale tests, a resin-bonded fuel stick containing fissile and fertile SiC-coated fuel particles was crushed in a jaw crusher with a $\frac{5}{8}$ -in. opening. The resulting product was tumbled, burned in a fluidized bed, and then sieved. Separation of the fissile and the fertile SiC-coated particles by this method was not successful. This fuel stick was an early model made with a thermosetting resin and a graphite-filler bonding agent. During the above operations, a component of the bonded matrix apparently reacted with the SiC layer to form a glassy surface. As a result, the glassy SiC particles formed small agglomerates and were only partially separable, even after being leached twice with 11 M HNO_3 —0.1 M Al^{3+} —0.05 M HF, tumbled in a $1\frac{1}{4} \times 12$ -in. Teflon pipe, and screened repeatedly. The crossover of ^{235}U to ^{232}Th was estimated to be 28 to 42% in the original fluidized-bed product and 4 to 18% after all treatments.

Unirradiated fuel samples containing Triso-coated Th O_2 and U O_2 particles were obtained as stand-ins for the Triso-coated particle fuels described above and were crushed in a hammer mill with $\frac{3}{4}$ - and $\frac{3}{8}$ -in. grate spacings. About 45% of the graphite in the product (i.e., pieces larger than 4 to 12 mesh) did not contain any fuel particles and could be easily separated from the fuel. In two separate tests, the SiC and pyrolytic-carbon coatings were broken on only 2.17 and 0.1% of the U O_2 particles and on 1.07 and 1.52% of the Th O_2 particles in the tests with the $\frac{3}{4}$ -in. grating.

The fraction of particles broken on burning the crushed fuel in a 2-in.-diam fluidized bed containing alumina as the fluidized heat-transfer medium was determined as a function of oxygen concentration in the reagent gas. When an oxygen concentration of 70% was used, the total breakage of coatings for both the crushing and burning operations was 5.7% for the U O_2 particles and 4.67% for the Th O_2 particles.

10.3 Head-end reprocessing studies with irradiated HTGR fuels – Study of Dragon compact 8375

Dragon reactor fuel compact 8375, which was previously irradiated to an exposure of 15,000 MWd/MT, was subdivided by sawing and crushing, and the resulting product was burned in a bed with fluidized alumina. This was followed by sieving to separate the SiC-coated fuel particles from the alumina. The fuel particles were ground to shatter the SiC shells, burned in a static bed, and leached to recover the heavy metals and fission products. Analyses of controls showed that the original fuel apparently contained 2 to 3% broken particles. Bead breakage was 1.0 and 11.3% in crushing at $\frac{5}{8}$ - and $\frac{1}{8}$ -in. jaw openings, respectively. These results show that crushing is preferable to sawing, since fewer particles are fractured during crushing if the fuel is reduced to a similar-sized product by each method. Crushing at a $\frac{5}{8}$ -in. jaw opening appears attractive for the first size reduction.

Fission gas (^3H and ^{85}Kr) releases were measured for each head-end reprocessing step. Essentially all the ^{85}Kr (~98%) was released on grinding and burning the SiC-coated particles. About 30 to 40% of the total ^3H was released in the first burning step, which removes the matrix graphite and outer pyrolytic-carbon coats. This ^3H was probably formed by neutron reactions with light atoms in the matrix graphite or ^3He in the coolant gas or both. Most of the ^3H produced by ternary fission was released when the SiC-coated particles were ruptured and burned. About 3 to 7% of the total tritium remained with the burned fuel and was released on dissolution. Burner conditions were probably not optimum for the complete release of ^{85}Kr and ^3H .

10.4 Procurement of irradiated HTGR fuels for head-end studies

Additional samples of irradiated Dragon compacts were requested for use in head-end studies. These compacts have fuel particles similar to the coated-particle HTGR fuels presently being considered in the United States. Another source of irradiated samples is ORNL sol-gel recycle fuel particles that have been irradiated as compacts in the Dragon reactor. Samples of both these materials should be available by late 1970. In addition, two capsules will be irradiated in the ETR, and six recycle test elements are undergoing irradiation in the Peach Bottom reactor.

11. Refabrication Development

11.1 Sol-gel studies and particle preparation

Sol-gel processes are being developed and applied to preparing ThO_2 , UO_2 , and $\text{ThO}_2\text{-UO}_2$ spheres for HTGR fuel elements. The sphere-preparation pilot plant is being modified for remote operation, and new procedures and equipment will be checked during the next runs with $\text{ThO}_2\text{-UO}_3$ sol. The new procedures include recycle of 2EH, as developed for UO_2 sols. As possible improvements for the CUSP flowsheets for preparing UO_2 sol by solvent extraction, spray column contactors were tested as an alternate to the mixer settlers, 0.5 *M* amine instead of 0.25 *M* amine, and 1.8 or 2.0 *M* U in the feed in place of 1 *M*. The spray column has advantages, but the 0.5 *M* amine and 1.8 *M* U concentrations gave poor sols.

11.2 Fueled-graphite fabrication development

Dual-purpose equipment is being designed for developing fuel fabrication concepts and fabricating small quantities of fuel for use in other parts of the program. The principal effort was the fabrication of the fuel required for the recycle test elements (RTE's) being irradiated in the Peach Bottom reactor. Fuel for six elements was fabricated in a combined effort of ORNL and Gulf General Atomic. Development efforts were principally on particle preparation, particle coating, and fuel-stick fabrication. The prototype remotely operated coating furnace, which was successfully used to coat RTE particles after only a very brief breakin period, is being modified to incorporate improved electrodes, unloading system, and off-gas systems.

A series of experiments was started for determining how variation of the parameters used in coating affect the amount of faceting and soot inclusions in high-density coatings. Also the construction of a fuel-stick fabrication line with the capacity of 400 in. of fuel sticks per day was started. This line will contain a coated particle batch blender for blending multiple batches of either fissile or fertile particles, a combination fissile-fertile particle blender, a fuel-stick mold loader, fuel-stick molds, a mold heater, a pitch injector, and a fuel-stick injector.

12. Fuel Irradiations

The irradiations in the HTGR recycle program have two main objectives: (1) to provide irradiated fuel for

head-end processing studies and (2) to proof test products of the process development program. The total program involves capsule irradiation tests in a thermal-neutron-flux test reactor, pilot-scale irradiation in the Peach Bottom reactor, and a series of tests that will eventually include tests of remotely fabricated recycle test elements (RTE) in the Fort St. Vrain reactor. For accelerated burnup-rate tests, two capsules are being fabricated that are to be irradiated in the ETR starting in the first quarter of 1971. Four fissile-fertile particle combinations will be irradiated at temperatures

of 750, 950, 1050, and 1300°C up to fast-neutron fluences of approximately 8×10^{21} neutrons/cm² ($E > 0.18$ MeV). These four combinations are those of principal interest to the HTGR recycle program and are the combinations that received emphasis in the RTE test. The first six RTE's were inserted in the Peach Bottom reactor and have been operating as planned since July 14, 1970. Exposures will vary from one to three years, and the corresponding fluences will be 1.4×10^{21} to 4.2×10^{21} neutrons/cm² ($E > 0.18$ MeV).

Part I. High-Temperature Gas-Cooled Reactor Development

Introduction

The HTGR program at ORNL is designed to develop the desirable features of high-temperature gas-cooled reactors, including low-cost fuel cycles, good fuel conversion ratios, high thermal efficiency, high on-stream factors, and to determine the safety margins of the system. A large portion of the program is concerned with the fabrication, characterization, and testing of fuel to understand and improve fuel performance. Other studies include the release, transport, and deposition of metallic fission products from fuel that has been subjected to high exposure and burnup or to anticipated transients and accidental corrosive environments. The program is coordinated with the HTGR development program at Gulf General Atomic and is related to the Fort St. Vrain and Peach Bottom reactor projects being carried out by GGA.

The fuel element studies have emphasized the development of coated fuel particles, coating materials, and bonded coated particle beds with high resistance to irradiation damage. Combinations of fast-neutron exposure and burnup to full HTGR requirements can now be obtained relatively quickly with irradiation facilities in the HFIR. In early experiments, bonded fuel sticks disintegrated to a large extent, and some particle coatings were broken. Modifications in fabrication technique and the use of isotropic filler materials in the binder improved the structure and density of the bonded fuel to such an extent that specimens successfully withstood HTGR temperatures and fast fluences without debonding or coating failure. Presently a

series of isotropic and natural-flake graphite fillers are being evaluated in fabrication and irradiation tests to more nearly optimize the composition of fuel-stick matrices. These are being tested both in the target position (static) and in reflector (sweep) capsules in HFIR.

The target capsules, in particular, are also used for testing both loose particles and specimens of coating materials to investigate the effects of coating parameters and properties on the changes induced by irradiation. In a recent target capsule, two 3-in.-long blended beds of carbon-coated particles were tested to full HTGR exposure. The shrinkage of the bed (18 vol %) was even greater than predicted and demonstrated the fuel shrinkage problems associated with using loose particle beds.

An important part of the present fuel development program concerns the preparation, characterization, and testing of coated fuel particles with kernels made from ion-exchange resins. These particles offer an attractive alternative to the present fissile particle, which would be exposed to very high burnup. The fueled-resin particles consist of a low-density glassy carbon particle with about 50 wt % uranium dispersed as UO_2 or UOS and about 30% porosity. Techniques for loading the resin spheres with uranium, carbonizing, and coating have been studied and developed. Coated particles of this type survived full HTGR fast-neutron exposure and approximately 9% burnup in a recent experiment.

Fission-product release from irradiated coated particles and bonded beds of pyrolytic carbon and SiC-coated particles are studied during long-term high-temperature annealing experiments. At normal operating temperatures the fission gases are completely retained, and metallic fission-product release is quite low. However, some coatings may fail during operation, and in other particles the SiC layer may be defective. The time-temperature relations for fission-product release under these conditions are studied and diffusion constants are measured when possible. The distribution of fission products within a bonded fuel stick or in a fuel element may be measured in this manner after long heating periods. The specimens studied in these experiments include irradiated coated particles typical of Fort St. Vrain and advanced HTGR fuel obtained from the programs at GGA. Similar studies being carried out in Europe for the HTGR programs in the United Kingdom and Germany are reported through relevant exchange agreements, and results are analyzed and correlated with data from GGA and ORNL programs.

In recent experiments the diffusion coefficients of cesium from bonded beds of particles and from loose particles were measured at temperatures of 1250 to 1400°C in long annealing experiments. The coefficients obtained indicate that diffusion through low-temperature isotropic pyrolytic carbon may be significantly greater than diffusion through high-temperature methane-derived coatings. The SiC layers in Triso-coated particles were observed to break down at temperatures above 1800°C and result in release of solid fission products without detection of fission-gas release. Analysis of the stress distribution in the coating layers of individual coated particles by using the "Stress 2" code developed for the Dragon Project showed a high probability of SiC-coating-layer fracture without simultaneous failure of the pyrolytic-carbon outer layer. The calculated fractures compared favorably with observed fractures in annealing experiments.

The studies of fission-product behavior are extended by investigations carried out in the fission-product deposition loop. The objective of this program is to develop analytical methods and experimental data that will permit an evaluation of fission-product contamination in the coolant circuit of HTGR's. The plateout characteristics of potentially hazardous strontium and cesium isotopes are especially important for all gas-cooled reactors of advanced design. In five experiments with cesium in the loop, the transport of cesium through graphite into turbulently flowing helium was measured, and the deposition pattern was studied. The transport of cesium into the loop system was several

orders of magnitude greater than predicted by diffusion coefficients and vapor pressure data. Transverse flow of helium in the evaporator was suggested as a mechanism for this transport.

Considerable work on safety studies in HTGR environments is carried out as part of the nuclear safety program and is reported in detail in safety program documents. The current work is also reported in condensed form in this report. The primary objective of the work is to provide information concerning the response of the reactor to accidental perturbations that might affect the distribution of heat and fission products or the mechanical integrity of the core. The program consists of three related studies: (1) defining the conditions that produce failure of particle coatings and measuring the consequent fission-product release, (2) studying the chemical and physical states of fission products that have been released into the circuit and their mobility during accidental depressurization, and (3) understanding the steam-graphite reaction so that the effects of water ingress into the core can be analyzed adequately. In other studies, the investigation of distribution and character of important fission products in the coolant circuit of an operating HTGR was begun by initiating probe measurements in the Peach Bottom primary circuit.

The study of steam-graphite reactions is designed to find a model that will describe the reactions of steam with a porous solid and demonstrate that reaction rate constants measured out of the reactor can describe the removal of carbon from operating HTGR fuel elements. The rate of graphite removal is broadly governed by steam concentration, temperature, type of graphite, and extent of reaction. The latter two conditions affect the reaction to such an extent that rate parameters reported are, in many cases, poorly descriptive of any graphite except the samples tested. In reactions conducted in steam at 1000°C it now appears possible to correlate the variation of reaction rate with the extent of reaction in terms of surface area changes in the sample. A program to demonstrate the model under irradiation has been started. A small fuel element heated only by nuclear reactions is monitored for reaction rate and condition of the fuel. In recent studies, both in a reactor and in the laboratory, pitting corrosion of graphite was observed that is indicative of catalysis by inhomogeneously distributed metallic impurities. This pitting corrosion severely damaged the fuel after several percent burnoff in the first in-reactor experiment.

In component studies, a series of tests was carried out to evaluate the corrosion resistance of welds in

conventional and advanced alloys. The materials investigated are those considered for use in the superheater and reheater sections of HTGR steam generators. The test schedule emphasizes dissimilar-metal welds because a variety of alloys may be used in the same component in order to optimize the performance of the system. In addition to compatibility tests with steam at 595 and 650°C, the stress-corrosion cracking susceptibility, weldability, and strength of the welds are being

studied. The compatibility tests are being conducted in a heated loop by using steam from a commercial power plant. Inconel 625, Hastelloy X, and IN 102 as both base and filler metals, Incoloy 800 as base metal, and Inconel 82 as filler metal exhibited very good corrosion resistance in the tests, which have now exceeded 8000 hr duration. No preferential or unusual attack was noted.

1. Fuel Element Development

J. H. Coobs

1.1 Coated Fuel Particles Derived from Carbonized Ion-Exchange Resins

C. B. Pollock J. L. Scott

Fuel particles made by carbonizing ion-exchange resins loaded with uranium are being investigated for potential HTGR applications. It has been demonstrated that fuel particles can be prepared that have uranium densities comparable to those of the present reference fissile fuel particles, which consist of fully dense UO_2

or UC_2 kernels surrounded by thick buffer layers of low-density carbon. The new alternative to the dense kernel and thick buffer layer is a low-density kernel without a buffer layer or with a thin buffer layer to protect the outer coating from fission recoil damage. In Fig. 1.1 a sketch of a reference fissile particle is compared with the proposed alternate fuel particles, which can be manufactured by utilizing fuel-loaded, carbonized, ion-exchange-resin kernels with conventional pyrolytic-carbon and silicon carbide coatings.

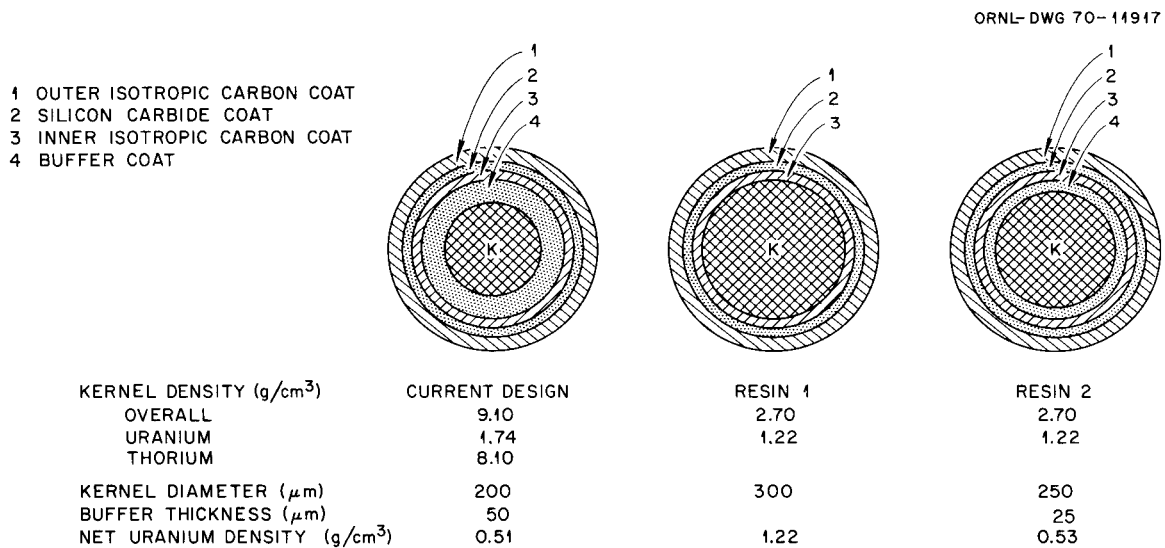


Fig. 1.1. Reference designs of current fissile-particle fuels and proposed fuel-loaded resin alternates.

Use of the resin-based kernel as a fuel material involves raw materials that are inexpensive. Also, kernel size and shape selection can be made before fuel loading. Figure 1.2 is a diagram of the proposed fuel-manufacturing process. Commercial ion-exchange resins would be dried, sized, and hydrated before contacting them with the uranyl nitrate solution, and after the exchange process was complete, the loaded beads would be dried and carbonized in a fluidized bed furnace with an inert atmosphere. The carbonized fuel beads would then be separated by shape prior to the application of pyrolytic-carbon and silicon carbide coatings.

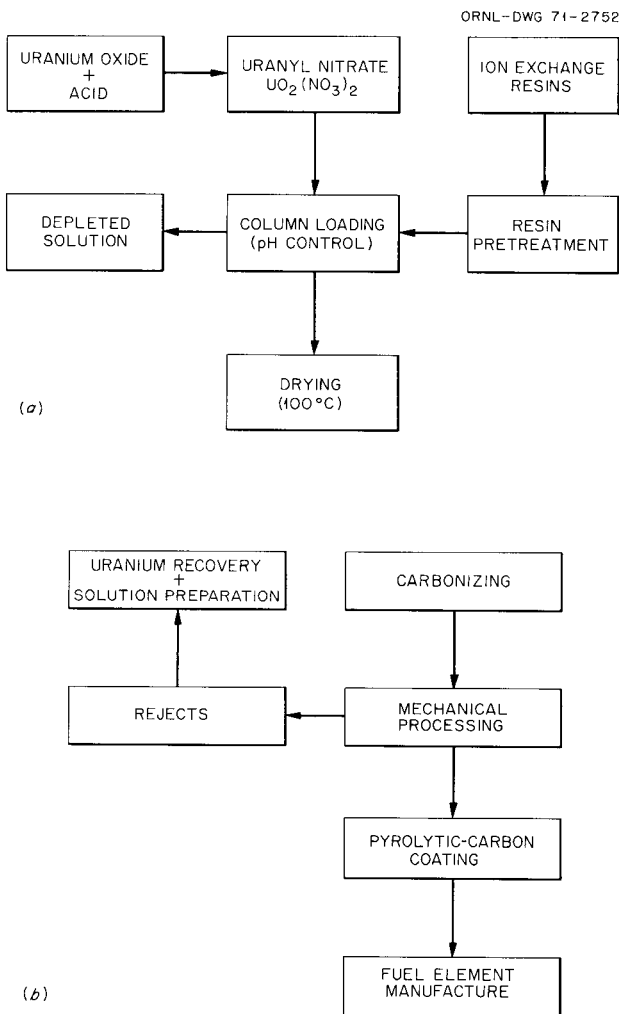


Fig. 1.2. Process diagrams for (a) loading ion-exchange resins with fuel and (b) converting fuel-loaded ion-exchange resins into fuel elements.

Another attractive feature of resin use is the variety of options available. The first fuel particles were made from sulfonated cation-exchange resin, and the fuel obtained contained uranium oxy-sulfide (UOS) finely dispersed in a glassy carbon matrix. It was also demonstrated that carboxylic cation-exchange resins could be used for preparing the particles. The fuel obtained was in the form of uranium dioxide (UO_2) finely dispersed in a glassy carbon matrix. The carboxylic cation-exchange resin gives a fuel particle that contains no residual sulfur and in which the fuel loading can be doubled (relative to use of the sulfonate type of resin).

The uranium compounds that exist in the glassy carbon matrix have been identified by x-ray analysis. The diffraction patterns are weak and diffuse because the phase is finely dispersed over the carbon matrix.

1.1.1 Chemistry of ion-exchange resins

The chemistry of ion-exchange resins is well understood,¹ but most of the previous experiments in this area involved loading ion-exchange resins to relatively low levels of metal concentration.² The ORNL experimental work has been designed to determine ways of achieving maximum loading of metal in various copolymers and to demonstrate repeatable loading curves. The two loading procedures used are a batch-type process and a column-loading technique. Table 1.1 gives a summary of data obtained with carbonized, fueled cation-exchange resins loaded in a batch-type procedure. Table 1.2 summarizes data collected from fuel particles loaded in the batch-type process under various conditions of temperature and time, with solution concentration being constant. In all batch-loading experiments the degree of uranium loading was substantially lower than theoretical, which is 51 wt % uranium. To increase the loading, a column-loading technique was developed in which the equilibrium was driven toward uranyl ion use so that the UO_2^{++} ion replaced all hydrogen ions. Table 1.3 summarizes data collected from a series of batches loaded in this manner. The results have been quite consistent, and means are now being investigated for increasing the uranium

1. J. L. Scott, J. M. Leitnaker, and C. B. Pollock, "Preparation of Coated Fuel Particles from Ion-Exchange Resins," pp. 3-7, *Gas-Cooled Reactor Program Semiann. Progr. Rept. Mar. 31, 1970*, USAEC Report ORNL-4589, Oak Ridge National Laboratory.

2. See, for example, *Duolite-Ion-Exchange Manual*, Chemical Process Company, Redwood City, California.

Table 1.1. Summary of results obtained in loading ion-exchange resins with uranium by a batch-type process^a

Time (min)	Analysis (wt %)			
	Uranium	Carbon	Sulfur	Oxygen
15	33.77	45.55	11.20	8.56
15	35.52	47.11	10.30	7.71
30	37.04	46.58	11.70	5.00
30	35.18	45.26	11.40	7.24
45	37.38	45.70	10.50	7.31
45	36.77	45.37	11.50	6.28
60	34.05	46.10	11.90	10.12
60	35.53	46.15	10.20	8.78
120	35.50	45.86	11.40	8.06
120	37.31	46.50	11.20	5.43

^aSolution concentration, 500 g UO₂(NO₃)₂/liter.

Table 1.2. Typical analysis obtained in loading ion-exchange resins with uranium at two temperatures^a

Sample No.	Temperature (°C)	Analysis (wt %)			
		Uranium	Carbon	Oxygen	Sulfur
130-1	23	36.60	46.52	5.96	11.20
130-2	23	34.75	46.00	6.96	11.60
130-1	35	37.76	42.72		7.40
130-2	35	38.62	46.56	3.62	11.30
160-1	23	38.99	46.01	4.99	10.40
160-2	23	42.85	48.44		9.80
160-1	35	37.93	43.95	6.64	11.20
160-2	35	38.03	44.08	6.24	10.90

^aSolution concentration, 500 g UO₂(NO₃)₂/liter.

Table 1.3. Summary of results obtained in loading ion-exchange resins with uranium by a column-loading technique^a

Sample	Analysis (wt %)			
	Uranium	Carbon	Oxygen	Sulfur
C1-1-1	46.71	36.85	7.03	10.57
C1-1-2	47.02	37.14	5.33	11.24
C1-2-1	48.68	35.62	4.89	10.54
C1-2-2	48.74	33.99	6.42	9.95
C1-107-709	46.60	35.60	8.12	10.26

^aSolution concentration, 775 g UO₂(NO₃)₂/liter.

density in the fuel particles. Figure 1.3 is a plot of uranium concentration as a function of time for a column-loading experiment, with the solution concentration constant at 775 g UO₂(NO₃)₂/liter.

Metal loading of ion-exchange resins is dependent on a number of variables, including temperature, time, solution concentration, number of active sites, and valence state of the metal ion. Temperature and time influence the rate of the exchange reactions, since it is a diffusion process. Solution concentration is significant only at low concentrations and has little effect in this work, since very concentrated solutions are used. The number of active sites in a sulfonated cation-exchange resin is indicative of the degree of sulfonation. Uranium loadings of 85 to 90% of theoretical are being achieved, and consequently it is thought that commercially available resins are only about 85 to 90% sulfonated. Consideration of the structure of cross-linked ion-exchange resins such as styrene-divinyl benzene, shown in Fig. 1.4, indicates why this is true. The sulfonic group prefers the *para* position in the benzene ring, but only about 85% of the sites are normally occupied. It is more difficult to attach sulfonic groups to the *meta* or *ortho* positions because of energy considerations. In the fuel-loading step the ionizable hydrogens of the sulfonic groups are replaced by uranyl ions.

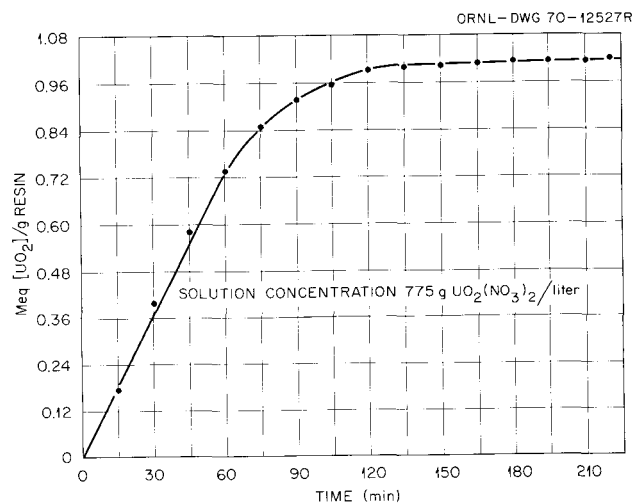


Fig. 1.3. Kinetics of loading UO₂⁺⁺ on cation-exchange resin Dowex 50-X8.

ORNL-DWG 70-4952R2

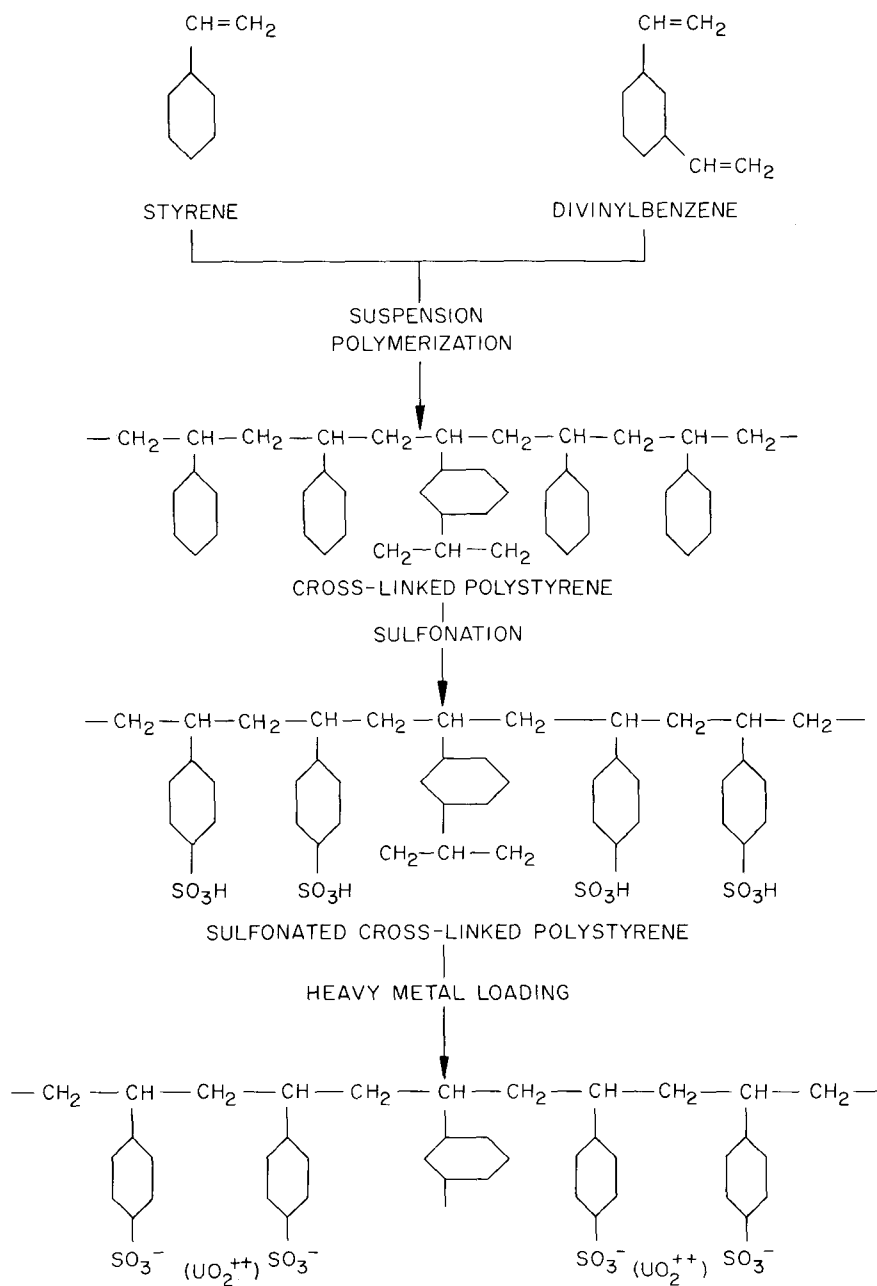


Fig. 1.4. Structure of polymerized and metal-loaded ion-exchange resins.

1.1.2 Carbonization of fueled resin microspheres

The carbonization of fuel-loaded ion-exchange resins is dependent on heating rate, and therefore investigations of the carbonization cycle were made. Figure 1.5 shows typical differential-thermal-analysis curves for resin particles with and without fuel. On heating, an

endothermic reaction occurs first that is indicative of a loss of water in both samples. This reaction starts very early and peaks prior to 200°C . Then there is a strong endothermic reaction in the unloaded resin that peaks near 325°C and a similar weaker reaction in the loaded resin that peaks earlier. This peak is indicative of decomposition of the resin or the creation of monomers

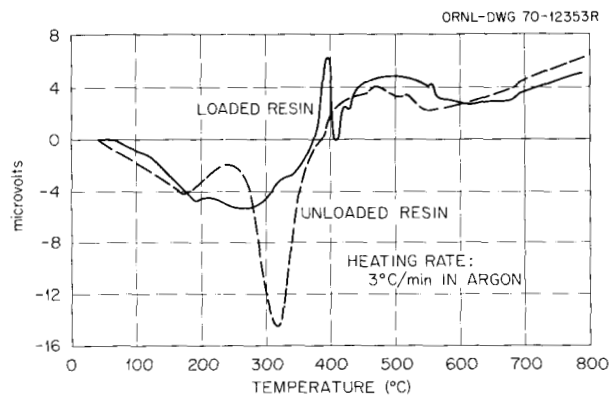


Fig. 1.5. Differential-thermal-analysis curve for a uranium-loaded sulfonated ion-exchange resin (solid curve) compared with the corresponding unloaded resin (dashed curve).

from the copolymers. In the fuel-loaded resin this reaction starts earlier and is apparently suppressed by the uranyl groups that are present.

The next event is a rather sharp exothermic peak in fuel-loaded resins and the start of a broad, weaker exotherm in the unloaded resin. The narrow exothermic peak appears to be due to loss of sulfur in the form of SO_2 prior to the start of carbonization, whereas the loss of sulfur in the unloaded resin is concealed by the sharp, steep endotherm representing the decomposition reaction. The broad, wide exotherm on both curves starting at about 400°C represents the advent of carbonization of the ion-exchange resins and also a reduction of surface area by the closing of surface pores. Carbonization is essentially complete by 700°C . The density of the carbon matrix obtained was approximately 1.4 g/cm^3 , while the density of the fueled particle was dependent on the concentration of uranium. Table 1.4 shows how density varies with degree of fuel loading. Figure 1.6 is a plot of uranium density as a function of particle density and porosity.

1.1.3 Irradiation testing

The fuel-loaded carbonized resin kernels can be coated with successive layers of pyrolytic carbon or silicon carbide, and particles with a variety of such coatings have been made. The low-density kernels require different coating conditions than the high-density oxide or carbide kernels for the initial buffer coating. Other coating steps are identical for the two types of particles. Table 1.5 lists the properties of three batches of coated particles prepared in this manner for irradiation testing. These samples were tested in HFIR

Table 1.4. Effect of uranium loading on porosity and particle density of fuel-loaded carbonized ion-exchange resins

Sample No.	Uranium (wt %)	Density (g/cm^3)	Porosity volume (%)
1	0	1.4	36.0
2	10.5	1.5	40.0
3	15.8	1.77	31.0
4	22.6	1.90	40.0
5	25.2	2.00	31.8
6	27.0	1.96	32.0
7	34.9	2.13	34.0
8	43.6	2.60	39.7
9	46.6	2.94	24.0
10	51.4	3.09	25.0
11	58.3	3.10	32.0

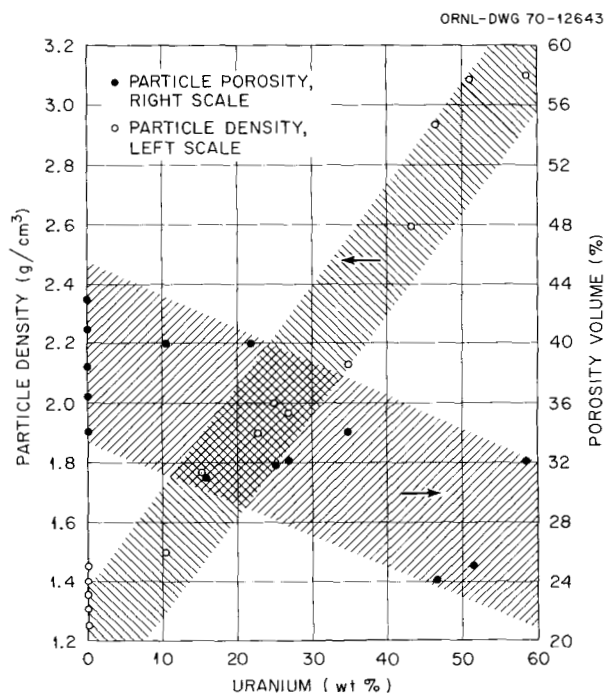


Fig. 1.6. Effect of uranium loading on particle porosity and particle density of fuel-loaded ion-exchange resins.

target experiment HT5 at 1050°C to a fluence of 6×10^{21} neutrons/ cm^2 ($E > 0.18 \text{ MeV}$). The fuel burnup was about 9% of the heavy metal. Postirradiation examination of the particles is in progress, and the results obtained thus far have been quite encouraging. Figure 1.7 shows coated particles before and after

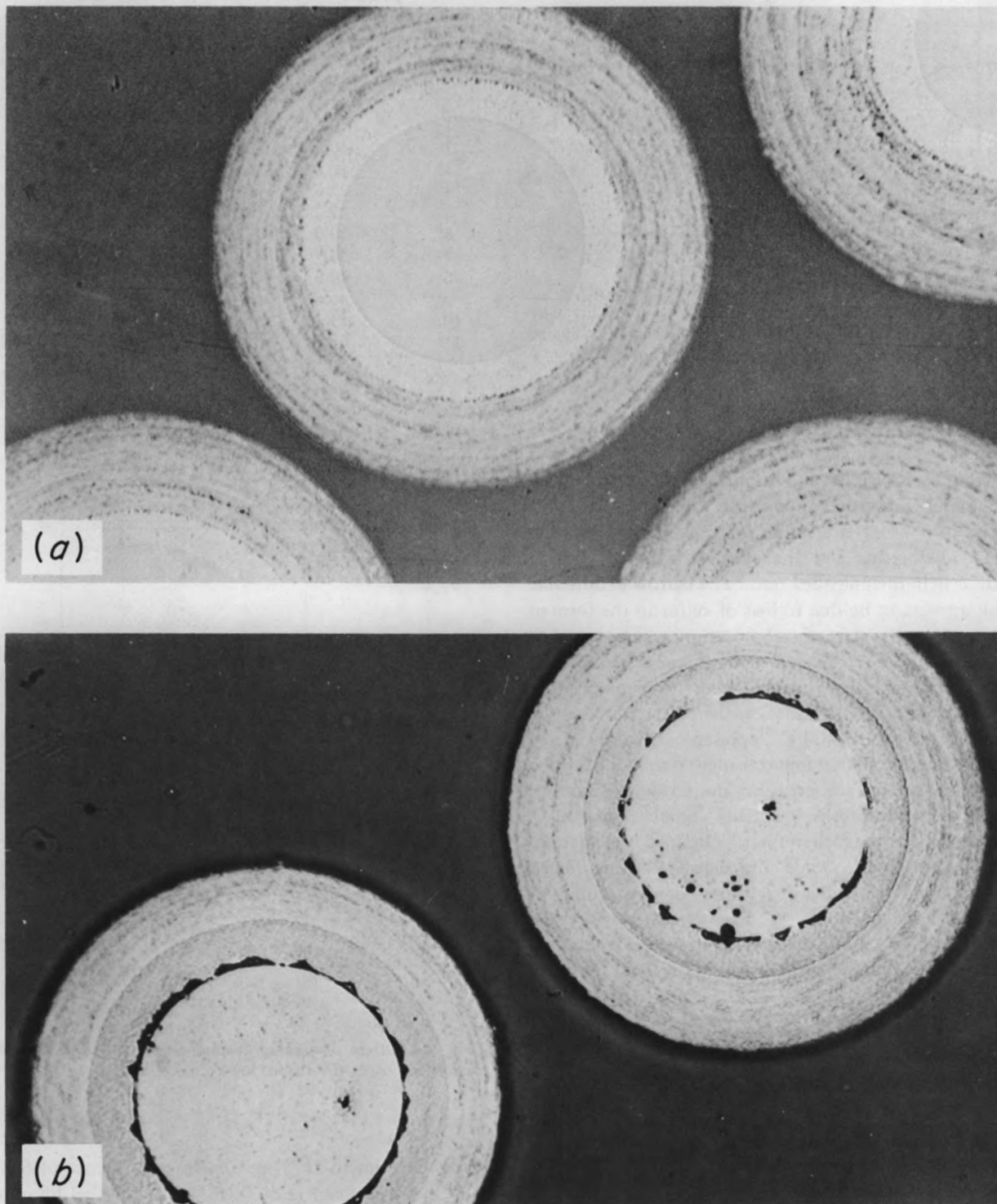


Fig. 1.7. Typical coated particles made from fueled, carbonized ion-exchange resins. (a) As coated. (b) Irradiated at 1050°C to 6×10^{21} neutrons/cm² ($E > 0.18$ MeV).

Table 1.5. Properties of coated particles prepared and used for HT5 irradiation experiment

Type of kernel: carbonized resin + UOS Diameter of kernel: 250 μm Fuel: natural uranium			
Coated particle designation	OR 1100	OR 1101	OR 1117
Heavy-metal content, wt %	9.24	7.22	6.95
Type of coating	Monolayer	Monolayer	Interrupted, two layers
Thickness of layer, μm			
Inner			24.4
Outer	55.6	73.6	58.0
Density of layer, g/cm^3			
Inner			2.07
Outer	1.68	1.64	1.55

irradiation. There is apparently no damage to the kernel, but the inner layer shows some damage from fission recoils. The outer coatings are completely intact.

1.2 Development of Bonded Beds of Coated Particles for HTGR Fuel Elements

J. M. Robbins J. H. Coobs

Results of irradiation tests of bonded beds in HFIR target capsule HT4 confirmed the suitability of bonded beds for HTGR fuel elements.³ The beds tested had Poco graphite as the filler material in a binder of 15V coal-tar pitch. Attempts are now being made to find less expensive filler materials that will perform satisfactorily. Some of the criteria for choosing materials for screening were (1) availability in commercial quantities, (2) relative cost, (3) workability, (4) graphitizability, and (5) formation of isotropic structure. HFIR capsules HT6 and HRB2 were designed and fabricated to screen several of these fillers. In addition, some fillers were included to confirm irradiation results obtained earlier both here and at Gulf General Atomic.

HFIR capsule HT6 contains both bonded fuel sticks and loose coated particles. Fabrication history and location within the capsule are given in Table 1.6, and Table 1.7 indicates the loading scheme of both GGA

and ORNL loose coated particles. The capsule is to be removed from the reactor November 10, 1970, after three cycles of operation.

Capsule HRB2 will contain both bonded fuel sticks and loose coated particles. The compositions of the bonded specimens are given in Table 1.8. All fuel sticks in HRB2 contain three types of kernels with Biso coatings and were bonded with 15V pitch as the binder. The three types of kernels are (1) 10.16%-enriched UO_2 in a carbonized resin particle, (2) sol-gel derived ThO_2 particles, and (3) inert, carbonized resin particles. Some pellets are to be used as unirradiated control specimens. The capsule is to be inserted November 10, 1970, and is scheduled for eight cycles of operation.

The Santa Maria flour was obtained through the Los Alamos Scientific Laboratory (LASL) and the Y-12 Chemical Engineering Development Department. It is reported to produce bodies similar in unirradiated properties to those formed with the Poco grades of graphite.⁴ When mixed with binder in concentrations up to 50 wt %, the Santa Maria flour makes a smooth-appearing matrix material that injects easily through a 0.7-in.-long bed of coated particles. The JOZ grade of graphite flour is derived from a petroleum coke and is the base material for the Great Lakes H-337 graphite. Interest in this material was evoked by the encouraging irradiation behavior of H-337 in HFIR experiments at 750°C and the availability of the material in large quantities. Only 42 wt % of the JOZ flour could be mixed with binder and still be usable. The mix shows a slight tendency toward dilatancy;⁵ however, injection through the 0.7-in.-long test specimen was not difficult. The Robinson flour is graphitized air-blown coke, which does not form a needle-like structure and therefore may form an isotropic matrix. It was possible to inject a mixture of 45 wt % of the Robinson flour in binder through the 0.7-in.-long test piece. When 50 wt % of the flour is mixed with binder, the mixture shows a marked degree of dilatancy and cannot be injected more than approximately $\frac{1}{2}$ in. into the test bed.

The Asbury flour is the natural flake graphite that was used in HT1 and HT3. Only 35 wt % can be added to binder and injected through the test piece. One mix was evaluated in which only Thermax carbon black was

3. J. H. Coobs et al., "Irradiation Tests on HTGR Fuel and Fuel Elements," pp. 18-36, *Gas-Cooled Reactor Program Semiann. Progr. Rept. Mar. 31, 1970*, USAEC Report ORNL-4589, Oak Ridge National Laboratory.

4. Los Alamos Scientific Laboratory, *Progress Report 9, February-April 1969*, USAEC Report LA-4171-MS.

5. A dilatant mix is one that seems reasonably fluid when at rest but becomes more viscous with increasing rates of shear.

Table 1.6. Bonded coated-particle specimens for HT6 experiment

Specimen designation	Filler Material		Type of particles	Carbonizing conditions	Temperature and fluence	Magazine	Temperature of preirradiation heat treatment (°C)
	Type	Amount (wt %)					
JF 270-2	Thermax	50	Mixed ^a	Packed bed ^b	Low	CP-23	1500
JF 270-4	Thermax	50	Mixed ^a	Packed bed ^b	High	CP-22	1500
JF 270-8	Santa Maria	40	Mixed ^a	Packed bed ^b	Low	CP-20	1500
JF 270-10	Santa Maria	40	Mixed ^a	Packed bed ^b	High	CP-22	1500
JF 270-14	JOZ	40	Mixed ^a	Tube holder ^c	Low	CP-20	1500
JF 270-16	JOZ	40	Mixed ^a	Tube holder ^c	High	CP-22	1500
JF 270-18	JOZ	40	Mixed ^a	Packed bed ^b	Low	CP-20	1500
JF 270-39	JOZ	40	Inert ^d	Packed bed ^b	Low	CP-20	1800
JF 270-20	H-378	35	Mixed ^a	Tube holder ^c	High	CP-21	1500
JF 270-50	H-378	35	Mixed ^a	Tube holder ^c	Low	CP-20	1500
JF 270-24	H-378	35	Mixed ^a	Packed bed ^b	High	CP-21	1500
JF 270-42	H-378	35	Inert ^d	Packed bed ^b	Low	CP-20	1500
JF 270-25	N.F. 6353	27	Mixed ^a	Packed bed ^b	Low	CP-23	1500
JF 270-28	N.F. 6353	27	Mixed ^a	Packed bed ^b	High	CP-22	1500
JF 270-31	Robinson	40	Inert ^d	Packed bed ^b	High	CP-21	1500
JF 270-32	Robinson	40	Inert ^d	Packed bed ^b	Low	CP-23	1500
JF 270-35	Poco AXZ	35	Inert ^d	Packed bed ^b	High	CP-22	1800
JF 270-38	Poco AXZ	35	Inert ^d	Packed bed ^b	High	CP-22	1500
JF 270-46	Poco FXA	40	Inert ^d	Packed bed ^b	High	CP-21	1500
JF 270-47	Poco FXA	40	Inert ^d	Packed bed ^b	Low	CP-23	1500

^aSufficient carbon-coated ThO₂ particles to give a concentration of 0.054 g Th/in. of fuel stick; ThO₂ particles mixed with carbon-coated SiC particles as the inert diluent.

^bSticks packed tightly in natural flake graphite during carbonization.

^cSticks restrained in a closely fitting graphite tube during carbonization.

^dCarbon-coated SiC particles.

Table 1.7. Loose coated particles in experiment HT6

Batch	Source	Kernel size (m μ)	Magazine	Temperature and fluence
GA-4000-176	GGA	>550	M-2	High
GA-4000-184	GGA	<475	M-2	High
GA-4000-176	GGA	>550	M-4	Low
GA-4000-176	GGA	475-550	M-2	High
GA-4000-176	GGA	475-550	M-4	Low
GA-4000-184	GGA	>550	CP-20	Low
GA-4000-184	GGA	475-550	CP-23	Low
GA-4000-184	GGA	475-550	CP-22	High
GA-4000-184	GGA	<475	M-4	Low
GA-4000-184	GGA	>550	CP-21	High
GA-4000-193	GGA	475-550	CP-22	High
GA-4000-193	GGA	>550	CP-20	Low
GA-4000-193	GGA	>550	CP-21	High
GA-4000-193	GGA	475-550	CP-23	Low
GA-4000-193	GGA	<475	M-2	High
GA-4000-193	GGA	<475	M-4	Low
OR-1298	ORNL	300-400	M-3	High
OR-1298	ORNL	300-400	M-1	Low
OR-1295	ORNL	400-500	M-3	High
OR-1295	ORNL	400-500	M-1	Low
OR-1316	ORNL	500-680	M-3	High
OR-1319	ORNL	350-700	M-1	Low

Table 1.8. Bonded specimens prepared for testing in HRB2

Pellet No.	Filler material		Maximum particle size (μ m)
	Type	Amount (wt %)	
1-4	Thermax	50	
5-8	Santa Maria	40	40
9-12	Robinson	40	27
13-16	JOZ	40	40
17-20	Asbury	35	40
21-24	Poco AXZ	35	40
25-28	H-378	35	27
29-32	N.F. 6353	27	40
33-36	Poco FXA	40	40

used as a filler. In this case, 58 wt % of the Thermax in the binder was usable. The amounts of the various fillers reported above are the maximum amounts for small specimens, and these were reduced in most cases for the HRB2 and HT6 specimens to obtain a more workable bonding material.

During the fabrication of the bonded beds for the recycle test elements (see Chap. 11), it was found to be expedient to pack the uncarbonized fuel stick in a bed of natural flake graphite during carbonization to prevent slumping in the early heating stage when the pitch becomes molten. Usually the fuel stick is contained in a close-fitting graphite tube during carbonization. However, the large number (about 1200) of fuel sticks required for the recycle test elements (RTE's) made this containment method cumbersome and created a bottleneck in the fabrication process. Therefore, fuel sticks were fabricated and evaluated to determine the effect of the containment method during carbonization on the final matrix density. All sticks contained the same amount of coated fuel particles and were bonded with 15V pitch. As shown in Table 1.9, the matrix density was higher in a stick carbonized in a graphite tube than in one carbonized in a bed of graphite. The higher density was primarily due to retention of more of the matrix material in specimens heated in the graphite tube than in the packed graphite bed. This is shown by the higher weights of matrix material in the tube-supported fuel sticks.

Many broken particle coatings were found upon examination of the first series of fuel stick specimens prepared for testing in the HRB2 experiment. Broken coatings were present in all specimens that were

carbonized in a close-fitting graphite tube. Apparently interaction of coatings with the high-density matrix that contained more binder coke produced high stresses in the outer coatings. This was especially true of low-temperature isotropic (LTI) coatings that were intermediate in density ($\sim 1.7 \text{ g/cm}^3$). Broken coatings on all types of particles were found in the specimens that had the highest matrix density; that is, those that contained either 50 wt % Thermax or 40% Santa Maria filler. Therefore all specimens for the HRB2 and HT6 experiments, except two types that contained JOZ and H-378 filler materials (see Table 1.6), were carbonized in a packed bed of natural flake graphite. The specimens tested in HT6 will yield comparative data on the two matrices carbonized by both methods.

The present observations of coating failure during carbonization are not consistent with prior fabrication experience and the results of irradiation testing of Varcum- and pitch-bonded particles in the HT4 experiment.³ Bonded specimens for this experiment were carbonized in close-fitting graphite tubes and contained no broken coatings. Apparently subtle changes in coating characteristics affect coating behavior during injection bonding and carbonization. The mechanisms of the interactions between coatings and matrix and the effects of carbonization support method on the structure of the matrix are being investigated further.

1.3 Irradiation Tests on HTGR Fuel Elements

J. A. Conlin B. H. Montgomery
 J. H. Coobs C. B. Pollock
 D. M. Hewette II J. M. Robbins
 R. E. MacPherson J. L. Scott

Table 1.9. Effect of method of fuel stick support during carbonization on final matrix density

Stick designation	Filler material		Support method	Matrix weight (g)	Matrix density (g/cm^3)
	Amount (wt %)	Type			
JF265-1	35	Poco	Tube ^a	0.4232	0.713
-2	35	Poco	Bed ^b	0.4118	0.654
-8	50	Thermax	Tube	0.6357	0.974
-11	50	Thermax	Bed	0.5456	0.899
-12	40	Santa Maria	Tube	0.5364	0.886
-14	40	Santa Maria	Bed	0.4470	0.732
-16	40	Robinson	Tube	0.4750	0.787
-19	40	Robinson	Bed	0.4467	0.720
-22	35	JOZ	Tube	0.4844	0.812
-23	35	JOZ	Bed	0.4062	0.674
-28	27	6353	Tube	0.5161	0.852
-31	27	6353	Bed	0.3887	0.643
-32	35	H-378	Tube	0.5344	0.872
-33	35	H-378	Bed	0.4038	0.701
-38	40	JOZ	Tube	0.5736	0.914
-39	40	JOZ	Bed	0.4576	0.774

^aSupported in a close-fitting graphite tube.

^bSupported in a tightly packed graphite flour bed.

The HTGR program at ORNL includes irradiation in two types of capsules in the HFIR where the combined effects of burnup and high values of fast-neutron exposure can be evaluated. The target capsules (HT) are small uninstrumented capsules designed to fit into one of the target positions in the HFIR. They contain small specimens of HTGR fuel and fuel element materials in the form of loose particles, bonded coated-particle beds, blended coated-particle beds, or pyrolytic-carbon disk specimens. The specimens can be irradiated at temperatures up to 1100°C and to representative HTGR end-of-fuel-life fast flux exposure in about two and one-half months. The HT capsules have the advantage of low cost and short irradiation time to attain representative exposure, but they have some limitations. Only small specimens with very small amounts of fissionable material can be accommodated.

Since the capsules are uninstrumented, temperatures are not monitored during irradiation but are deduced by postirradiation analysis of silicon carbide monitors. The capsules are sealed and no gas sweep is possible. Therefore the composition of the atmosphere is somewhat uncertain, and fission-gas release cannot be measured during irradiation.

The second type of HFIR capsule is irradiated in the removable beryllium (HRB) facility. These capsules are large (1.3-in.-OD) instrumented gas-swept capsules with provision for specimen temperature control and fission-gas release measurement. The capsules accommodate fuel specimens in a graphite support sleeve that is geometrically representative of a single fuel channel of a Fort St. Vrain type of HTGR fuel element. Fuel loading, temperature, power density, and burnup rate are limited only by the capability of the fuel.

1.3.1 HTGR-HFIR target capsules

Five target capsules, HT1 through HT5, have been irradiated. Design information and irradiation history were previously reported for capsules HT1 through HT4.⁶⁻⁹

Postirradiation examination of target capsule HT4. Capsule HT4 contained three types of bonded beds made with large amounts of filler materials in pitch and Varcum binder. The dimensional changes and metallographic examination of specimens bonded with 29 wt % Poco graphite and 29 wt % Thermax in pitch or Varcum binder were reported previously. Four such samples irradiated at two different temperatures showed no broken particle coatings on more than 2000 coated particles exposed in the polished sections.⁶ This was the first demonstrated irradiation of injection-bonded beds of coated particles to the full fluence specified for HTGR's.

Two more specimens that were bonded with a mixture of 40% Poco graphite in pitch were examined

recently. One was irradiated in magazine CP-14 to a fast-neutron fluence of 8×10^{21} neutrons/cm² ($E > 0.18$ MeV) at 1050°C, and the second was tested at 750°C to a fluence of 5×10^{21} neutrons/cm². No broken particle coatings were found in polished sections of either specimen. The matrix showed some gross porosity and much microporosity, as illustrated in Fig. 1.8. These two specimens have matrices that are similar in composition and structure to the matrix of fuel sticks fabricated at ORNL for testing in the recycle test elements (see Chapter 11).

Target capsule HT5. The capsule most recently irradiated in this series (capsule HT5, described previously⁶) was installed in HFIR target position A-3 December 11, 1969. The capsule was removed February 22, 1970, after a scheduled three-cycle (69-day) irradiation to a peak fast-neutron exposure of approximately 7.5×10^{21} neutrons/cm² ($E > 0.18$ MeV) at temperatures ranging from 890 to 1020°C for the various specimens. The results of neutron radiography, gamma scanning, and visual examination were given previously.³ The results of metallographic examination of fueled resin particles tested in the experiment are given in Section 1.1 of this chapter. Metallographic examination of additional samples is in progress.

Target capsule HT6. The sixth capsule was inserted in target position A-3 August 28, 1970, to be irradiated for three HFIR cycles, and removal is scheduled for November 10, 1970. The capsule, which is similar to previous target capsules, is shown in Fig. 1.9. Four graphite holders (magazines) labeled CP-20, -21, -22, and -23 are used to support bonded beds containing coated particles fueled with ²³²Th, ²³⁵U, and ²³⁸U. Small longitudinal slots were machined in the ends of each graphite holder to contain loose ThC₂ fuel particles from Gulf General Atomic that represent Fort St. Vrain reactor preproduction material. The bonded beds are unfueled in the vicinity of these loose particles to avoid excessive heat flux. The capsule also includes two graphite bodies, labeled M-2 and M-4, that contain SiC temperature monitors. They are located between the bonded-bed holders. These graphite bodies also contain ²³²Th-fueled loose particles in longitudinal slots.

Table 1.10 lists the design temperature and expected fast fluences for the magazines, which are designed to operate at a uniform axial temperature. This is accomplished by tapering to provide a varying gap for insulating gas between the magazine and the water-cooled capsule wall to compensate for the axial variation in gamma and fission heating within the capsule. The maximum temperatures are expected to

6. J. H. Coobs et al., "Irradiation Experiments in HFIR," pp. 20-25, *Gas-Cooled Reactor Program Semiann. Progr. Rept. Mar. 31, 1969*, USAEC Report ORNL-4424, Oak Ridge National Laboratory.

7. J. H. Coobs et al., "Irradiation of Loose and Bonded Coated Particles in HFIR Target," pp. 47-54, *Gas-Cooled Reactor Program Semiann. Progr. Rept. Sept. 30, 1968*, USAEC Report ORNL-4353, Oak Ridge National Laboratory.

8. *Ibid.*, pp. 29-30.

9. H. C. McCurdy et al., "Instrumented Capsules for Fuel Tests in HFIR," pp. 27-37, *Gas-Cooled Reactor Program Semiann. Progr. Rept. Sept. 30, 1969*, USAEC Report ORNL-4508, Oak Ridge National Laboratory.

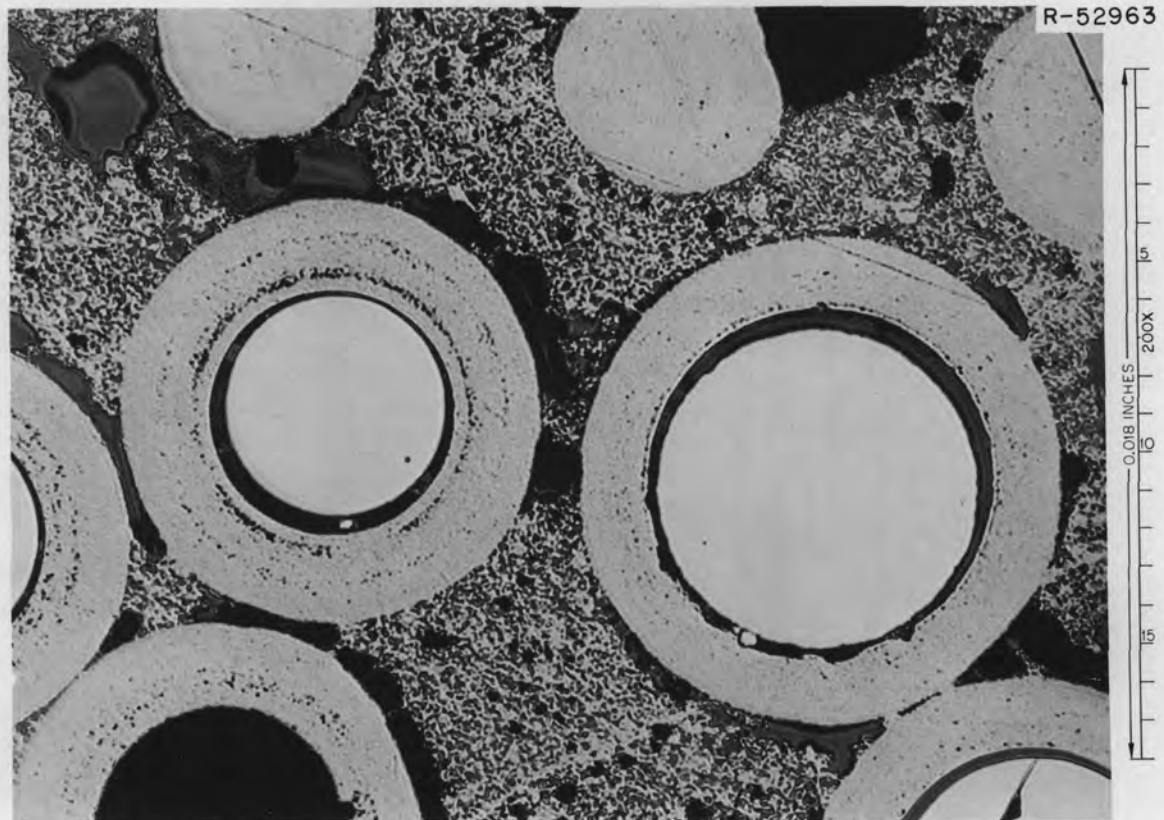


Fig. 1.8. Polished section of bonded coated-particle bed tested in experiment HT4 to fast-neutron fluence of 8×10^{21} neutrons/cm² ($E > 0.18$ MeV) showing intact particle coatings and structure of matrix.

Table 1.10. HT6 graphite magazine design temperature and expected fast fluence

Magazine	Design temperature (°C)		Expected fast fluence ($E > 0.18$ MeV) (10^{21} neutrons/cm ²)
	Initial	Maximum	
CP-20	800	~870	2.8–6.3
CP-21	1070	~1200	6.6–7.9
CP-22	1070	~1200	6.4–8.0
CP-23	800	~870	2.5–4.8
M-2	1130	~1250	7.9–8.0
M-4	1000	~1100	5.1–6.1

occur at the start of the third cycle, at which time the buildup of ²³³U plus ²³⁵U in the fuel will be at a maximum. A detailed description of the bonded beds and coated particles being tested in capsule HT6 is given in Section 1.2 of this chapter.

1.3.2 HTGR-HFIR instrumented capsules

HRB1. Irradiation of the first instrumented fueled capsule in the HFIR was completed, and examination is in progress. This capsule, HRB1, contained several fueled bonded-bed specimens in a graphite sleeve. The test element was designed to represent a single fuel region within a fuel element of the type used in the Fort St. Vrain reactor. The element simulated the geometry and was irradiated at temperatures and fast-neutron fluence representative of the Fort St. Vrain reactor. The capsule was described previously,⁶⁻⁹ and the results of fission-gas release measurements during irradiation and the postirradiation examination by neutron radiography were reported.³

Dismantling and visual examination of HRB1. The capsule was gamma scanned and then dismantled. The differential scan permitted identification of all fueled samples in the experiment and verification of their positions. The capsule was opened by cutting off both ends and slitting the inner and outer containment

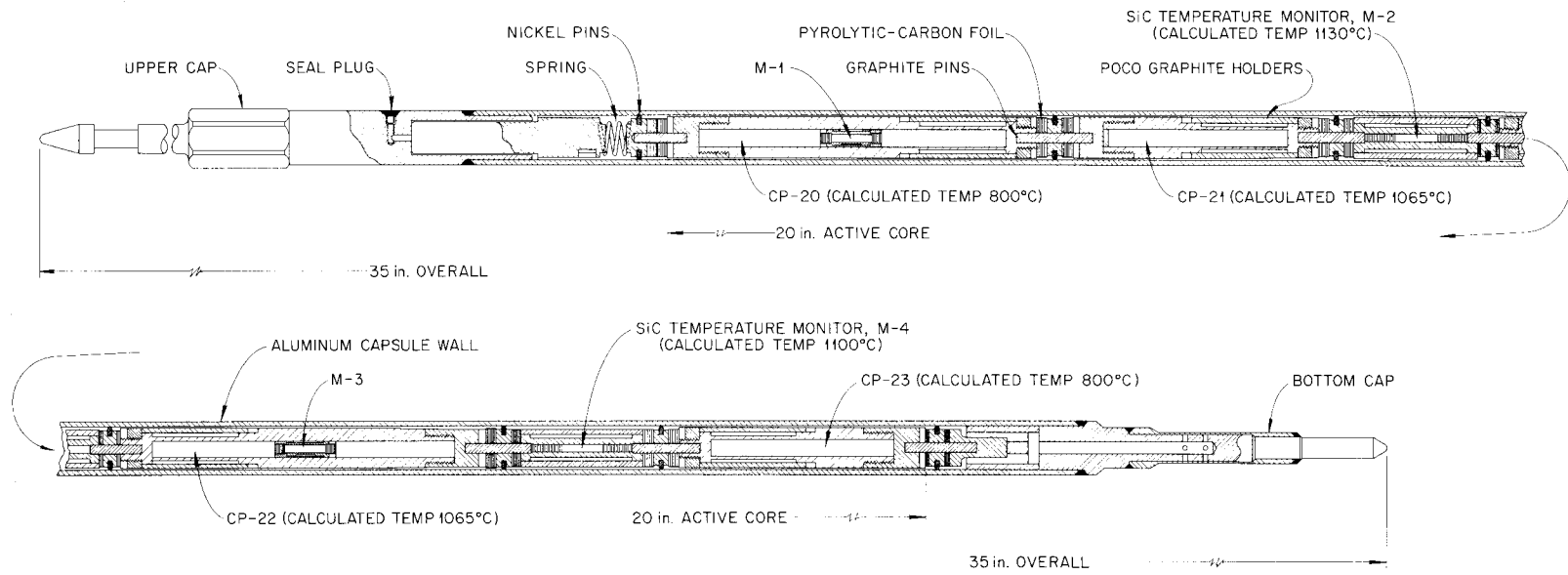


Fig. 1.9. HTGR-HFIR target capsule HT6.

vessels so they could be separated from the graphite sleeve. The inner surfaces of the secondary containment vessel were bright and clean, while the primary containment vessel was stained and had a small amount of a light-colored deposit at the top end. The segmented graphite sleeve came out intact and seemed unaffected by the high exposure, except for severe warping of each segment. No cracking at the joints could be detected, and no surface roughening or staining was observed on the sleeve. The Lucalox (Al_2O_3) spacers were in place on the graphite sleeve and were intact. These were later recovered and are being examined.

The lower and upper segments were then separated from the long midsection by slipping the joints apart. The bonded beds and other specimens were pushed out of the end segments and recovered. However, the middle segment had to be cut into three parts and, finally, split before all specimens could be removed.

The conditions of the several types of bonded coated-particle specimens were quite variable. Those specimens that were made with a matrix consisting of 15% Asbury graphite in phenolic resin (low-density matrix) were very weak and crumbled easily. This was especially true of specimens 4A and 4B, which were exposed to maximum fluence. On the other hand,

specimens prepared with the high-density matrix (40% Poco graphite in Varcum, or 29% Poco-29% Thermax in Varcum) were intact, except for two that were damaged during dismantling of the capsule. This condition is best illustrated by comparing the appearance of bonded-bed specimens 4B and 5A in Fig. 1.10. The samples with high-density matrices could be measured and handled readily. Specimens from positions 3 and 5 were easily broken in two (to obtain samples for metallographic examination), while a specimen from position 8, which contained only inert particles and was exposed to the minimum fluence, was very strong and could be broken only by using a vise.

The dimensional changes of the bonded specimens are given in Table 1.11. Changes in diameter appear to be more a function of fluence than composition. Specimens 3A, 3B, 5A, and 6B, which contained coated fuel particles and received high exposure of 5×10^{21} neutrons/cm² ($E > 0.18$ MeV) or more, swelled slightly during irradiation, while the other specimens shrank as much as 1.5%. The swelling was as much as 0.005 in. on specimens 3A and 5A and could account for much of the difficulty in removing the specimens from the H-327 graphite sleeve. As mentioned before, the central segment of the graphite sleeve was cut into three parts

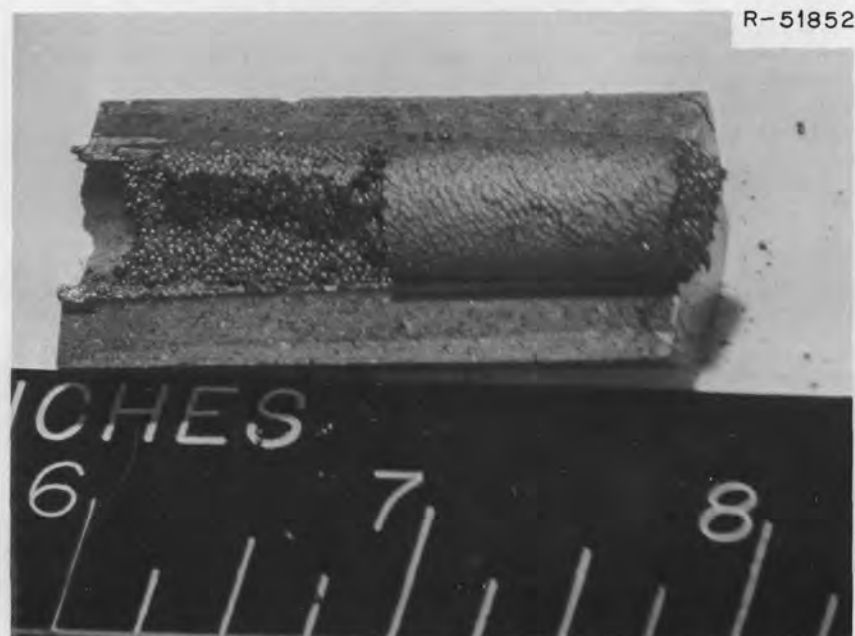


Fig. 1.10. Resin-bonded (left) and Varcum-bonded specimens after irradiation in HRBI to a fast fluence of 6×10^{21} neutrons/cm² ($E > 0.18$ MeV). Specimen 4b, on left, which was bonded with 15 wt % Asbury graphite in phenolic resin, crumbled and almost completely debonded; only small fragments could be recovered.

and finally split before all specimens could be removed. The shrinkage of matrix specimens S1 and S2 was equivalent to about 10% change in volume, which is much less than the 20 to 35 vol % shrinkage observed in specimens of resin-base matrix.⁶

The postirradiation analysis of the flux monitors from capsule HRB1 was completed, and the results were compared with the data from experiment HRB- γ -2. The

measured flux was lower than the calculated flux, and as a result the fast-fluence values and burnups were somewhat lower than predicted. Table 1.12 lists the HRB1 fuel stick specimens, the corresponding measured neutron fluxes, and the exposure doses and burnups based on these fluxes. The calculated fluxes had predicted a peak fast fluence (in fuel stick 5) of about 8×10^{21} neutrons/cm² ($E > 0.18$ MeV).

Table 1.11. Dimensional changes of bonded beds irradiated in experiment HRB1

Specimen ^a	Filler material		Type of binder	Change in dimensions (%)	
	Type	Amount (wt %)		Length	Diameter
2A	Asbury	15	Resin		1.5
3A	Poco AXM	40	Varcum	-3.5	+0.2 to 1.4
3B	Poco AXM	29	Varcum		+0.4 to 0.9
	Thermax	29			
S1 ^b	Poco AXM	40	Varcum	-0.3	-3.3
S2 ^b	Poco AXM	29	Varcum	-3.0	-4.1
	Thermax	29			
5A	Poco AXM	40	Varcum		+1.1 to +1.4
6B	Poco AXM	29	Varcum	-0.9	+0.6
	Thermax	29			
8A ^c	Poco AXM	29	Varcum	-1.7	-1.5
	Thermax	29			
8B ^c	Poco AXM	29	Varcum		-1.4
	Thermax	29			

^aAll specimens contained coated (Th,U)O₂ and ThO₂ particles unless otherwise noted.

^bMatrix specimen; no coated particles.

^cContained coated inert (ZrO₂) particles only.

Table 1.12. Capsule HRB1 measured fluxes and corresponding exposure doses and heavy-metal burnups

Fuel stick	Thermal flux ($E < 0.414$ eV) (10^{15} neutrons/cm ² ·sec)	Fast flux ($E > 0.18$ MeV) (10^{14} neutrons/cm ² ·sec)	Fast fluence ($E > 0.18$ MeV) (10^{21} neutrons/cm ²)	Fissile ^a particle burnup (%)	Fertile ^b particle burnup (%)
1	0.45	1.8	2.9	9.8	0
2A	0.57	2.2	3.4	10.2	3.8
2B	0.69	2.5	4.0	16.6	4.6
3	0.86	3.0	4.8	12.7	5.9
4A	1.02	3.3	5.3	13.8	7.1
4B	1.10	3.5	5.6	22.6	7.7
5	1.17	3.6	5.8	14.9	8.2
6	1.06	3.4	5.4	14.0	7.4

^aFissile particles contained (U,Th)O₂ or UO₂.

^bFertile particles contained ThO₂ only.

Metallographic examination of HRB1. Metallographic examination of six bonded-bed specimens from HRB-1 was completed. These specimens are described in Table 1.13.

The four Varcum-bonded specimens were intact and strong enough to handle and measure, while only fragments from the severely debonded resin-matrix specimens could be recovered for examination. In addition to the above specimens, samples 1A and 1C and the loose particles from holders D1 and D2 were examined. The results of all examinations to date are summarized in Table 1.14.

Some failures of coatings on UO_2 and $(\text{Th,U})\text{O}_2$ particles were observed in all specimens that contained these particles. Fracture and deformation of the outer isotropic pyrolytic-carbon coatings, shown in Fig. 1.11a, were typical of these failures. Most of the fissile particles were intact, however, as illustrated in Fig. 1.11b, and none exhibited broken SiC coating layers. Considerable swelling of the fuel and densification of

the buffer coating occurred as a result of the high burnup (~ 22 at. %) in the particle shown in Fig. 1.11a. However, no significant damage to the inner isotropic coating layer was observed.

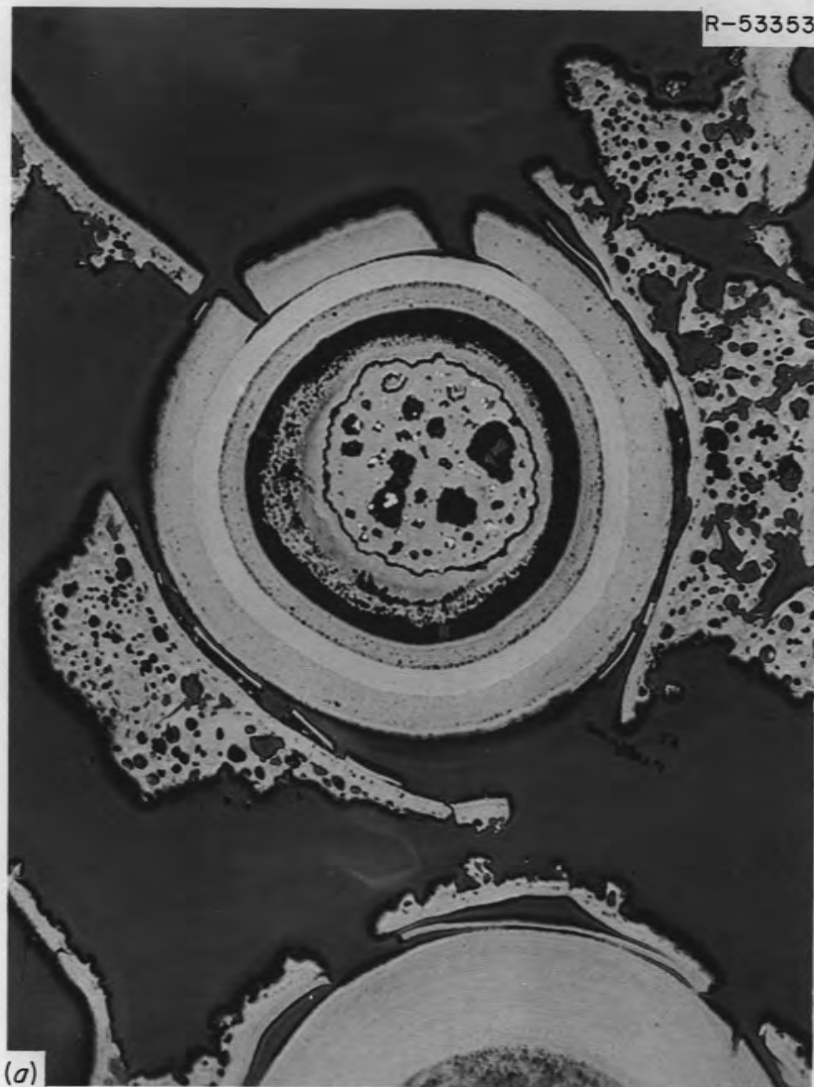
All coated ThO_2 particles were intact in all specimens except 2B, which was bonded with the resin-base matrix and irradiated at 1200°C to an exposure of 4.0×10^{21} neutrons/cm². In this specimen, 30% of the ThO_2 particles showed fractured outer carbon coatings and 10% had SiC layers that were cracked. An important observation about the performance of the outer coatings was the marked increase in anisotropy induced by the irradiation. This was observed on the coated fissile particles and on the ThO_2 particles, as illustrated in Fig. 1.12, but was even more evident on the Biso-coated inert ZrO_2 particles that were used in many specimens. This is illustrated by the polarized-light micrographs of unirradiated and irradiated particles shown in Fig. 1.13. A large fraction ($>75\%$) of

Table 1.13. Compositions of specimens examined after irradiation in HRB1

Experimental position	Specimen	Filler material		Binder type	Type of particles
		Type	Amount (wt %)		
3B	JF 30-10	Poco + Thermax	29:29	Varcum	$(\text{Th,U})\text{O}_2$, ThO_2 , ZrO_2
4B	JF 108-7	Asbury	15	Resin	UO_2 , ThO_2 , ZrO_2
5A	JF 30-14	Poco AXM	40	Varcum	$(\text{Th,U})\text{O}_2$, ThO_2 , ZrO_2
2B	JF 108-5	Asbury	15	Resin	UO_2 , ThO_2 , ZrO_2
6A	JF 30-16	Poco AXM	40	Varcum	$(\text{Th,U})\text{O}_2$, ThO_2 , ZrO_2
8A	JF 30-15	Poco + Thermax	29:29	Varcum	ZrO_2 only

Table 1.14. Summary of results obtained from metallographic examination of Triso-coated particles irradiated in experiment HRB1

Specimen	Fast fluence ($E > 0.18$ MeV) (10^{21} neutrons/cm ²)	Percentage of particles with broken outer coatings		
		ThO_2 (OR-1056)	$(\text{Th,U})\text{O}_2$ (YZ-233)	UO_2 (YZ-231)
1A	2.9		100	
D1	3.0	0	12	0
2B	4.0	30		76
3B	4.8	0	7	
D2	5.6	0	8	5
4B	5.6	0		60
5A	5.8	0	35	
6A	5.4	0	10	
8A	4.0			



(a)

(b)

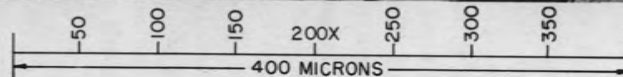
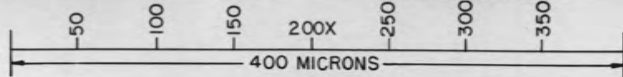
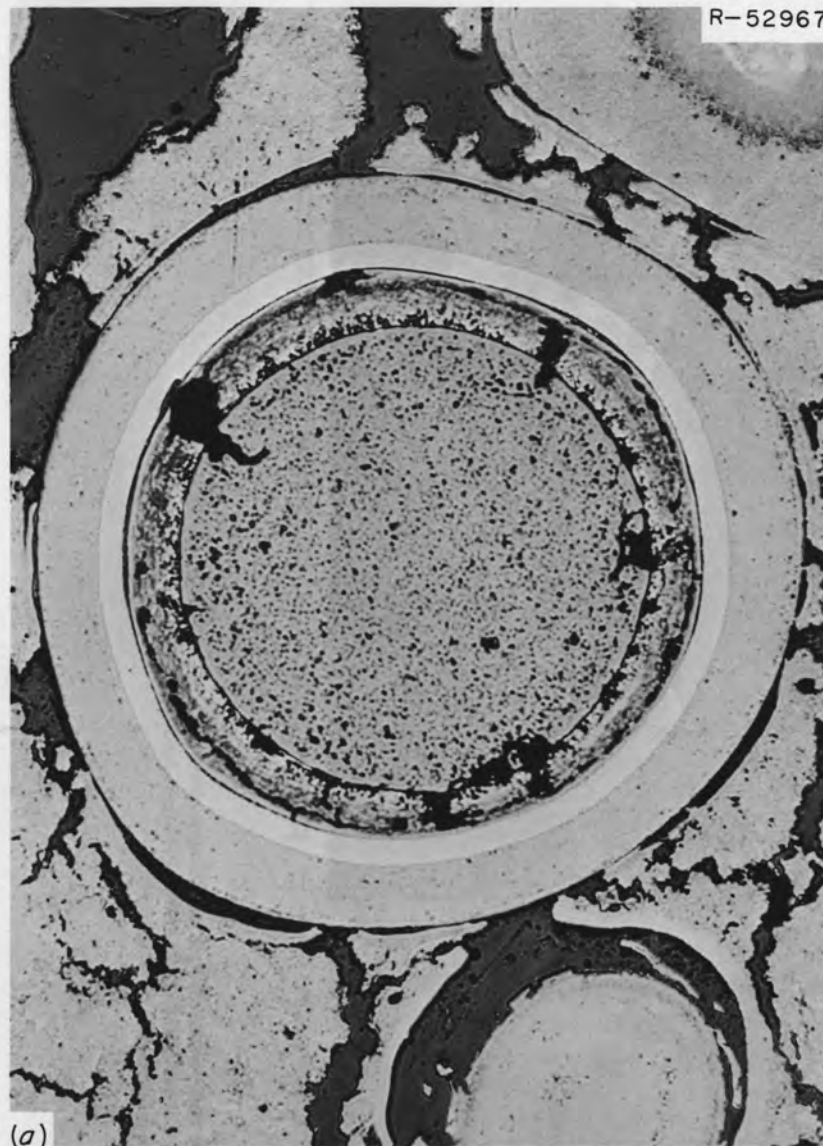


Fig. 1.11. Polished sections of Triso-coated fuel particles irradiated to a fast fluence of approximately 5.8×10^{21} neutrons/cm² ($E > 0.18$ MeV). (a) Triso-coated UO₂ particle after 22 at. % burnup. (b) Triso-coated (Th,U)O₂ particles after 15 at. % burnup. As polished. 200X.



R-52967

(a)

0.018 INCHES
15 15 200X 15 15

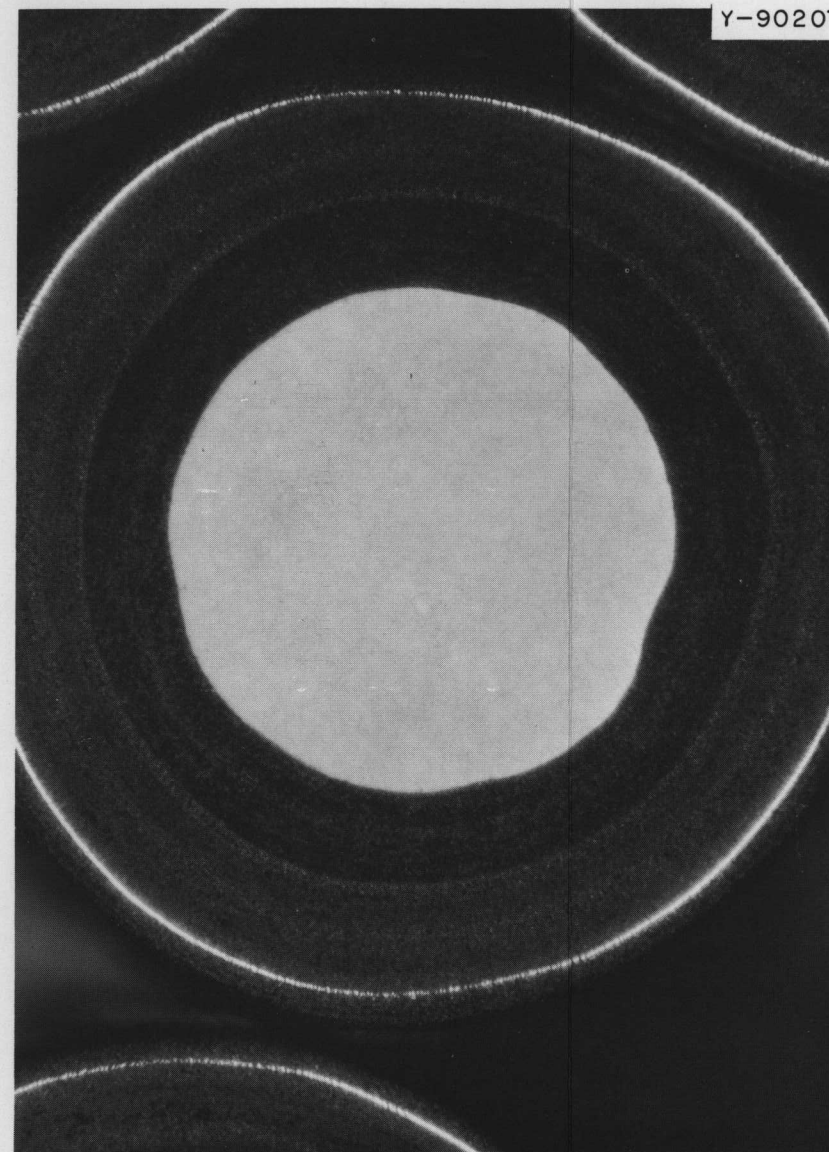


R-52973

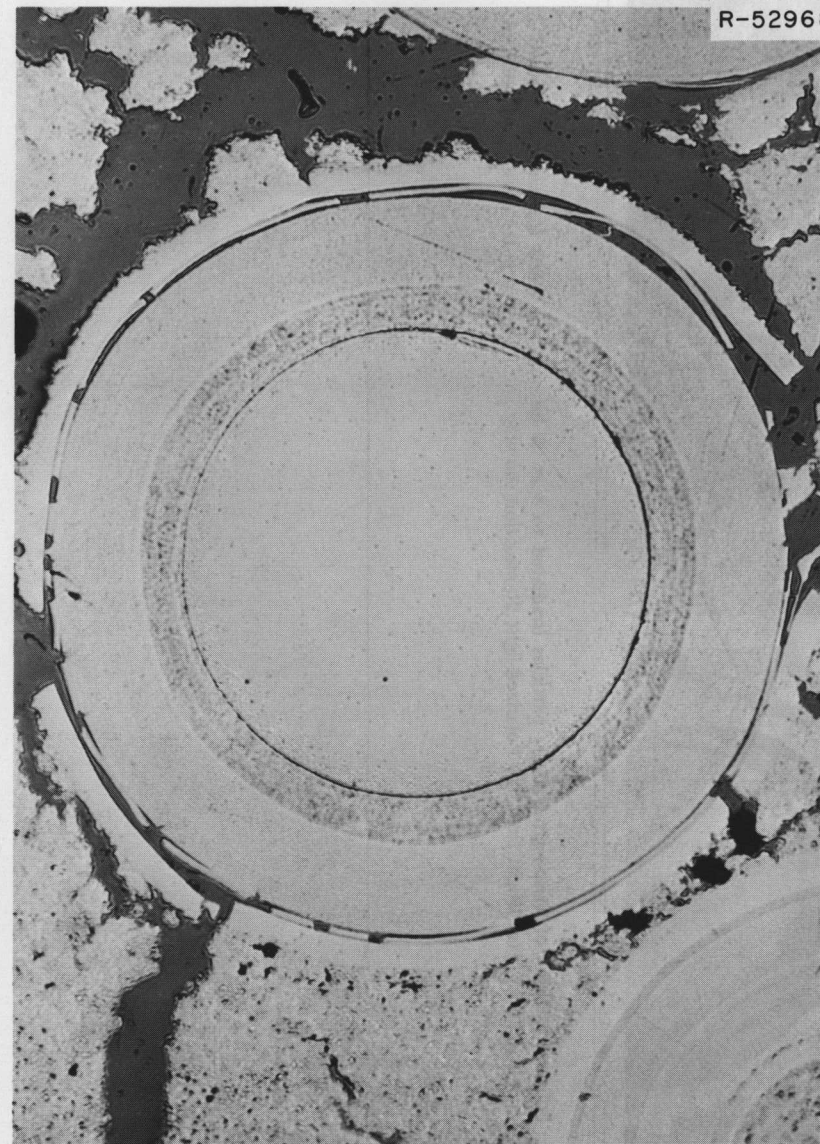
(b)

0.018 INCHES
15 15 200X 15 15

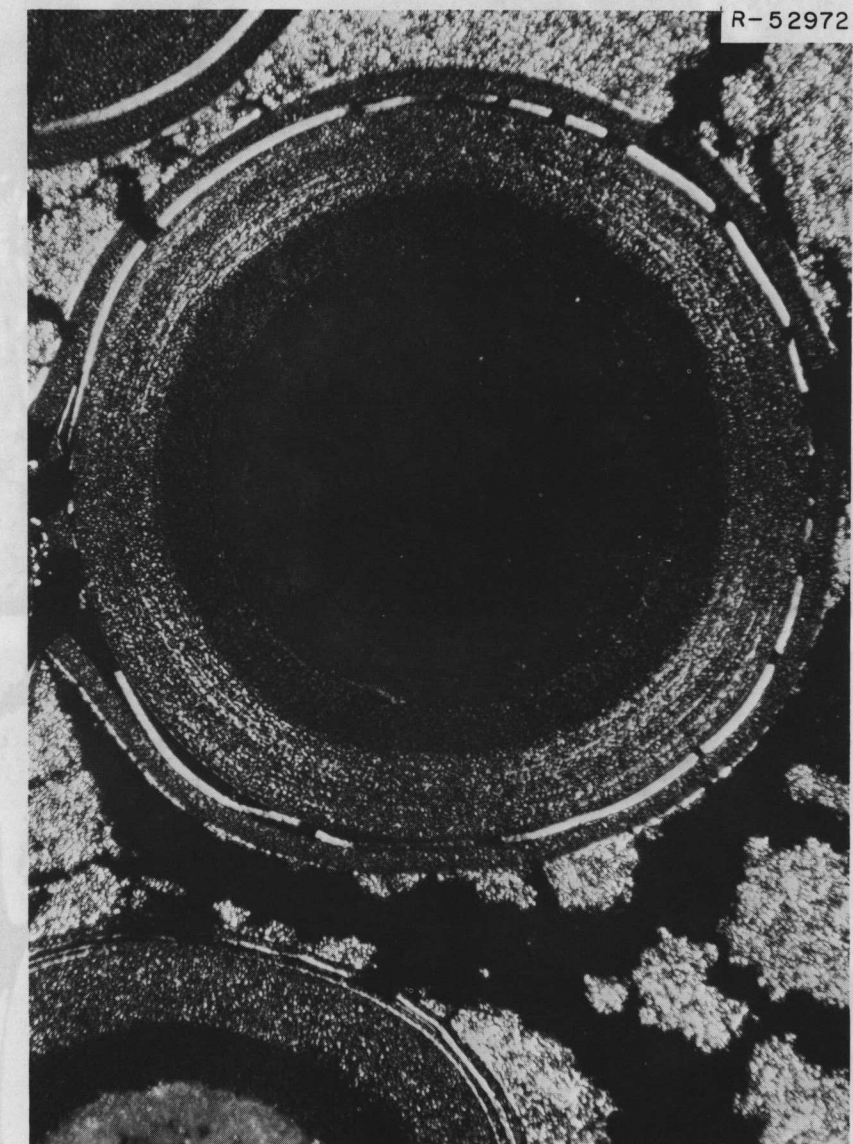
Fig. 1.12. Polished sections of Triso-coated ThO_2 particles irradiated to 8 at. % burnup and a fast fluence of 5.8×10^{21} neutrons/cm² ($E > 0.18$ MeV). (a) Bright field. (b) Polarized-light illumination showing anisotropy in outer coating. As polished. 200X.



(a)



(b)



(c)

Fig. 1.13. Polished sections of Biso-coated ZrO_2 particles. (a) Unirradiated specimen under polarized-light illumination showing no anisotropy in outer coating. (b) Specimen irradiated to a fast fluence of 5.8×10^{21} neutrons/cm² ($E > 0.18$ MeV); bright-field illumination. (c) Irradiated specimen under polarized light showing distinct and significant anisotropy in coating.

these inert particles failed in specimens that received exposures of 5×10^{21} neutrons/cm² or greater.

The behavior of the sacrificial and nonbonding layers on all particles was also significant. The isotropic sacrificial layer bonded tightly to the matrix carbon and pulled away from the nonbonding layer. On the other hand, the anisotropic nonbonding layer generally remained bonded to the Biso coating but broke into short segments due to the severe shrinkage induced by the fast-neutron damage. These effects are well illustrated in Figs. 1.11, 1.12, and 1.13.

The integrity of the matrix was mentioned above while describing the condition of the various specimens after irradiation. The microstructure of fragments of the resin-base matrix that contained 15 wt % natural flake graphite filler is shown in Fig. 1.11a. Shrinkage of this matrix was so severe that the specimen debonded almost completely. Specimens bonded with the Varcum-base matrix that contained 40 wt % Poco graphite were intact, and the structure of this matrix is illustrated in Figs. 1.11b, 1.12, and 1.14. While some shrinkage occurred and produced additional cracking of the matrix, specimens bonded with this matrix were in good condition. Typical fractures induced in the Biso coatings on a large fraction of the inert particles are shown in Fig. 1.14.

Discussion and conclusions. The good performance of outer coatings on ThO₂ particles and the fracture of outer coatings on some fissile particles are consistent with the properties of these coatings. All were quite isotropic in the as-deposited condition, but the density of outer layers on the two fissile particle batches was low — 1.78 and 1.80 g/cm³. In these coatings considerable shrinkage would occur early in the experiment that would induce significant anisotropy, and continued exposure would then lead to fracture. The outer coatings on the ThO₂ particles had a somewhat higher density, 1.88 g/cm³, and would therefore shrink less as densification occurred. It is notable that a detectable degree of anisotropy was induced in the outer coatings on the ThO₂ particles, even though they performed well. The fracture of some outer coatings on these particles in specimen 2B can be attributed to the interaction of the resin-base matrix and nonbonding layers with the outer carbon coating.

On the other hand, the excellent performance of SiC-coating layers on all particles is very encouraging. Even in those cases where a large fraction of the outer carbon coatings failed the SiC layer was intact, indicating that some possibility exists for the use of Triso coatings without the outer pyrolytic-carbon layer.

From the results of examinations and the foregoing discussion several tentative conclusions may be stated:

1. The Varcum-bonded matrix containing either Poco graphite or Poco plus Thermax filler materials will remain intact after irradiation to a fast fluence of 6×10^{21} neutrons/cm². However, resin-bonded matrices containing only 15 wt % graphite filler will completely debond during this exposure.

2. The swelling observed in diametral measurements of some specimens can be attributed to the fracture and subsequent deformation of coatings on a large fraction of the inert ZrO₂ particles used in the experiment.

3. The fracture of some outer coatings on both types of fueled particles can be attributed to increases in anisotropy induced by fast-neutron damage. The outer coatings on the ThO₂ particles were higher in density and would therefore be more stable, and very few of these particles showed fractured coatings.

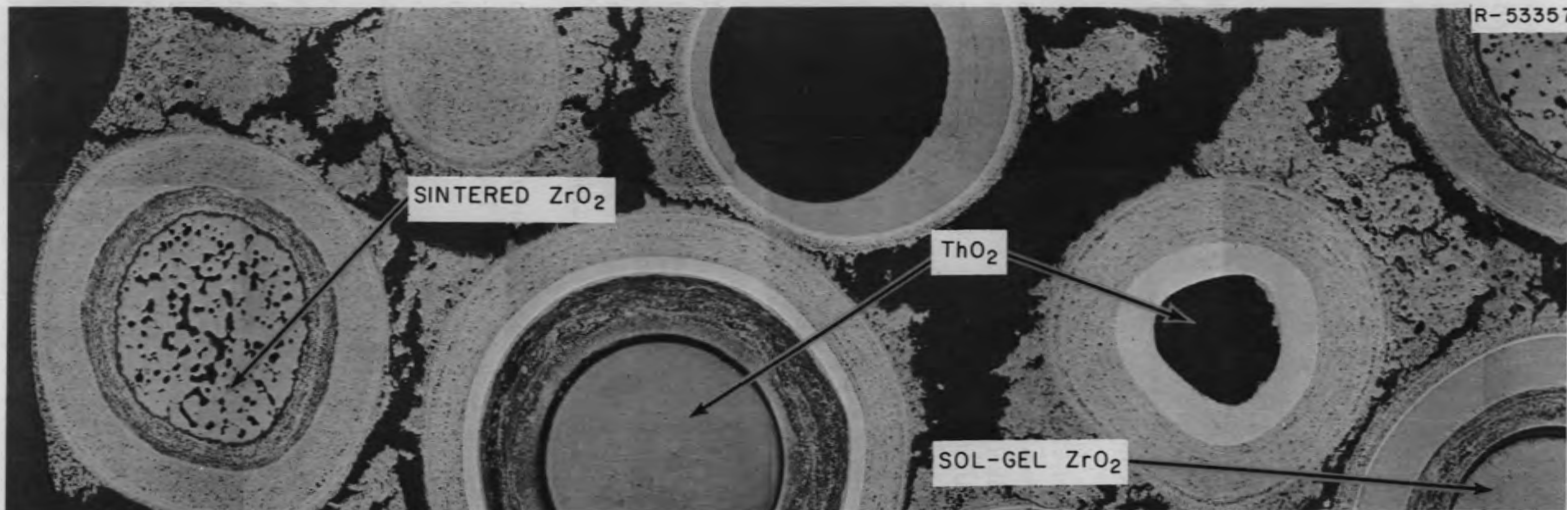
4. The good performance of the SiC coating layers indicates that the coated particles were adequately designed for the fuel burnup achieved in this experiment and that some possibility exists for the use of such particles without the outer pyrolytic-carbon layers.

5. The failure of outer coatings was highest in the two resin-bonded specimens, 4B and 2B, and was lowest in the samples of loose particles tested in holders D1 and D2. However, the sacrificial coating layers were broken and deformed even on the loose particles and probably contributed to stressing of the coatings in all specimens. These observations indicate that the resin-base matrix and the sacrificial and nonbonding layers are both detrimental to the successful performance of coated particles.

6. In only one specimen, 2B, were any particles with failed SiC coating layers found. The slight but significant increase in fission-gas release after about 120 days of irradiation is consistent with this result; that is, the failure of 10% of the SiC coatings on the ThO₂ particles in only one of the five specimens examined.

HRB2. The second of the removable beryllium capsules, HRB2, has been designed, and assembly is nearly complete. The capsule is identical to the first capsule, HRB1, but the test element differs in that the temperature-instrumented graphite sleeve that holds the bonded-bed specimens is in one piece and is made of Poco graphite, while the sleeve in HRB1 was comprised of three pieces of H-327 graphite.

The graphite sleeve will contain 15 in. of bonded beds, together with small batches of loose particles in graphite holders. No attempt has been made to adjust



UNIRRADIATED

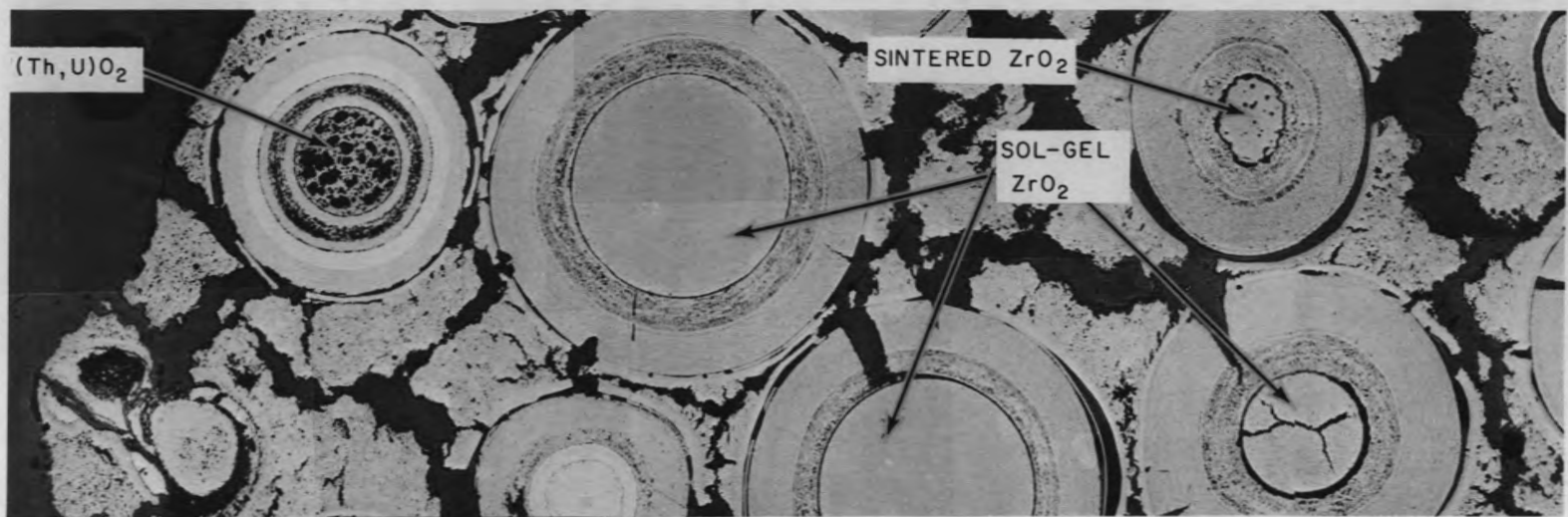
IRRADIATED AT 1150°C TO FLUENCE OF 6×10^{21} NEUTRONS/cm² ($E > 0.18$ MeV)

Fig. 1.14. Typical appearance of unirradiated and irradiated specimens of HTGR fuel particles bonded with Varcum containing 40 wt % Poco AXM graphite. Note severe cracking of matrix and sacrificial coating layers and the mode of failure of the coated inert ZrO₂ particles.

the fuel loading to compensate for the axial variation in neutron flux. Instead the graphite sleeve is tapered axially to compensate for the axial flux gradient and thus provide approximately uniform temperatures along the length of the fuel. The design peak fuel temperature is 1180°C. The types of fuel stick specimens prepared for this experiment are described in Section 1.2 of this chapter. In addition to the ORNL specimens, pre-production samples of Fort St. Vrain coated particles and fuel rods are being prepared by Gulf General Atomic for testing in HRB2. The irradiation is scheduled to begin early in December. The expected fast fluence at the midplane will be approximately 8×10^{21} neutrons/cm² ($E > 0.18$ MeV).

1.3.3 Irradiation experiments at DFR – Experiment DN-5

The three niobium capsules containing ORNL specimens¹⁰ irradiated in experiment DN-5 (DFR 287/6) were returned to ORNL from KFA, Jülich, after irradiation for 55 days in row 10 of DFR. The capsules were opened without difficulty, and the graphite magazines were recovered and inspected. Magazine 13 was stuck to the molybdenum foil that separated it from the niobium can, although all metal surfaces were

bright. This capsule was designed to operate at the highest temperature, 1250°C; apparently superficial bonding occurred. The SiC temperature monitors from each magazine were packaged and returned to Dounreay for analysis, as requested by KFA.

The magazines were then dismantled and all specimens were recovered. The threads were broken in one-half of magazine 7 during disassembly, but no specimens were damaged. The graphite disks containing loose particles and the disk specimens of matrix material were recovered and stored for later examination. The bonded beds of Biso-coated ThO₂ particles were photographed, weighed, measured, and retained for metallographic examination. These specimens were bonded with matrices consisting of pitch containing 40 wt % Poco graphite or Varcum containing 29 wt % Poco graphite and 29 wt % Thermax. All specimens were intact, but the pitch-bonded specimens had fewer cracks and suffered only slight weight loss (0.3 to 1.6%). The Varcum-bonded specimens debonded slightly on the edges and showed weight losses of 1.7 to 3.8%. All specimens shrank about to the extent expected; diametral changes ranged from -2.0 to -2.9%; and length changes varied from -2.3 to -3.3%. Shrinkage of the pitch-bonded specimens was more consistent than that of the Varcum-bonded specimens, but otherwise the behaviors were quite similar. The irradiation conditions and dimensional changes are summarized for all bonded specimens in Table 1.15. Specimen 7A, which was outgassed at 1500°C before irradiation, will be the first examined metallographically.

10. J. M. Robbins and D. M. Hewette, "Coated Particle Bonding Development for HTGR Fuels," pp. 3-8, *Gas-Cooled Reactor Program Semiann. Progr. Rept. Sept. 30, 1969*, USAEC Report ORNL-4508, Oak Ridge National Laboratory.

Table 1.15. Properties and dimensional changes of bonded coated-particle beds irradiated in experiment DN-5

Experiment position	Binder	Filler		Preirradiation heat treatment temperature (°C)	Design conditions for irradiation		Average dimensional change (%)	
		Type	Amount (wt %)		Temperature (°C)	Fast fluence ($E > 0.18$ MeV) (10^{21} neutrons/cm ²)	Diameter	Length
13A	15V pitch	Poco AXM	40	2100	1250	8.0	-2.2	-2.9
7A	15V pitch	Poco AXM	40	1500	1150	7.8	-2.1	-3.3
4A	15V pitch	Poco AXM	40	1500	830	5.6	-2.1	-2.9
13B	Varcum	Poco and Thermax	29 + 29	2100	1250	8.0	-2.9	-2.3
7B	Varcum	Poco and Thermax	29 + 29	1500	1150	7.8	-2.8	-3.1
4B	Varcum	Poco and Thermax	29 + 29	1500	830	5.6	-2.2	-3.3

2. Fission-Product Release and Transport Studies

O. Sisman M. D. Silverman

2.1 Fission-Product Release from High-Burnup Coated Fuel Particles by Postirradiation Anneals

C. D. Baumann M. T. Morgan
R. L. Towns

2.1.1 Fission-product release from coated fuel particles in a bonded bed during postirradiation anneals

Two bonded-bed samples from capsule B9-41, which had been irradiated to 20% FIMA, were annealed to determine the retention of cesium and strontium by the coated particles and the matrix of the bonded bed. The bonded beds were 0.28 in. in diameter and 0.22 in. long, and each contained approximately 100 Bisocoated UO_2 particles from batch OR-1010. The bonded beds were contained in graphite cans and annealed in a purified helium atmosphere in a resistance-heated tube furnace at 1250°C . The helium stream was continuously monitored for ^{85}Kr , since its appearance would indicate coating failures. No ^{85}Kr was noted during the anneals.

The first sample, B-51, was annealed for 2500 hr, and the furnace tube was periodically analyzed for ^{137}Cs . The cesium release versus annealing time is plotted in Fig. 2.1. Cesium and its compounds are highly volatile at 1250°C , and holdup in porous media is slight at this temperature. During short postirradiation annealing experiments on cracked coated UO_2 particles, only 2% of the cesium released remained on the graphite crucibles at 1000°C , and less than 1% remained at 1300°C .^{1,2} During in-reactor experiments at 1250°C , 81 to 92% of the cesium released from coated particles was collected outside the massive graphite holder, which had a temperature gradient across it of 250°C .³

A diffusion coefficient was calculated from the following relation⁴ by assuming that the holdup of

cesium would be negligible in this bonded-bed experiment and that the only deterrent to cesium escape was the outer pyrolytic-carbon coating of the coated UO_2 particles:

$$D = 0.166L^2/t,$$

where

D = diffusion coefficient, cm^2/sec ,

L = thickness of pyrolytic-carbon coating, cm,

t = delay time, sec (taken from intercept on graph).

The diffusion coefficient based on Fig. 2.1 was $5.0 \times 10^{-12} \text{ cm}^2/\text{sec}$. The total cesium release at 1000 hr was 8.3%, which is high compared with results from an in-pile experiment on similar coated particles, which released 3% of the cesium in approximately 1000 hr during irradiation at 1250°C .²

1. M. T. Morgan and R. L. Towns, "Fission-Product Release from High-Burnup Coated Fuel Particles by Postirradiation Annealing," pp. 89-90, *GCRP Semiann. Progr. Rept. Mar. 31, 1967*, USAEC Report ORNL-4133, Oak Ridge National Laboratory.

2. M. T. Morgan, J. G. Morgan, and R. L. Towns, "Cesium Release from Coated Fuel Particles During Postirradiation Anneals," pp. 53-55, *GCRP Semiann. Progr. Rept. Mar. 31, 1969*, USAEC Report ORNL-4424, Oak Ridge National Laboratory.

3. P. E. Reagan, J. G. Morgan, and O. Sisman, "Solid Fission-Product Release from Coated Particle Fuels During Irradiation," pp. 38-42, *GCRP Semiann. Progr. Rept. Mar. 31, 1970*, USAEC Report ORNL-4589, Oak Ridge National Laboratory.

4. J. Crank, *Mathematics of Diffusion*, pp. 47-48, Clarendon Press, Oxford, England, 1956.

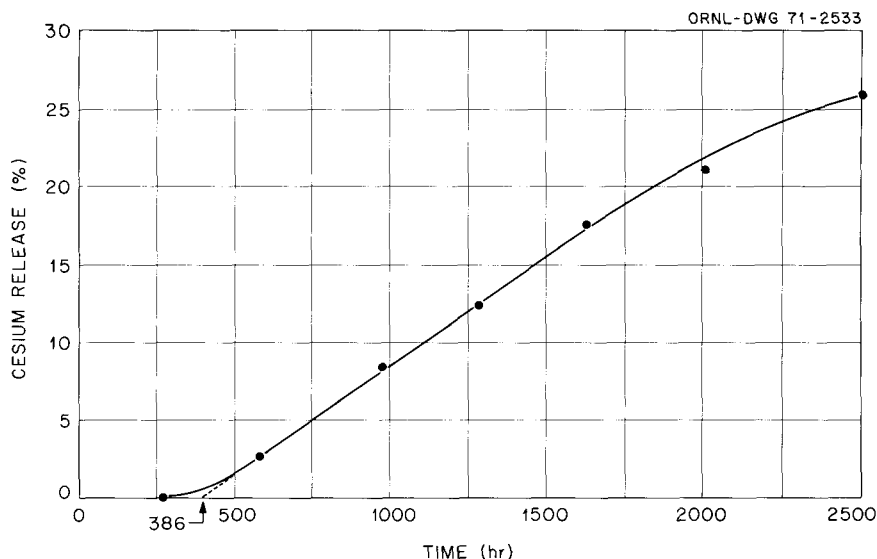


Fig. 2.1. Cesium release from bonded-bed sample B-51 during annealing at 1250°C.

A second identical bonded bed, B-50, was annealed at 1250°C to check the results for the B-51 sample. This anneal was terminated at 369 hr when a leak in the system introduced air into the helium stream. The cesium release at 369 hr was 6%, or a factor of 10 higher than the release from the B-51 sample at the same annealing time.

The graphite cans containing the B-50 and the B-51 samples were wrapped in tantalum foil. The tantalum took up most of the oxygen in the helium stream during the anneals. Postannealing examinations of the tantalum showed some evidence of corrosion in both samples; however, of the graphite components, only the graphite cap of sample B-50 appeared to be pitted, and the bonded beds inside the graphite cans showed no evidence of attack, as illustrated in Fig. 2.2.

Bonded-bed samples B-50 and B-51 are being disintegrated by an electrolytic method with 2.5 M HNO₃. The strontium and cesium quantities in the coated fuel particles, the matrix, and the graphite can will be determined. Some of the coated fuel particles will be sectioned and polished for metallographic examination.

2.1.2 Diffusion of cesium in pyrolytic-carbon coatings

Capsule B9-42 contained bonded-bed samples identical to those in capsule B9-41 but was irradiated to only 10% FIMA. One of the graphite cans in both capsules contained loose coated particles (identical to those used in the bonded beds) packed in graphite

powder. Some of the loose Biso-coated UO₂ particles from batch OR-1010 were annealed to determine cesium diffusion coefficients in the pyrolytic-carbon coatings.

Three of these coated particles (those numbered 1, 3, and 4 in Table 2.1) were annealed separately at 1400°C, but since the results varied widely, a graphite crucible was fitted with five tungsten tubes arranged in a circle so that they could be heated together. The error in temperature measurements was estimated to be within 35°C, but the variation in temperatures across the graphite crucible (sighting into empty holes) was less

Table 2.1. Cesium release and diffusion coefficients obtained from Biso-coated particles annealed at 1400°C

Coated particle No.	Cesium release in 72 hr (%)	D (10^{-11} cm ² /sec)
1	0.5	2.6
2	2.6	12
3	4.6	7.0
4	6.2 ^a	6.5
5	7.2	8.4
6	15	12
7	17	13
8	32	

^aExtrapolated from cesium release at 42 hr.

PHOTO 100148

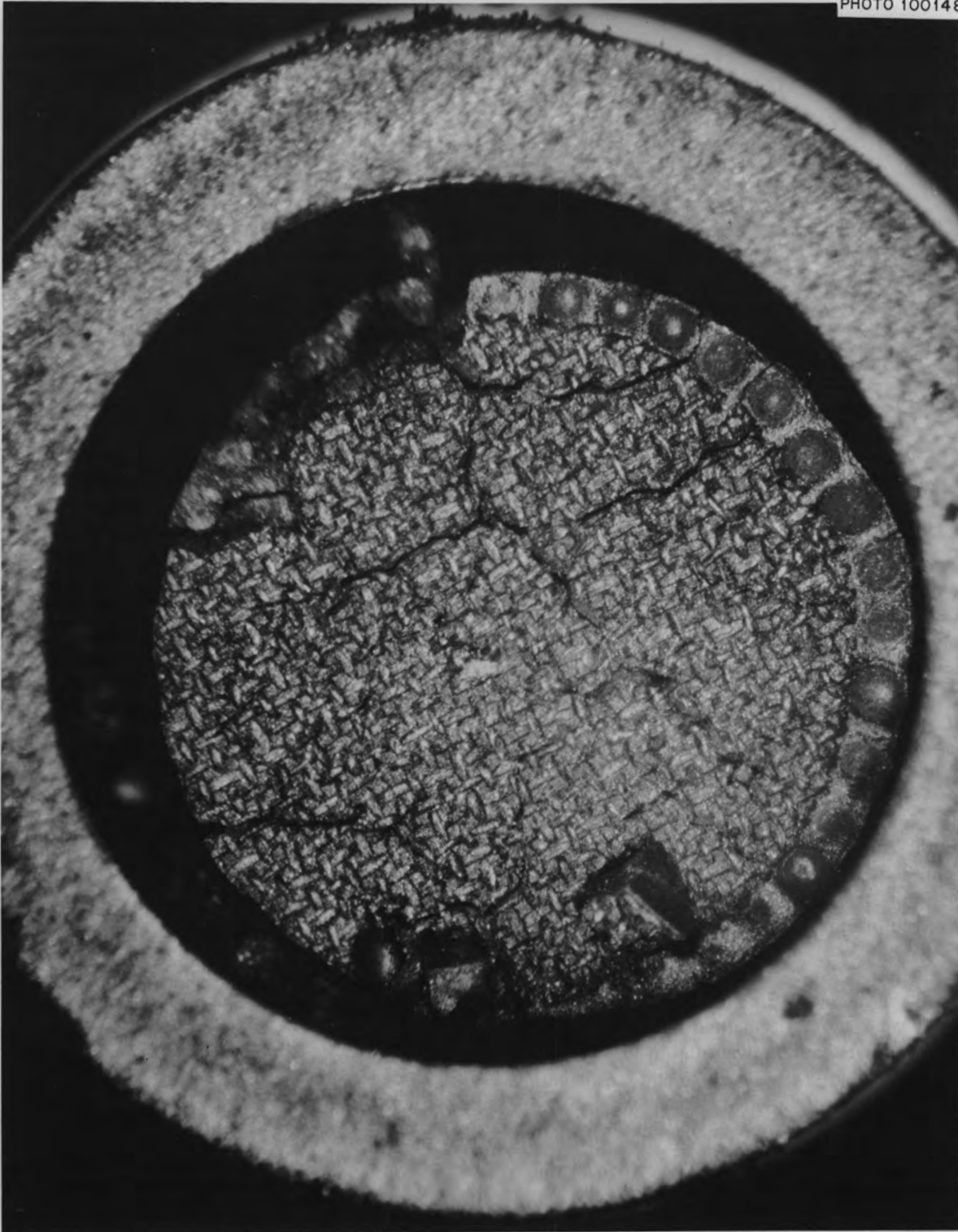


Fig. 2.2. Bonded-bed sample B-51 in graphite can. (The pattern is derived from a screen used to hold the bed of particles in place during bonding.)

than 10°C. The $\frac{1}{16}$ -in.-OD tungsten tubes were $4\frac{1}{2}$ in. long. This provided a sufficient cold zone above the crucible so that the cesium released by each coated particle would be deposited on the tube wall.

Five of the B9-42 Biso-coated particles (those numbered 2, 5–8 in Table 2.1) were annealed at 1400°C, one in each tungsten tube, and the tungsten tubes were analyzed for cesium periodically to obtain the cesium release as a function of time. Only the results from four of the particles were used to determine diffusion coefficients. The fifth (coated particle 8) had an exceptionally high total cesium release and did not provide a usable indication of cesium release versus time. Since there was no ^{85}Kr release during irradiation or annealing, it is presumed that the particle coatings remained intact. The total cesium release at 72 hr and the diffusion coefficients calculated from the delay times are given in Table 2.1. A graph of cesium release versus annealing time for one of the coated particles is shown in Fig. 2.3.

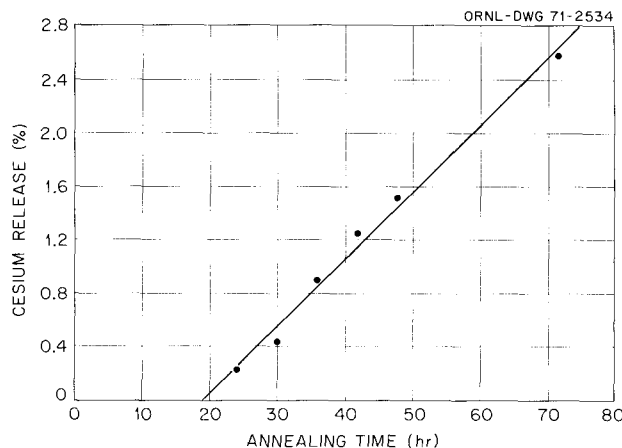


Fig. 2.3. Cesium release from Biso-coated UO_2 particle during postirradiation annealing at 1400°C.

2.1.3 Cesium release through Triso coatings at high temperatures

Triso-coated UO_2 particles from batch OR-818, irradiated to 20% FIMA in capsule B9-41, were annealed at high temperatures to measure cesium release and coating stability. A previous experiment proved that cesium was not released in 6 hr at 2000°C through Triso coatings, but over longer periods the coatings deteriorated and released cesium and other fission

products but not the noble gases. Since pyrolytic-carbon coatings at high temperatures do not retain cesium, barium, strontium, and other solid fission products but do retain the gases and iodine, the loss of solid fission products through Triso coatings during high-temperature anneals without the simultaneous loss of gaseous fission products indicates a breakdown of the SiC layer.

During several anneals of the Triso-coated particles at temperatures above 1800°C, cesium was released from some of the coated particles but not from others in the same sample. In one experiment, ten Triso-coated particles from B9-41 were heated in steps of 100°C from 1300 up to 2200°C and maintained at each temperature for 10 min. No ^{85}Kr was released, so no coatings failed catastrophically, but appreciable cesium was released from eight of the ten coated particles. The coated particles were radiographed and then sectioned and polished for metallographic examination.³ The photomicrographs showed no cracks in the SiC layers of the two coated particles that did not release appreciable cesium, while all the others were cracked. Since cracking of the SiC layers can occur as a result of polishing, more evidence was desired. The outer pyrolytic-carbon coating was burned off some coated particles, which released cesium to expose the SiC layer, and these coatings were examined under the optical microscope. No cracks were apparent. Fragments of the SiC from some of the same coated particles were then examined under the electron microscope.³ One micrograph showed what appeared to be porosity associated with the fractured surface of an SiC coating fragment from a coated particle annealed at 2000°C for 11 hr (this coating released approximately 50% of the cesium). Subsequent micrographs of SiC fragments from other coated particles in the same sample did not indicate porosity.

Intact irradiated coated fuel particles cannot be examined under the scanning electron microscope because of the radioactivity; however, replicas of a large fraction of the exposed SiC coatings of four coated particles that released cesium were examined under the scanning electron microscope at magnifications up to 5000X, and no evidence of cracks was found at this time. Examples of the details shown in these micrographs may be seen in Figs. 2.4 and 2.5. Figure 2.4 is a micrograph of a replica of a hemisphere of an SiC coating at a magnification of 500X. The other half of this coated particle was buried in the mount and was not examined. The fine detail at a magnification of 5000X is apparent in Fig. 2.5. The surface of the SiC is



Fig. 2.4. Scanning electron micrograph of surface of SiC coating from coated UO_2 particle that released cesium. 500X.

similar to an orange peel. The ridge in Fig. 2.5 on the replica represents a valley on the surface of the SiC.

2.1.4 Failure model analysis of irradiated Triso-coated particles (C. D. Baumann, H. C. Roland⁵)

The Walther "Stress-2" computer code⁶ was used to analyze the failure of irradiated OR-818 coated fuel particles as indicated by ^{137}Cs release during postirradiation anneals. The fully enriched UO_2 kernels were coated with a low-density buffer layer, a thin high-density pyrolytic-carbon sealing layer, an SiC layer, and a high-density outer pyrolytic-carbon coating. The coated particles were irradiated in the ORR B9-41 experiment at 630°C to a burnup of 20% FIMA at a

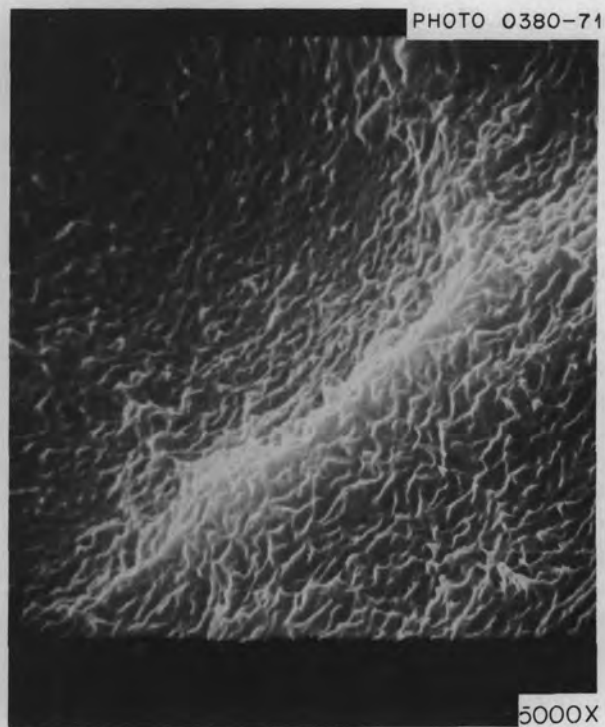


Fig. 2.5. Scanning electron micrograph of surface of SiC coating from coated UO_2 particle that released cesium. 5000X.

fast-neutron (>0.18 MeV) fluence of 2.38×10^{20} neutrons/cm². Ten coated particles were then annealed for 10 min at 100°C intervals from 1300 to 2200°C . The ^{95}Zr and ^{137}Cs activities of each coated particle were measured after the anneal. X-ray radiographs and metallographic micrographs were made, and from these the average dimensions of the components of each coated particle were obtained.

The Walther "Stress-2" code for calculating the in-pile performance of a coated particle was modified for use on the ORNL computers. The values of the tangential rupture stress for the sealing layer, SiC, and outer pyrolytic-carbon coating were adjusted until the code gave a reasonable description of the performance of the particles as indicated by the ^{137}Cs release fraction. Table 2.2 lists the results of the calculations when the rupture stresses of the sealing layer, SiC, and outer pyrolytic-carbon coating were 45,000, 160,000, and 50,000 psi, respectively. While these results are not exactly replicative of the particle performance as indicated by ^{137}Cs release, they are qualitatively correct. There are, however, probably other combinations of different values of the rupture stresses that

5. Consultant, University of Tennessee.

6. H. Walther, *A Model for Stress Analysis in Coated Fuel Particles*, Dragon Project Report 604 (August 1968) and Dragon Project Report 683 (October 1969).

Table 2.2. Failure model analysis of irradiated OR-818 Triso-coated particles^a

Particle No.	¹³⁷ Cs Release (%)	Annealing temperature at which sealing layer breaks (°C)	Burnup at which SiC layer breaks (%)	Annealing temperature at which outer coating breaks (°C)	Ratio of core volume to buffer volume
1	<1	No break	No break	No break	0.54
2	<1	No break	No break	No break	0.60
3	47	No break	19.6	No break	0.94
4	43	No break	18.9	No break	0.98
5	45	No break	19.1	No break	1.03
6	45	2000	17.0	No break	1.13
7	50	1900	17.3	No break	1.13
8	58	2000	17.1	No break	1.16
9	59	2000	16.8	No break	1.20
10	64	1500	16.3	2000	1.25

^aAssumed rupture stresses: sealing layer, 45,000 psi; SiC, 160,000 psi; outer coating, 50,000 psi.

would describe the performance just as well or perhaps better. Additional trial and error calculations will be made to determine better combinations of rupture stresses, but the successful description of many more than ten particles would probably be required before any unique set of rupture stresses could be considered valid.

It was found that a rather simple geometric parameter, the ratio of the core volume to buffer volume (which roughly corresponds to the internal gas pressure), results in a surprisingly good qualitative description of particle performance, as indicated in Fig. 2.6. Apparently the reason for this is that the effect of the variation in the thickness of the SiC and outer pyrolytic-carbon coatings was much less than the effect of variation in the core-to-buffer volume ratio.

2.2 Fission-Product Transport and Deposition

M. D. Silverman M. N. Özişik⁷
G. E. Mills

Cesium transport and deposition studies continued in the fission-product deposition loop (FPD), and experiment C-5A was completed during this reporting period. In addition, a number of modifications to the loop were made during the past several months.

The changes in the loop proper are discussed below; Fig. 2.7 shows the schematic diagram of the loop before

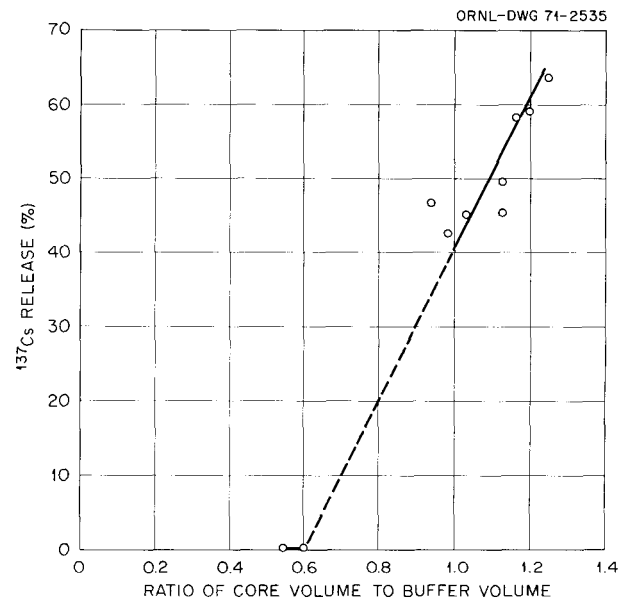


Fig. 2.6. ¹³⁷Cs release versus ratio of core volume to buffer volume.

the changes and Fig. 2.8 shows it after the modifications.

1. The filter trap upstream of the cesium injector, which contained the uranium turnings used for gas cleanup, along with a sintered-metal filter to trap any uranium dust, was removed and placed downstream of the deposition test section. Relocation of this large flanged trap, along with removal of the flange just

7. Consultant to the Reactor Division, Oak Ridge National Laboratory, from North Carolina State University, Raleigh.

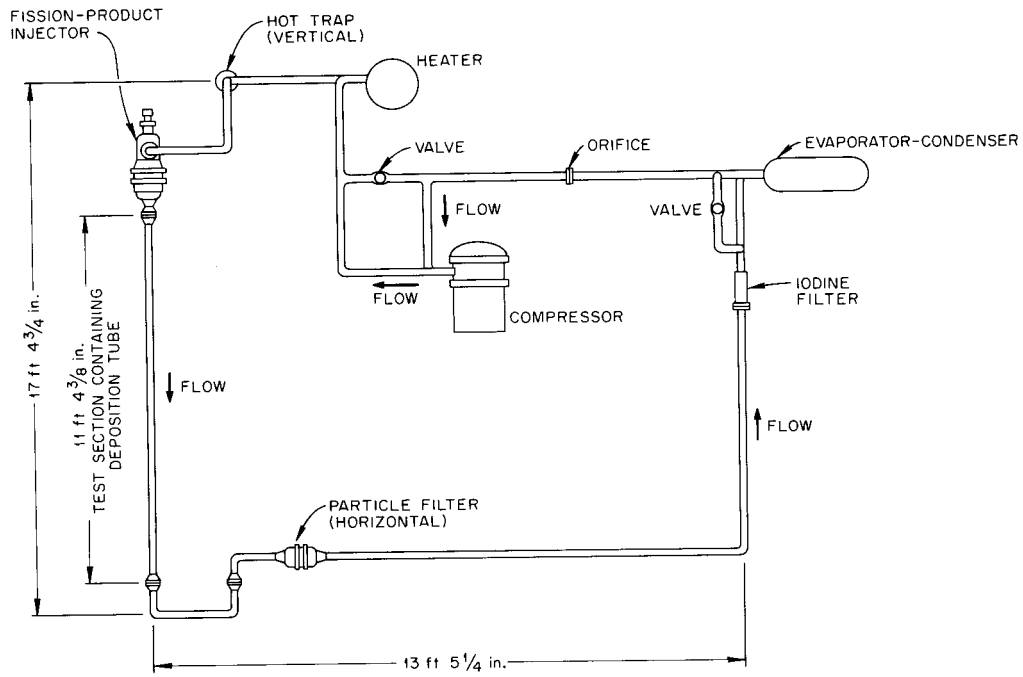


Fig. 2.7. Schematic diagram of FPD loop piping and components before rearrangement.

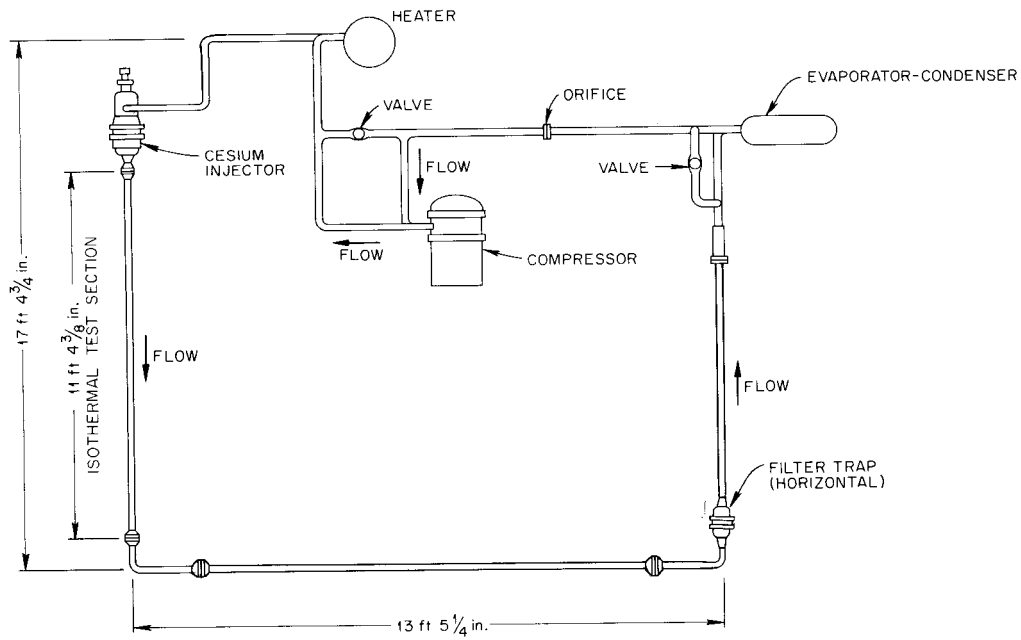


Fig. 2.8. Schematic diagram of FPD loop piping and components after rearrangement.

upstream of the cesium injector, should result in decreased maintenance.

2. The filter trap was installed at a new position to eliminate the second large flange (which contained a second sintered-metal filter for cesium trapping) in the dog-leg after the isothermal deposition test section. Elimination of this sintered-metal filter should cut down on pressure drop in the loop and consequently decrease the load on the compressor. The remaining filter will serve to trap both uranium dust and cesium metal.

3. The heater bundle was installed directly ahead of the cesium injector. This rearrangement should decrease heat losses previously encountered in this region.

4. The dog-leg after the isothermal test section was eliminated, and approximately 10 ft of straight run pipe was installed to serve as a nonisothermal deposition test section. Heat transfer calculations indicate that a temperature drop of about 200°C should be obtainable along this section.

Previous reports⁸⁻¹² have presented detailed descriptions of the loop and its components. To summarize, cesium is released from a quartz capsule and allowed to diffuse through static helium down a molybdenum tube to which is brazed a graphite section that acts as an evaporator. The metallic cesium vapor, which moves through the evaporator into turbulently flowing helium, deposits downstream on a test deposition tube monitored by a traveling sodium iodide crystal counter and on other metallic surfaces in the loop. Chemical and radiochemical analyses are made at the end of each experiment to determine cesium concentrations for the appropriate portions of the loop and its components.

8. M. D. Silverman and F. H. Neill, "Fission-Product Deposition Loop," pp. 69-73, *GCRP Semiann. Progr. Rept. Sept. 30, 1968*, USAEC Report ORNL-4353, Oak Ridge National Laboratory.

9. D. L. Gray and F. H. Neill, *Design Report for Fission-Product Deposition Tests up to 1500°F*, USAEC Report ORNL-TM-2532, Oak Ridge National Laboratory, June 1969.

10. M. D. Silverman and F. H. Neill, "Fission-Product Transport and Deposition," pp. 55-58, *GCRP Semiann. Progr. Rept. Mar. 31, 1969*, USAEC Report ORNL-4424, Oak Ridge National Laboratory.

11. M. D. Silverman, F. H. Neill, and G. E. Mills, "Fission-Product Transport and Deposition," pp. 42-49, *GCRP Semiann. Progr. Rept. Sept. 30, 1969*, USAEC Report ORNL-4508, Oak Ridge National Laboratory.

12. M. D. Silverman and G. E. Mills, "Fission-Product Transport and Deposition," pp. 50-56, *GCRP Semiann. Progr. Rept. Mar. 31, 1970*, USAEC Report ORNL-4589, Oak Ridge National Laboratory.

Five experiments have been completed. Except for the initial test, in which difficulties were encountered with uniform inductive heating of the graphite and poor placement of a graphite guide bracket in the molybdenum tube (which soaked up cesium vapor and thereby limited vaporization of the metal), the experimental results have correlated with a model based on the transverse flow of helium resulting from pressure differentials. No reference to this specific problem could be found in the literature; however, experiments have been reported on the determination of the permeability of graphite to a variety of gases.¹³⁻¹⁵

The model is based on fully developed turbulent flow over a graphite tube in which a fission product is released at a steady rate, as illustrated in Fig. 2.9, where P_o is the gas pressure outside the tube, P_i is the pressure inside the tube, P_1 is P_o evaluated at the gas inlet, and P_2 is P_o evaluated at the gas outlet. Since graphite is porous, differences between the pressures inside and outside the tube give rise to a complex flow pattern from the outer region into the graphite tube and back outside, and thus some fission products are carried into the outer stream.

13. R. B. Evans III, J. Truitt, and G. M. Watson, *J. Chem. Eng. Data*, 6: 522 (1961); also, *Superposition of Forced and Diffusive Flow in a Large-Pore Graphite*, USAEC Report ORNL-3067, Oak Ridge National Laboratory, 1961.

14. R. B. Evans III, G. M. Watson, and E. A. Mason, "Gaseous Diffusion in Porous Media, II. Effects of Pressure Gradient," *J. Chem. Phys.*, 35: 1894 (1962).

15. G. F. Hewitt, M. J. C. Moore, and E. W. Sharratt, *The Permeability of Nuclear Grade Graphite to a Variety of Gases*, British Report AERE-R-3994, 1966.

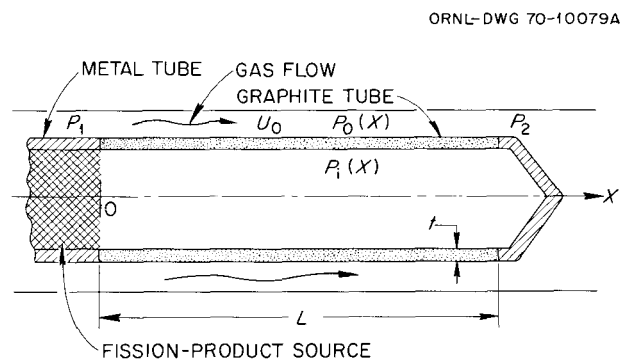


Fig. 2.9. Flow over a porous tube with an internal source.

The frictional pressure gradient for turbulent flow outside the graphite tube is

$$-\frac{dP_o(x)}{dx} = f \frac{\rho U_o^2}{2gd_{eo}} \equiv F, \quad (1)$$

where f is the frictional factor, ρ the density of the gas, U_o the velocity of the gas on the outside of the graphite tube, g the gravitational constant, and d_{eo} the equivalent diameter for gas flow (annulus).

The flow inside the graphite tube also gives rise to a pressure gradient in the axial direction; however, since internal flow is small, the resulting pressure drop inside is negligible compared with that on the outside. Therefore it is assumed that

$$\frac{dP_i(x)}{dx} = 0. \quad (2)$$

Integration of Eq. (1) with the boundary condition $P_o(x) = P_1$ at $x = 0$ yields

$$P_o(x) = P_1 - Fx, \quad (3)$$

and integration of Eq. (2) gives

$$P_i = C = \text{Constant}. \quad (4)$$

The integration constant C is determined by using the conservation equation for the transverse flow of gas through the graphite. Application of Darcy's equation¹⁶ for purely viscous, isothermal flow of an ideal gas to the transverse flow through porous graphite gives

$$w_g(x) = K \frac{M}{RT\mu t} [P_o^2(x) - C^2]. \quad (5)$$

Here $w_g(x)$ is the transverse mass flow rate of gas per unit area of tube surface; M is the molecular weight of the gas; R is the gas constant; T is the absolute temperature; μ is the viscosity of the gas; t is the thickness of the septum; and the permeability constant K is usually determined experimentally for each type of porous medium.

Under steady-state conditions, conservation of mass for transverse flow through the graphite tube requires

that

$$\int_0^L w_g(x) dx = 0. \quad (6)$$

Substitution of Eq. (5) into Eq. (6) and integrating yields

$$C^2 = P_1^2 - P_1 FL + \frac{1}{3} F^2 L^2, \quad (7)$$

which establishes the pressure inside the graphite tube. The physical significance of Eq. (7) is envisioned better if it is expressed as

$$C^2 = \left(\frac{P_1 + P_2}{2} \right)^2 + \frac{1}{12} (P_1 - P_2)^2, \quad (8)$$

since

$$\frac{P_1 + P_2}{2} = P_1 - \frac{1}{2} FL,$$

$$P_1 - P_2 = FL.$$

For most reactor applications the second term on the right-hand side of Eq. (8) is negligible compared with the first term, so

$$C \cong \frac{1}{2} (P_1 + P_2). \quad (9)$$

This result implies that the transverse flow will enter the graphite tube in the region $0 \leq x < L/2$ and leave it in the region $L/2 < x \leq L$. Then the amount of transverse flow of gas into the graphite tube, W_g , is given by

$$W_g = \pi d \int_{x=0}^{L/2} w_g(x) dx, \quad (10)$$

where d is the diameter of the tube. Integrating gives

$$W_g = \frac{KAM}{4RT\mu t} (P_1 - P_2) \left[P_1 - \frac{1}{2} (P_1 - P_2) \right]. \quad (11)$$

When $(P_1 - P_2) \ll P_1$, Eq. (11) simplifies to

$$W_g = \frac{KAM}{4RT\mu t} P_1 (P_1 - P_2). \quad (12)$$

16. P. C. Carman, *Flow of Gases Through Porous Media*, Academic Press, 1956.

By using the perfect gas law, this relation can be rewritten as

$$W_g = \frac{KA\rho_g}{4\mu t} \frac{P_1}{P_m} (P_1 - P_2), \quad (13)$$

where A is the surface area of the graphite tube and P_m the mean gas pressure.

Equation (13) also represents the total transverse flow of gas from the graphite tube back into the outer stream. If β is the weight fraction of the fission product in the gas inside the tube (i.e., grams of fission product per gram of gas), the transport of fission product through the graphite tube to the outside is

$$W_f = \beta \frac{KA\rho_g}{4\mu t} \frac{P_1}{P_m} (P_1 - P_2). \quad (14)$$

If it is assumed that the gas density inside is approximately the same as that outside,

$$\beta\rho_g \equiv m_f, \quad (15)$$

where m_f is the mass of fission product per unit volume of gas inside the graphite tube. Then Eq. (14) becomes

$$W_f = m_f \frac{KA}{4\mu t} \frac{P_1}{P_m} (P_1 - P_2), \quad (16)$$

where

W_f = rate of transport of fission product through the graphite tube into the outer stream, g/sec,

A = surface area of graphite tube, cm²,

P_1, P_2 = inlet and exit gas pressures, atm,

P_m = mean gas pressure, atm,

μ = viscosity of gas, centipoise,

m_f = mass fraction of fission product in the gas inside the graphite tube, g/cm³,

K = permeability coefficient for graphite, Darcy.

Here it may be noted that $P_1 \cong P_m$ for most practical cases.

Equation (16) was used to predict cesium transport in experiments with the ORNL fission-product deposition loop,⁹ where helium at 15 atm and 900°K flows turbulently over a 15-cm-long 2.5-cm-diam 0.2-cm-thick graphite test section. A K value of 0.05 Darcy, obtained

from measurements on similar graphite,¹⁷ was used for these calculations. The pressure drop along the graphite tube was estimated to be approximately 1.4×10^{-3} atm. Table 2.3 lists the values of W_f predicted from Eq. (16) and those determined experimentally.^{11,12}

Table 2.3. Experimental and predicted values of cesium transport through a graphite tube

Experiment	W_f from Eq. (16) (10^{-8} g/sec)	W_f from experiment (10^{-8} g/sec)
C-2	9.8	2.8
C-3	11.6	4.0
C-4	7.4	13.0
C-5A	13.2	2.0

If a solid-state diffusion mechanism were assumed, the values of W_f would be of the order of 3.0×10^{11} for a cesium diffusion coefficient, D , of 10^{-7} cm²/sec. It is apparent that for the cases considered here, diffusion alone underestimates the cesium transport through the graphite tube by several orders of magnitude. However, the values obtained from transverse flow considerations [Eq. (16)] are in reasonable agreement with the experimental data, when the variation in permeability obtained on samples of the same graphite and the precision of the experimental measurements are considered. The calculations also indicate that transverse flow will occur in reactor fuel elements in which a 5-mil gap exists between the fuel stick and the graphite.

It should be emphasized that in these experiments cesium vapor pressures of about 10^{-3} atm were used, which are greater by orders of magnitude than those expected to exist in reactor fuel (i.e., $\sim 10^{-10}$ atm and lower). It is therefore not possible to state a priori that these much smaller quantities of cesium will not be adsorbed by fuel element graphite. Future work is to be directed toward providing information concerning the behavior of cesium at low concentrations.

17. Personal communication with R. B. Evans III and J. Truitt of ORNL.

3. Nuclear Safety Program Studies

H. J. de Nordwall O. Sisman

The prime objective of safety studies of the HTGR is to provide information concerning the response of the reactor to accidental perturbations that might affect the distribution of temperature and fission products or the mechanical integrity of the core. Since in abnormal situations, important parameters such as temperature, oxygen concentration, and coolant velocity may vary more widely than under normal operating conditions, the basic approach is to obtain an understanding of the mechanisms and parameters.

The specific topics being examined are (1) the causes of fuel-particle coating failures at abnormally high temperatures, (2) the steam-graphite reaction, and (3) the chemical species and physical entities present in the cooling circuit.

In addition to the laboratory programs, experimental programs were recently begun in order to increase the amount of information available about the fission products in the coolant circuits of operating HTGR's that are less volatile than krypton and xenon. The specific objectives of this program, which is known as the HTGR fission-product surveillance program, are the following:

1. to demonstrate that the rates of release of the important fission-product isotopes of cesium, strontium, and other group IIA and IIIA metals lie within the currently predicted limits after fuel has operated for a whole fuel cycle,
2. to determine the location of important deposited fission products in the primary circuit, particularly ^{90}Sr , ^{137}Cs , ^{131}I , ^{132}I , and ^{140}Ba , as a function of time over an indefinite period,
3. to determine whether dust plays a part in the transport of fission products in the coolant circuit.

The program calls for fission-product monitoring instruments to be placed in early HTGR's, particularly where a new fuel is being used for the first time or where significantly higher temperatures will be attained. At the moment, ORNL, Gulf General Atomic, and Philadelphia Electric Company are working together to obtain information from the Peach Bottom HTGR.

3.1 Fuel Integrity and Fission-Product Release

C. D. Baumann M. T. Morgan

Coated particles containing silicon carbide coatings have been observed to become transparent to cesium upon heating to temperatures above 1800°C .¹ Attempts have therefore been made to use the Stress-2 computational model obtained from the Dragon Project to calculate whether such postirradiation annealing could lead to fracture of the SiC without fracture of the outer pyrolytic-carbon coating. By choosing suitable values for the rupture stresses of the coatings within the ranges of available measurements, a qualitatively correct description of the behavior of a small number of individual particles was obtained on the assumption that cesium release could be equated with SiC fracture.

It was also observed that variation of the core-to-buffer volume ratio yielded a surprisingly good qualitative description of particle performance. It should be noted that in these experiments the thickness of the SiC

1. C. D. Baumann et al., "Fuel Integrity and Fission Product Release," pp. 93-100, *Nuclear Safety Program Ann. Progr. Rept. Dec. 31, 1969*, USAEC Report ORNL-4511, Oak Ridge National Laboratory.

and outer pyrolytic-carbon coatings did not vary as much as the core-to-buffer volume ratio.

3.2 Studies of Reactions of Graphite with Steam

C. M. Blood S. H. Freid
H. J. de Nordwall² A. P. Malinauskas²

The reactions of steam with various graphites are being studied to determine reaction rate constants needed in calculating the effects of steam on HTGR graphite integrity and associated rates of hydrogen and carbon monoxide production. Investigations are also under way concerning why the observed rate of reaction varies with the extent of reaction. Further, an in-pile program is being conducted to determine the influence of reactor irradiations on graphite-fuel-steam reaction rates.

In out-of-pile studies, laboratory experiments with H-327 graphite revealed that different specimens that were nominally similar corroded in steam by different mechanisms. One specimen with a high iron content (~150 ppm) was found to corrode faster than others and to exhibit pitting; the latter phenomenon is usually taken to be a sign of inhomogeneously distributed metallic impurities. Laboratory work on reaction rates and corrosion mechanisms will continue with a block of H-327 graphite obtained from Gulf General Atomic that did not exhibit pitting and which has a low iron content. This is the graphite being used in the Fort St. Vrain reactor core. More detailed reports of this work may be found in the reports of the Nuclear Safety Program.^{1,3}

Initial in-pile studies have been performed with fuel sticks contained in graphite. These studies were made to investigate both the steam-graphite reaction and the resistance of coated particles to steam. Evaluation of results is incomplete, but some preliminary conclusions may be drawn. The fuel stick contained UC₂ fuel coated with silicon carbide and pyrolytic carbon and was encased in a graphite sleeve.⁴ The element was

exposed to a mixture of 4% steam in helium at about 1 atm total pressure. The temperature of the graphite casing ranged from 730 to 900°C, and the central temperature of the fuel reached 1040°C. Exposure was continued until 25% of the carbon in the fuel element had been removed. At the end of the experiment the fuel could be poured out of the fuel box, and the binder had all but disappeared. The fuel element plug, which had been cemented in place, could be removed. The graphite casing had corroded by pitting, so easy access of steam to the fuel was possible. Figure 3.1 shows the large pits in the graphite. Further, during the experiment, significant fuel coating fracture occurred. In addition, the average radial thermal conductivity of the fuel was halved. With respect to graphite attack, it appears that the influence of irradiation on induced corrosion was insignificant, as expected.

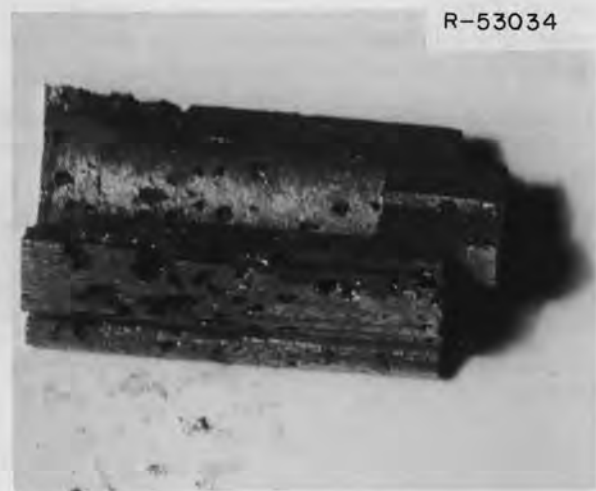


Fig. 3.1. Section of fuel element after exposure to steam.

These in-pile studies will continue, and in future experiments fuel surface temperatures will be kept constant. A more detailed report on this work is presented in the Nuclear Safety Program report for September–October 1970.³

3.3 Fission-Product Behavior in an HTGR Coolant Circuit

It is desirable to know the behavior of fission products and other impurities in HTGR coolant circuits. ORNL work in this area involves laboratory

2. Part time.

3. C. M. Blood et al., "Studies of Reactions of Graphite with Steam," pp. 54–59, *ORNL Nuclear Safety Research and Development Program Bimonthly Report for September–October 1970*, USAEC Report ORNL-TM-3212, Oak Ridge National Laboratory; see also preceding reports in this series.

4. B. F. Roberts, W. H. Montgomery, and O. W. Thomas, "In-Pile Studies of Oxidation of Model Fuel Elements by Steam," pp. 63–67, *Gas-Cooled Reactor Program Semiann. Progr. Rept. Sept. 30, 1969*, USAEC Report ORNL-4508, Oak Ridge National Laboratory.

programs on dust behavior, and experiments are being planned for studying fission-product behavior in the Peach Bottom HTGR.

3.3.1 Experiments on dust behavior (E. Hoinkis,⁵ J. Kolb²)

A wind tunnel is being constructed for use in studying deposition and reentrainment of dust. The fluid used will be air at 1 atm pressure. Flow conditions will be adjusted to bracket the Reynolds numbers and linear velocities expected in HTGR's. Aerosols of carbon or metal oxides will be generated with electric arcs.

3.3.2 Fission-product surveillance program (F. F. Dyer,² H. J. de Nordwall,² J. Kolb²)

After a visit to the Peach Bottom HTGR and discussions with Gulf General Atomic and Philadelphia Electric Company personnel, plans are being made to make the following measurements in the primary coolant circuit of the Peach Bottom reactor:

1. mass and number concentrations of aerosol particles, solid fission products, and corrosion products leaving the core,
2. concentrations of solid fission and corrosion products leaving the steam generator,

5. Visiting scientist from Hahn-Meitner Institute, Berlin, Germany.

3. concentrations of very short-lived rare gases in the circuit,
4. distributions of gamma-emitting fission products that have settled on the walls of the primary circuit.

A few samples of particulate matter collected by GGA with existing instruments have been examined microscopically and by electron diffraction.⁶ The predominant gas-borne materials appeared to be oxides of iron, chromium, and manganese. Some amorphous carbon was present. Crystalline graphite whiskers were found on the body of the diffusion probe. The black deposits on the two fine filters examined were found to be composed of agglomerates of particles. Because of overcrowding on the filters the sizes of gas-borne agglomerates were indeterminate, but the primary particles were typically as small as 0.02 μm in diameter. Chain-like nondiffracting structures characteristic of smokes were seen, as well as more crystalline bodies, with the latter usually consisting of mixtures of corrosion-product oxides. No large carbon particles that could have originated as graphite grit or pyrolytic carbon were observed. The deposits, particularly the carbon whiskers, found on the diffusion-probe body were not necessarily representative of deposits or reaction products elsewhere in the circuit.

6. E. Hoinkis, J. Kolb, and H. J. de Nordwall, "Fission Products in an HTGR Coolant Circuit," pp. 87-95, *ORNL Nuclear Safety Research and Development Program Bimonthly Report for May-June 1970*, USAEC Report ORNL-TM-3061, Oak Ridge National Laboratory.

4. Corrosion Studies of Welds in Alloys for Advanced Steam Generators

P. Patriarca G. M. Slaughter
J. P. Hammond

The corrosion resistance of welds in several high-temperature alloys being considered for use in steam generators for advanced high-temperature gas-cooled reactors is being studied to determine how well these weldments will resist both general and preferential corrosion in steam at 595 to 760°C. The program includes four areas of investigation: (1) general corrosion (formation of a uniform scale) at 595 and 650°C, including an evaluation of the general weldability of various combinations of base and filler metals; (2) general corrosion at 705 to 760°C; (3) preferential corrosion (e.g., oxidation at the fusion line, pitting, and stress cracking); and (4) mechanical properties.

4.1 General Corrosion at 595 and 650°C

4.1.1 Studies of similar- and dissimilar-metal weldments

The amounts of corrosion of steam-generator-alloy weldments were determined for a total accumulated steam exposure of 12,000 hr at 595 and 650°C, and averaged corrosion rates were added to the weight-gain corrosion curves. These data points were the first determinations made since the 8000-hr mark.¹ All the curves continued to show an approximately linear relationship between corrosion and time. Where devia-

tions from linearity were observed, they were slight, and almost invariably the corrosion rate decreased with time, suggesting that the protective nature of the scales improved with exposure.

The calculated amounts of corrosion in terms of metal penetrated in 20 years for the similar-metal weldments of Inconel 625, Hastelloy X, and IN 102 welded with themselves was less than 1/2 mil after exposure at 595 and 650°C. Dissimilar-metal weldments of these alloys joined to Incoloy 800 with themselves and with Inconel 82 as filler metal were about as good at 595°C and only moderately inferior at 650°C. Inconel 600, which showed the highest amount of corrosion of the high-nickel alloys, gave a 20-year penetration of 2 mils after exposure at 595°C and 3 mils at 650°C.

The corrosion results of these weldments were usually substantially lower than had been reported for these same materials in the wrought form.^{2,3} Wozaldo and Pearl² investigated the isothermal corrosion of the base metals being considered (except for IN 102) in superheated steam at 565 and 620°C. A comparison of

1. J. P. Hammond et al., "Corrosion of Advanced Steam Generator Alloy Weldments in 1100 and 1200°F (595 and 650°C) Steam," paper 46 presented at the National Association of Corrosion Engineers, 26th National Conference, March 2-6, 1970, Philadelphia; to be published in the proceedings.

2. G. P. Wozaldo and W. L. Pearl, "General Corrosion of Stainless Steels and Nickel-Base Alloys Exposed Isothermally in Superheated Steam," *Corrosion*, 21: 355-369 (1965).

3. F. Eberle and J. H. Kitterman, "Scale Formations on Superheater Alloys Exposed to High Temperature Steam," pp. 67-113 in *Behavior of Superheater Alloys in High Temperature, High Pressure Steam*, sponsored by American Society of Mechanical Engineers Research Committee on High Temperature Generation, Library of Congress No. 68-19904 (copyright 1968).

results obtained at ORNL at 650°C with their 620°C data showed that, in spite of the temperature difference, the ORNL similar-metal weldments after 8000 hr exposure corroded only one-half to two-thirds as much as Wozaldo and Pearl's wrought samples, except for type 304 stainless steel, which corroded less than one-ninth as much. Although the steam used by Wozaldo and Pearl contained 20 ppm O and 2.5 ppm H, compared with undetectable levels in the present work, the reason for lower corrosion at ORNL is probably associated with a difference in surface condition of the specimens in the respective studies. The ORNL specimens were ground on a 100-mesh Carborundum belt to achieve an economical standard finish, whereas the specimens of the other investigation were pickled and probably had little cold work in their surfaces.

To determine how large an effect surface condition has on corrosion of steam generator materials, two sets of specimens from three alloys were exposed to superheated steam at 595 and 650°C; one set had the 100-mesh ground finish and the second identical set had the ground finish removed by electropolishing 3 mils of material from the surfaces. The results, for exposure times to 8000 hr, are given in Table 4.1. It may be

observed that for type 304 stainless steel and Incoloy 800, the amounts of corrosion are one to two orders higher for the electropolished specimens than for the ground specimens. On the other hand, for the nickel-base alloy Inconel 625, surface condition had only a minor influence, with slightly improved performance for the electropolished specimens indicated. It is significant to note with respect to stainless steel and Incoloy 800 that the difference in amounts of corrosion for the respective surface conditions is not attributable entirely to differences in the early, parabolic stage of corrosion. The linear rates of corrosion for these materials appear to be significantly higher for the electropolished condition. This consideration is important from the point of view of the extrapolated long-term corrosion represented.

4.1.2 Studies on simulated "root-pass" compositions

The total accumulated exposure of a set of corrosion specimens specially synthesized to simulate the root passes of weldments in both composition and structure has now reached 4000 hr. The root passes are receiving special attention because they generally are more highly

Table 4.1. Steam corrosion of steam generator alloys as influenced by surface finish

Exposure temperature (°C)	Material	Corrosion weight gain ^a (mg/cm ²)				
		Exposure time				
		1000 hr	2000 hr	4000 hr	6000 hr	8000 hr
595	Type 304 stainless steel					
	As-ground	0.07	0.10	0.14	0.22	0.29
	Electropolished	5.19	6.87	(b)		
	Incoloy 800					
	As-ground	0.055	0.095	0.100	0.120	0.140
	Electropolished	3.97	4.66	5.24	5.45	5.61
650	Inconel 625					
	As-ground	0.050	0.065	0.070	0.075	0.085
	Electropolished	0.050	0.055	0.055	0.070	0.080
	Type 304 stainless steel					
	As-ground	0.11	1.20	1.21 ^c		
	Electropolished	6.33	(b)			
650	Incoloy 800					
	As-ground	0.215	0.310	0.415	0.475	0.535
	Electropolished	5.32	5.57	5.79	5.90	5.99
	Inconel 625					
	As-ground	0.115	0.130	0.150	0.185	0.205
	Electropolished	0.065	0.055	0.060	0.080	0.085

^aValues listed are, in most cases, an average of three determinations.

^bSpecimen spalled badly while being weighed; test discontinued.

^cSpecimen apparently had flaked substantially during exposure and weighing; test discontinued.

alloyed (from base-metal dilution) than subsequent passes, and it is the root pass that is actually exposed to steam in service. These synthetic root-pass compositions were designed to match the compositions corresponding to the 50% dilution factor obtained in welds for the general corrosion studies.

After establishing the surprisingly large effect of surface finish on corrosion resistance, the number of root-pass compositions selected for investigation was expanded, as were the conditions of their surfaces. The alloys to be examined and their status are listed in Table 4.2. All are being studied in the as-welded, electropolished, sand-blasted, and belt-ground conditions; in addition, some are being studied in the belt ground-and-annealed condition. To date, examinations show two orders of magnitude difference in the amounts of corrosion between the materials showing highest corrosion rates (type 304 stainless steel welded with type 308 stainless steel and Incoloy 800 welded with Inconel 82, as-welded finish) and those of lowest corrosion rate (Hastelloy X joined to Incoloy 800 with Inconel 82, all four finishes).

4.2 Preferential Corrosion

The construction of the Incoloy 800 steam-corrosion loop equipped for injecting chloride and oxygen contaminants to investigate stress-corrosion cracking of weldments was completed. This unit operated successfully in a shakedown test designed to prove out its functional units and provide a stress-relieving thermal exposure to critical portions of the loop. U-bend test specimens and holding fixtures were completed, and the first of two test runs was begun. These runs will be conducted under "low corrosion" conditions, and the tests are designed primarily to determine whether chloride stress-corrosion cracking can occur under "dry" steam conditions. Subsequent tests will include cycling below the steam saturation temperature (to

Table 4.2. Composition and status of root-pass specimens

Code	Composition	Status
A2	50% Inconel 82, 50% Incoloy 800	As-welded and electropolished specimens exposed 4000 hr; other specimens prepared
A3	50% Inconel 600, 50% Inconel 82	Specimens being prepared
A4	50% type 304 and 50% type 308 stainless steel	As-welded, electropolished, and ground specimens prepared; other specimens prepared
A6	75% Hastelloy X, 25% Incoloy 800	Specimens being prepared
A7	50% Inconel 82, 25% Hastelloy X, 25% Incoloy 800	As-welded and electropolished specimens exposed 4000 hr; other specimens prepared
A12	50% Inconel 82, 25% Inconel 625, 25% Incoloy 800	As-welded and electropolished specimens exposed 4000 hr; other specimens prepared
A13	75% Inconel 625, 25% Incoloy 800	Specimens being prepared
A19	75% IN 102, 25% Incoloy 800	Specimens being prepared
A20	50% Inconel 82, 25% IN 102, 25% Incoloy 800 100% Inconel 82	Specimens being prepared Specimens being prepared

introduce moisture), and chloride and oxygen contaminants will be introduced at higher levels (2 to ~8 ppm each).

Specimens with and without purposely introduced welding flaws (to act as corrosion crevice) are being prepared in all the weldment combinations of the general corrosion study. Additionally, similar-metal weldment specimens are being made in types 316 and 410 stainless steel, an 18 Cr-18 Ni-2 Si (wt %) stainless steel (especially marketed for use in stress-corrosion environments by United States Steel Corporation), and Inconel 601.

Part II. Gas-Cooled Breeder Reactor Development

5. GCBR Fuel Studies

A. L. Lotts J. A. Conlin
R. B. Fitts

A joint ORNL-Gulf General Atomic (GGA) irradiation testing program is being conducted to evaluate the performance of fuel pins representing various design concepts proposed for use in gas-cooled fast breeder reactors (GCBR). The concepts under consideration are based on oxide fuel contained in metallic cladding. Two major types of fuel pins are being considered – the sealed pin and the vented pin. Fuel pins of the sealed type (capsules P-1 through P-8) have been tested in the ORR poolside thermal-flux irradiation facility under various steady-state and cyclic conditions of fission power, cladding temperature, and coolant overpressure. A test of a vented fuel pin (capsule P-9) is in progress in the ORR, and eight pins (the F-1 series) containing charcoal fission-product traps and large plenum volumes to minimize fission-gas-pressure buildup and thus simulate vented pins were encapsulated and shipped to the EBR-II for fast-flux irradiation.

The principal variable in the irradiations of the sealed pins was the mechanical stability of the pins as it was influenced by cladding material (Hastelloy X and type 316 stainless steel), cladding thickness, operating temperatures, and pressure differential across the cladding wall. These tests showed that a sealed pin with a practical, economic cladding thickness can be built that will perform successfully in a thermal-neutron flux at

GCBR operating conditions.¹ This type of pin is the backup concept for the GCBR.

The current irradiations, both in thermal and fast fluxes, are for examining the performance of the reference GCBR fuel-pin concept – the vented pin. In this concept the pressure differential across the cladding is maintained at a nearly constant low value (about 25 psi) by connection of the internal fuel-pin gas space either to an external pressure control system or directly to the reactor coolant system. This type of pin has the advantages that it eliminates any large pressure differential across the cladding and permits utilization of fuel and cladding technology developed in the LMFBR program.

5.1 Irradiation of GCBR-ORR Capsule 04-P9

A. W. Longest J. A. Conlin
K. R. Thoms E. D. Clemmer

The 04-P9 capsule test is a joint effort of ORNL and GGA. The capsule was designed to permit evaluation of

1. R. B. Fitts et al., "Gas Cooled Fast Reactor Fuel-Element Development," pp. 864–878 in *Proceedings of the Gas Cooled Reactor Information Meeting, Oak Ridge National Laboratory, April 27–30, 1970*, USAEC Report CONF-700401, 1970.

the overall performance of a vented fuel pin under conditions typical of a GCBR and to provide for monitoring of the fission-product release from the charcoal trap and blanket regions of the pin during operation. The irradiation of this capsule, which began in April 1970, is proceeding satisfactorily. The third irradiation cycle in the ORR poolside facility was completed on September 13, 1970. At this time the accumulated irradiation time at full power was 138 days, and the estimated fuel burnup was approximately 15,000 MWd/MT.

The capsule design, fabrication, planned operating conditions, and initial operation were discussed previously.²⁻⁴ The capsule is shown in Fig. 5.1; it contains one fuel-pin specimen of the vented concept, as indicated in Fig. 5.2. In this concept the fuel-pin internal-to-external pressure differential is maintained near zero, and by this means the gas-pressure stresses in the cladding are essentially eliminated. In the reference reactor,⁵ the low pressure differential is controlled by manifolding the fuel pins to an external fission-product trapping and cleanup system maintained at a pressure slightly below that of the coolant. The concept of interest in this case also employs a small charcoal trap in each fuel pin to reduce the fission-product load on the external system, particularly the iodines and very short-lived fission gases. A detailed summary of data for the fuel pin is given in Table 5.1.

The fission-product release from the trap and from the blanket region of the fuel pin is being monitored during irradiation by means of a high-pressure (1000-psig) high-purity-helium sweep-gas system. The system is designed so that the fission-gas release from the charcoal trap can be measured with the helium sweep

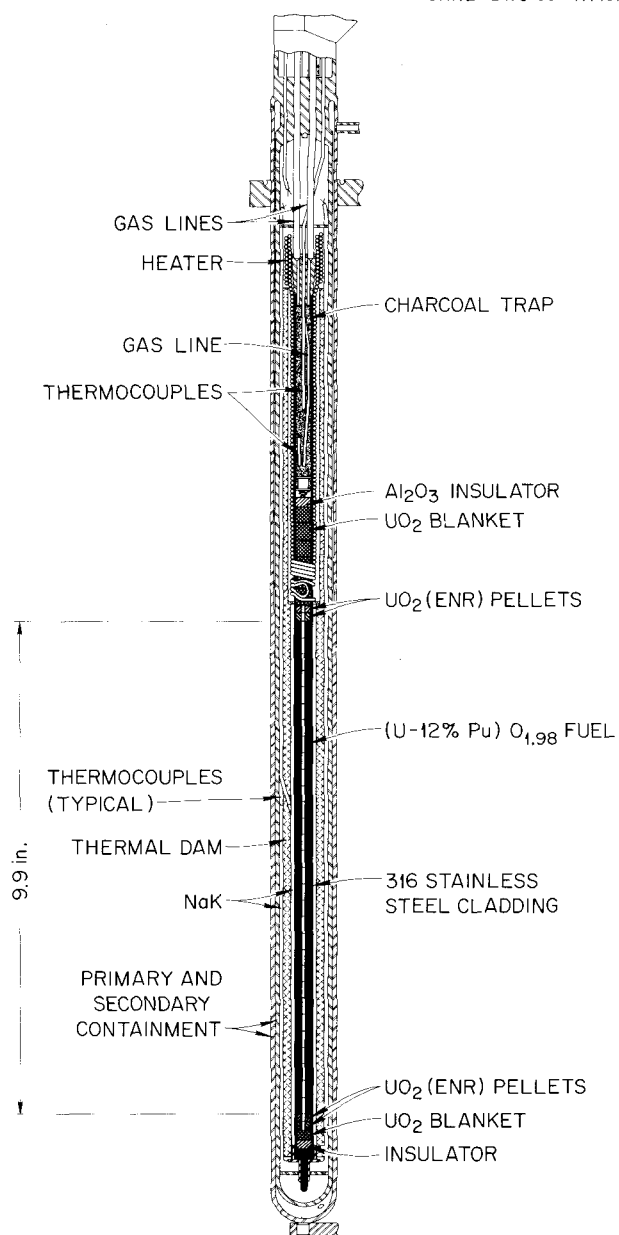


Fig. 5.1. Capsule 04-P9.

flowing either across the top of the trap (normal case) or upward through the trap when the inlet flow is transferred to the line that terminates at the bottom of the trap. In the latter case the gaseous effluent is swept through the trap. Calculations (made by GGA) indicated that sorption holdup time in the charcoal trap at its normal operating temperature of 300°C and at the

2. A. W. Longest et al., "Design and Fuel Rod Fabrication for Capsule O4-P9," pp. 87-97, *GCRP Semiann. Progr. Rept. Sept. 30, 1969*, USAEC Report ORNL-4508, Oak Ridge National Laboratory.

3. J. R. Lindgren et al., *Planned Thermal Irradiation of Manifolded-Vented (U,Pu)O₂-Fueled Rod in ORR Capsule P-9* USAEC Report GA-9896, Gulf General Atomic, 1970.

4. A. W. Longest et al., "Installation and Startup of Capsule O4-P9," pp. 91-96, *GCRP Semiann. Progr. Rept. Mar. 31 1970*, USAEC Report ORNL-4589, Oak Ridge National Laboratory.

5. P. Fortescue and W. I. Thompson, "The GCFR Demonstration Plant Design," pp. 795-811 in *Proceedings of the Gas Cooled Reactor Information Meeting, Oak Ridge National Laboratory, April 27-30, 1970*, USAEC Report CONF-700401, 1970.

Table 5.1. GCBR-ORR irradiation capsule 04-P9 fuel-pin data

Fuel-pin designation	GA-20
Pin type	Vented, with integral charcoal trap
Cladding data	
Material	Type 316 stainless steel
OD, in.	0.3535
Wall thickness, in.	0.0245
OD/ID ratio	1.161
Length, in.	16.312
Fuel data	
Pellet dimensions	
OD, in.	0.301
ID, in.	0.060
Length (U,Pu)O ₂ , in.	0.273–0.319
Length UO ₂ , in.	0.148–0.162
End-dish depth, in.	0.006
Total fuel-stack height, ^a in.	9.872
Pellet material	(U,Pu)O ₂ , sol-gel derived
Number of (U,Pu)O ₂ pellets	32
Composition, %	
UO ₂	88
U enrichment	9
PuO ₂ ^b	12
Oxygen-to-metal ratio	1.983–1.992
Density, % theoretical	91–92
Stack smear density of (U,Pu)O ₂ pellets, % theoretical	85
BET surface area, m ² /g	<0.05
(U,Pu)O ₂ stack height, in.	9.240
UO ₂ power-peak-reducing half-pellets	
Material	UO ₂
Number of pellets	2 at each end of fuel stack
Pellets adjacent to fuel stack	
Enrichment, % ²³⁵ U	14.9
Oxygen-to-uranium ratio	2.004
Density, % theoretical	91–92
Outer pellets	
Enrichment, % ²³⁵ U	8.3
Oxygen-to-uranium ratio	2.005
Density, % theoretical	90
Blanket-pellet data	
Pellet material	UO ₂
Enrichment, % ²³⁵ U	0.22
Number of pellets	6 at top, 1 at bottom
OD, in.	0.301
Length, in.	0.321–0.328
Stack height, in.	1.959
Oxygen-to-uranium ratio	2.004
Density, % theoretical	88–90
Fission-product trap ^c	
Material	Activated coconut charcoal, Barnebey-Cheney
Bed length, in.	3.22
Charcoal weight, g	1.29
Charcoal type	MI 6736
Particle mesh size	10–14
Density, g/cm ³	0.448
BET surface area, m ² /g	1004
Impurity content, ppm	
Ba	4
B	<1
Fe	40
Cu	120
Sr	<80
Mn	<0.20
Al	20
Cu	4
Si	400
Mg	20
Ti	2
Na	<120
P	<200

^aIncludes the (U,Pu)O₂ and the UO₂ half-pellets.

^bPlutonium isotopic composition: ²³⁹Pu, 88.7%; ²⁴⁰Pu, 9.97; ²⁴¹Pu, 1.23%; ²⁴²Pu, 0.101%.

^cContained between 30- to 40-mesh type 316 stainless steel screens.

sampling flow rate of approximately 1300 cm³ STP/min (actual flow rate is 19 cm³/min at pressure) is only about 10 to 15 sec for krypton and xenon.

During most of the first three cycles of irradiation the fuel pin and its charcoal trap were operated at steady-state design conditions; these are a linear heat rating of 16 kW/ft, 685 ± 15°C peak cladding outer surface temperature, 300°C charcoal trap temperature, 1000-psig cladding internal pressure (sweep-gas pressure), and 975-psig cladding external pressure (NaK blanket-gas pressure). Sweep-gas samples were taken periodically and analyzed by gamma-ray spectrometry.

A normal set of gas samples consists of two samples with the sweep gas flowing across the top of the trap, followed by two samples with the sweep gas flowing through the trap. The latter two samples are taken 1 to 2 hr after transferring the flow to the bottom of the trap. One sample taken under each flow condition is held 15 min to allow the short-lived noble gases to decay. These samples are then evacuated to remove the longer lived noble gases before counting for the plated-out daughter products of the short-lived gases. The other two samples are counted without evacuation.

Fission-gas release-rate-to-birth-rate ratios (*R/B*) calculated from data obtained under the constant-pressure steady-state design conditions are shown in Figs. 5.3 and 5.4 for the two flow configurations. The effectiveness of the trap in reducing the release rates of the various isotopes is shown by the release-rate ratios given in Table 5.2. All these samples were taken at a sweep-gas flow rate of approximately 1300 cm³ STP/min, which yields a sweep-gas transient time of about 47 sec from fuel pin to sampling point.

During nonsampling periods the flow rate is throttled to approximately 200 cm³ STP/min to reduce helium consumption. When the sweep-gas flow is increased for sampling, a pressure decrease of about 1.0 psi occurs in the sweep-gas system while the change is being made, and then the sweep-gas pressure-control system returns the pressure to normal. Because of this pressure disturbance, gas samples are taken only after about 2½ hr of steady operation following the flow-rate increase. At constant flow rates the pressure-control system maintains the 25-psi pressure differential between the static NaK blanket gas and the flowing sweep gas to within ±0.1 psi.

All the data shown in Figs. 5.3 and 5.4 and Table 5.2, with the exception of those taken at 4 and 46 days at power, were obtained with the ORR poolside-facility gamma-ray spectrometer (3- by 3-in. NaI detector, 512-channel analyzer) at 10 keV per channel. Some of

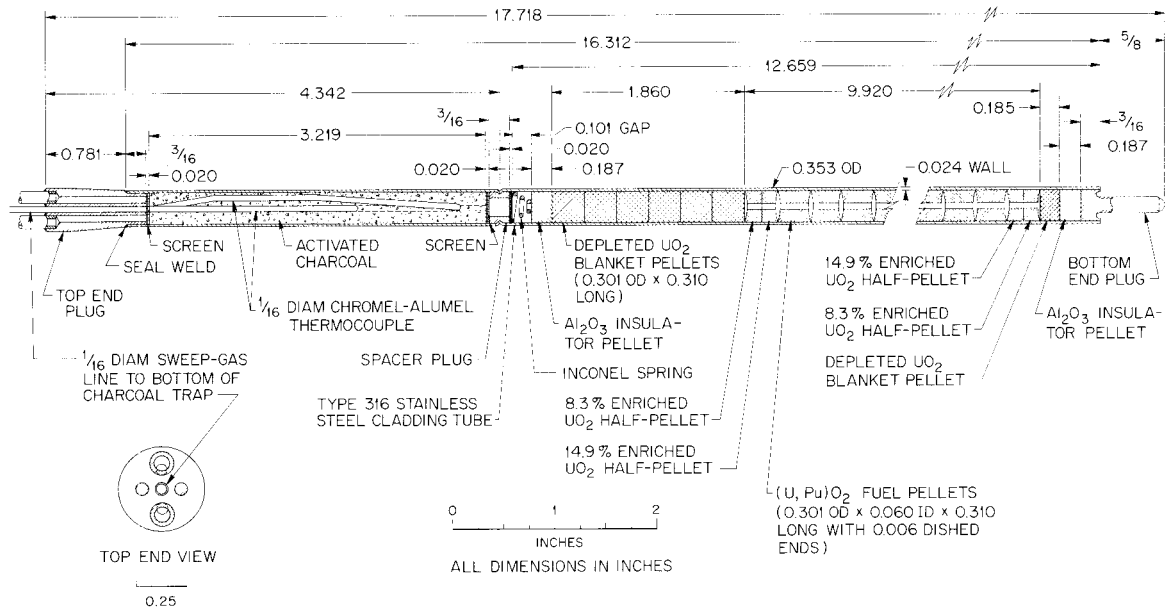


Fig. 5.2. Gas-cooled fast breeder reactor fuel-rod specimen in capsule 04-P9. Specimen designed by Gulf General Atomic.

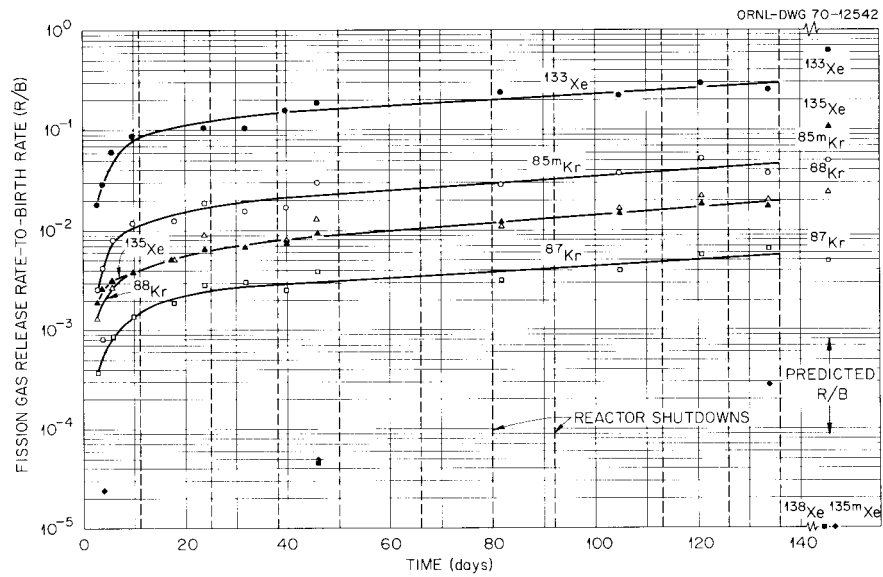


Fig. 5.3. Steady-state fission-gas release from GCBR-ORR capsule 04-P9 versus time at full power for case of sweep-gas flow across top of trap.

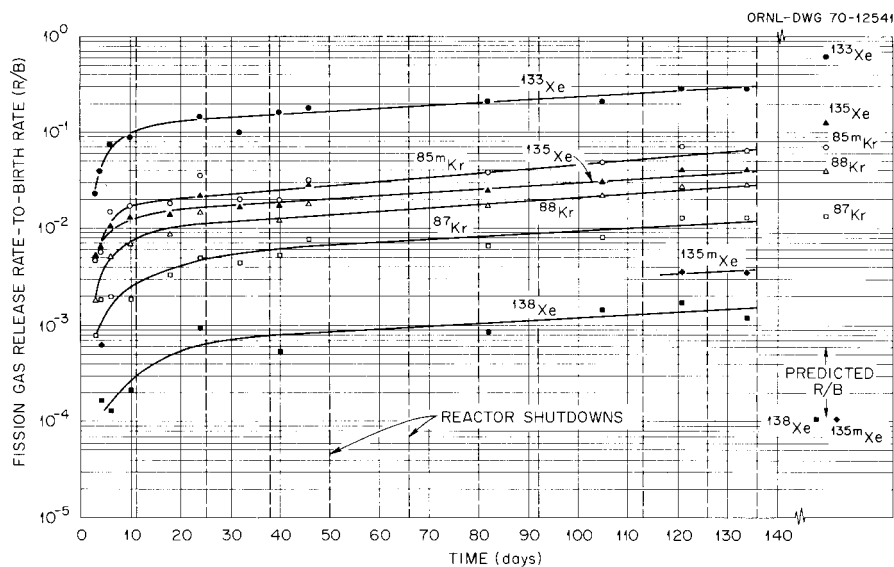


Fig. 5.4. Steady-state fission-gas release from GCBR-ORR capsule 04-P9 versus time at full power for case of sweep-gas flow through trap.

Table 5.2. Effectiveness of charcoal trap in fuel pin in reducing the steady-state fission-gas release from GCBR-ORR capsule 04-P9

Sampling date	Peak cladding outer surface temperature ^a (°C)	Calculated fuel-rod total power (kW)	Accumulated time at full power (days)	Ratio of fission-gas release rate with sweep-gas flow across top of trap to that with sweep-gas flow through trap							
				4.4-h ^{85m} Kr	2.8-h ⁸⁸ Kr	1.3-h ⁸⁷ Kr	3.2-m ⁸⁹ Kr	5.27-d ¹³³ Xe	9.13-h ¹³⁵ Xe	17.0-m ¹³⁸ Xe	15.3-m ^{135m} Xe
4-7-70	348	5.74	0	0.81	0.81	0.49		0.81	0.56		
4-9-70	530	9.41	0	0.85	0.83	0.53		0.89	0.41		
4-13-70	667	12.1	3	0.54	0.71	0.47		0.79	0.38		
4-14-70	677	12.3	4	0.74	0.72	0.43		0.71	0.41	0.036	0.038
4-16-70	677	12.3	6	0.53	0.53	0.44		0.81	0.30		
4-20-70	673	12.2	10	0.69	0.74			0.99	0.30		
4-28-70	675	12.3	18	0.68	0.58	0.52			0.37		
5-4-70	677	12.4	24	0.52	0.61	0.58		0.73	0.30		
5-12-70	667	12.2	32	0.76		0.68		1.0	0.41		
5-21-70	686	12.2	40	0.85	0.65	0.48		0.97	0.44		
5-22-70	683	12.2	41								
5-27-70	692	12.5	46	0.95	0.72	0.51		1.0	0.35	0.040	
7-9-70	683	11.9	82	0.74	0.65	0.48		1.1	0.50		
8-10-70	680	12.1	105	0.75	0.73	0.49		1.1	0.49		
8-27-70	683	12.1	121	0.73	0.79	0.45		1.0	0.46		
9-10-70	686	12.0	134	0.59	0.70	0.51		0.89	0.43		0.082
Average of full-power values				0.70	0.67	0.52		0.92	0.40	0.038	0.060
Predicted (ref. 3)				0.71	0.60	0.38	10 ⁻⁴	0.98	0.81	0.10	0.10

^aCalculated on the basis of thermocouple indications of temperature along the inner surface of the Zircaloy-2 sleeve surrounding the fuel rod. The calculation takes into account the radial dislocation of the thermocouple junction from the cladding surface and the circumferential displacement from the hot-side location.

the samples were also counted at 5 and 2.5 keV per channel in an attempt to obtain better resolution. However, it has not been possible to obtain a satisfactory count of ^{89}Rb from which the release of 3.2-m ^{89}Kr can be determined. Also, the amount of ^{138}Cs in the samples (from which 17.0-m ^{138}Xe release is determined) is frequently too low for a good count when the sample is taken with the sweep gas flowing across the top of the trap.

Samples taken after 4 and 46 days at power were submitted for counting with a 6-cm³ planar Ge(Li) detector and 400-channel analyzer. Those results were in reasonably good agreement with our data for the longer lived fission gases and gave ^{89}Kr R/B values for the case of sweep flow through the trap of 9.4×10^{-6} and 2.0×10^{-5} after 4 and 46 days at power, respectively. These R/B values are close to the value of 10^{-5} predicted by GGA. For the case of sweep-gas flow across the top of the trap, the results indicated the R/B for ^{89}Kr to be less than 5×10^{-6} after 46 days at power.

The predictions of fission-gas release data were made by GGA on the basis of diffusional delay processes in the fuel pin and experimental studies of the adsorption holdup in the charcoal trap. Diffusion experiments were performed by using ^{85}Kr . Because of a lack of xenon data, the effectiveness of the trap was assumed to be the same for xenon as for krypton. Additional experiments and analyses are in progress at GGA.

As may be seen in Figs. 5.3 and 5.4, the steady-state release rates increased rapidly at first and then showed a steady slow increase toward the predicted release fractions. The measured krypton release rates are now about equal to their predicted release rates. The measured ^{133}Xe and ^{135}Xe releases are lower than predicted, while the results for ^{135m}Xe and ^{138}Xe are about a factor of 10 higher than predicted. The effectiveness of the charcoal trap (see Table 5.2) is a function of the half-life of the isotopes and is reasonably close to the values predicted. The better-than-predicted trap performance for the holdup of ^{135}Xe is probably due to burnup of the ^{135}Xe in the high thermal-neutron flux in the trap, which in effect reduces the ^{135}Xe half-life. Reactor shutdowns and frequency of sampling are factors affecting the buildup and release of the longer lived ^{133}Xe .

Reactor refueling shutdowns are denoted in Figs. 5.3 and 5.4 by vertical lines. These shutdowns are important in interpreting the data because all indications of fission-gas release, including the radiation monitors on the effluent sweep-gas line, show an appreciable

increase during the life of each reactor core. The variation in fuel-pin total power during a given fuel loading is small. However, there is an upward shift of the temperature profile over the fueled portion of the pin associated with the gradual withdrawal of the reactor control rods. Cladding temperatures near the top end of the fuel column increase by as much as 50°C during a core life.

Special tests conducted to date have included steady-state operation at several different fuel-pin trap temperatures and slow cycling of the sweep-gas pressure. During the week of June 8, sets of sweep-gas samples were taken at fuel-pin trap temperatures of 200, 250, and 300°C to determine the effect of trap temperature on fission-gas release. These sample results were erratic, perhaps caused in part by the wait of only one day between each step increase in temperature. Several minor modifications were made to the sampling system immediately prior to the trap temperature tests, and changes in the sampling procedure may also have been a factor. It is planned to repeat the trap temperature tests later and allow more time to reach equilibrium at each temperature.

During the period from June 18 to July 2 several pressure cycling tests were conducted at sweep-gas pressure decrease rates of about 2.5 and 7.5%/hr down to pressures of 900 and 750 psig. Two consecutive cycles down to 900 psig at the rate of approximately 2.5% pressure decrease per hour were conducted on June 18. The remaining tests, all at about 7.5% pressure decrease per hour, consisted of three consecutive cycles down to 750 psig on June 25, a single cycle to 750 psig on June 29, and a single cycle to 775 psig on July 2. Several days were allowed before each test for the fission products to reach steady-state levels. In each test, sweep-gas samples were taken during the depressurization half of the cycle. The sweep-gas flow was across the top of the trap at all times.

The results of the pressure cycle tests are plotted in Fig. 5.5, where the response of the ionization chamber on the high-pressure side of the effluent sweep-gas line (RR-451) and the R/B results obtained for the longer lived fission gases are given. During each of the depressurizations, the volumetric flow rate (actual cm³/sec) of sweep gas past the ionization chamber (RR-451) was approximately constant. This was a consequence of the manner in which the depressurizations were conducted (exponential decay of pressure at pressure-decay half-lives of 23.4 and 8.5 hr for the two depressurization rates, respectively) and was verified by examination of the pressure and flow rate

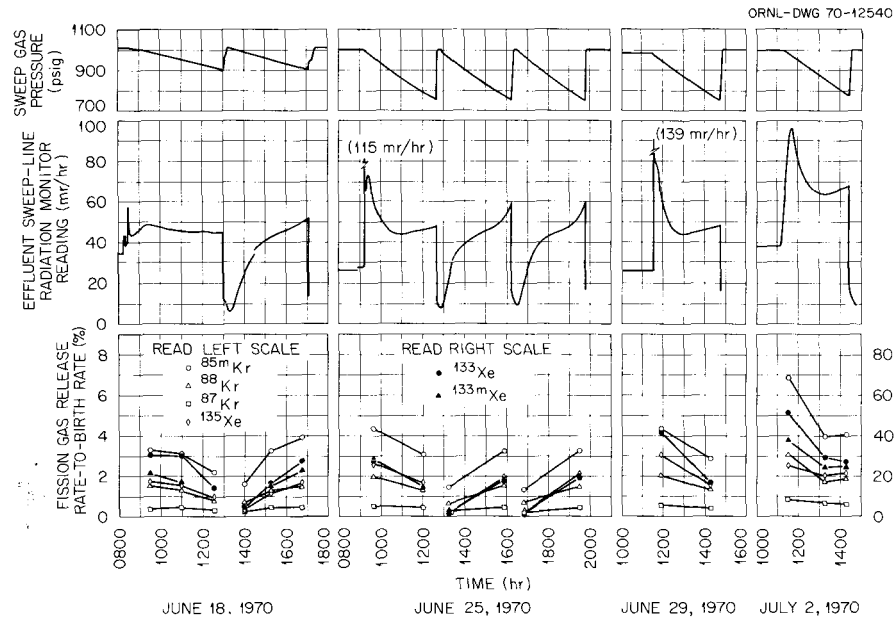


Fig. 5.5. Activity release from GCBR-ORR capsule 04-P9 during slow pressure cycling tests conducted on June 18, June 25, June 29, and July 2, 1970.

data obtained. Therefore, the response of the ionization chamber can be interpreted as changes in the gross activity release rate from the fuel pin.

During the first few depressurizations it was difficult to start the pressure decay smoothly. The activity spikes at the start of the tests on June 18, 25, and 29 were caused by small pressure fluctuations. Experience has shown that a decrease in the 1000-psig sweep-gas pressure of as little as 0.5 psi within 1 min or less following a period of steady operation with the sweep-gas flowing across the top of the trap will cause a distinct activity spike of as much as 30% above normal.

The *R/B* results obtained during the pressure-cycle tests appear to be consistent with the on-line radiation monitor readings, with the exception of the third sample set (two samples) taken during the first depressurization on June 18. This set of *R/B* results appears to be low compared with the radiation monitor readings.

The ^{138}Cs activity found in the samples taken on June 18 was too low to count except for the first sample set. In each of the depressurizations at the higher pressure decay rate, ^{138}Xe release (determined from counting ^{138}Cs) was low early in the depressurization but increased to an appreciably higher level (*R/B* of $\sim 1.5 \times 10^{-4}$) by the latter half of the depressurization.

The activity peaking that occurred early in the first cycle of each test is believed to have been caused by the dumping of a portion of the fission-gas inventory contained in the charcoal as a consequence of increasing the flow rate through the charcoal. The volumetric flow rate out of the charcoal trap was calculated to be about $0.0013 \text{ cm}^3/\text{min}$ during the approximately 2.5%/hr depressurizations and $0.0036 \text{ cm}^3/\text{min}$ during the depressurizations at the higher pressure decay rate. The void volume in the charcoal trap is slightly more than half the approximately 5.0-cm^3 total void in the fuel rod; therefore, gas from below the trap would not be expected to break through the trap during the depressurization. In fact, a large portion of the activity dumped from the charcoal would have had time to decay before entering the sweep-gas flowing across the top of the trap. Thus, the activity peak at the monitor would be expected to decay off in a manner similar to the decay of the dumped activity in the trap. A dose-rate calculation based on the release data obtained from the first sample set on June 18 indicated that 2.8-h ^{88}Kr accounted for about two-thirds of the radiation-monitor reading at that time. Additional dose-rate calculations will be made to permit more direct comparison of the radiation-monitor readings and *R/B* data.

The steady increase in gross activity release that followed the activity peaks in the case of the latter tests

at the higher pressure decay rate may have been caused by a gradual upward shift (or flattening) of the fission-product concentration profiles in the trap. Other factors that could have influenced the shape of the activity curves include the buildup of ^{138}Cs deposition in the gas lines and increased release of the shorter lived fission gases (^{138}Xe and ^{135m}Xe) during the latter half of the depressurizations.

Soon after the start of the pressurization half of each pressure cycle, the radiation monitor reading dropped quickly to a level between 10 and 20 mR/hr as a result of the inflow of clean gas into the fuel pin. The subsequent decay of the radiation monitor reading indicates ^{88}Rb and ^{138}Cs deposition in the line.

As was discussed in the preceding progress report,⁴ the indicated moisture level in the effluent sweep gas remained high even after weeks of purging with the inlet moisture probe indicating less than 1.0-ppm moisture. When the capsule was initially brought up in power, the sweep-gas effluent moisture level decreased slowly from 60 to about 40 ppm. Currently, the indicated level is approximately 35 ppm. One difference between the two probes is that the inlet probe has about 6 ft of electrical lead between it and the readout instrument and the outlet probe has about 70 ft because of its remote location in a shielded valve box. A recent reading taken at a lead connection 20 ft from the outlet probe was less than 1 ppm compared with a reading of 35 ppm at the 70-ft distance, indicating that the instrument lead is responsible for the high reading.

5.2 F-1 Irradiation Capsules for EBR-II

T. N. Washburn

Eight capsules were fabricated in conjunction with GGA for irradiation testing of GCBR fuel pins in the EBR-II. The planned irradiation tests will provide the initial evaluation of GCBR-type fuel pins with internal charcoal fission-product traps under fast reactor operating conditions. A typical capsule is shown in Fig. 5.6. The fuel pin consists of $(\text{U}_{0.85}\text{Pu}_{0.15})\text{O}_{1.98}$ clad with 0.300-in.-OD 0.263-in.-ID type 316 stainless steel tubing. These fuel pins are encapsulated in an outer container (0.778 in. OD) with an inner sleeve separating (radially) the sodium heat transfer medium into two regions. The inner sleeve acts as a thermal barrier. A series of cladding midwall temperatures between 590 and 790°C are achieved by having sleeves of different thicknesses. Each of the fuel pins will operate at a linear heat rate of approximately 15 kW/ft, and pins will be removed from the reactor at 25,000, 50,000, and 100,000 MWd/MT. The specific cladding temperature, heat-generation rate, and burnup for each capsule are given in Table 5.3.

In this cooperative program, GGA performed the test and engineering design and supplied all hardware components. Oak Ridge National Laboratory fabricated the fuel, fuel pins, and irradiation capsules.

The fuel column in these pins is 13.5 in. of 0.260-in.-OD 0.056-in.-ID annular pellets of 91% theoretical density. The pellet ends are dished 0.006 in.

Table 5.3. F-1 capsule assemblies for GCBR fast-flux irradiation tests

Capsule designation	Conditions			Purpose of test
	Cladding temperature (°C)	Heat generation (kW/ft)	Burnup (MWd/MT)	
G-3	700	15.5	25,000	Temperature calibration
-6	710	14.4	50,000	Comparison of performance in fast and thermal fluxes ^a
-4	700	14.9	100,000	Evaluation of effect of burnup ^a
-7	590	13.8	50,000	Evaluation in LMFBR temperature range ^a
-5	650	14.3	50,000	Evaluation in intermediate temperature range
-2	755	15.5	50,000	Evaluation in upper temperature range
-1	790	16.1	50,000	Evaluation in upper temperature range
-8	700	15.5	75,000	Evaluation of effect of burnup ^b

^aThe fuel pins contain active fission-product traps.

^bCapsule G-8 replaces capsule G-3 after the initial 25,000-MWd/MT exposure in a B-7 type subassembly.

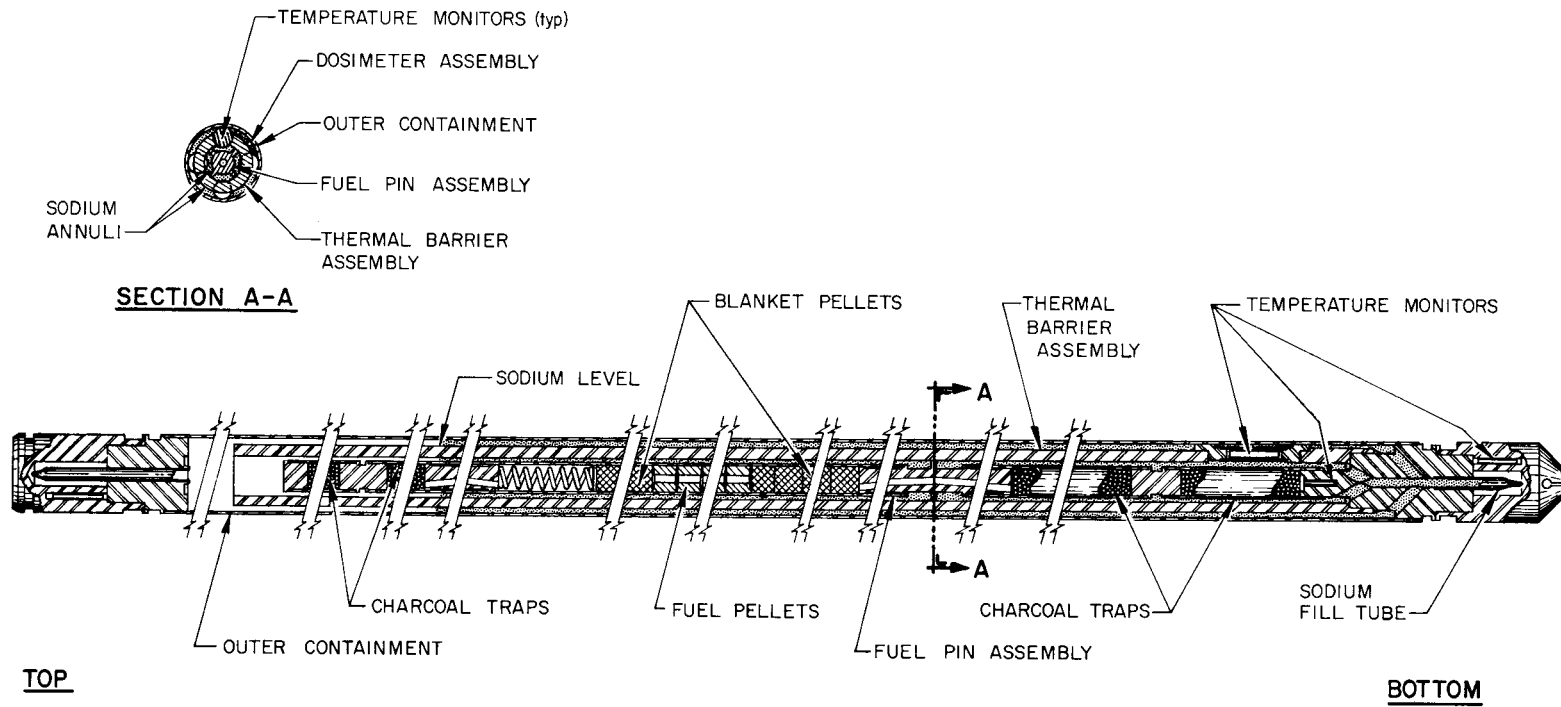


Fig. 5.6. GCBR F-1 irradiation assemblies.

There is 3 in. of natural UO_2 pellets at each end of the fuel column. All pins contain two 1.2-in.-long sealed containers filled with activated charcoal for the purpose of evaluating the effects of irradiation on sorption characteristics. Three of the lower temperature pins contain active charcoal fission-product traps about 11 in. long at each end of the pins. Fluence and temperature monitors are incorporated into each capsule.

5.2.1 Fuel fabrication (R. A. Bradley, J. D. Sease)

About 2 kg of powder was required for process development, pellet fabrication, and samples for characterization of the powder and sintered pellets. The powder was prepared by the standard sol-gel powder preparation process. Briefly, this process consists of blending PuO_2 and UO_2 sols, drying to a gel at 100°C , and grinding to -325-mesh powder in a fluid energy mill. For criticality reasons it was necessary to blend and dry this material in six batches, but these batches were interblended and reduced to two larger batches prior to grinding in the fluid energy mill. The powder was calcined by an oxidation-reduction technique which has been successful in producing powder that will sinter to 91%-dense pellets. Test sinters produced pellets with densities below that required; therefore, the powder was milled in a neoprene-lined ball mill with tungsten-carbide grinding media. This powder was prepressed at 80,000 psi and granulated to -20 mesh and then pressed into pellets at 16,000 psi. The pellets were sintered at 1550°C in an atmosphere of Ar-4% H_2 and centerless ground to final dimensions. Approximately 400 pellets were required for loading into fuel pins.

5.2.2 Fuel-pin fabrication (J. D. Sease, R. A. Bradley)

The fuel pins consist of separate sections for the charcoal traps, reflector spacers, plenums, and fuel, and all sections are joined by welds. The unique fuel-pin design, with its provision for incorporation of either active charcoal traps or empty plenum chambers, requires an unusually large number of seal welds on the primary fuel pin. Six fusion welds are employed in connecting and sealing the fueled region, the two reflector spacers, and the two trap (or plenum) chambers that comprise each fuel pin. Preproduction weld-qualification samples were examined by liquid-penetrant inspection, x-ray radiography, helium leak testing, and metallography. Each of the fuel-pin welds successfully passed each of the nondestructive tests listed above.

The design specification was $91 \pm 1\%$ -dense pellets to yield fuel-pin smear densities of 85% or less theoretical density. Pellets in four of the fuel pins exceeded 92% theoretical density. The smear density of two of these pins was less than 85% theoretical density, while for two pins it was more than 85% theoretical density. These deviations from design specification were approved by the GGA representative. The fuel loading for each pin is listed in Table 5.4.

5.2.3 Capsule fabrication (M. K. Preston, E. J. Manthos)

All hardware items were received from GGA and inventoried, and critical assembly dimensions were checked. All the capsule welds were qualified prior to assembly of the capsules, as required in EBR-II specifications. The capsules were then welded and inspected, and the welding and inspection data were

Table 5.4. Fuel loading of F-1 capsules

Capsule designation	Oxygen-to-metal ratio	Pellet density (% theoretical)	Smear density (% theoretical)	Fuel column length (in.)	Oxide weight (g)
G-1	1.992	91.8	82.6	13.63	109.5
-2	1.971	92.8	84.1	13.65	111.1
-3	1.987	94.3	85.5	13.54	111.9
-4	1.983	91.5	82.5	13.48	107.7
-5	1.990	92.8	83.5	13.60	110.2
-6	1.972	91.4	82.7	13.46	107.8
-7	1.984	91.5	82.5	13.51	107.9
-8	1.985	94.7	86.1	13.30	111.3

forwarded to GGA for inclusion in the data package. The procedures followed covered welding of end fittings to capsule tubes, helium leak testing, x-ray radiography, dimensional inspection and weighing, and inspection of sodium-bond quality by eddy current techniques. In addition, procedures for capsule fabrication were written.

Fabrication and inspection of the eight capsules were completed by the end of June. Chemical analyses of the sodium showed that oxygen contamination during filling was negligible. Eddy-current inspection of the outer-annulus sodium bond showed that the void size in general was less than $\frac{1}{16}$ in. in diameter and the largest void detected was about $\frac{3}{64}$ in. in diameter; the acceptance standard was $\frac{1}{8}$ in. On the basis of this, the bond quality is judged to be excellent. The inspection results were most encouraging because bonding of this quality in the outer annulus infers satisfactory bonding

in the inner annulus. It is not possible to inspect the quality of bonding in the inner annulus. The properties of the sodium bond for each capsule are listed in Table 5.5.

The as-fabricated data for the capsules were compiled as an addendum to the GGA data package. This addendum was forwarded to the EBR-II Project, GGA, and to the AEC as required by the *Guide for Irradiation Experiments in EBR-II*. The following items were sent to the EBR-II Irradiation Coordinator: four sample capsule welds (two each of top and bottom closures), radiographs of all capsule closure welds (with and without shape-correction form), radiographs of the overall capsule lengths, and radiographs showing the sodium level in each capsule.

The eight F-1 capsules were shipped to the EBR-II on July 20, 1970. Irradiation testing is tentatively scheduled to begin in November 1970.

Table 5.5. Sodium-bond quality in F-1 capsules

Capsule designation	Sodium-bond thickness (in.)			Thermal-barrier thickness (in.)	Sodium-bond discontinuities ^a	
	Inner annulus	Outer annulus	Total		Number	Maximum diameter (in.)
G-1	0.037	0.024	0.061	0.152	0	
-2	0.037	0.039	0.076	0.136	6	0.047
-3	0.067	0.050	0.117	0.095	5	0.052
-4	0.061	0.039	0.100	0.112	4	0.050
-5	0.037	0.047	0.084	0.129	5	0.047
-6	0.067	0.065	0.132	0.081	4	0.062
-7	0.090	0.075	0.165	0.047	6	0.040
-8	0.067	0.050	0.117	0.095	3	0.047

^aDiscontinuities over the fuel in the outer sodium annulus. Acceptable diameter of nonbond is 0.125 in. or less.

Part III. Prestressed-Concrete Pressure Vessel Research and Development

Introduction

G. D. Whitman

Program activities are now concerned with the completion of the concrete materials investigations and models studies. Work was reactivated on the thermal cylinder test, which had been deferred for a year, and the investigations on the effects of high temperature on concrete strength were terminated with the testing of a first series of specimens.¹

The concrete materials investigations are now concerned with the moisture migration experiments and the multiaxial creep projects. The former have been in operation for approximately two years, and data have been obtained routinely with no significant problems. It is now evident that free moisture movement in the

concrete chosen for study under a simulated thermal environment and mass configuration proceeds at a much slower rate than had been anticipated. Data on multiaxial concrete creep behavior are now being evaluated with the completion of a major portion of this phase of the concrete materials investigations. The techniques that were developed have been demonstrated to be adequate, and summary reports are in preparation.

The structural model tests on head-region behavior were analyzed in more detail, and two additional models were constructed to obtain more detail on crack initiation and propagation during overpressure loading. Work on the small thermal-cylinder experiment was reactivated after being suspended for a year. Most of the component parts for this experiment had been procured, and plans are now under way to cast the concrete structure during this fiscal year.

1. V. Bertero and M. Polivka, "Concrete Strength Properties as a Function of Temperature," pp. 132-139, *GCRP Semiann. Progr. Rept. Mar. 31, 1970*, USAEC Report ORNL-4509, Oak Ridge National Laboratory.

6. Concrete Materials Investigations

G. D. Whitman

The concrete materials investigations are planned to provide information that could be used in predictions of vessel behavior for the many regimes of loading experienced under design and hypothetical accident conditions. These investigations will also provide specific input for the predictions of the thermal cylinder experiment behavior.

A concrete made with Tennessee limestone aggregate was designated as the main mixture for study in the program. A limited number of studies are being made with two other concretes containing Alabama gray-wacke and chert aggregates to provide data on creep behavior for concretes having a range of elastic moduli. These three concretes have a nominal 28-day compressive strength of 6000 psi and are made with type II cement and $\frac{3}{4}$ -in. maximum-sized aggregate. The materials used in all tests were specified and furnished by the Waterways Experiment Station of the Corps of Engineers, Department of the Army, Vicksburg, Mississippi.

Work still in progress includes studies of time-dependent deformation of concrete under multiaxial stress conditions (creep-test program) and a moisture-distribution test on a simulated segment of a concrete pressure vessel (moisture-migration test). Work on concrete properties as a function of temperature has been terminated because of funding limitations.

The concrete creep projects are being conducted at the University of Texas and the Waterways Experiment Station. All experimental work on the phase I portion of the program at the University of Texas has been completed, including a destructive examination of the test specimens. The creep program at the Waterways Experiment Station is well along, and a major segment of the first phase of the experimental work is completed. The techniques developed by these organizations appear to have been generally satisfactory, and the data are being obtained as originally planned.

Since the temperature gradient was applied to the moisture-migration specimen in March 1970, there has been little change in moisture content in the specimen. Although there may be the first indication of moisture movement at this time the relative change has been much slower than had been anticipated when the experiment was designed.

6.1 Triaxial Creep Tests at the University of Texas

Thomas W. Kennedy Ervin S. Perry
Subcontract No. 2864

During the current reporting period, project activities included (1) analysis of data obtained from phase 1 of the project and the preparation of reports summarizing the findings and conclusions, (2) disassembly and examination of all specimens used in phase 1, (3) loading of specimens that had been allowed to cure one year, and (4) collection of data from all specimens still under test.

6.1.1 Data analysis and preparation of reports

The major activities during this period involved analyses of the data obtained from phase 1 of the investigation. These analyses consisted of a preliminary evaluation of all the data obtained from phase 1 and the development of a method of predicting long-term triaxial creep behavior for triaxially loaded specimens based on data obtained from short-term uniaxially loaded specimens.

The preliminary evaluation essentially consisted of a statistical analysis to determine the effects on creep behavior produced by changes in temperature, curing history (moisture condition), axial and radial stress levels, and time to evaluate the interaction effects of these factors. The findings from this preliminary evaluation have been summarized in Research Report 2864-2, "Experimental Investigation of Creep in Concrete Subjected to Multiaxial Compressive Stresses at Elevated Temperatures," along with the data obtained from the investigation. This report was completed and approved for publication, and it is currently being published in final form. Conclusions from this analysis are summarized in this progress report.

The second phase of the evaluation resulted in the development of predictive equations and techniques that can be utilized to predict multiaxial creep strains in specimens loaded under various combinations of multiaxial compressive stresses. The equations were derived by establishing a linear time-dependent relationship between creep strain and stress from uniaxial creep tests and by assuming that the law of superposition is applicable to creep. The development, theory, and evaluation of these equations and techniques were summarized in Research Report 2864-3, "An Approach

to Estimating Long-Term Multiaxial Creep Behavior from Short-Term Uniaxial Creep Results," which was approved for publication and is currently being printed in final form.

In addition, a third report, which summarizes the techniques utilized in conducting the experimental program, was completed as Research Report 2864-1, "An Experimental Approach to the Study of the Creep Behavior of Plain Concrete Subjected to Triaxial Stresses and Elevated Temperatures," and was approved for publication. Final publication was delayed by the extensive effort involved in the analyses of data and the preparation of reports summarizing the findings from these analyses.

Major conclusions and findings obtained from the preliminary analysis and the analysis to develop predictive equations are summarized below. These conclusions were based on data from 6- by 16-in. concrete cylindrical specimens prepared from a crushed-limestone aggregate and loaded 90 days after casting. They had a nominal 28-day compressive strength of 6000 psi. As-cast specimens were sealed in copper 48 hr after casting and were allowed to cure at 75°F, and the air-dried specimens were cured at 75°F and 60% relative humidity for 82 days before sealing in copper.

6.1.2 Conclusions from preliminary evaluation

Some of the general conclusions are the following:

1. After 90 or more days of curing, the unconfined compressive and indirect tensile strengths of as-cast concrete were greater than those of air-dried concrete. Concrete cured in lime-saturated water (standard ASTM curing) until tested, however, exhibited greater compressive and tensile strengths than concrete cured by either of the previous procedures.

2. The secant modulus of elasticity was greater for as-cast concrete than for air-dried concrete.

3. An increase in temperature at time of loading decreased the modulus of elasticity.

4. The elastic Poisson's ratio did not appear to be significantly affected by curing history, temperature, or stress conditions.

5. The thermal expansion of air-dried concrete was greater than that of as-cast concrete, and the thermal expansion of the concrete used in this study was less than that of steel.

6. Little or no shrinkage strain occurred in sealed specimens.

7. During the first 84 days after casting, the air-dried specimens exhibited shrinkage strains of approximately 220 micro-units, with shrinkage strains approximately

60 micro-units greater in the axial than radial direction. Beyond this time the axial and radial strains began to converge. At approximately 100 days after casting, the radial and axial strains became essentially equal and remained essentially constant throughout the remainder of the test period. Thus, little or no shrinkage occurred after 84 days, the time at which these specimens were sealed.

The results of this study show that creep in plain concrete under multiaxial compressive stress is a very complex phenomenon involving many interaction effects. Some of the conclusions on creep behavior are given below.

1. Several factors and interactions of factors produced highly significant effects on creep strain in plain concrete. The main factors were stress and nonlinear effect of stress, temperature during loading, curing history, and time after loading and nonlinear effect of time. The interactions were (a) temperature during loading times stress and temperature during loading times nonlinear effect of stress, (b) curing history times stress and curing history times nonlinear effect of stress, (c) time after loading times stress, (d) axial stress times radial stress, and (e) temperature during loading times type of curing times stress and temperature during loading times type of curing times nonlinear effect of stress.

2. Applied stress was the most important factor affecting creep strain. It was not only the most significant main effect, but it also produced highly significant interaction effects with each of the other main factors in this experiment. Radial stress was generally more significant than axial stress, since it involved two, rather than one, principal stress fields.

3. Compressive and tensile creep strains were larger for a higher constant temperature during loading; air-dried concrete, except for the case when the stress conditions produced a low tensile creep strain; increased time after loading; and increased stress for uniaxial and biaxial states of stress.

4. Under triaxial states of stress in comparable environmental conditions, creep strain increased or decreased depending on the magnitude of the changing stress and on the stress direction. For a relatively high constant stress in either the axial or radial direction, increasing the stress from zero in the direction perpendicular to the direction of the constant stress decreased the compressive creep strain in the direction of constant stress and changed the creep strain from tension to greatly increased compression in the direction of the changing stress. When the constant stress was relatively

low, an increase in stress in the direction perpendicular to the constant stress changed the creep strain in the direction of the constant stress from compression to tension and in the direction of the changing stress from tension to compression.

5. As the level of stress increased, the creep strain increased, but the increase was larger for concrete at a higher temperature relative to concrete at a lower temperature, for air-dried concrete relative to as-cast concrete, and as time after loading increased.

6. Increasing the confining pressure reduced the overall creep strains; that is, the sum of the absolute creep strains in all principal stress directions decreased.

Conclusions regarding Poisson's ratio for creep were the following:

1. A Poisson's effect did occur and the Poisson's ratio ranged from approximately 30% of the elastic Poisson's ratio to approximately equal to the elastic Poisson's ratio, the magnitude of which depended primarily on curing history and on the state of stress. The average Poisson's ratio for creep for the entire test period was 0.17, which was approximately 30% less than the average elastic Poisson's ratio.

2. Poisson's ratio for creep of air-dried concrete was approximately 25% less than for as-cast concrete.

3. The magnitude of stress and the state of stress influenced Poisson's ratio, but this influence was less at the higher temperatures and for air-dried concrete.

Conclusions on elastic recovery strains are given below.

1. The modulus of elasticity and Poisson's ratio for elastic recovery were essentially equal to the modulus of elasticity and Poisson's ratio at the time of loading.

2. The elastic recovery strains were generally slightly higher than the initial elastic strains, except for the air-dried specimens loaded at 150°F and for most hydrostatically loaded specimens.

Conclusions on creep recovery were that

1. Curing history appeared to be the only factor studied that significantly affected the percentage of creep recovered. A larger percentage of the creep strain, which occurred during one year under load, was recovered from the as-cast concrete than from the air-dried concrete.

2. Factors that caused larger creep strains generally caused larger total recovery strains, although they did not necessarily cause a larger percentage of the creep strains to be recovered.

Conclusions from development of predictive equations were that

1. Unit creep (creep strain per unit stress) of concrete under constant temperature and with a given curing history is a function of concrete age at loading, time after loading, and stress levels. When the applied stress is less than the creep proportional limit, unit creep of concrete is independent of stress levels.

2. The Poisson's ratio for creep of as-cast specimens was higher than that for air-dried specimens. At 75°F, the average Poisson's ratios for creep were 0.150 for as-cast specimens and 0.108 for air-dried specimens. At 150°F, the average Poisson's ratios were 0.149 for as-cast specimens and 0.140 for air-dried specimens.

3. The creep prediction technique developed by employing the unit creep function was satisfactory for predicting creep strains resulting from multiaxial stresses when stress levels were less than the creep proportional limit. For stress levels higher than the creep proportional limit, the measured creep strains were higher than the predicted values.

4. The unit creep function based on one-year creep test results can be used for predicting creep at later ages. However, creep tests longer than one year are needed to validate this technique.

6.1.3 Inspection and evaluation of test specimens

All creep and shrinkage specimens utilized in phase I were dismantled and destructively inspected five months after the creep specimens were unloaded. This inspection consisted of removing the specimens from the test frames, weighing the specimens to determine whether moisture loss had occurred, and visually inspecting the copper seal. Subsequently the copper was removed and the specimen broken in order to inspect the interiors and the gages to determine whether oil had penetrated the specimens and to ascertain the condition of the gages. This evaluation of the specimens has been completed and documented, but analysis of the findings has not begun.

6.1.4 Loading of specimens to evaluate the effect of age prior to loading

On June 17, 1970, four specimens, two as-cast and two air-dried, which had been allowed to cure for one year were loaded under uniaxial stress levels of 600 and 2400 psi. These specimens were loaded to obtain an estimate of the effect of age prior to loading and will be compared with similar specimens loaded December 17, 1969, six months after casting, and three months after casting (phase 1). No evaluation of the effects of age has been conducted; nevertheless, total strain data are presented in Table 6.1 to illustrate the nature of the

Table 6.1. Summary of instantaneous and 84-day total strain data obtained from phase 1A specimens

Uniaxial stress (psi)	Curing time (days)	Axial strain (micro-units)				Radial strain (micro-units)			
		As-cast		Air-dried		As-cast		Air-dried	
		Instantaneous	84-day total ^a	Instantaneous	84-day total ^a	Instantaneous	84-day total ^a	Instantaneous	84-day total ^a
600	90	93.1 ^b	126.4	87.3	140.2	-26 ^b	-12.1	-25.1	-24.3
	183	77.4	98.1	90.9	136.0	-22.6	-32.5	-23.2	-20.5
	365	99.8	92.6	73.7	99.2	-20.4	-31.9	-19.9	-17.0
2400	90	379.5	647.2	384.7	607.9	-103.8	-112.8	-93.5	-120.8
	183	385.7	589.7	385.1	600.7	-93.5	-118.7	-84.2	-102.1
	365	441.7	593.3	327.8	470.5	-84.9	-104.9	-89.6	-99.6

^aTotal strains include instantaneous, creep, and shrinkage strains.

^bPositive values indicate compressive strains, and negative values indicate tensile strains.

behavior being observed. Due to the short time the one-year specimens have been under load and the lack of detailed evaluation, no conclusion can be drawn at this time.

6.1.5 Data collection

During the first part of the reporting period, creep-recovery data were collected for the specimens in phase 1. In addition, creep data were also collected for all specimens from the portion of the study concerned with the effect of age at loading (phase 1A). This collection of data will continue for approximately one more year, but it is hoped that a meaningful analysis of the data can be made prior to the end of the total test period.

6.2 Multiaxial Creep Tests at Waterways Experiment Station

D. E. Harrison

The Waterways Experiment Station's part of an overall investigation of time-dependent deformation of concrete under multiaxial loading is concerned with one strength (6000 psi at 28 days), three aggregate types (chert, limestone, and graywacke), one cement (type II), two types of specimens (as-cast and air-dried), two levels of temperature during testing (73 and 150°F), and four types of loading (uniaxial, hydrostatic, biaxial, and triaxial). Creep recoveries of unloaded specimens in batches I through V are being monitored after being loaded for one year. Measurements of creep strains are continuing on specimens in batches VI, VII, and VIII.

6.2.1 Unloading procedure

Gages in specimens to be unloaded were read for two days prior to unloading. On the day of unloading, gages were read immediately before and following unloading and then at 3 and 6 hr after unloading. Readings were then taken once a day for two weeks and twice a week for three additional weeks. Specimens are being monitored once a week for the remainder of the three-month monitoring period. Results indicate that this procedure is satisfactory for monitoring creep recovery as a result of unloading.

6.2.2 Status of testing

All gage conditions are summarized in Table 6.2. The condition "NR" (Not Reading) means the gage has failed to read completely. The condition "Weak" means

the gage indicates a reading but is not necessarily reliable for true strain measurement.

On August 12, 1970, the unconfined compressive strength tests were completed. The 455-day tests were run on strength specimens cast in the first low-modulus batch to be cast. Complete results of this phase of testing are shown in Table 6.3. Generally the results are averages for three test cylinders; however, at least two cylinders were tested in all cases.

Representative plots for uniaxial specimens are shown in Figs. 6.1 through 6.4. These plots represent specimens at both temperatures (73 and 150°F) and both moisture conditions (air-dried and as-cast) and are corrected for environmental effects. In some cases, the data are incomplete due to gage failure.

6.2.3 Testing failures

All gages have failed in two main-modulus specimens subjected to biaxial loading ($\sigma_R = 2400$ psi) at 150°F. The membrane around two low-modulus specimens subjected to biaxial loading ($\sigma_R = 600$ psi) at 150°F ruptured and released all pressure on the 600-psi loading-manifold system. The membrane has been replaced, and the specimens have been reloaded with no adverse effect on the gages involved.

6.3 Moisture-Migration Test at Waterways Experiment Station

J. E. McDonald

The experimental study of moisture migration in a pie-shaped specimen (shown in Fig. 6.5) representing a section through a cylindrical wall of a prestressed-concrete reactor vessel was continued, with strain, temperature, and moisture data being obtained at various increments of time after application of the temperature gradient (80°F). The variation in concrete temperature along the specimen's center line is being determined with Carlson strain meters embedded as shown in Fig. 6.6. The temperature profile along the specimen has tended to stabilize as shown in Fig. 6.7. Latest temperature measurements (204 days after heating) are essentially the same as shown for 21 days. Temperature variations with time for typical individual gages are shown in Fig. 6.8.

A surface backscatter nuclear gage is being used to determine concrete moisture contents at the various stations indicated along the top surface of the specimen in Fig. 6.9. Representative plots of moisture content determined in this manner are presented for typical stations in Fig. 6.10. Curves of best fit calculated for

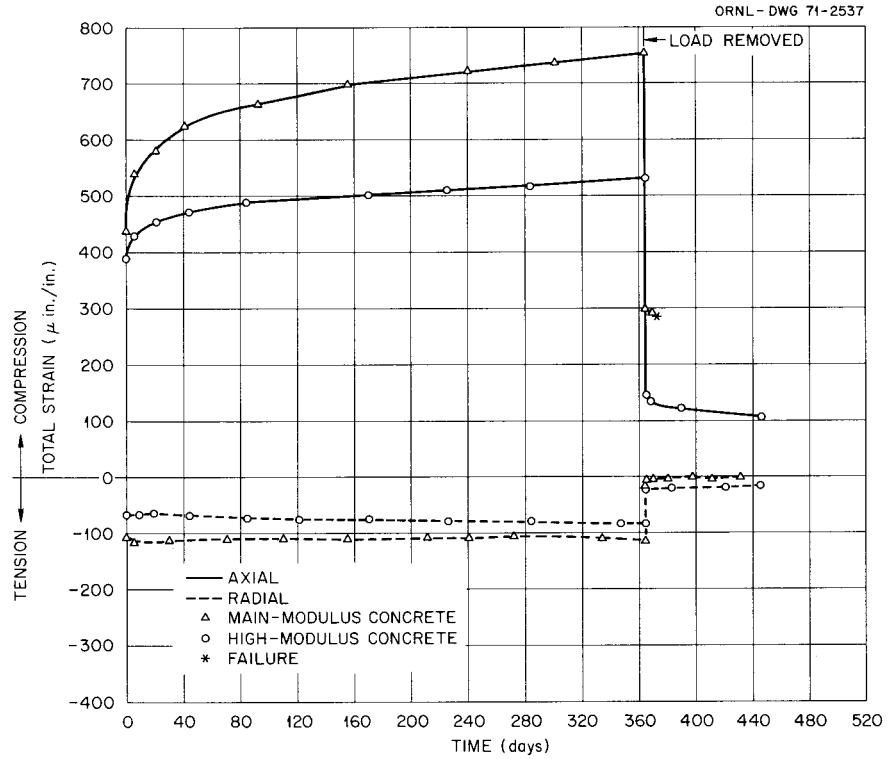


Fig. 6.1. Strain versus time curves for uniaxially loaded air-dried specimens tested at 73° F; $\sigma_z = 2400$ psi.

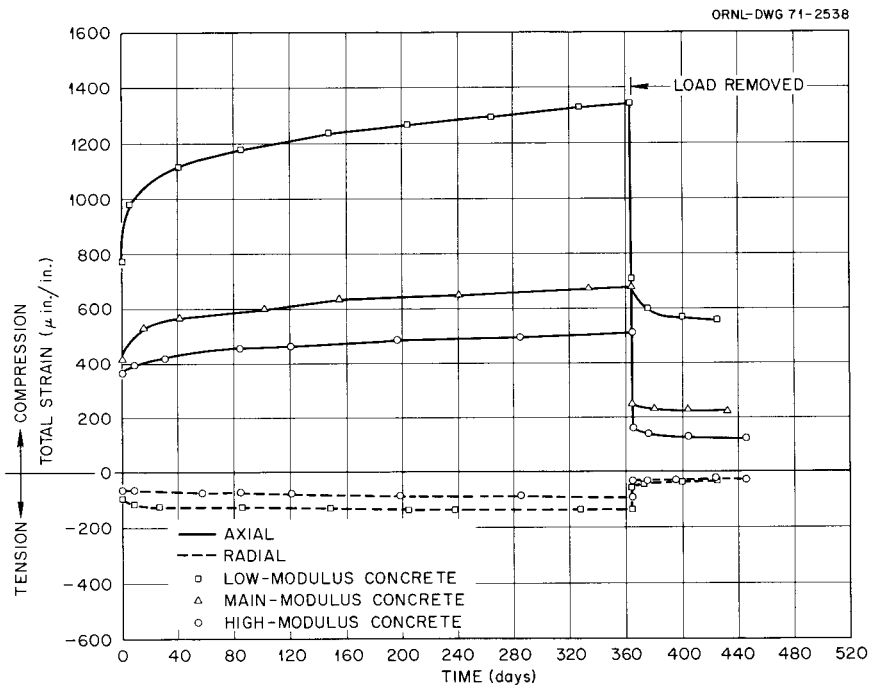


Fig. 6.2. Strain versus time curves for uniaxially loaded as-cast specimens tested at 73° F; $\sigma_z = 2400$ psi.

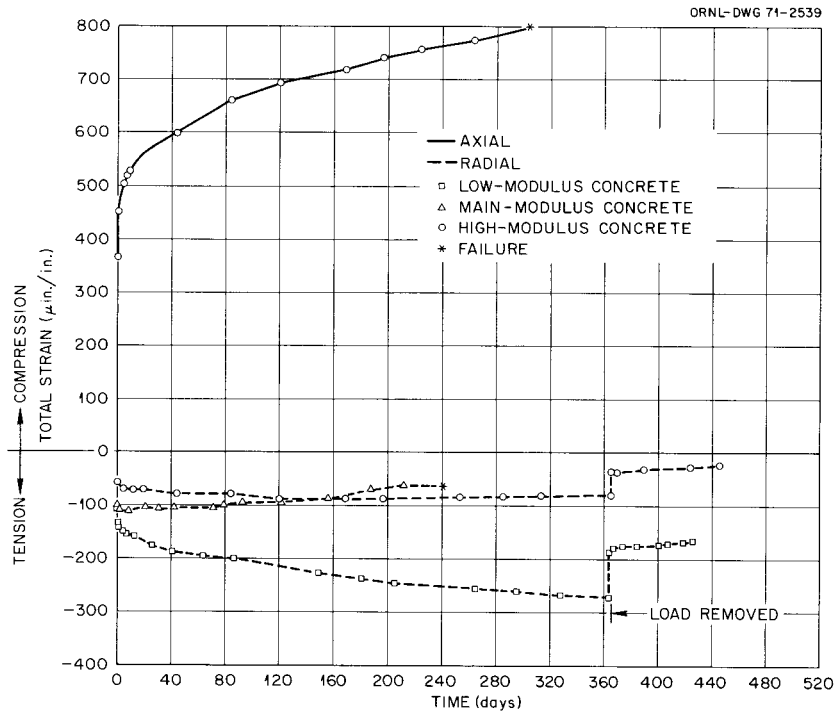


Fig. 6.3. Strain versus time curves for uniaxially loaded air-dried specimens tested at 150° F; $\sigma_z = 2400$ psi.

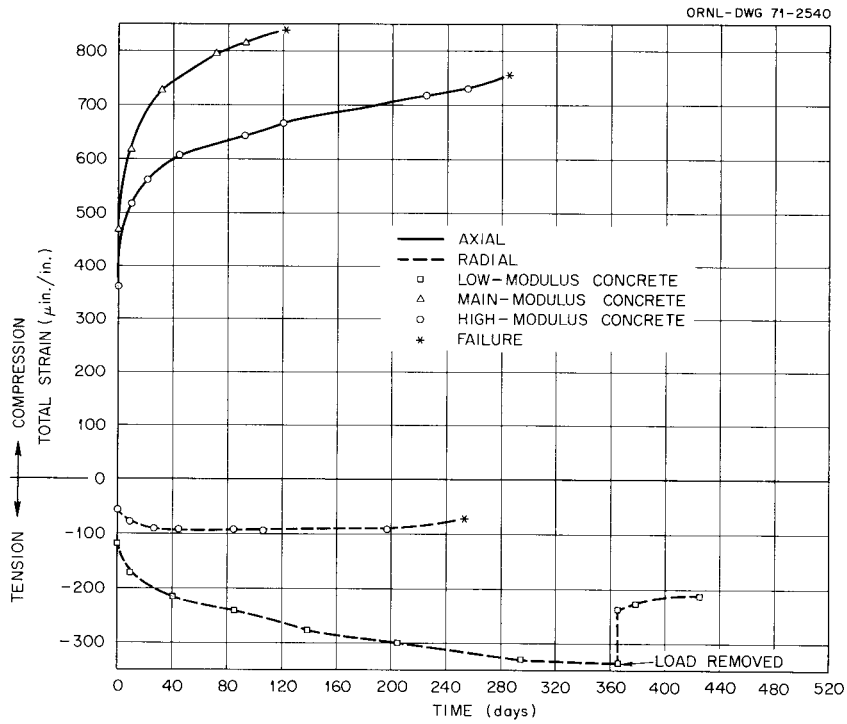


Fig. 6.4. Strain versus time curves for uniaxially loaded as-cast specimens tested at 150° F; $\sigma_z = 2400$ psi.

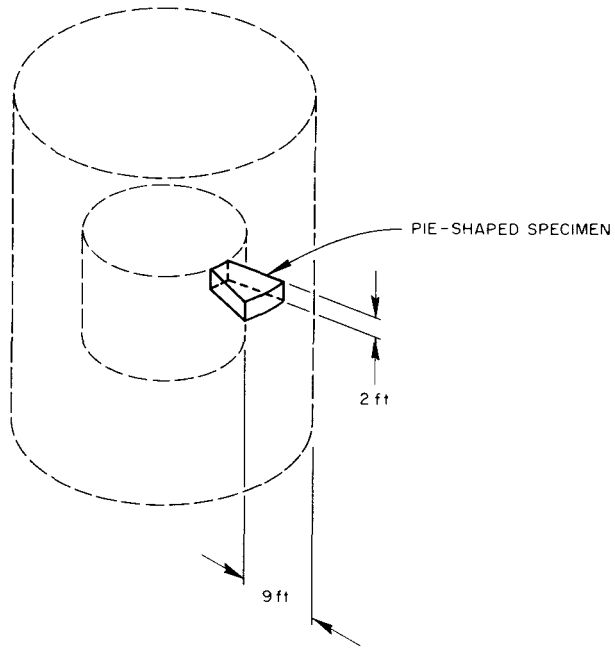


Fig. 6.5. Simulated location of specimen in vessel.

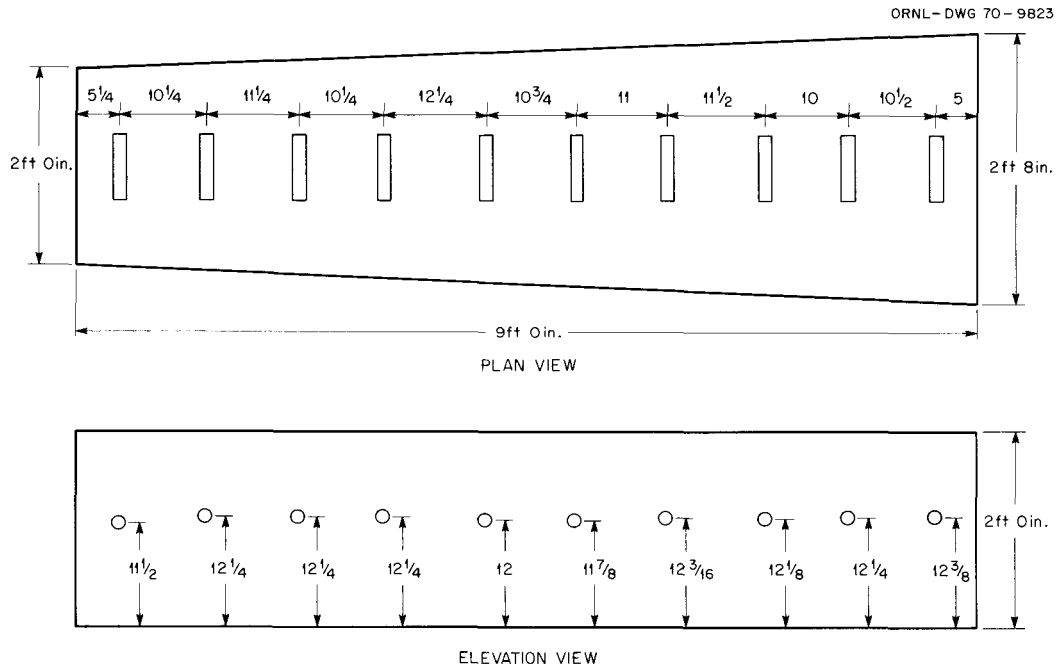


Fig. 6.6. Carlson strain meter locations.

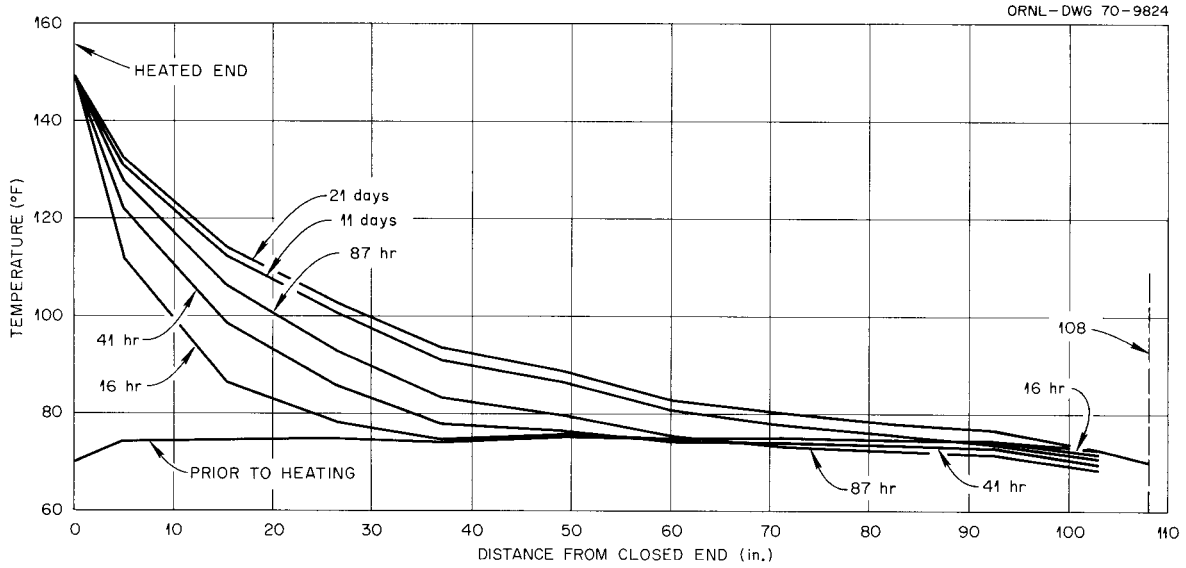


Fig. 6.7. Temperature variation along center line of specimen.

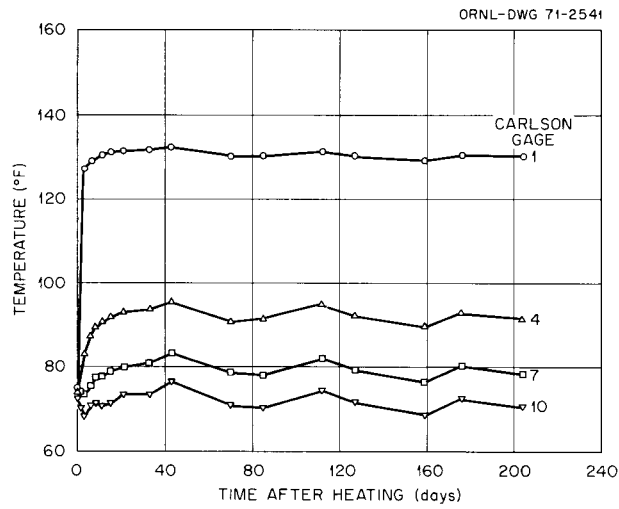
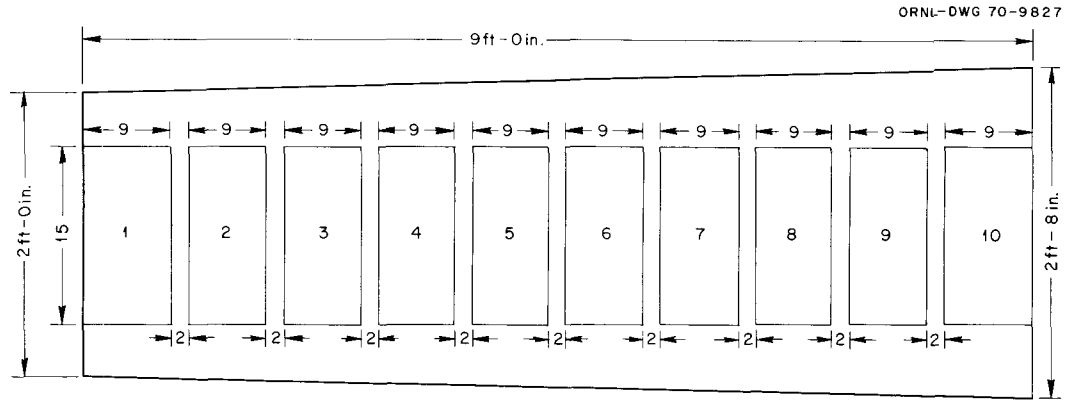


Fig. 6.8. Temperature versus time at Carlson gage locations.



DIMENSIONS ARE IN INCHES
EXCEPT WHERE NOTED

Fig. 6.9. Nuclear moisture gage stations.

Table 6.2. Summary of status of phase I creep program

Concrete modulus	Test condition	Date of casting	Date of loading	Age at loading (days)	Temperature (°F)	Load (psi)		Strain-gage performance in creep specimens				Remarks	
						Axial	Radial	As-cast		Air-dried			
								Axial	Radial	Axial	Radial		
High	Uniaxial	4-21-69	7-23-69	93	150	600	0	OK	OK	OK	OK		
		4-21-69	7-23-69	93	150	2400	0	OK	OK	OK	OK		
		4-21-69	7-23-69	93	73	2400	0	OK	OK	OK	OK		
	Hydrostatic	4-21-69	7-23-69	93	73	600	0	OK	OK	OK	OK		
		5-21-69	8-20-69	91	150	2400	2400	NR	NR	NR	NR		Test failed
		5-21-69	9-17-69	119	73	600	600	OK	NR	OK	OK		
	5-21-69	9-10-69	112	73	2400	2400	NR	NR	OK	OK			
	Biaxial	11-3-69	2-2-70	91	150	0	2400	NR	NR	OK	OK		
		11-3-69	2-2-70	91	150	0	600	Weak	Weak	Weak	Weak		
	Triaxial	11-3-69	2-3-70	92	150	2400	600	Weak	OK	OK	Weak		
11-3-69		2-3-70	92	73	2400	600	OK	OK	OK	OK			
Main	Uniaxial	5-7-69	8-5-69	90	150	600	0	OK	OK	Weak	Weak		
		5-7-69	8-5-69	90	150	2400	0	Weak	Weak	Weak	Weak		
		5-7-69	8-5-69	90	73	600	0	OK	OK	OK	OK		
		5-7-69	8-5-69	90	73	2400	0	OK	Weak	OK	OK		
	Biaxial	6-4-69	9-3-69	91	150	0	600	OK	Weak	OK	OK		
	Hydrostatic	6-4-69	9-17-69	105	150	2400	2400	OK	OK	OK	OK		
		6-4-69	9-3-69	91	73	0	600	OK	OK	OK	OK		
	Hydrostatic	6-4-69	10-3-69	121	73	600	600	NR	OK	OK	Weak		
		6-4-69	9-17-69	105	73	2400	2400	OK	OK	OK	OK		
	Biaxial	7-30-69	12-8-69	131	150	0	2400	NR	NR	NR	NR	Test failed	
	Triaxial	7-30-69	11-12-69	105	150	2400	600	Weak	OK	OK	Weak		
		7-30-69	10-30-69	92	73	2400	600	OK	OK	NR	OK		
	Biaxial	7-30-69	11-4-69	97	73	0	2400	OK	OK	OK	NR		
Low	Uniaxial	5-14-69	8-12-69	92	150	2400	0	Weak	OK	Weak	OK		
	Hydrostatic	5-14-69	8-19-69	99	150	2400	2400	NR	NR	NR	NR	Test failed	
	Uniaxial	5-14-69	8-12-69	92	73	2400	0	OK	OK	OK	OK		
	Hydrostatic	5-14-69	10-3-69	143	73	2400	2400	NR	NR	Weak	Weak		
	Uniaxial	11-18-69	2-16-70	90	150	600	0	OK	OK	OK	OK		
	Biaxial	11-18-69	2-17-70	91	150	0	2400	OK	NR	OK	Weak		
		11-18-69	2-16-70	90	150	0	600	OK	OK	OK	OK		
	Triaxial	11-18-69	2-16-70	90	150	2400	600	NR	NR	Weak	OK		
11-18-69		2-16-70	90	73	2400	600	OK	OK	Weak	OK			

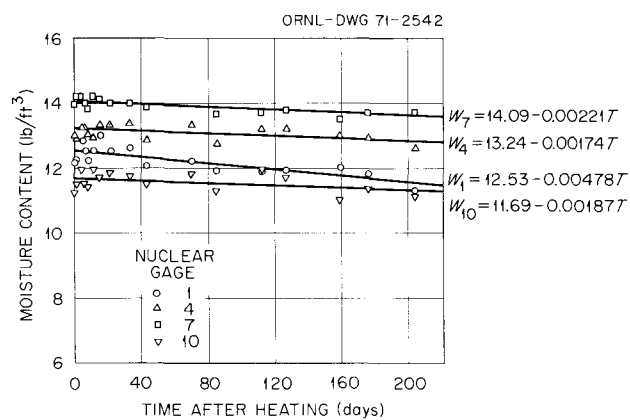


Fig. 6.10. Moisture content versus time.

Table 6.3. Compression test results

Batch	Modulus	Age (days)	Temperature (°F)	Average strengths of three cylinders (psi)		
				Air-dried	As-cast	Limewater
I	High	28	73	6970	6690	6840
		90	73	8010	7890	8400
		189	73	9250 ^a	7480 ^a	
		189	150	8880 ^a	8660 ^a	
		365	73	8840 ^a	8160 ^a	
		365	150	8410 ^a	10010 ^a	
		455	73	9480 ^a	8160 ^a	
		455	150	9030 ^a	9855 ^a	
II	Main	28	73	7320	6600	7420
		90	73	8110	7480	8840
		183	73	8590 ^a	8590 ^a	
		183	150	7890 ^a	8560 ^a	
		365	73	8660 ^a	9110 ^a	
		365	150	8380 ^a	9430 ^a	
		455	73	8980 ^a	9140 ^a	
		455	150	8380 ^a	8690 ^a	
III	Low	28	73	6700	6320	6370
		90	73	7570	7160	7940
		183	73	8220 ^a	8370 ^a	
		183	150	7990 ^a	8690 ^a	
		365	73	8530 ^a	9350 ^a	
		365	150	8710 ^a	8200 ^a	
		455	73	8345 ^a	9350 ^a	
		455	150	9295 ^a	9250 ^a	
IV	High	28	73	6540 ^b	5670 ^b	6290
		90	73	7430	7030 ^b	7610
V	Main	28	73	6800 ^b	6010 ^b	
		90	73	7870	7250 ^b	8140
VI	Main	28	73	7350	6080 ^b	7650
		90	73	8250	7490 ^b	9060
VII	High	28	73	7080	6190	6950 ^b
		90	73	8250	7470	8490 ^b
VIII	Low	28	73	7500	6330	7010 ^b
		90	73	8050	8150	8630 ^b

^a Average for two cylinders.^b Average for six cylinders.

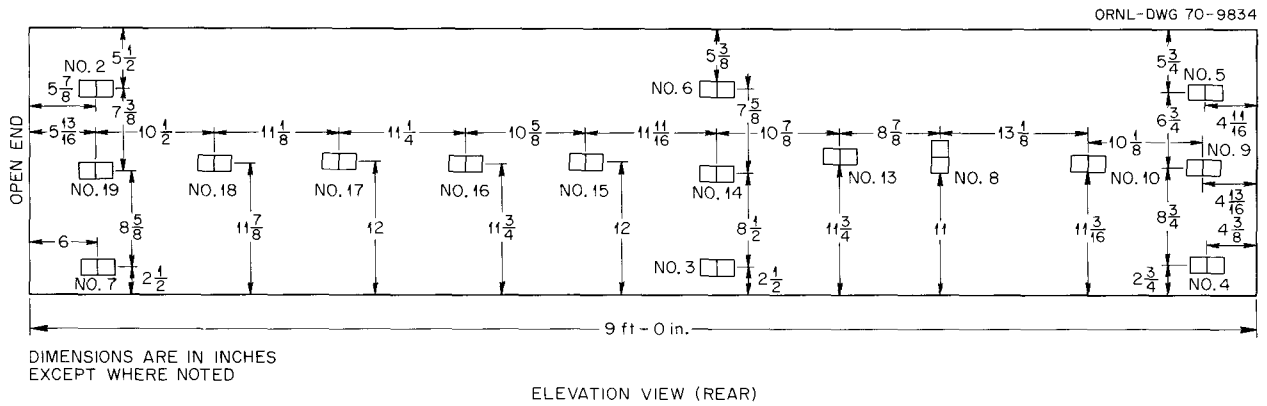


Fig. 6.11. Position of open-wire line gages.

each station indicate decreases in moisture content with the largest decrease occurring at the station nearest the heated end and generally uniform decreases at the other stations.

Open-wire-line (OWL) probes are being used to determine relative dielectric constants at various stations along one side of the specimen, as shown in Fig. 6.11. Null frequencies and, consequently, the relative dielectric constants are affected not only by the moisture content in the concrete but also by the temperature; therefore application of the temperature gradient resulted in apparent increases in the relative dielectric constant, as shown in Fig. 6.12. However, as the temperature tended to stabilize at approximately 20 days, output from the OWL probes located at the closed end and middle of the specimen began to exhibit slight decreases in relative dielectric constant, which would indicate a decrease in moisture content. Output from probes near the open end is quite erratic; however, from about 40 days after heating, the trend indicates a decrease in moisture content.

Prior to application of heat, the Monfore relative humidity probe indicated that the relative humidities in each well were in an essentially steady state at approximately 96%. Upon application of heat, the indicated relative humidity in those wells nearest the heat increased rapidly to 100% and, within 21 days, all wells, with the exception of the three nearest the open end, were at 100% relative humidity. These wells near the open end continue to indicate relative humidities ranging from 90 to 97%.

Variations in concrete strain along the specimen's center line as a result of applying a temperature

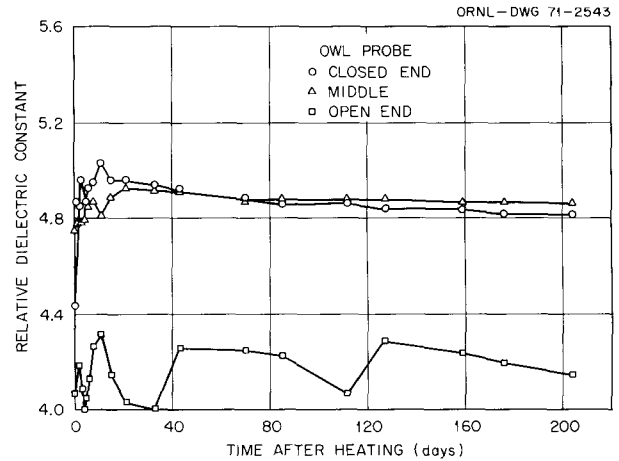


Fig. 6.12. Relative dielectric constant versus time.

gradient are presented in Fig. 6.13. The highest indicated strain is about 325 micro-units at the station nearest the heat. From this maximum, indicated strains decrease in a generally linear manner to less than 25 micro-units near the open end. Strain variations with time at typical stations are shown in Fig. 6.14. As expected, these curves are of the same general shape as those of temperature versus time. When the total strains are corrected for thermal expansion of the specimen (Fig. 6.15), the two stations nearest the heated end (1 and 4) appear to indicate a slight expansion, with the stations nearest the open end exhibiting a slight contraction.

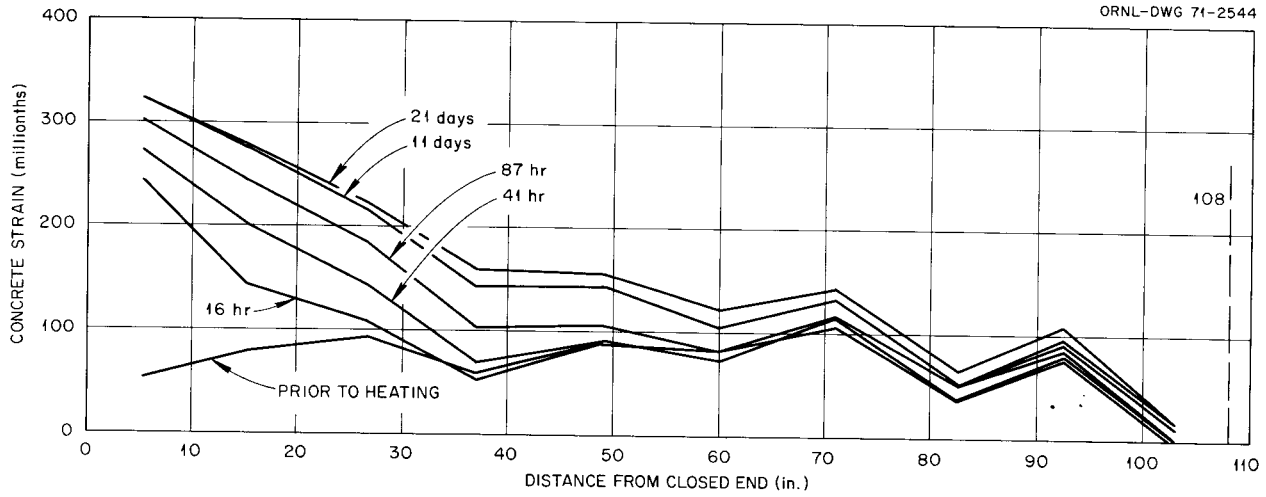


Fig. 6.13. Indicated strain distribution versus time.

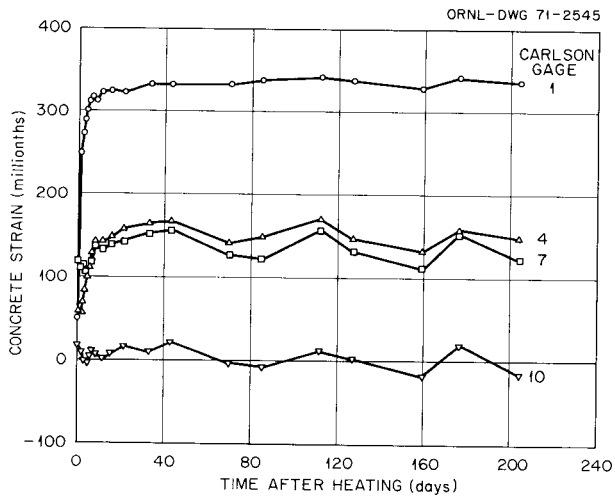


Fig. 6.14. Indicated strain versus time.

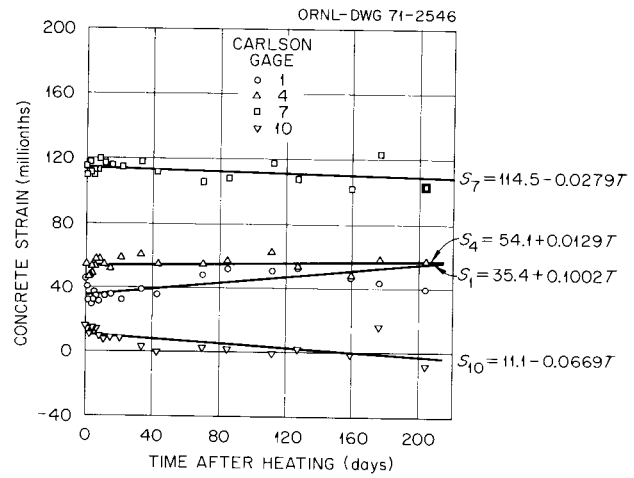


Fig. 6.15. Corrected strain versus time.

7. Model Studies

7.1 Structural Behavior of Prestressed-Concrete Reactor Vessels

M. A. Sozen W. C. Schnobrich
S. L. Paul

University of Illinois, Subcontract No. 2906

One of the critical structural failure modes of cylindrical prestressed-concrete pressure vessels with flat end slabs is the failure of the end slab in shear. The study of this type of failure is of importance because the dimensions of end slabs of pressure vessels make them susceptible to shear failures and because the failure mechanism for shear failures is not clearly defined.

As indicated in the previous progress report,¹ a series of tests of pressure vessels with and without openings in the end slab have defined the series of events leading to shear failure. As the internal pressure is increased, an inclined crack forms near the middepth of the end slab and in the vicinity of the anchorage plates of the longitudinal reinforcement. This crack propagates in both directions; it reaches the edge of the anchorage plates at a nearly constant angle of 45° in one direction and to the center of the slab in the other direction at an increasingly flatter angle. In effect, the fully developed inclined crack carves a dome out of the end slab. Final collapse is associated with the failure of the inverted dome when the concrete is subjected to a critical combination of normal and shearing stresses. Accordingly a quantitative prediction of the shear strength of

the end slab requires (1) the prediction of the load corresponding to the initiation of the inclined crack, (2) the prediction of the trajectory of the fully developed inclined crack or the shape of the inverted dome that results from development of the inclined crack, and (3) the prediction of the failure of the dome with the use of a suitable failure criterion for concrete subjected to triaxial stresses. Analytical and experimental studies relative to these three objectives have been in progress and are described briefly in the following section.

7.1.1 Test vessels with special instrumentation

Study of the shear failures that occurred in some of the specimens of the preceding series of 21 test vessels indicated that one of the important factors in developing a theory for the strength of end slabs was the correct prediction of the stress or strain distributions within the end slab of the vessel. To this end, two new test vessels were designed, constructed, and instrumented. These vessels are indicated in Fig. 7.1 and have the same overall dimensions as test vessel PV16, which was used as the basic module for the series of five tests investigating the effect of openings in the end slab. As indicated in Fig. 7.1, one of the vessels has a solid end slab, while the slab of the other one contains openings.

In addition to the usual complement of instrumentation measuring strains and deformations on the inner and outer surfaces of the pressure vessels, these test vessels contained a total of 180 strain gages embedded in the end slab to measure radial and circumferential strains, as shown in Figs. 7.2 and 7.3. The primary function of these gages is to trace the development of strain leading to the initiation of the inclined crack within the end slab and to measure strain distributions in the dome that result from formation of the fully developed inclined crack.

1. M. A. Sozen, W. C. Schnobrich, and S. L. Paul, "Shear Failures in End Slabs of Prestressed Concrete Pressure Vessels," *Proceedings of Gas-Cooled Reactor Information Meeting*, Oak Ridge National Laboratory, April 1970, USAEC Report CONF-70041, 1970.

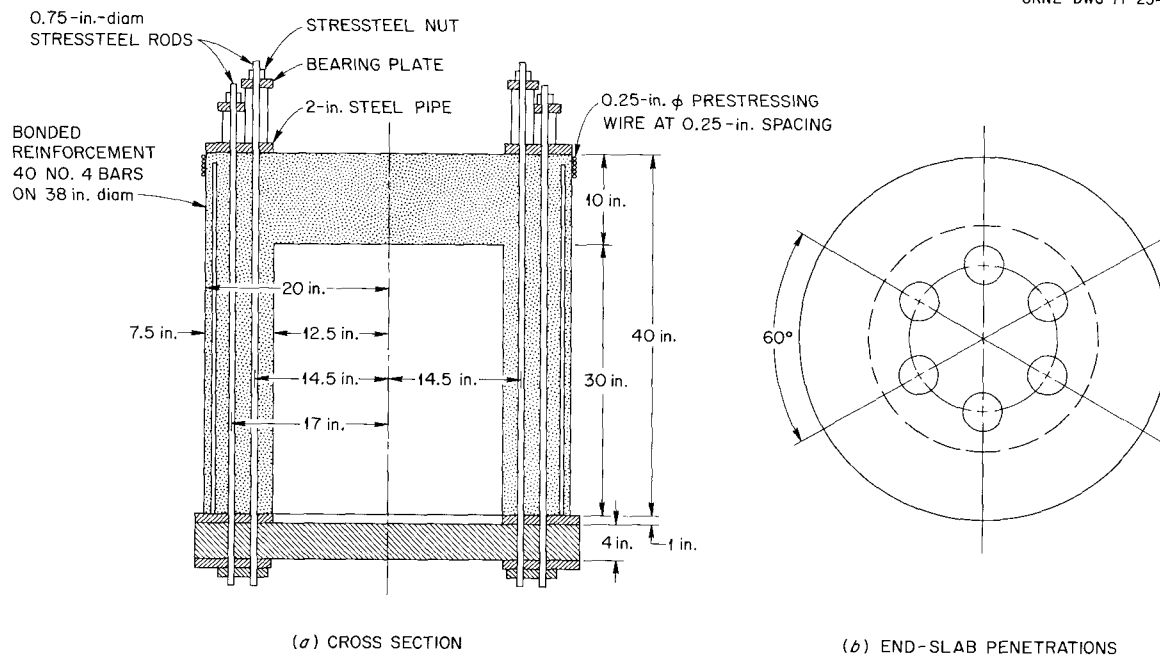


Fig. 7.1. Overall dimensions of test vessels PV22 and PV23.

7.1.2 Studies of experimental data

The correct interpretation of the available data is essential to a meaningful confirmation of any theory that may be developed as a result of these studies. Because strain measurements made at any location in the pressure vessels can be affected not only by one but by various phenomena and because these phenomena are of importance in understanding the mechanism of shear failure, a series of analytical studies was undertaken in order to interpret the strain data. An example is provided in the following paragraphs.

Figure 7.4 shows the extent of an assumed radial crack in the end slab in a finite-element model representing PV16, one of the test vessels. The calculated radial strains in the end slab are plotted in Fig. 7.5. The plot is based on an arbitrarily selected value of the internal pressure, 3200 psi. The solid lines indicate the radial strains calculated for an uncracked end slab at 3200 psi, while the broken lines indicate the radial strains calculated for an end slab with a radial crack as shown in Fig. 7.4 at an internal pressure of 3200 psi. The plotted strains indicate that the radial crack will cause an increase in strain on the outside of the vessel at locations close to the interior edge of the sidewall.

Figure 7.6 shows, in two dimensions, the locations of an idealized inclined crack in the end slab. Calculated radial strains are plotted in Fig. 7.7, which show, at an internal pressure of 3200 psi, strains calculated for an end slab with no cracks and for an idealized end slab with the inclined crack shown in Fig. 7.6. The strains plotted in this figure indicate that on the outer surface of the end slab and near the inner edge of the vessel wall, the development of the inclined crack results in a decrease of the radial strain. As in Fig. 7.5, the solid lines refer to strains in the uncracked slab, and broken lines refer to strains in the slab with the idealized shear crack.

Figure 7.8 shows the strains measured on the outer surface of the end slab of vessel PV16 at a radius of 12 in. It may be seen that at an internal pressure of 1500 psi, there is a sudden increase of the measured compressive strain rate that is reversed at approximately 2500 psi. On the basis of the trends shown by the calculations, it is evident that the strain-gage readings were affected initially by the development of radial cracks and then by the development of the inclined crack to the tension surface of the end slab. Thus, it becomes possible to make reasonably firm conclusions about internal crack development on the basis of strains measured on the surface.

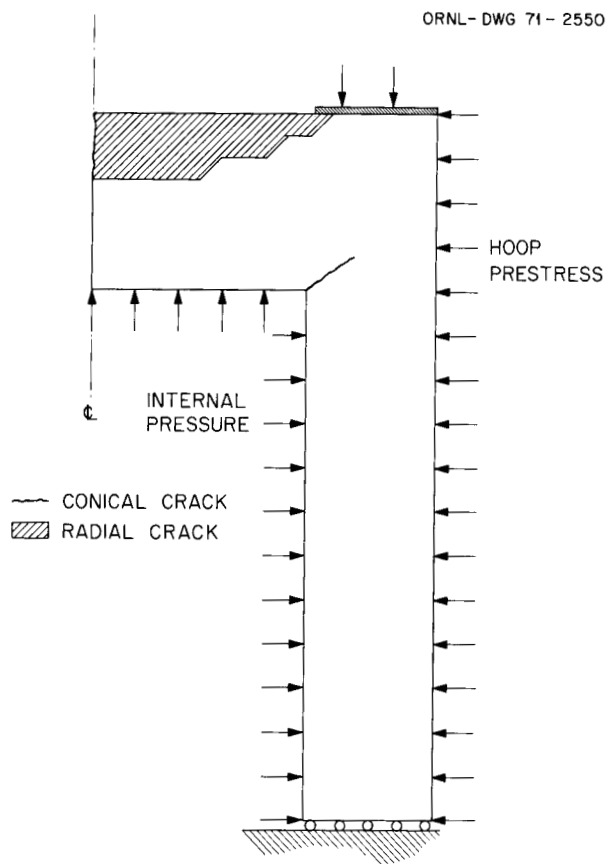


Fig. 7.4. Extent of assumed radial cracking in the finite-element analysis.

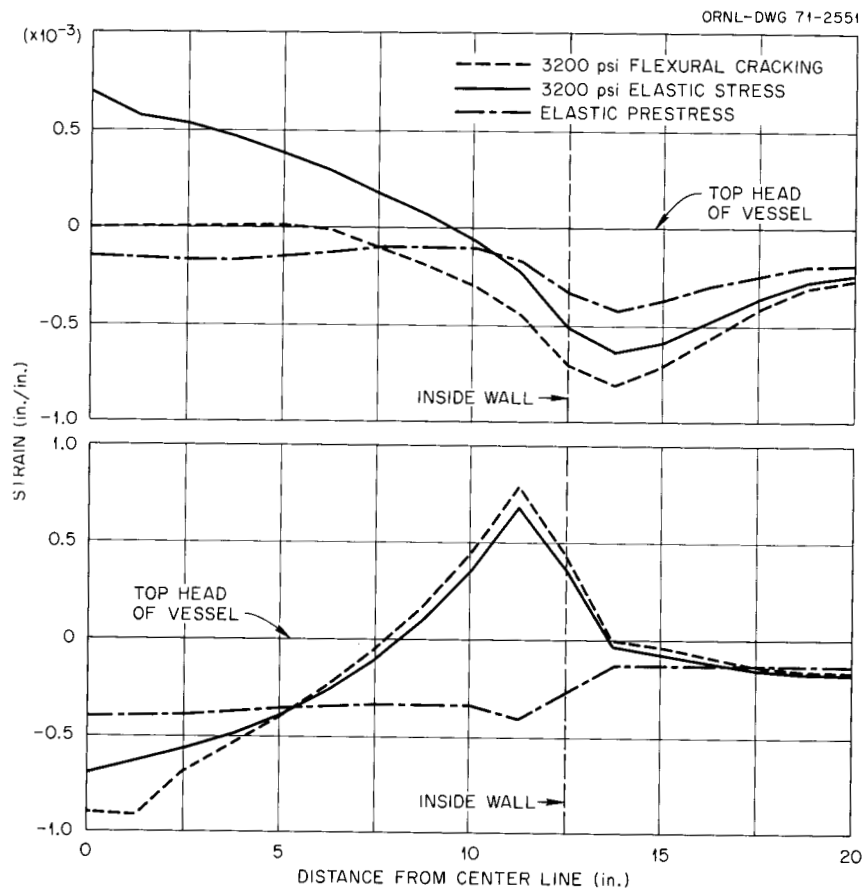


Fig. 7.5. Calculated radial strains at 3200 psi for PV16 before introduction of assumed radial crack.

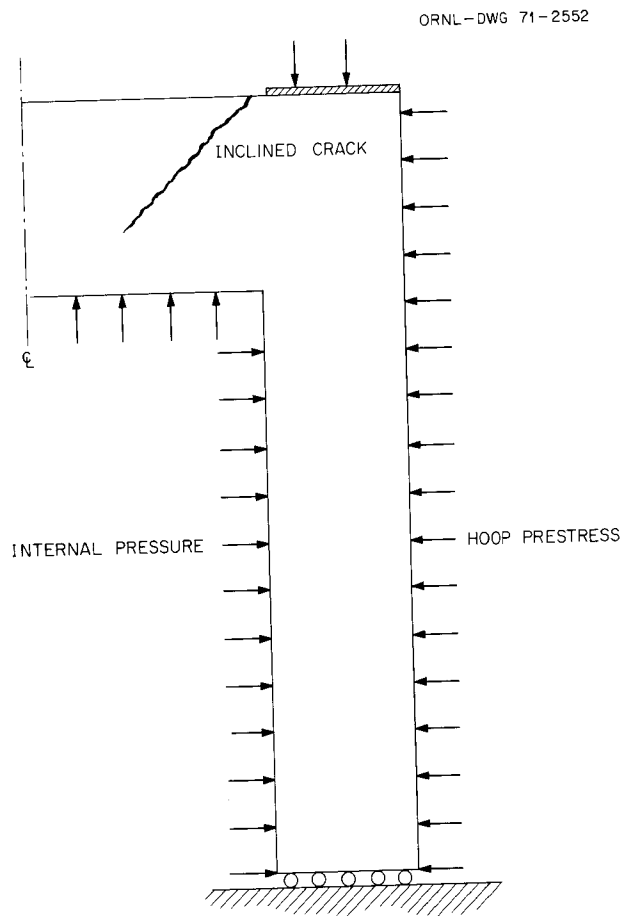


Fig. 7.6. Extent of assumed inclined crack in the finite-element analysis.

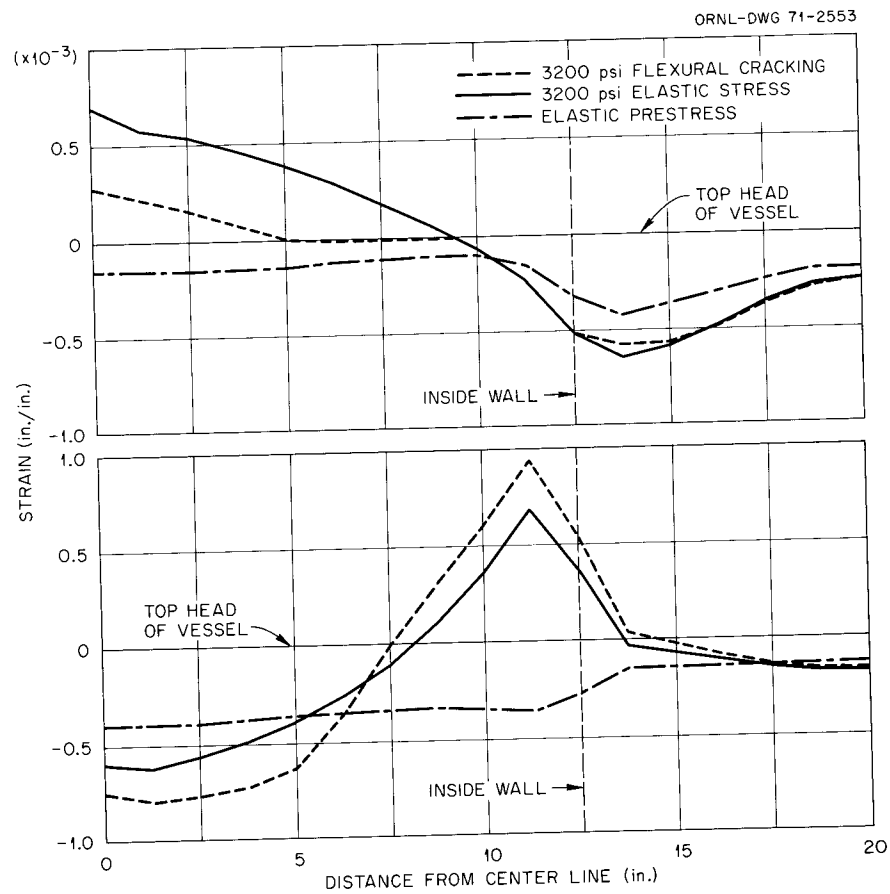


Fig. 7.7. Calculated radial strains at 3200 psi for PV16 before and after introduction of assumed inclined crack.

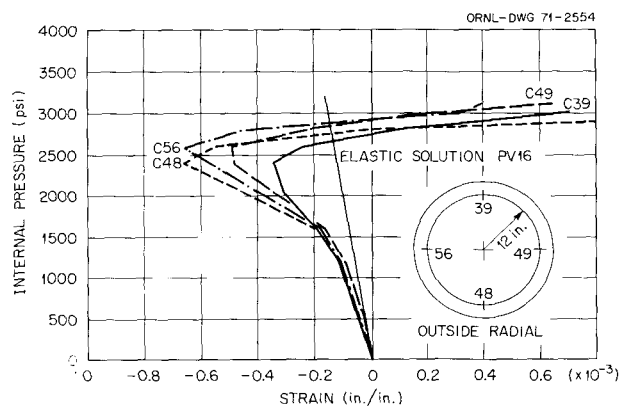


Fig. 7.8. Radial strains on outer surface of end slab at a radius of 12 in. for PV16.

7.1.3 Supporting analytical studies

Two analytical programs are being used to define the stress field and the cracking state in the end slab of the test vessels. A lumped-parameter model,² as illustrated in Fig. 7.9, has the material properties of the vessel concentrated at selected points. By varying the material properties at these points the crack development can be computed and propagated with increasing load levels. This procedure predicts an early formation of an inclined crack at about middepth in the end slab. This crack then propagates upward with increasing load toward the anchorage plate of the longitudinal rods and down toward the center of the vessel head. Additional circumferential as well as radial cracks form during this time. A cracking state is thus predicted, as shown in Fig. 7.10. The main inclined crack tends to become shallow and propagate horizontally near the center of the vessel head. Varying the hoop constraint of the circumferential prestressing and the effect of the anchorage plates for the longitudinal rods shows that these factors have a strong influence on the inclined crack.

The lumped-parameter model also provides stress, strain, and displacement values at the various load levels. Figure 7.11 shows a comparison of the numeri-

2. R. Higashionna and W. C. Schnobrich, Lumped-Parameter Analysis for Shear Failure in the End Slab of Cylindrical Prestressed Concrete Pressure Vessels, Civil Engineering Studies, Structural Research Series No. 363, University of Illinois, August 1970.

cally computed strain versus the experimentally obtained values at the same position in the vessel. Similar plots for other locations also show good correlation. A plot of the center deflection, Δ , versus pressure is shown in Fig. 7.12. Here the correlation is not so good. The figure also shows the influence of increasing the hoop constraint from the circumferentially continuous anchorage plate.

In order to define the elastic strain state around the openings in the vessel head, an isoparametric finite-element³ approach was developed. These elements have the advantage that they can have curved surfaces for their faces. Also these elements do not have directional problems like many other elements. An array of elements, such as that shown in Fig. 7.13, was used to compute the stress and strain values around the opening in the head of vessel PV18. A typical plot of the radial stresses in the vessel head is shown in Fig. 7.14.

7.2 PCR V Thermal-Cylinder Test

J. M. Corum J. P. Callahan
M. Richardson

Preparations for the thermal cylinder test at ORNL were reactivated after being suspended during fiscal year 1970 due to the reduction in PCR V funding. The test specimen and the testing plan were described in ref. 4. The time schedule shown in ref. 4 has in effect been moved up one year.

The objective of the thermal-cylinder test is to simulate, as closely as possible, the middle section of the cylindrical portion of a prestressed-concrete reactor vessel and the conditions imposed on it. The resulting test specimen is shown, in simplified form, on the right in Fig. 7.15. The specimen is sealed at top and bottom and on the inner and outer surfaces to eliminate any net moisture loss, and the ends are also insulated thermally. The moisture flow and heat flow will thus be confined primarily to the radial direction and will simulate conditions near the middle of the actual vessel. The specimen is prestressed axially and circumferentially, and internal pressure can be applied to the inner

3. B. M. Irons and O. C. Zienkiewicz, "The Isoparametric Finite Element System - A New Concept in Finite Element Analysis," paper presented at Conference on Recent Advances in Stress Analysis, Royal Aeronautical Society, March 1968.

4. J. M. Corum and G. C. Robinson, Jr., "Thermal-Cylinder Test to Simulate Behavior of Cylindrical Portion of a Prestressed-Concrete Vessel," pp. 225-239, *GCRP Semiann. Progr. Rept. Mar. 31, 1969*, USAEC Report ORNL-4424, Oak Ridge National Laboratory.

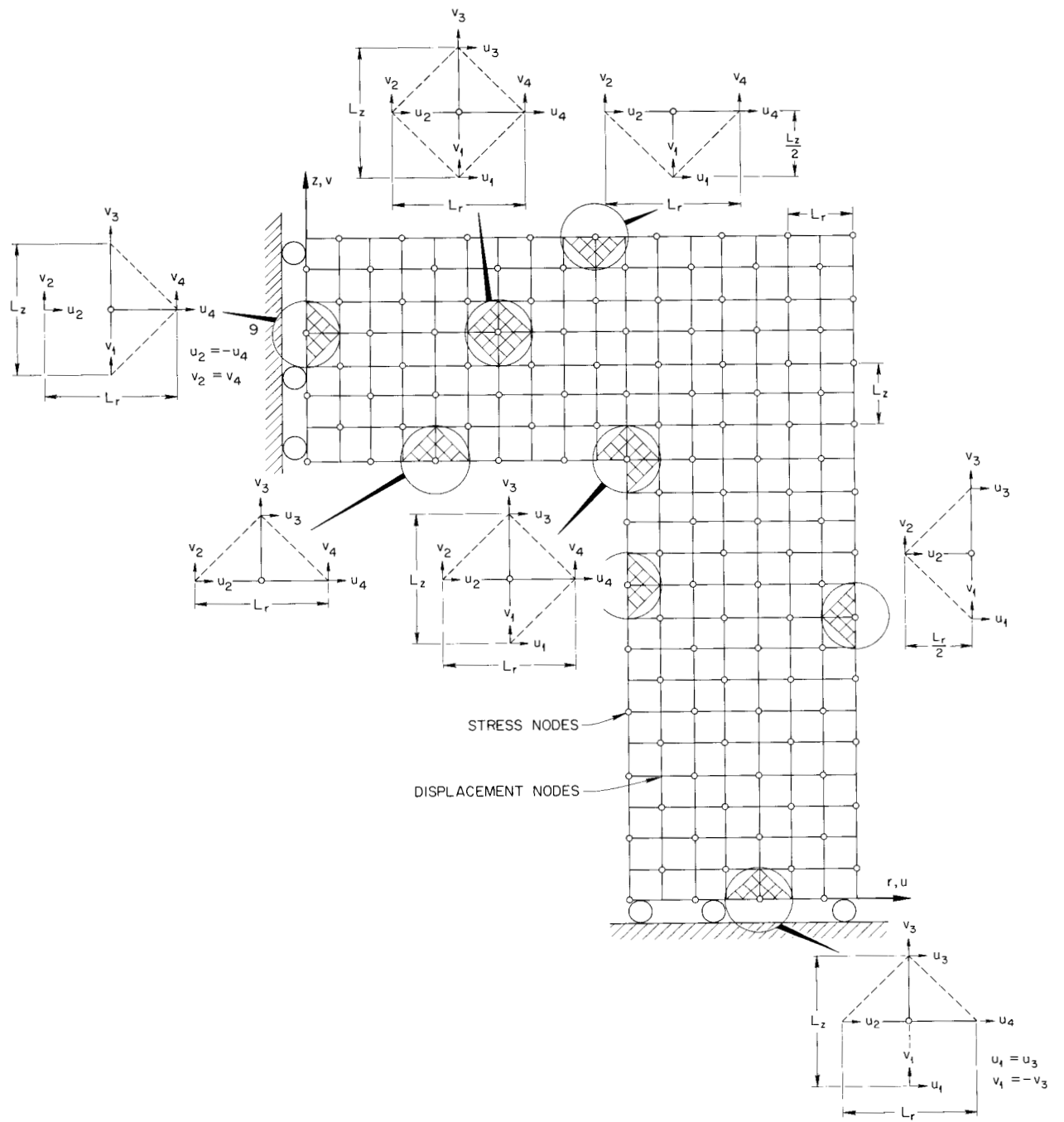


Fig. 7.9. Lumped-parameter representation of the pressure vessel.

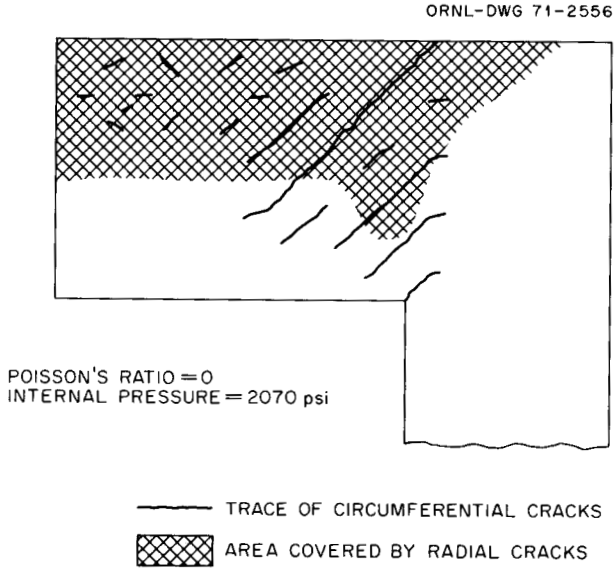


Fig. 7.10. Crack trajectories.

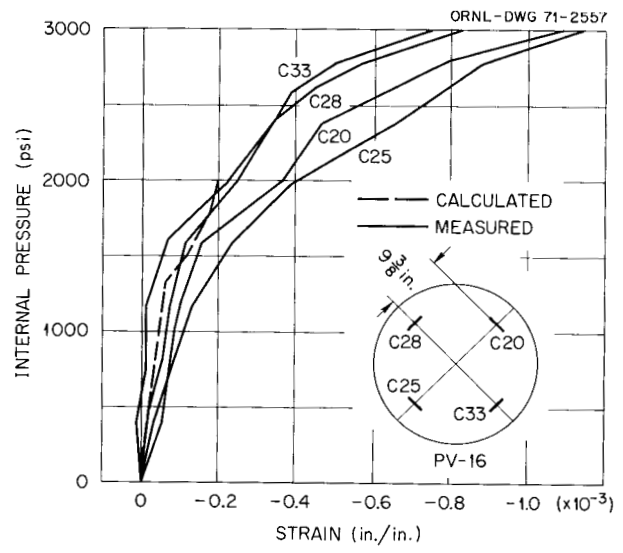


Fig. 7.11. Internal pressure versus inner circumferential strain at radius of 9 3/8 in. for PV16.

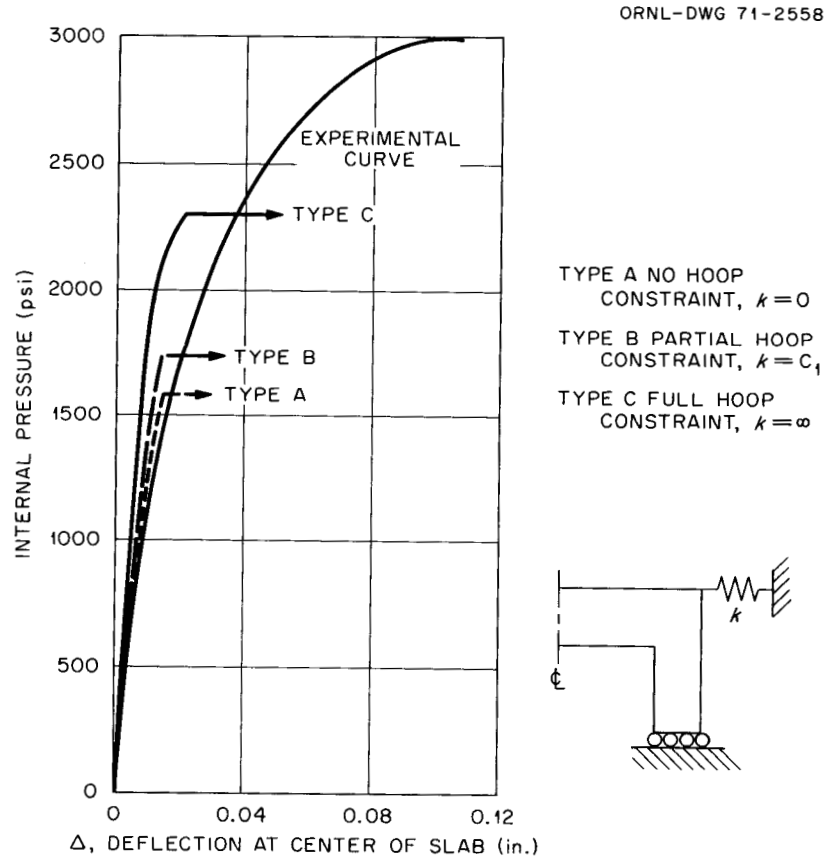


Fig. 7.12. Comparison of load-deformation curves for a Poisson's ratio of 0.15, PV16.

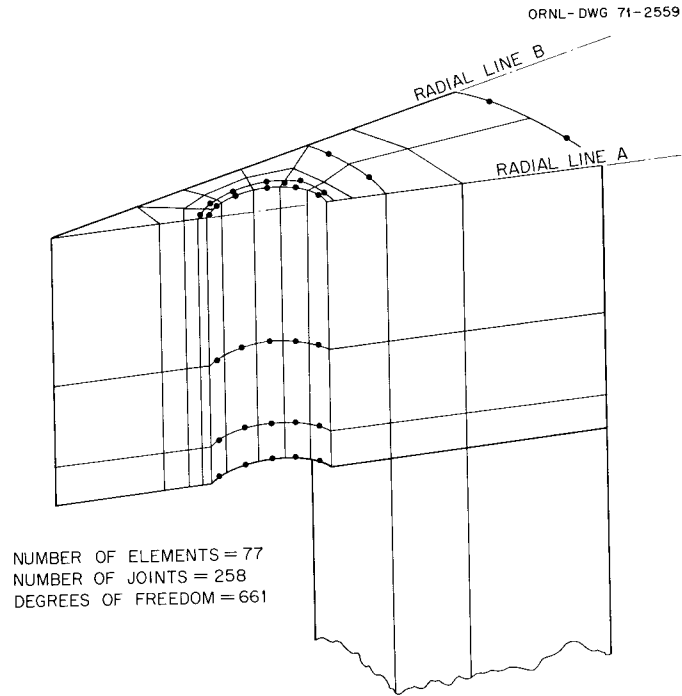


Fig. 7.13. Isoparametric element arrangement around opening in vessel head (PV18).

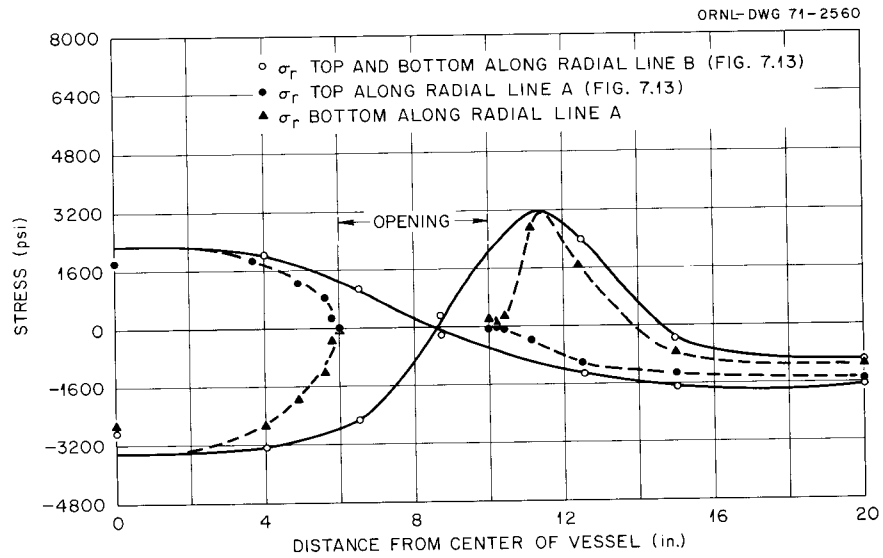


Fig. 7.14. Variation of radial stress in vessel PV18 with pressure of 3000 psi.

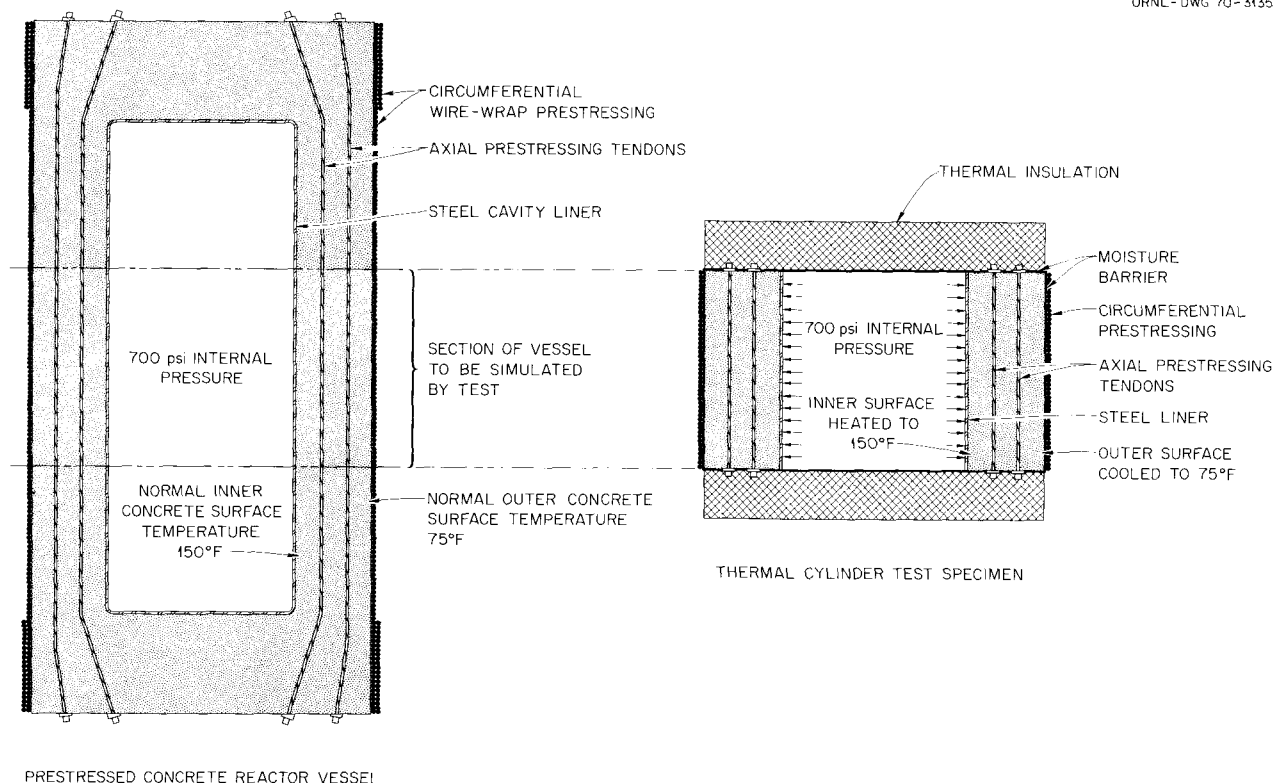


Fig. 7.15. Thermal-cylinder test specimen relationship to prestressed-concrete reactor vessel.

surface. The temperature distribution is simulated by heating the inner surface and cooling the outer surface. The actual detailed thick-walled cylinder test structure, as depicted and described in ref. 4, is 48 in. high, 18 in. thick, and 81 in. in outside diameter.

Prior to suspension of the program last year, most of the equipment required for the test had been procured. Exceptions were parts of the control system for heating and cooling the specimen, parts of the internal pressurization system, and the top and bottom torus weldments that close off the annular region between the cylinder test specimen and the inner concrete core, or island. In addition, not all the required instrumentation had been procured. Since reactivation this fiscal year, all the control and pressurization system parts have been obtained or are on order, and assembly of the control system is under way. The top and bottom torus weldments are on hand, and thus all the structural framing and forms have been obtained, and assembly is on schedule.

It is expected that the test structure will be cast in January 1971. Verbal agreement for casting the thermal

cylinder and associated test specimens has been reached with an outside organization.

7.2.1 Instrumentation

Instrumentation work is proceeding satisfactorily. The 20 weldable strain gages and five thermocouples have been attached to the inner surface of the liner, the 12 tendon load-transducers have been prepared and instrumented (48 strain gages), and strain gages are now being applied to the prestressing tendon strand.

Instrumentation work has also included the development of two types of embedment devices for measuring stress in the thermal-cylinder concrete. These are (1) a stress cell made of titanium, and (2) a system consisting of two concrete embedment strain gages, one of which has a pressure diaphragm attached.

Preliminary prototypes have been fabricated and are now undergoing testing. The titanium stress-cell prototype has been subjected to axial loading cycles to evaluate stiffness, sensitivity, and repeatability of the instrumental drift-monitoring system. The modulus of

elasticity of the cell was found to be 10^7 psi. Fifteen of these cells have been fabricated for use in the thermal cylinder and associated control specimens.

The second device for measuring stress consists of a system of two embedment strain gages cast into the concrete in parallel positions. One gage will have a pressure diaphragm attached perpendicular to the axis of the gage. The pressure in the diaphragm will be controlled so that at any time the two strain gages read the same. The diaphragm pressure reading is then a measure of the stress in the concrete.

Finite-element analyses of the concrete-pressure diaphragm system were carried out for diaphragm diameters of 3, 4, and 6 in. The analytical results indicated that a 4-in.-diam diaphragm is well matched with the 4-in.-long Microdot embedded strain gages that will be used. With a 4-in.-diam diaphragm, each 1000 psi of actual concrete stress will create a differential reading in the two strain gages associated with the diaphragm of $100 \mu\text{in.}$ when the diaphragm pressure is zero. The diaphragm pressure required to reduce the differential reading to zero is theoretically equal to the concrete stress.

In addition to the analyses, a number of diaphragms of various design were fabricated and embedded in 6- by 12-in. concrete cylinders. The behavior of the diaphragms was then investigated by pressurizing them and taking associated strain-gage readings. The final design chosen as being satisfactory was a 4-in.-diam diaphragm consisting of two 20-mil sheets spaced 20 mils apart.

7.2.2 Preliminary inelastic analysis

To verify the adequacy of the design, a preliminary time-dependent finite-element creep analysis was performed. The analysis was used to predict the stress and strain behavior of the specimen starting with the initial prestressing and extending through the 45-day period during which the internal pressure was removed.⁴ The finite-element computer program, SAFE-CREEP,⁵ which was developed for PCRV's by Gulf General Atomic, Inc., was used. This is a linear viscoelastic program based on the superposition principle. It is a two-dimensional analysis that will treat either axisymmetric or plane concrete structures. A specific set of

concrete creep data, which includes age at loading as a variable, is built into the program.

Although any other set of creep data can, with very little trouble, be programmed into the SAFE-CREEP program, the preliminary analysis was performed with the data currently in the program. The initial creep data from the basic creep investigations indicate that the actual thermal cylinder concrete will exhibit slightly less primary creep than indicated by the data used in the computer program and about the same amount of secondary creep.

The finite-element layout for the analysis was shown in ref. 4. Typical results from the preliminary time-dependent analysis of the cylindrical specimen are presented in Figs. 7.16, 7.17, and 7.18. The circumferential and axial stresses on the inner and outer surfaces of the cylinder at midheight are shown in Fig. 7.16 as a function of time after prestressing. The heavy lines are the viscoelastic predictions, while the fine lines indicate the variations predicted by a purely elastic analysis. The circumferential and axial strain variations at the same points are shown in Fig. 7.17, while the circumferential and axial stresses in the steel liner at midheight are shown in Fig. 7.18.

While the analytical technique used for the preliminary analysis is only one of several possibilities that will be utilized in the thermal-cylinder investigation, the results presented do give an indication of the general stress and strain behavior expected during the test. The results show that during periods that are predominantly load controlled (for example, when only the prestressing forces are acting) the time-dependent behavior is primarily creep with the strains changing more rapidly than the stresses. During periods that are predominantly strain controlled (for example, when the thermal gradient plus the prestressing is acting) the behavior is primarily relaxation, with the stresses changing more rapidly than the strains.

The effect of stress relaxation on the stresses due to prestressing plus the thermal gradient can be seen in the circumferential stress on the inner surface in Fig. 7.16. Calculated on an elastic basis, the stress is about 3200 psi in compression. Principal compressive stresses are generally limited to $0.45f'_c$, where f'_c is the specified 28-day compressive strength and is 6000 psi. This compressive limit is thus 2700 psi, which is exceeded by the circumferential stress calculated on an elastic basis. With stress relaxation taken into account the maximum stress is 2550 psi in compression, which is below this limit.

5. F. J. DeArriago and Y. R. Rashid, *SAFE-CREEP - A Computer Program for the Viscoelastic Analysis of Axisymmetric and Plane Concrete Structures*, USAEC Report GA-8111, General Atomic Division, General Dynamics Corporation, July 31, 1967.

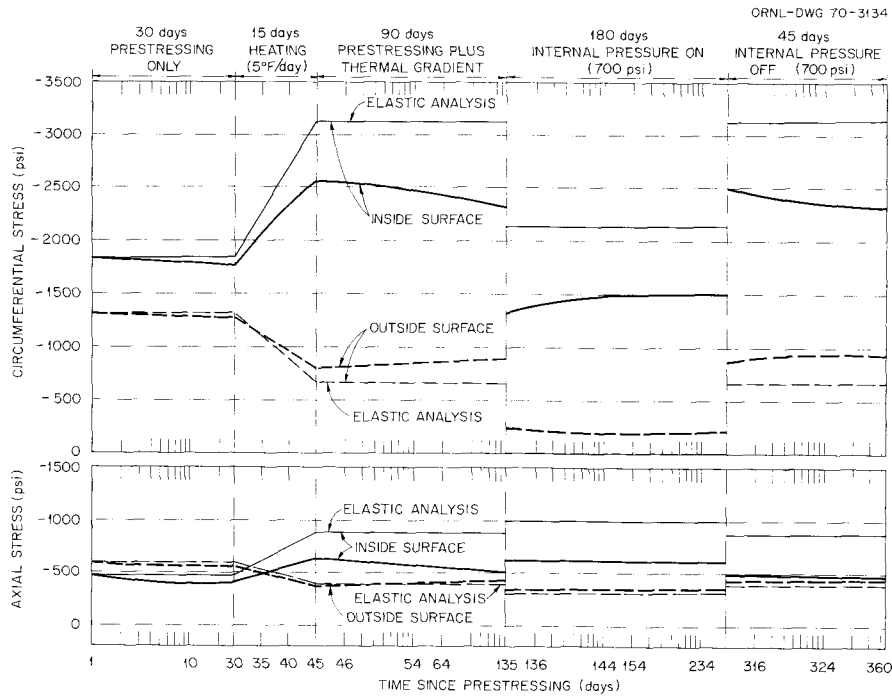


Fig. 7.16. Predicted circumferential and axial concrete stress variation with time on inner and outer surfaces of thermal cylinder at midheight.

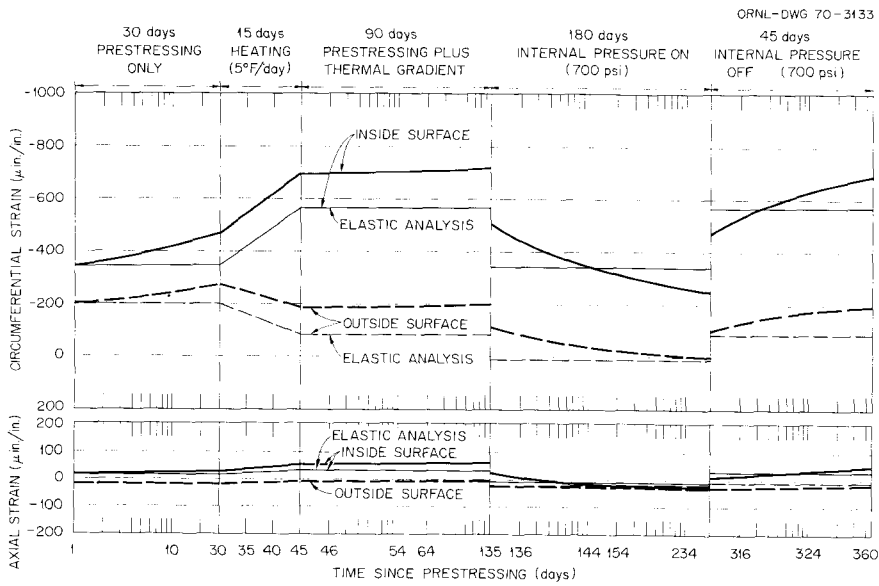


Fig. 7.17. Predicted circumferential and axial concrete strain variation with time on inner and outer surfaces of thermal cylinder at midheight.

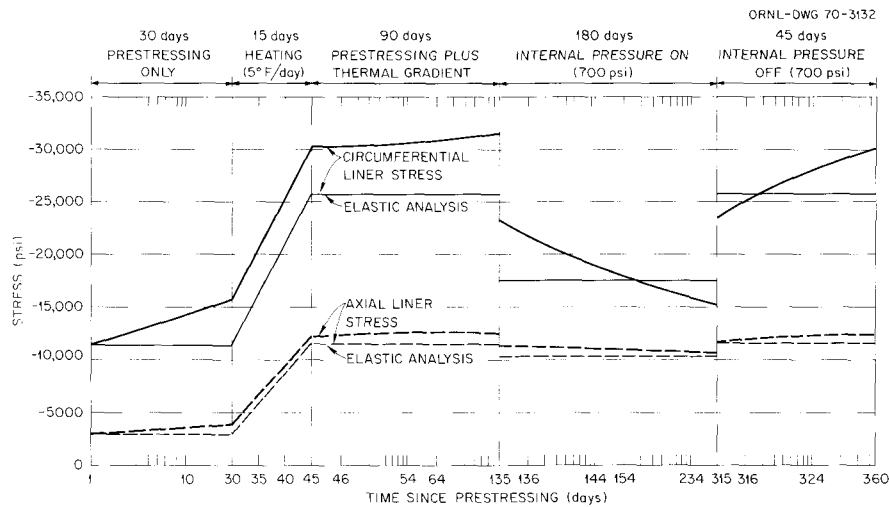


Fig. 7.18. Predicted circumferential and axial stress variation with time in steel liner at midheight.

This is generally the case in actual PCRV's. Early designers found that for a design to remain within practical and economic limits, account had to be taken of the beneficial effects of creep. Some designers have used various methods to approximately account for the effects of creep in their stress analyses, notably by simply using a reduced elastic modulus value, while others have relaxed the allowable stress limits for thermal plus mechanical load stresses calculated on an elastic basis.

To accurately predict the actual stresses, more realistic and rigorous creep-analysis methods must be used. The linear viscoelastic method employed by SAFE-CREEP is one possibility. It is known, however, that the principle of superposition used in SAFE-CREEP does not agree, in all cases, with experimental observations on concrete behavior, and, in fact, one of the objectives of the thermal-cylinder test is to evaluate the accuracy of this method.

Other analytical techniques, including a viscoelastic analysis based on a modified superposition principle, the simplified effective modulus method, and an analysis based on the rate of creep method, will also be investigated and utilized for comparisons with the experimental results from the thermal-cylinder test.⁶

6. G. L. England, "Elastic and Thermal-Creep Analyses of Cylindrical Model Concrete Pressure Vessel," pp. 262-273, *GCRP Semiann. Progr. Rept. Sept. 30, 1968*, USAEC Report ORNL-4353, Oak Ridge National Laboratory.

From these comparisons the most suitable creep theory and methods of analysis will be identified.

The computer program SAFE-CRACK⁷ was developed by Gulf General Atomic under ORNL sub-contract, and it uses a modified superposition principle as mentioned above. The SAFE-CRACK program is a modification of SAFE-CREEP, and it is expected to provide improved predictions of inelastic behavior, particularly in those situations where the temperature varies with time, as is the case of the thermal cylinder.

The SAFE-CRACK program has been converted to use at Oak Ridge. The trial problem supplied with the program has been satisfactorily run and the program has been enlarged to handle the input data for the thermal cylinder that was originally used with the earlier SAFE-CREEP program. The enlarged program is presently being debugged with the thermal-cylinder input data. When this analysis is carried out satisfactorily, the creep behavior representation that was programmed into the analysis by GGA will be modified based on the Corps of Engineers and University of Texas creep data. The latter data are for the same concrete mixture as will be used in the thermal cylinder. The SAFE-CRACK program will then be used for one of the final time-dependent analyses of the concrete thermal-cylinder test.

7. Y. R. Rashid, *Nonlinear Quasi-Static Analysis of Two-Dimensional Concrete Structures*, USAEC Report GA-0004, Gulf General Atomic, Inc., Mar. 23, 1970.

Part IV. Thorium Utilization Program

8. Introduction

A. L. Lotts R. G. Wymer

Development of the thorium fuel cycle for the economical production of nuclear energy has been the aim of extensive programs of government and industry for many years. The present effort is part of the planned HTGR fuel recycle development program, which is being pursued by the AEC, GGA, and ORNL. Emphasis is being placed on development of the fuel recycle technology required to demonstrate and support commercial HTGR recycle operations based on use of the thorium fuel cycle.

The planned HTGR fuel recycle development program to attain the above objectives includes studies of spent fuel reprocessing; recycle fuel fabrication; fuel receiving, handling, storage, and shipping; waste treatment and disposal; recycle fuel irradiations; and conceptual design studies of a commercial recycle plant. Present emphasis is on developing the recycle technology for a reference fuel element composed of graphite blocks containing fuel sticks of pyrolytic-carbon-coated ceramic fuel particles. Alternative fuels will be investigated as necessary to determine their relative merits. Technology developed in connection with nonrecycle fuels will be adapted where practical to the fabrication of recycle fuels.

The reference fuel cycle is the thorium cycle with ^{235}U as the initial fissile fuel. This cycle is illustrated in Fig. 8.1. The bred ^{233}U will be recovered and recycled. Since the conversion ratio of the type of HTGR under consideration is approximately 0.8 with a fuel exposure time of four years, makeup fuel will be required

throughout the life of the reactor. Although ^{235}U is considered as the reference material for initial and

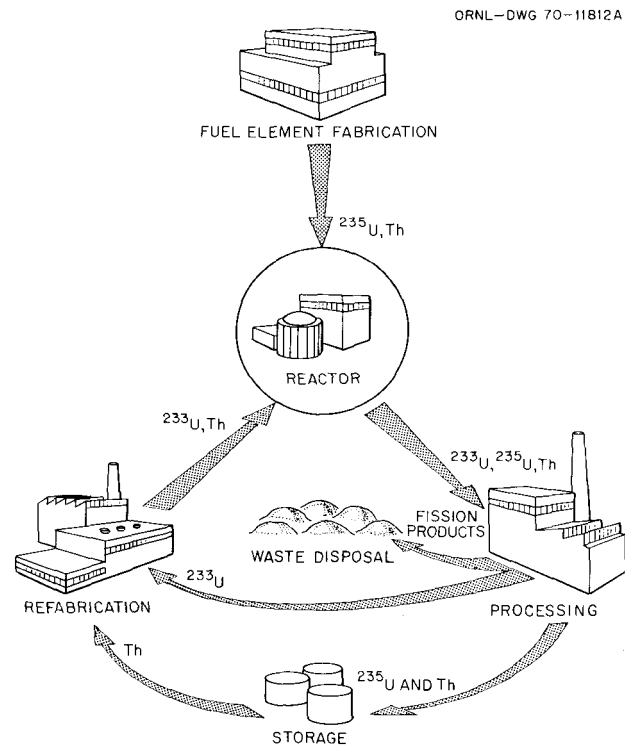


Fig. 8.1. Steps in HTGR fuel recycle.

makeup fuel, plutonium from light-water reactors is an alternate fuel.

The reference fuel element for commercial HTGR's is a hexagonal block of graphite approximately 31 in. long and 14 in. across flats, as shown in Fig. 8.2. In both the reference 1000-MW(e) HTGR and the Fort St. Vrain Reactor currently being constructed, these fuel elements will be stacked together in a close-packed array. No supporting structure or additional moderator material is used. The typical fuel element contains 102

helium coolant holes and 210 fuel holes. A fuel element modified for control rods is shown in Fig. 8.3.

The reference fuel is in the form of ceramic kernels (microspheres) coated with pyrolytic carbon and silicon carbide and is bonded into sticks that fit into the fuel holes in the graphite blocks. The coatings on the kernels prevent the spread of fission products into the coolant system. An inner layer of low-density pyrolytic carbon is applied to all kernels to provide voids for the fission products and to protect the outer coating from fission

ORNL-DWG 70-10233

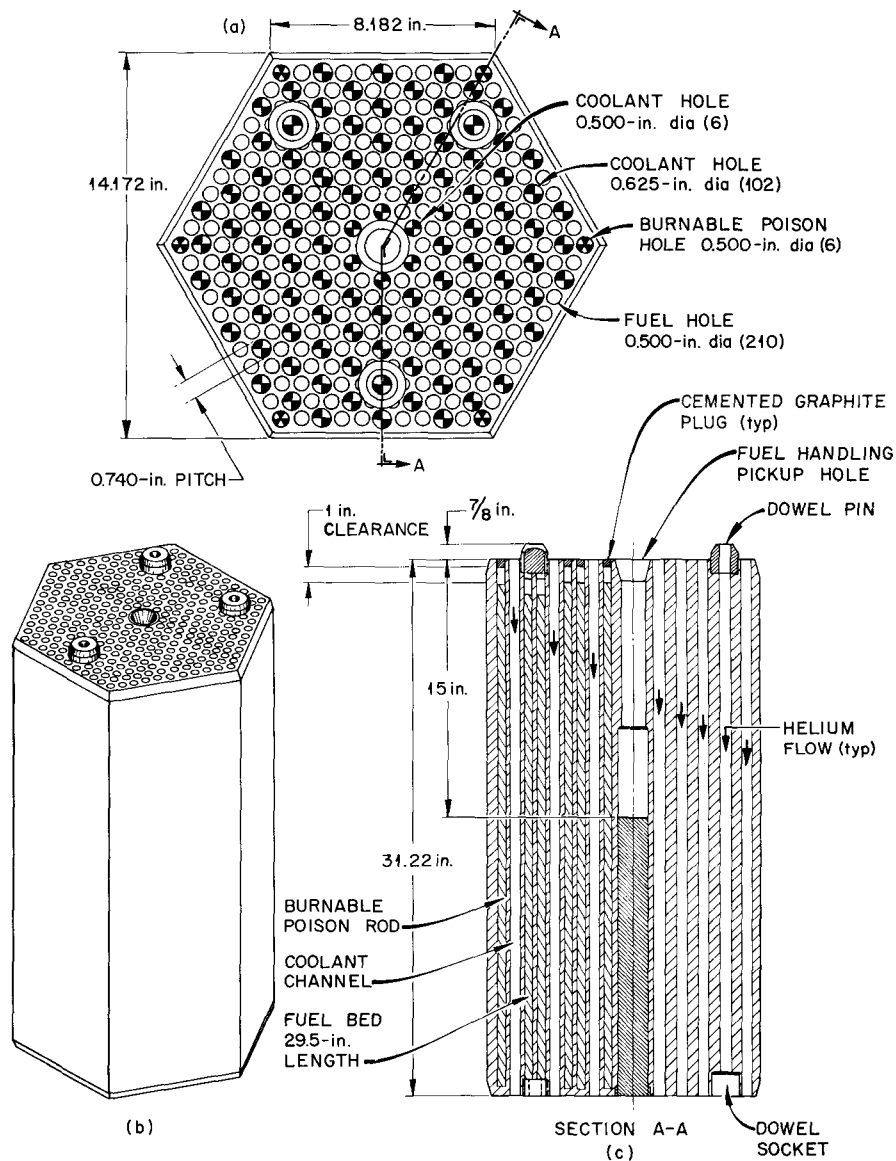


Fig. 8.2. Typical HTGR fuel element.

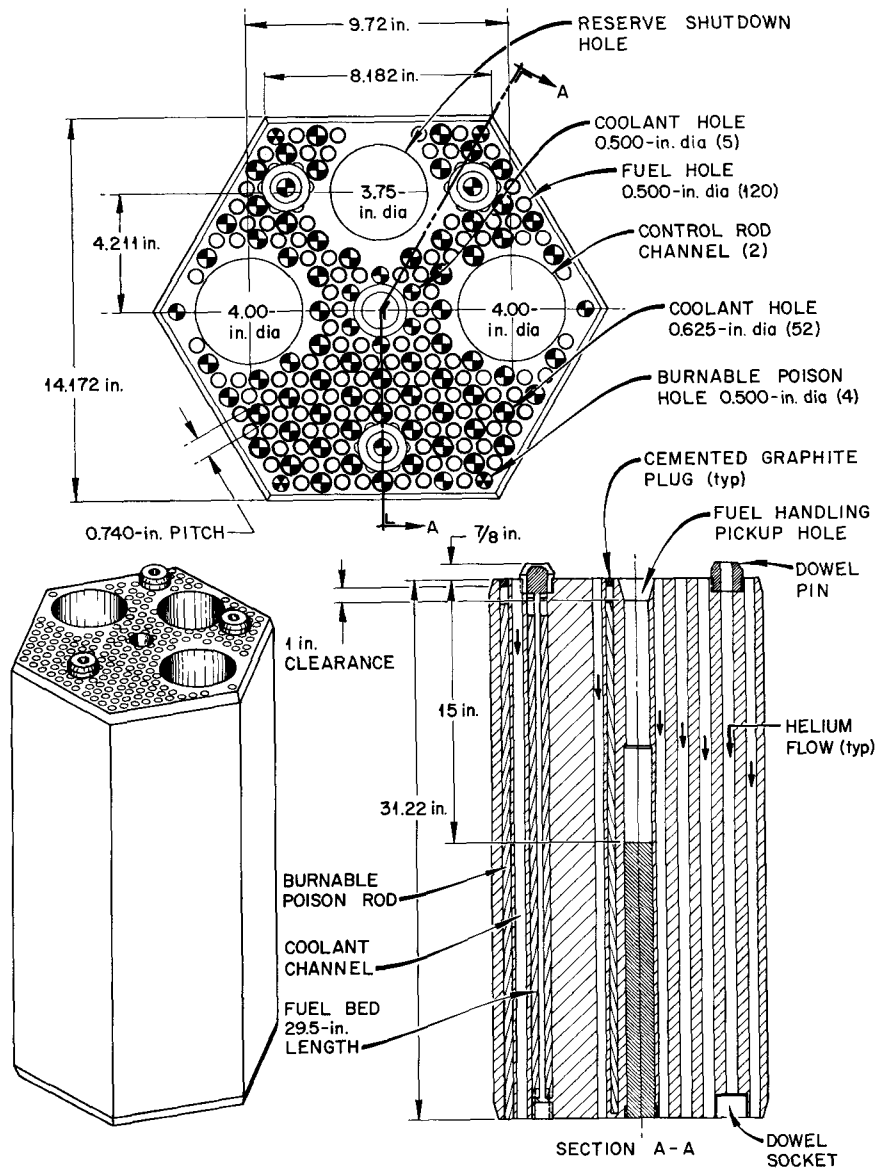


Fig. 8.3. Typical HTGR fuel element with control rod channels.

recoil damage. The outer layers, either of a single layer of high-density pyrolytic carbon or of a layer of silicon carbide sandwiched between two layers of high-density pyrolytic carbon, act as a pressure vessel to contain the fission products.

Four types of particles are used to provide for isolation of spent ^{235}U (containing ^{236}U) from ^{233}U and to lower the fabrication costs. The cost reduction is possible because particles containing only thorium or ^{235}U can be fabricated at lower cost in a facility

separate from the shielded ^{233}U particle refabrication facility. The four particle types are (1) a fertile particle containing Th, (2) a fissile particle containing ^{235}U with a pyrolytic-carbon coating – called the Biso fissile particle, (3) a fissile particle containing ^{235}U coated with both pyrolytic carbon and silicon carbide – called the Triso fissile particle, and (4) a fissile particle containing ^{233}U with a pyrolytic-carbon coating – called the recycle particle. Only one type of fissile particle is used in any one fuel element. Fissile particles

are mixed with fertile particles before the fuel stick is formed. The nomenclature of the elements that contain the various fissile particles is outlined in Table 8.1. Every element contains the ThC₂ fertile particle. Two types of elements are used at one time in the core — elements A and B. The Triso fissile particle is contained in element B. Initially, until ²³³U is available, element A contains the Biso fissile particle. In later core loadings, the same element B as in the initial fueling will

be used, and the recycle particle will be used in element A.

To implement this development program, facilities are required for demonstrations of head-end reprocessing, solvent-extraction reprocessing, and fuel refabrication; recycle fuel proof test irradiations; and laboratory development work preceding and supporting the demonstrations. This laboratory development work includes both process development and engineering-scale equipment development. Laboratory development work will be done in available chemical and engineering laboratories and hot cell facilities at ORNL and GGA.

The demonstrations of head-end reprocessing and fuel refabrication will be performed in pilot plants located in the Thorium-Uranium Recycle Facility (TURF) at ORNL. The demonstration of solvent-extraction reprocessing will be accomplished either in TURF or in the ORNL Building 3019 Facility, which presently contains Thorex pilot plant equipment. The irradiations will be done in the Peach Bottom Reactor, the Engineering Test Reactor, ORNL irradiation facilities, and the Fort St. Vrain Reactor. The overall schedule for the development program is shown in Fig. 8.4.

Table 8.1. Particle types in the reference HTGR fuel elements^a

	Element A	Element B
Initial fuel	²³⁵ UC ₂	²³⁵ UC ₂ (Triso)
	ThC ₂	ThC ₂
Recycle fuel	(Th- ²³³ U)O ₂	²³⁵ UC ₂ (Triso)
	ThC ₂	ThC ₂

^aAll particles have Biso coating except as noted.

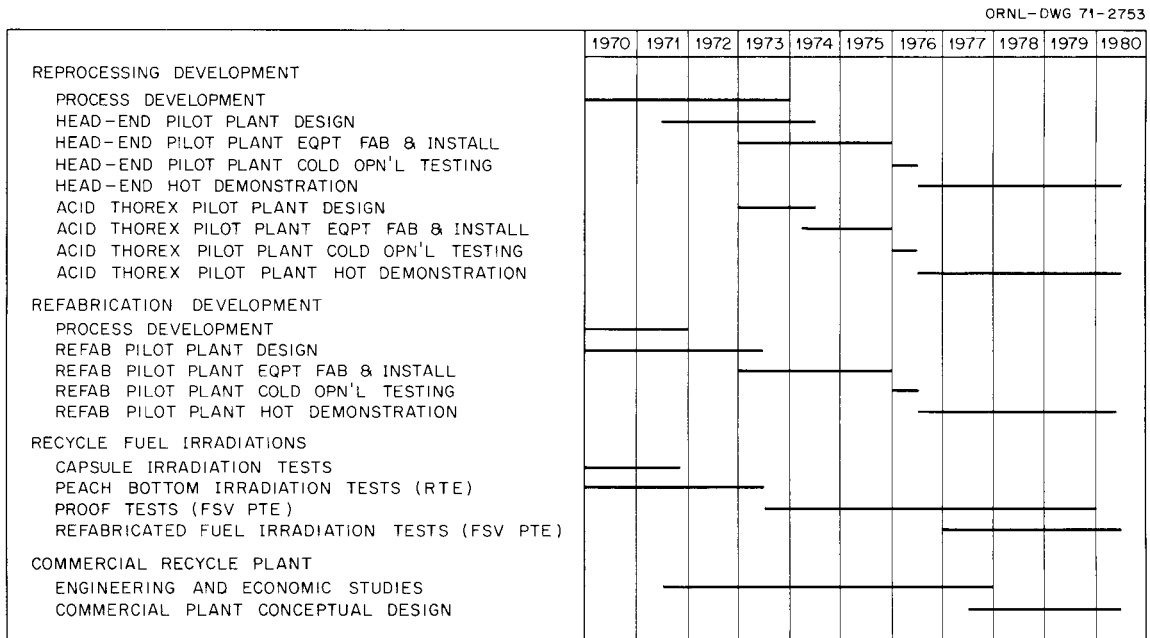


Fig. 8.4. HTGR recycle development program schedule.

9. HTGR Fuel Recycle Development Program Plan

A. L. Lotts J. W. Anderson

9.1 Background

The HTGR fuel recycle development program is being documented in a formal report that states the objectives of the development program and outlines the activities necessary to accomplish these objectives. A summary of the current status of recycle fuel reprocessing and refabrication technology is included, and the additional technology needed to permit commercial fuel recycle is identified. The plan is intended to provide the basis from which a well-organized and systematic approach can be taken to recycle fuel development.

The initial draft of the program plan was prepared several years ago, and since that time the plan has been reviewed periodically by Gulf General Atomic, ORNL, and the AEC. Updated drafts were prepared on several occasions, but a final report was not issued or completed. Efforts are now proceeding to update and complete the program plan and to issue it as a formal report.

9.2 Scope

The plan reflects a progression of work activities that began in 1970 and extends into 1981; the planning is such that a commercial recycle plant can be designed, constructed, and placed into operation on a time schedule that minimizes HTGR fuel recycle costs.¹ The plan thus describes the actions that must be taken by both government and private industry to realize

1. F. J. Furman, R. B. Pratt, and A. L. Lotts, *Prediction of the Economically Optimum Time to Initiate Recycle for the High-Temperature Gas-Cooled Reactor Industry Using Computer Program DELAY*, USAEC Report ORNL-TM-2704, Oak Ridge National Laboratory, December 1969.

maximum benefit from an HTGR economy. It defines in detail the tasks and the subtasks that must be performed in the development program so that the overall objective of developing and demonstrating the technical and economic feasibility of HTGR fuel recycle can be achieved. The tasks are therefore all oriented toward developing processes and equipment for remotely reprocessing the irradiated HTGR fuel and then remotely refabricating recycle fuel. Also included are the design, construction, and operation of an integrated pilot plant for demonstration of fuel recycling. The demonstration will involve a six-month operating period during which approximately 1000 spent fuel elements will be treated by the planned processing methods; the bred ^{233}U will be recovered; and recycle fuel elements containing ^{233}U will be refabricated. The plan considers the proof testing of recycle fuel and the development of the conceptual design for a commercial reprocessing plant.

9.3 Organization

The plan is divided into the following major sections:

- Summary
- Introduction
- Technical and Economic Background
- Task 100 – Reprocessing Development
- Task 200 – Refabrication Development
- Task 300 – Recycle Irradiation
- Task 400 – Commercial Recycle Plant Studies
- Appendix A
- Appendix B

The introduction to the plan provides an overall description of the program and the economic justification for it, as well as information relative to the

reference HTGR fuel and fuel elements. The introduction also presents the program budget, schedule of activities, and important milestones and events that must occur during implementation in order to realize the objectives.

The program tasks are organized according to the outline given below:

PROGRAM TASK	
100	REPROCESSING DEVELOPMENT
110	Head-End Process Development
111	Burner feed preparation
112	Burner technology
113	Burner ash handling
114	Treatment of classified burner ash
115	Alternate methods of maintaining isolation of ^{233}U and ^{235}U
116	Scrap recycle
117	Off-gas handling and decontamination
118	Waste treatment and disposal
120	Head-End Processing Demonstration
121	Design
122	Procurement and testing of equipment
123	Installation of equipment
124	Cold operational testing of equipment
125	Hot demonstration of equipment
126	Waste treatment and disposal
127	Materials handling
128	Process development support
130	Acid Thorex Processing Demonstration
131	Design
132	Procurement and testing of equipment
133	Installation of equipment
134	Cold operational testing of equipment
135	Hot demonstration of equipment
136	Waste treatment and disposal
137	Materials handling
138	Process development support
200	REFABRICATION DEVELOPMENT
210	Refabrication Process Development
211	Sol preparation
212	Microsphere preparation
213	Particle coating
214	Particle handling and inspection
215	Fuel stick fabrication
216	Fuel element fabrication
217	Internal recycle of off-specification material

220	Fuel Refabrication Demonstration
221	Design
222	Procurement and testing of equipment
223	Installation of equipment
224	Cold operational testing of integrated equipment
225	Hot demonstration of integrated equipment
226	Waste treatment and disposal
227	Materials handling
228	Process development support

300	RECYCLE FUEL IRRADIATIONS
311	Capsule irradiation tests
312	Peach Bottom irradiation tests
313	Proof tests
314	Fuel irradiation tests
400	COMMERCIAL RECYCLE PLANT STUDIES
410	Engineering and Economic Studies
411	Process evaluation
412	Fuel shipping methods and cost
413	Irradiated fuel storage
414	Waste management and byproduct recovery
420	Conceptual Design of a Commercial Recycle Plant

The 110 subtask relates to the laboratory development of head-end processing, while the 210 subtask relates to the development of refabrication processes. These laboratory development subtasks include both the development of processes and equipment for performing fuel processing and refabrication.

The 120, 130, and 220 subtasks relate to the design, construction, and operation of the integrated pilot plant, which is to demonstrate the technical and economic feasibility of HTGR fuel recycling.

The 300 series subtasks relate to the preparation of either capsules containing fuel for irradiation or test fuel elements for irradiation. These irradiations are designed to be proof tests of the adequacy of the fuel and the fuel recycle processes that are being developed for HTGR's. Another objective of these subtasks is providing irradiated material that can be used in early studies concerning the development of processes and equipment.

The 400 series subtasks relate to the engineering efforts that must be directed toward the preparation of a conceptual design for a commercial fuel recycling plant.

Within the plan each major task description provides (1) background information and a description of the activities required, (2) the schedule, (3) the funding requirements, and (4) the facilities that are necessary to carry out the task. Each subtask description provides a basic statement of requirements, status of the tech-

nology that relates to the task, and a work plan for achieving the identified objectives.

9.4 Status

Currently the program plan is in the final stages of preparation before issue as a formal report. The technical work on the plan has been completed, and the draft material is presently being edited and reviewed. It is anticipated that the document will be issued early in 1971.

10. Head-End Reprocessing Development

R. S. Lowrie V. C. A. Vaughen

Head-end methods are being developed for the reprocessing of HTGR fuel. The reprocessing studies cover fuels for both Fort St. Vrain (FSV) and the 1000-MW(e) reference reactors with the primary emphasis on FSV fuel, since it will be the first HTGR fuel to become available for use in recycle studies in the Thorium-Uranium Recycle Facility (TURF). Present head-end reprocessing studies are based on use of bonded graphite fuel sticks in the graphite block. Fuel sticks for the FSV reactor contain Triso-coated $^{235}\text{U}\text{C}_2$ fissile and Triso-coated ThC_2 fertile particles, which are expected to maintain their integrity during exposure in the reactor and throughout the reprocessing steps.¹ A method is being developed to separate fertile from fissile particles based on size difference after the block graphite, the binder graphite, and the outer carbon layer are removed by burning.

The fuel presently being considered for the reference 1000-MW(e) reactor comprises Triso-coated $^{235}\text{U}\text{C}_2$ fissile and Biso-coated ThC_2 and $(\text{U,Th})\text{O}_2$ fertile particles.¹ Burning converts the ThC_2 particles to a finely powdered oxide, which must be separated from the fissile particles. The $(\text{Th,U})\text{O}_2$ fertile particles are expected to maintain their integrity during the burning step. A method is being developed to recover the fertile material by leaching all the ash from the fluidized-bed burner, except the recycle alumina. The bred uranium will be separated from the thorium in the acid-thorex solvent extraction process. Although fissile particles will probably be stored, the uranium and thorium can be recovered by a separate crush, burn, and leach process followed by a solvent-extraction step. The previously

published reprocessing flowsheet² was modified to reflect these changes and is given in Fig. 10.1.

The lowest calculated power cost for an HTGR occurs when the bred uranium (^{233}U) is selectively recycled. Since partial cost penalties accrue for "crossover" of ^{233}U to the discarded ^{235}U fraction and ^{235}U to the ^{233}U fraction, emphasis has been placed on determining the efficiency of separation of the fertile particles from the fissile particles in both engineering-scale and hot-cell tests. Crossover can occur by particle breakage or by inefficient particle separation or both. For example, the particles cannot be separated by screening if they stick together in small agglomerates after burning. Cost penalties of about 0.015 mill/kWhr were calculated for a loss of 5% of the ^{233}U to the ^{235}U fissile fraction. The same cost penalty accrues for 10% retention of the ^{235}U (and attendant ^{236}U) in the ^{233}U recycle fraction when reactor equilibrium conditions are assumed, which takes 100 years, and for 25% retention when a 30-year reactor lifetime is assumed.

10.1 Engineering Studies

Engineering studies of the head-end methods to be used in reprocessing HTGR fuel elements were resumed. Detailed process flowsheets of the head-end and the acid-Thorex solvent-extraction steps are being prepared, based on the principal reprocessing effort indicated in Fig. 10.1, to determine major problem areas. The compositions and flow rates of the inlet and outlet streams, shown in Figs. 10.2 and 10.3, are based on the assumption that during the hot demonstration of the

1. Triso coatings consist of a porous carbon buffer layer on the fuel kernel, a thin sealing layer, and two outer isotropic pyrolytic-carbon layers separated by a silicon carbide layer; Biso coatings consist of two pyrolytic-carbon layers.

2. Oak Ridge National Laboratory, *Chemical Technology Division Annual Progress Report for Period Ending May 31, 1968*, USAEC Report ORNL-4272, p. 57.

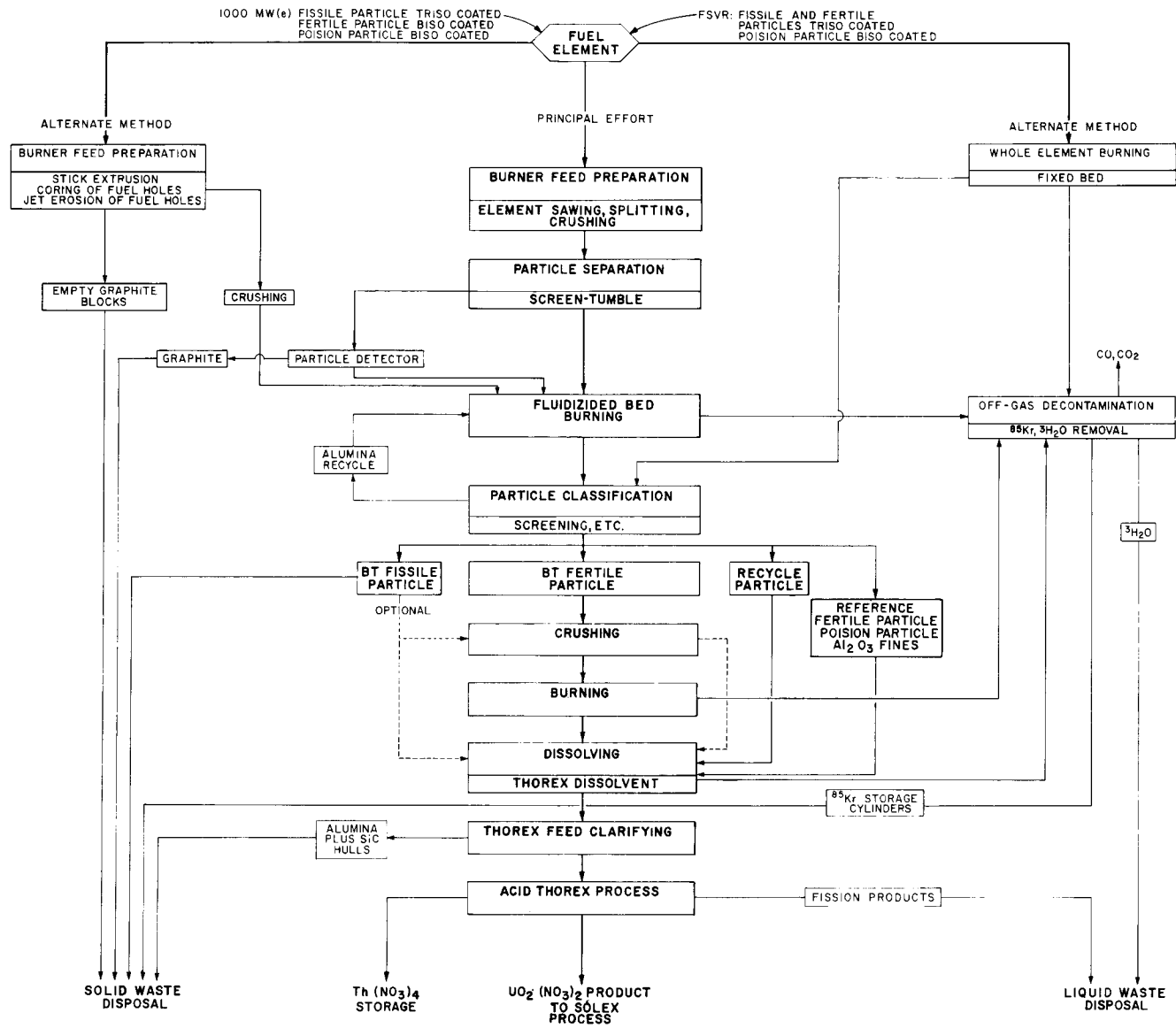


Fig. 10.1. Generalized head-end reprocessing diagram.

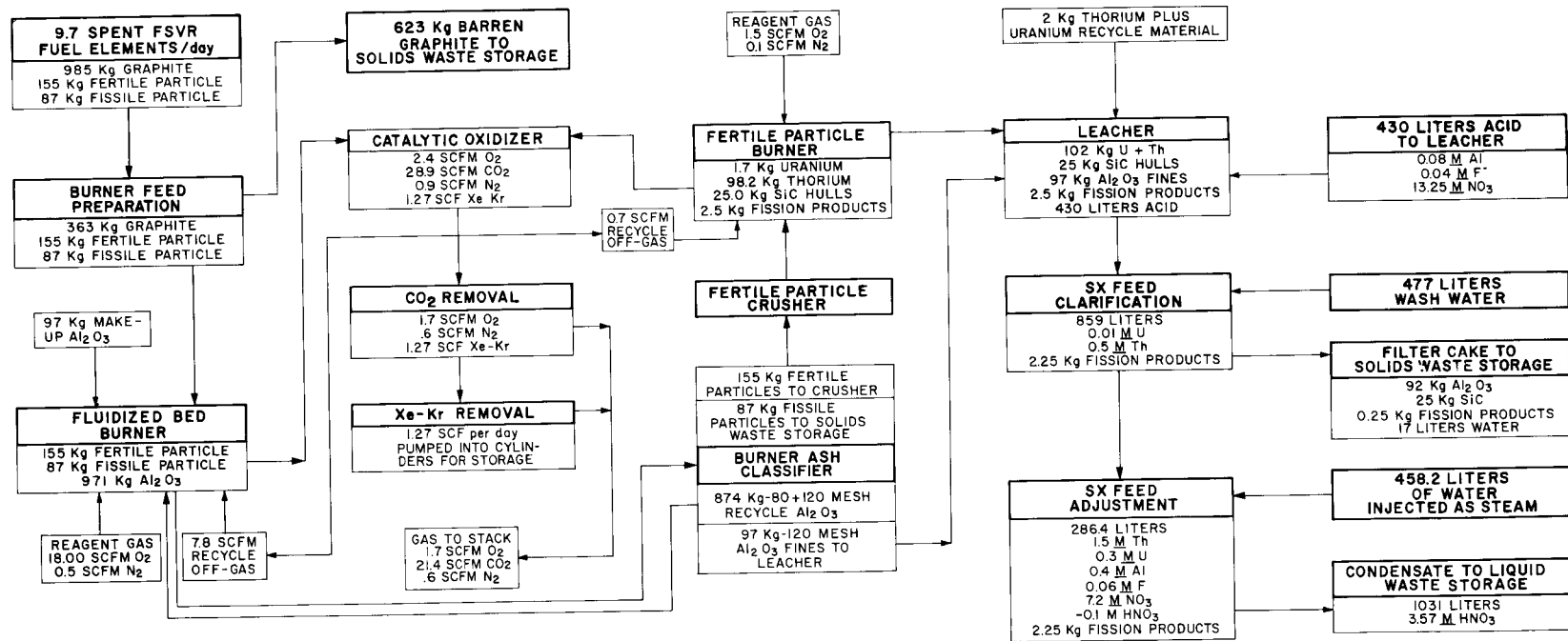


Fig. 10.2. Head-end reprocessing flowsheet.

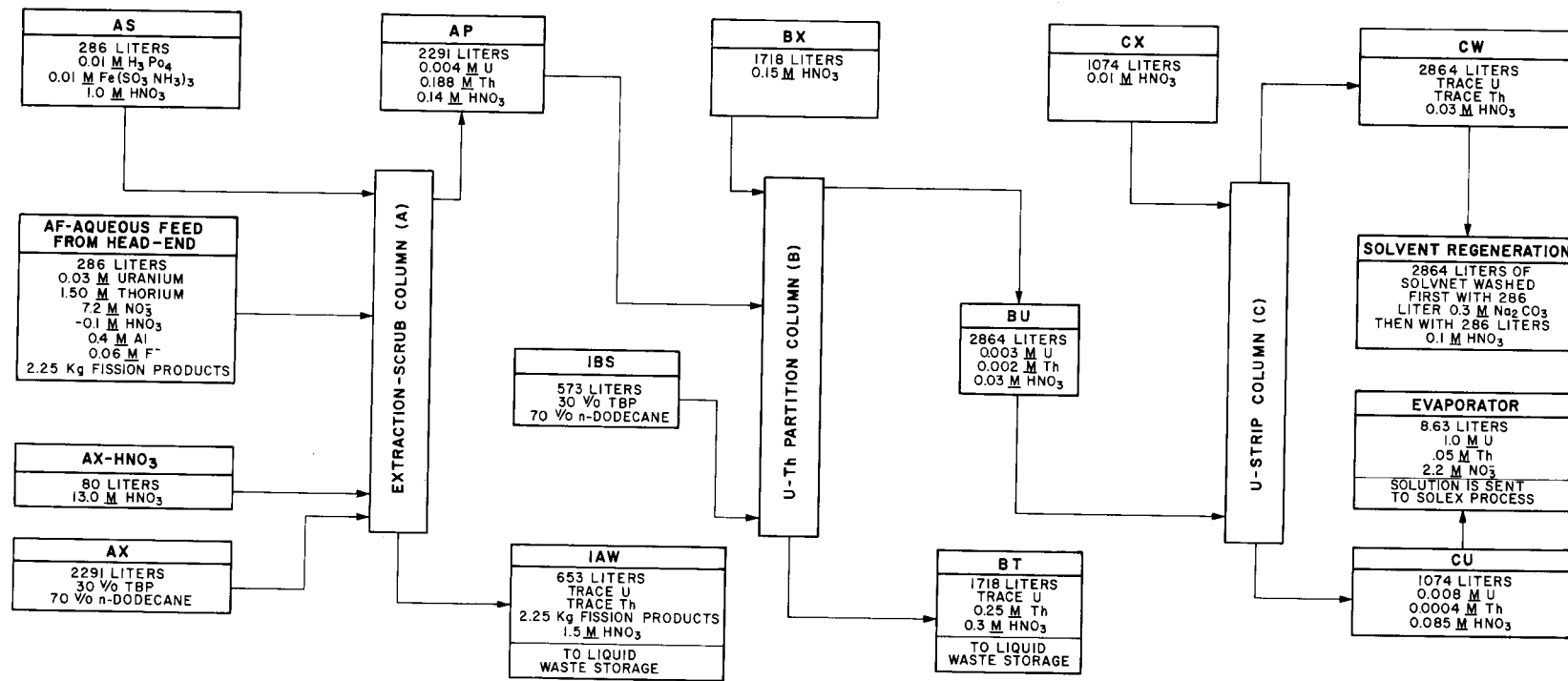


Fig. 10.3. Acid Thorex solvent-extraction flowsheet.

reprocessing and refabrication of HTGR recycle fuel elements, the production capacity of TURF will be 12 kg/day of (Th,U)O₂ microspheres with a thorium-to-uranium ratio of 4.25:1. It was further assumed that all the ²³³U required will be supplied by reprocessing spent FSV fuel elements. For simplicity the fission-product concentration, the uranium concentration, and the isotopic composition calculated by the ORIGEN code for fertile-particle fuel discharged after two years in the FSV reactor were used in these calculations as the average values for all fuel elements. These values, given in Table 10.1, indicate that reprocessing about ten fuel elements per day will provide sufficient uranium, when combined with the internal uranium recycle stream, to produce 12 kg of microspheres per day.

Major problem areas are listed below:

1. separation of particles from barren graphite by a screen tumbling or other physical technique, to-

gether with the development of a particle detector to scan the barren graphite waste stream,

2. development of suitable burners, fluidized bed or other, which will permit separation of the SiC-coated particles from all external graphite,
3. efficient separation of the burner ash into fertile and fissile fractions,
4. development of a burner to remove all graphite in the crushed fertile particle fraction before leaching, and
5. development of a method for decontaminating large amounts of burner off-gas from both entrained solids and small amounts (ppm) of ⁸⁵Kr and ³H.

Table 10.1. Nuclide concentrations in fertile particle in fuel leaving Fort St. Vrain reactor after a two-year exposure^a

Power: 9.24 MW/MT Burnup: 8437 MWd/MT Flux: 4.84×10^{13} neutrons/cm²·sec

Nuclide	Concentrations (g/MT of fuel charged to reactor)				
	Charge	After 90 days	After 150 days	After 365 days	After 730 days
²²⁸ Th	0	1.26×10^2	1.42×10^2	1.94×10^2	3.79×10^2
²²⁹ Th	0	7.81×10^2	8.59×10^2	1.14×10^1	5.45×10^1
²³⁰ Th	0	1.86×10^1	1.87×10^1	1.89×10^1	2.19×10^1
²³² Th	7.70×10^5	7.50×10^5	7.50×10^5	7.50×10^5	7.50×10^5
²³¹ Pa	0	5.44	5.44	5.44	5.43
²³³ Pa	0	9.58×10^1	2.10×10^1	1.82×10^1	1.36×10^8
²³² U	0	1.59	1.59	1.58	1.45
²³³ U	0	1.13×10^4	1.14×10^4	1.14×10^4	1.14×10^4
²³⁴ U	0	1.24×10^3	1.24×10^3	1.24×10^3	1.24×10^3
²³⁵ U	0	1.64×10^2	1.64×10^2	1.64×10^2	1.64×10^2
²³⁶ U	0	1.22×10^1	1.22×10^1	1.22×10^1	1.22×10^1
²³⁷ Np	0	3.95×10^1	3.95×10^1	3.95×10^1	3.95×10^1
²³⁸ Pu	0	5.51×10^2	5.50×10^2	5.48×10^2	5.11×10^2
²³⁹ Pu	0	7.77×10^3	7.77×10^3	7.77×10^3	7.76×10^3
²⁴⁰ Pu	0	2.18×10^3	2.18×10^3	2.18×10^3	2.18×10^3
Total	7.70×10^5	7.63×10^5	7.63×10^5	7.63×10^5	7.63×10^5

^aThese values are at variance with results obtained from GGA because GGA's results were calculated from a more accurate knowledge of fuel loading and fuel patterns in the Fort St. Vrain reactor. They are, nonetheless, suitable for use here, and in conjunction with results for other exposures, they provide a self-consistent set of values.

10.2 Head-End Reprocessing Studies with Unirradiated HTGR Fuels

10.2.1 Resin-bonded fuel stick from early Fort St. Vrain reactor prototype fuel

A resin-bonded unirradiated fuel stick obtained from Gulf General Atomic (GGA) was crushed, burned, and leached to test the head-end reprocessing characteristics of unirradiated prototype FSV reactor fuel. The fuel stick, enclosed in a graphite sleeve (1 in. in diameter, $15\frac{5}{8}$ in. long, and weighing 379.21 g), was fabricated at GGA from Triso-coated fertile (ThC_2) and fissile particles [$(\text{Th,U})\text{C}_2$ with a thorium-to-uranium ratio of 4] bonded with a thermosetting resin and graphite filler. The coated particles are described in Table 10.2. Agglomeration of the particles occurred during the burning of the crushed fuel because a component in the bonding material formed a glassy surface on the SiC layer. Consequently, further grinding and leaching to determine ^{233}U - ^{235}U crossover were omitted. Results showed that only limited success was achieved in tests in which leaching, tumbling, and screening were used to break up the small agglomerates and separate the fissile and fertile particles.

Crushing. The fuel stick was crushed in the laboratory jaw crusher (DFC model 20830) at a $\frac{5}{8}$ -in. jaw opening to simulate a large-scale crusher. Since the fuel stick was not bonded to the graphite sleeve, the crushed fuel was

easily separated from most of the graphite splinters. The products were screened to give the following distribution of sizes:

Mesh	Size (μm)	Quantity (%)
Large pieces (no fuel)		67.6
+4	>4760	16.5
+9	>2000	4.1
+20	>840	2.8
+42	>354	8.5
+60	>250	0.58
+100	>149	0.12
-100	<149	0.24

Several larger lumps of fuel and one end plug were removed from the +4-mesh material for an archive sample. The fines fractions (-100 mesh) were combined for leaching tests. Each of the remaining sieve fractions was "split" (or divided) into eight equal portions, and these portions were combined to make eight random samples of crushed fuel (without the large sleeve fragments) for head-end tests. (This procedure has been standardized to give random samples of crushed HTGR fuels.) The samples weighed 14.29 ± 0.24 g, and the median weight was 14.33 g. The material balance through the sample splitting step was 100.1%, and the measured loss was 0.18 g of a total of 379.2 g of original fuel plus sleeve.

Release of broken particles to the crusher fines. Fines from the crushing step (1.42 g) were leached twice with 11 M HNO_3 -0.05 M HF -0.1 M Al^{3+} . Soluble organic compounds colored the leach solutions dark brown. The total breakage in the -60-mesh fraction was 0.03% of the fissile particles and 0.25% of the fertile particles at a $\frac{5}{8}$ -in. jaw spacing. This level of breakage is insignificant from a head-end processing standpoint. Additional broken particles were found after fluidized-bed burning studies (see below). In a second test, two of the samples (R3 and R4) were recrushed at a nominal $\frac{1}{8}$ -in. jaw opening for small-scale burner tests. The distribution of sizes for the crushed product is given in Table 10.3. Estimates of breakage are given in the discussion of fluidized-bed burning (see below).

Tumbling to subdivide fuel stick. One sample of crushed fuel (R4) was tumbled in a $1\frac{1}{4}$ -in.-diam by 12-in.-long Teflon pipe for 6120 revolutions (6 hr) and then rescreened. Since the fertile-particle fraction (+35 mesh, 76.6 wt %) contained significant amounts of conglomerated fissile particles and resin, no further

Table 10.2. Description of coated particles in an unirradiated resin-bonded fuel stick^a obtained from GGA

	Fertile particle	Fissile particle
Kernel composition	ThC_2	$(\text{Th,U})\text{C}_2$; Th/U ratio of 4
Kernel diameter, μm	295-589	104-275
Thickness of Triso coating, μm	86/21/43	55/19/28
Final Triso-coated particle diameter, μm	400-870	250-450
Weight of coated particle, g	51	44
Weight of SiC-coated particle, ^b g	41.97	31.91
Weight of U, ^b g	0.0	3.08
Weight of Th, ^b g	26.16	12.32

^aThe coated particles were bonded with a thermosetting resin and carbonized before insertion in the graphite sleeve.

^bCalculated.

Table 10.3. Distribution^a of sizes of the product obtained from the crushing step

Screen Mesh	Size (μm)	Crushed product (total fuel) obtained at $\frac{5}{8}$ -in. jaw opening (%)	Recrushed product obtained at $\frac{1}{8}$ -in. jaw opening (%)	
			Sample R3	Sample R4
+4	4760	50.7	1.6	1.3
+9	2000	12.5	37.9	31.6
+20	840	8.5	18.7	21.7
+42	354	26.1	38.3	42.2
+60	250	1.2	2.3	2.6
+100	149	0.4	0.4	0.1
-100 ^b		0.7	0.8	0.4
Total, %		100.1	100.1	99.9
Total weight, g		123.43	14.39	14.25
Total weight after sieving, g		123.32	14.55	14.09

^aFraction (in %) caught on a screen of the given mesh size.

^bFraction (in %) passed by a 100-mesh screen.

analysis of crossover was made. The total particle breakage in the -60-mesh fraction was less than 1.5% of the original sample weight – or an increase of 1% due to the tumbling operation. It was concluded that tumbling in this device is not effective for separating fertile and fissile particles.

Fluidized-bed burning. Three samples (R1, R2, and R3) of crushed fuel were burned at 750°C in a fluidized-bed burner with 28 g of T-61 alumina screened to -80 +100 mesh. In each case, the burner product was free-flowing; however, the fertile and fissile SiC-coated particles adhered to each other and formed

small clusters that prevented separation by sieving. Sticking was attributed to a glassy surface on the SiC layer caused by a component in the resin bonding agent. Two of the samples were leached and resieved, and then all three were tumbled and screened several times in an attempt to separate the two particle fractions. Although there was an improvement in separation after the leaching and tumbling operations, the combined treatment did not yield a clearly defined separation. In addition, some variability was noted in the three runs. The ratio of the weight of the +42-mesh fraction (fertile plus adhering fissile particles) to that of the -42 +60 mesh material (i.e., fissile plus broken fertile particles) is given in Table 10.4.

The weight ratio of fertile to fissile particles in the original fuel stick was about 1.32. A rough estimate of crossover may be made by dividing half the difference between the fertile-to-fissile particle ratio for the final product and the original ratio (1.32) by the original ratio; for example, (100) (1.43 - 1.32)/2(1.32) = 4.2% crossover for sample R1 (see Table 10.4). The original crossover for the fluidized-bed burner product was about 28 to 42%. After the various steps and treatments described, this value was reduced to about 4 to 18%.

Alumina retentions were low; about 1% of the Al₂O₃ remained with the SiC-coated particles (0.02 g Al₂O₃ per gram of SiC-coated particles).

Particle breakage due to crushing and fluidized-bed burning. The leachable heavy-metal content (a measure of particle breakage) in the coated particle and alumina fractions of the fluidized-bed burner product was determined by leaching the sieved products twice with 11 M HNO₃ - 0.1 M Al³⁺ - 0.05 M HF. The results obtained are listed in Table 10.5. The use of a $\frac{5}{8}$ -in. jaw

Table 10.4. Comparison of weight ratios of +42-mesh to (-42 +60)-mesh sieved burner products^a

Sample	Fluidized-bed burner product ratio ^b	Original crossover (%)	Separation step			Final product ratio	Final crossover ^c (%)
			Tumbler product ratio	Leacher product ratio	Tumbler product ratio		
R1	2.06	28		1.59	1.55	1.43	4.2
R2	2.20	33		1.84	1.82	1.60	10.6
R3	2.42	42	2.14			1.80	18.2
R4	Unburned		3.50				

^aSieve analysis made after each listed step.

^bOriginal ratio of materials in the fuel stick was 1.32.

^c²³⁵U that went to the thorium fraction.

Table 10.5. Particle breakage due to crushing and fluidized-bed burning

Sample	Jaw setting (in.)	Breakage (% of calculated total heavy metals)									
		Leachate from +42-mesh fraction		Leachate from -42 +60-mesh fraction		Al ₂ O ₃ leachate		Al ₂ O ₃ residue		Total breakage	
		U	Th ^a	U	Th ^a	U	Th ^a	U	Th ^a	U	Th ^a
R1	5/8	0.18	0.16	0.66	~0	1.1	0.05	0.06	0.01	2.0	0.2
R2	5/8	0.20	0.06	0.44	0.07	0.81		0.07	0.01	1.5	0.1
R3	1/8	(b)	(b)	(b)	(b)	7.1		0.07	0.02	>7.2	

^aCorrected for thorium from fissile particles (Th-to-U ratio of 4).

^bNot analyzed.

opening did not result in the breakage of more than about 1.5 to 2.0% of the fissile particles, whereas breakage in excess of 7.2% was obtained with a 1/8-in. jaw opening. Breakage of the fertile particles was 0.1 to 0.2% with the 5/8-in. jaw opening. An additional 0.03 to 0.25% breakage was found with the crusher fines (see above). Approximately 0.07% of the uranium and 0.01% of the thorium were lost to the alumina residues.

10.2.2 One-sixth section of a prototype Fort St. Vrain fuel element

Comminution studies. Unirradiated graphite fuel samples containing resin-bonded Triso-coated ThO₂ and UO₂ particles³ were crushed in a hammer mill with 3/4- and 3/8-in. grate spacings, and the crushed material was sieved to determine the particle size distribution (Table 10.6). No fuel particles were found in +4-mesh or larger size fractions with a 3/4-in. grate spacing or in the +12-mesh or larger size fractions with a 3/8-in. grate spacing. Apparently the increased time in the hammer mill with a 3/8-in. grate spacing freed the particles from the +12-mesh fractions so that the total amount of barren graphite (free from fuel particles) was about the same (~42 to 46%) for each spacing. Further treatment in a screen tumbler should increase the amount of particle-free graphite. The barren graphite could be stored instead of burned if storage proved to be more economical.

The breakage of particle coatings was determined by leaching the hammer-mill product with Thorex dis-solvent (13 M HNO₃ - 0.04 M F⁻ - 0.10 M Al³⁺). In two

Table 10.6. Size distribution of the product obtained by crushing HTGR graphite fuel^a in a hammer mill

Size fraction	Hammer mill ^b product (wt %)			
	3/4-in. grate spacing		3/8-in. grate spacing	
	Sample 1	Sample 2	Sample 1	Sample 2
+3/4 in.	2.2 ^c	3.2 ^c		
-3/4 + 1/2 in.	9.0 ^c	12.2 ^c		
-1/2 in. +4 mesh	33.0 ^c	30.8 ^c	14.4 ^c	23.4 ^c
-4 +12 mesh	14.5	14.6	27.6 ^c	19.83 ^c
-12 +20 mesh	11.1	11.7	14.5	11.72
-20 +35 mesh	19.8	18.0	10.7	19.7
-35 +50 mesh	3.6	2.6	8.5	6.6
-50 +80 mesh	2.5	2.5	7.4	5.4
-80 mesh	4.8 ^d	4.4 ^d	16.7 ^d	13.2 ^d

^aOne-sixth section of a prototype FSV fuel element containing Triso-coated fertile and fissile fuel particles in resin-bonded fuel sticks.

^bType A Jeffrey swing hammer.

^cNo fuel particles were found in these fractions.

^dContained only a few pieces of broken UO₂ and ThO₂ particles.

batches of graphite fuel, the coatings on 2.17 and 0.1% of the UO₂ particles and on 1.07 and 1.52% of the ThO₂ particles were broken by crushing at a 3/4-in. grate spacing.

Fluidized-bed burning studies. Tests were made in a 2-in.-diam fluidized-bed burner with crushed graphite (material passing a 3/4-in. grate spacing) containing Triso-coated UO₂ and ThO₂ fuel particles to determine the direct and indirect effects of oxygen concentration

3. These particles were made and coated at ORNL.

in the reagent gas on particle-coating breakage (Table 10.7). The oxygen concentration was varied from 20% (air) to 100%, while other operating conditions were held constant. Norton RR grade alumina was used as the heat-transfer medium. The bed temperature was 750°C.

The percentages of particles with broken coatings (as determined by leaching the product with Thorex dissolvent) are shown in Table 10.8. Breakage of the UO₂ particle coatings decreased from 6.09 to 2.97% as the oxygen concentration increased from 20 to 100%, primarily due to the decreased time in the fluidized bed. The breakage of the ThO₂ particle coatings decreased from 6.9 to 3.6% as the oxygen concentra-

tion increased from 20 to 70% and then increased sharply to 11.3% with 100% oxygen. However, since pure oxygen reagent can produce sintering of the bed, a feed containing 100% oxygen would probably not be used in a routine operation. When a 70% oxygen reagent is used, the overall coating breakage for both the crushing and the burning steps is 5.7% for UO₂ and 4.67% for ThO₂ particles. Operation was smooth, and no wall "hot spots" or plugs developed. Oxygen utilization averaged greater than 95% during the major portion of the burning period; the burner residue was free-flowing and had a carbon content of less than 1%. When the residue was screened, the ThO₂ particles went to the +35-mesh fraction and the UO₂ particles went to the -35 +50 mesh fraction.

Table 10.7. Fluidized-bed burning tests with Triso-coated fuel

	Run BT-14	Run BT-15	Run BT-16
Burner charge, g			
Alumina ^a	1600	1600	1600
Crushed fuel ^b	2000	2038	1835
Reagent gas	Air (20% O ₂)	70% O ₂ + 30% N ₂	100% O ₂
Operating conditions			
Superficial gas velocity, fps	1.25	1.25	1.25
Temperature, °C	750 ± 25	750 ± 25	750 ± 25
Burning time, hr	14.75	7.25	4.25
Burner residue, g	1894	1954	1879

^a—90-mesh Norton RR alumina.

^bHammer mill set to produce $-\frac{3}{4}$ -in. product.

Table 10.8. Breakage of particle coatings in fluidized-bed burning tests with Triso-coated fuel

	Fraction of particles with broken coatings (%)		
	Run BT-14	Run BT-15	Run BT-16
UO ₂ particles, as charged	2.17	2.17	2.17
ThO ₂ particles, as charged	1.07	1.07	1.07
UO ₂ particles in burner ash	8.26	5.7	5.4
ThO ₂ particles in burner ash	7.97	4.67	12.37
UO ₂ particles broken in test	6.09	3.53	2.97
ThO ₂ particles broken in test	6.90	3.6	11.30

10.3 Head-End Reprocessing Studies with Irradiated HTGR Fuels – Study of Dragon Compact 8375

Flowsheet variables for the head-end reprocessing of HTGR fuels were tested on a small scale with irradiated HTGR fuels in a hot cell. The objectives of the hot-cell studies are to (1) test the operational feasibility of the proposed flowsheets, for example, crush-burn-sieve-grind-burn-leach, (2) test the stability of coated particles in head-end steps, (3) obtain information on releases of the fission products ^3H , ^{85}Kr , ^{90}Sr , ^{106}Ru , and ^{137}Cs in off-gases, (4) obtain information for the design of a head-end pilot plant to be located at TURF, and (5) obtain estimates of product losses and waste stream compositions. Unirradiated fuels were also studied in similar equipment to insure that the results of the small-scale studies are comparable with those of the larger scale studies with unirradiated fuels and to permit evaluation of irradiation effects by comparison with the tests on unirradiated fuels.

Dragon compact 8375, a hollow cylinder, contained "standard" Dragon fuel with Triso coatings of buffer pyrolytic carbon, silicon carbide, and isotropic pyrolytic carbon having thicknesses of 27, 17, and 64 μm , respectively. Based on ^{137}Cs analyses, the compact was irradiated to a burnup of approximately 15,000 MWd/MT. The purposes of the tests made with this compact were to (1) confirm that the crusher jaw opening was the major variable in the breakage of the SiC-coated particles, (2) determine the extent of breakage during sawing, (3) measure ^{85}Kr and ^3H releases during head-end reprocessing steps, and (4) obtain data on leaching, fission-product behavior, and uranium and thorium losses to residues. The experiments were completed, but not all the data have been analyzed. Details of the experimental procedures were published.⁴

The Dragon compact was first sawed into two rings, and then one of the rings was further sawed into four sections of about equal size. All the sawdust was brushed off the cut edges and collected as fines for leaching. Two of the four sawed sections were burned as large pieces (in a static bed), and the residual fuel particles were leached to determine the fraction of particles broken during the sawing step. The final two

sawed sections were crushed with a $1/8$ -in. jaw opening in the crusher, burned in a static bed, and leached to determine the amount of particle breakage. (It should be remembered that FSV-type fuel blocks can be cut without encountering fuel particles, whereas this is not possible with Dragon fuel compacts.)

The second ring was crushed into nine large pieces with a $5/8$ -in. opening on the jaw crusher. Three samples (R5, R6, and R7) were burned in a fluidized bed with Al_2O_3 , sieved to recover the SiC-coated particles from the Al_2O_3 , ground to -60 mesh to break all the particles, burned again in a static bed, and leached to obtain the uranium, thorium, and fission-product contents of the compact and the losses of these materials to the residue. The amounts of ^3H and ^{85}Kr released in each step were also determined.

10.3.1 Crushing studies

The hot-cell crusher (DFC model 20830) has a nominal $5/8$ -in. jaw opening but was shimmed to a nominal $1/8$ in. to produce a product suitable for small-scale burner tests.

With the $5/8$ -in. jaw opening, unirradiated compacts are crushed to a few large lumps, which are satisfactory feed for a 2-in.-diam fluidized burner. In the case of irradiated compact 8375, a quarter ring broke into nine pieces; consequently, size distribution of the product cannot be defined. However, two of the sawed sections (R3 and R4) were recrushed at a $1/8$ -in. jaw opening and analyzed by screening. The results, along with some earlier data for comparison, are given in Table 10.9. The important points are that the fueled compacts release a larger fraction of +42-mesh material (free beads) than is obtained from machined cylinders and, except for some variability in the amounts of +4- and +9-mesh material, that the size distributions of the crushed product in each case are quite similar.

10.3.2 Breakage during size-reduction studies

Experiments with compact 8375 confirmed that the jaw crusher opening was a significant variable in the breakage of fuel particles. In general, the composition of the fines (-42 mesh) was representative of the composition of the compact. With unirradiated fuels (and compact 8368), significantly fewer particles were ruptured; hence, the fines were richer in graphite than the overall average composition of the fuel, indicating that the cleavage was around (rather than through) the particles dispersed in the hot-pressed matrix.

The fraction of broken particles present in the original compact was estimated at 2.3% from static-bed

4. V. C. A. Vaughn, *Head-End Studies of SiC-Coated HTGR Fuels: Unirradiated Dragon Compact No. 8232*, USAEC Report ORNL-TM-2389, Oak Ridge National Laboratory, February 1969.

Table 10.9. Size distribution of product obtained with the hot-cell crusher at $\frac{1}{8}$ -in. jaw opening

	Fraction (%) of total product on screen of indicated size					
	+4 mesh	+9 mesh	+20 mesh	+42 mesh	+100 mesh	-100 mesh
Machined cylinders of graphite (no fuel)	~9	~60	12.6	6.6	4.9	6.9
Unirradiated compact 8232	2.6	62.6	9.1	18.1	2.9	4.8
Irradiated ^a compact 8368	5.9	48.0	12.2	22.8	3.8	7.3
Irradiated ^a compact 8375						
Sample R3	18.3	44.1	11.5	17.6	3.9	4.6
Sample R4	9.1	52.4	12.9	18.0	3.1	4.5

^aIrradiated to a burnup of approximately 15,000 MWd/MT.

burn-leach tests on two sawed segments (R1 and R2). This fraction was considered to be broken prior to the sawing step, since the sawed surfaces were brushed free of broken fines before burning, and neither hacksawing nor static-bed burning is expected to fracture particles that are surrounded by fuel matrix. The burner product was leached twice with 11 M HNO₃–0.1 M Al³⁺–0.05 M HF without grinding the SiC-coated particles, and the uranium and thorium contents of this product were compared with the uranium and thorium contents of the crushed fuel samples determined by analysis of fractions R5, R6, and R7.

Crushing with a $\frac{5}{8}$ -in. jaw opening produced a –42-mesh fines fraction containing 1.4% of the sample (by weight) and about 1% of the calculated uranium and thorium present in the half cylinder. Crushing to a nominal $\frac{1}{8}$ -in. jaw opening produced a fines fraction averaging 8.1% of the sample weight. After the crushed product was burned in a static bed and the residue was leached (without grinding), 13.6% of the calculated fuel particles present were found to be broken. Breakage due solely to crushing at a $\frac{1}{8}$ -in. jaw opening is estimated at 11.3%, of which 28% was retained with the +42-mesh material. These results indicate that a significant number of fractured particles were retained with the larger lumps (+42 mesh) of fuel.

10.3.3 Release of ³H and ⁸⁵Kr

Three samples of fuel crushed at the $\frac{5}{8}$ -in. opening (i.e., R5, R6, and R7) were put through the complete burn-grind-burn-leach processing. In each step, a purge of either 4% H₂ plus argon or moist oxygen-nitrogen

mixtures was used to provide adequate carrier water for trapping the ³H on molecular sieves. The off-gases were passed over a hot copper oxide bed to convert all the hydrogen to water before trapping. The entire gas output was collected and analyzed for ⁸⁵Kr (Table 10.10). About 1% of the total ⁸⁵Kr was collected in the off-gas from the first burner; this represents a release of ⁸⁵Kr from broken particles. There was some variation in the amounts released during grinding and the second burning; however, the sum of these two steps averaged 98%. The remainder (~1 to 2%) was found in the dissolver off-gas. The fact that ⁸⁵Kr was found in the dissolver off-gas probably indicates that the burning conditions were not optimum for complete removal in this step.

Tritium release data are also given in Table 10.10. As reported previously,⁵ a major fraction of the total tritium (~30 to 40%) exists outside the SiC-coated particles and is released in the first burning step. This tritium is believed to be a product of neutron reactions with materials in the bonding matrix and ³He in the coolant gas. Most of the ternary-fission-produced tritium is thought to be retained within the SiC coating until the particles are crushed and heated or burned. Residual tritium (2.6 to 6.8%) in the second burner product was recovered during leaching. The presence of residual tritium indicated a lack of optimum burning conditions.

5. Oak Ridge National Laboratory, *Chemical Technology Division Annual Progress Report for Period Ending May 31, 1969*, USAEC Report ORNL-4422, pp. 114–119.

Table 10.10. Release of ^3H and ^{85}Kr during head-end steps performed on samples of Dragon compact 8375

	^{85}Kr release			^3H release		
	Sample R5	Sample R6	Sample R7	Sample R5	Sample R6	Sample R7
Fraction, %, present in off-gas from						
First burning step	>0.4 ^a	1.04	0.98	32.3	(b)	29.7
Grinding step	27.6	81.1	16.7	0.3		5.6
Second burning step	71.7	15.7	81.3	60.6		62.0
First leach	0.3	2.1	1.0	3.8 ^c		2.2 ^c
Fraction in first leach liquor, %				3.0		0.4
Total activity, dis/min	4.13×10^{10}	3.34×10^{10}	3.32×10^{10}	7.45×10^8	5.44×10^8	1.80×10^8
Sample weight, g	16.35	14.55	11.11	16.35	14.55	11.11

^aCollected on dry ice-charcoal trap; CO_2 displaced some of the ^{85}Kr ; subsequent samples were taken from the collected gases.

^bPercentage values not realistic because the value for ^3H in the off-gas of the second burn cycle was very low.

^cAccuracy doubtful because of low counting rate.

10.4 Procurement of Irradiated HTGR Fuels for Head-End Studies

Additional samples of irradiated Dragon fuel compacts have been requested for head-end reprocessing tests. These compacts contain coated fuel particles similar to those proposed for the Fort St. Vrain and commercial 1100-MW(e) HTGR's and will provide meaningful tests of reprocessing flowsheet concepts, even though the Dragon fuels differ from GGA-HTGR fuels. Dragon fuels are hot-pressed compacts rather than bonded fuel sticks; they have larger particle kernel sizes and thicker coatings; and, among other differences, they are one-particle rather than two-particle fuels.

A comprehensive study of the following prototype HTGR fuels is also planned:

1. ORNL Biso-coated $(\text{Th,U})\text{O}_2$ sol-gel microspheres, which were irradiated as compacts in the Dragon reactor,
2. ORNL test capsules to be irradiated in the ETR for combined head-end reprocessing studies and irradiation performance testing, and
3. recycle test elements (RTE's) fabricated jointly by GGA and ORNL and being irradiated in the Peach Bottom reactor.

10.4.1 ORNL Biso-coated $(\text{Th,U})\text{O}_2$ sol-gel microsphere compacts

Several types of Dragon fuels of particular interest in head-end work have been requested and should arrive in the early part of fiscal year 1971. These and ORNL sol-gel irradiated compacts are described in Table 10.11.

Many important fuel types and head-end reprocessing steps can be simulated, as shown in the last column of this table.

10.4.2 ORNL test capsule

The irradiation performance and behavior of small quantities of three types of candidate coated-particle 1100-MW(e) HTGR fuels under proposed methods of head-end reprocessing will be studied jointly by the Metals and Ceramics and the Chemical Technology Divisions. The three types of fuel-particle combinations that will be tested in small, loose beds and in fuel sticks (~2.5 in. long) are the alternate block A recycle $[(4.2 \text{ Th,U})\text{O}_2 + \text{ThO}_2]$, block B recycle $[\text{UC}_2(\text{Triso-coated}) + \text{ThC}_2]$, backup block B recycle $[\text{UO}_2 + \text{ThO}_2]$ fuels, and the accelerated-burnup alternate block A recycle fuel $[(2\text{Th,U})\text{O}_2 + \text{ThO}_2]$. Only the UC_2 particles have Triso coatings. The particles in blended beds and in fuel sticks will be irradiated in two capsules at temperatures of 750, 950, 1050, and 1300°C to burnups of approximately 4×10^{21} to 6×10^{21} neutrons/cm²·sec fast fluence in the ETR. Although the quantities of fuel are quite small, they will be adequate for an early preliminary determination of the head-end reprocessing behavior of highly irradiated recycle and alternate fuels. They will be available before the first recycle test elements are removed from the Peach Bottom reactor (at about 1.4×10^{21} neutrons/cm²·sec fast fluence). Studies will include the separation of fertile and fissile particles (Biso and Triso coated), determination of uranium crossover, estimates of particle breakage, and measurement of the release of

Table 10.11. Irradiated Dragon compacts^a requested for ORNL head-end studies

Experimental designation	Th-to-U atom ratio (93% ²³⁵ U)	Kernel composition	Kernel diameter (μm)	Type of coating	Thickness of coatings (μm)	Comments
2M4	10	(U,Th)O ₂	500	Biso	130	Simulates (²³³ U,Th)O ₂ reference (Biso) recycle particle for 1100-MW(e) HTGR; will be compared with ORNL sol-gel recycle particle
2M7	10	(U,Th)O ₂	500	Triso	160	Simulates (²³³ U,Th)O ₂ alternate (Triso) recycle particle for 1100-MW(e) HTGR
2M10	10	(U,Th)C ₂	500	Triso	150	Suitable for comparison of carbides and oxides in head-end studies; simulates FSV fertile-fissile particle
3M	10	(U,Th)C ₂	900	Triso	50/30/80	Large kernel size; can be mixed with other fuels for particle-separation studies of Triso-Triso and Triso-Biso mixes (18M and ORNL sol-gel Biso-coated fuels)
18M		UC ₂₀	500	Triso	25/30/70	Simulates fissile (²³⁵ U) particle; will be used in particle separation studies
19M		ThC ₂ UC ₁₀	900 500	Triso Triso	25/30/70 25/30/70	Simulates FSV fuel particles; will be used in particle separation studies
38M	5	(U,Th)C ₂	500	Biso	40/80	1100-MW(e) HTGR simulated fertile-fissile particle with accelerated burnup; could be mixed with UC ₁₀ Triso-coated particles (which are presently available) for separation studies
ORNL sol-gel ^b	3, 4.5	(U,Th)O ₂	290	Biso		1100-MW(e) reference recycle fuel (fertile)

^aIrradiated to a burnup of about 7% fissions per initial metal atom and 2.5×10^{21} neutrons/cm² · sec fast fluence.

^bIrradiated to 12 to 18% fissions per initial metal atom.

volatile fission products, such as ⁸⁵Kr, ³H, ⁹⁰Sr, and ¹³⁷Cs, in various head-end steps.

10.4.3 Recycle test elements

Eight recycle test elements are to be irradiated in the Peach Bottom reactor. Six were inserted in the summer of 1970 and two may be inserted later in a cooperative program between GGA and ORNL. Reference and advanced recycle and makeup fuel particle mixtures in these elements are being tested at operating temperatures (1050 to 2250°F) of interest for use in commercial HTGR's. Bonded beds and some loose particles (blended beds) will be irradiated for one, two, or three years at exposures of 1.4×10^{21} , 2.8×10^{21} , and 4.2×10^{21} neutrons/cm² · sec fast fluence, respectively.

These irradiated elements will be more representative of the products of the large-scale production of fuel elements than the materials that are being used in capsule irradiation tests. In addition, they will provide significant quantities of irradiated fuels for head-end reprocessing studies and will probably be the first irradiated fuel used in a head-end process demonstration in TURF.

The types of fuel combinations in the recycle test elements and an indication of the reasons for their inclusion are given in Table 10.12. A more detailed breakdown of the loading combinations and irradiation conditions is given in Table 10.13. Odd-numbered elements are the primary source of material for the hot-cell head-end studies. The emphasis is on particle combinations a, c, f, and g, which are the reference

Table 10.12. Fuel combinations in the recycle test element program

Particle combination	Particle makeup in combinations		Justification ^a
	Fissile particle and coating	Fertile particle and coating	
a	(Th, 20% U)O ₂ , Biso		Reference recycle fuel
b	UO ₂ , Biso	ThC ₂ , Biso	Backup fuel type if economics indicate that Th should be eliminated from recycle fissile particle
c	(Th, 33% U)O ₂ , Biso	ThO ₂ , Biso	Th/U ratio of 2 to obtain reference burnup in three years; ThO ₂ backup if oxide process is adopted for economic reasons; over a period of time, the desired Th-to-U ratio will move from 4 toward 2
d	(Th, 33% U)O ₂ , Biso	ThC ₂ , Biso	Reference-type recycle combination with a Th-to-U ratio of 2 for accelerated burnup in fissile particle
e	UC ₂ , Biso	ThC ₂ , Biso	Reference startup loading
f	UC ₂ , Triso	ThC ₂ , Biso	Reference B block makeup fuel loading; Triso coating necessary to permit required separation of particles during reprocessing
g	UO ₂ , Biso	ThO ₂ , Biso	Backup fertile particle if thorium is eliminated from recycle particle; backup fertile particle if sol-gel process is used
h	UC ₂ , Biso	ThO ₂ , Biso	Backup B block loading; possible particle separation by chemical processes (e.g., selective burning or leaching)
i	UC ₂ , Triso	ThC ₂ , Triso	Needed if cleaner primary heat exchanger circuit becomes requirement; FSV-type fuel

^aAll combinations will be evaluated for equipment and chemical process checkout, bed sticking, metallic fission-product behavior, and kernel migration.

Table 10.13. Recycle test element (RTE) loading combinations

Position of fuel body in element	Center-line temperature range (°F)	Loading combinations ^a							
		First discharge (one-year irradiation)		Second discharge (two-year irradiation)		Final discharge (three-year irradiation)			
		RTE 1	RTE 2	RTE 3	RTE 4	RTE 5	RTE 6	RTE 7	RTE 8
6 (top of reactor)	2050–1950	b,d,e,i	f	b,d,e,i	e ^b	b,d,e,i	g	a,c,f,g	f
5	2250–2050	b,d,e,h	a ^b	b,d,e,h	d	b,d,e,h	f	a,c,f,g	i
4 (maximum flux)	2250–2300	a,c,f,g	e	a,c,f,g	f	a,c,f,g	f	b,d,g,h	d
3 (maximum flux)	2050–2250	a,c,f,g	f ^b	a,c,f,g	a ^b	a,c,f,g	d	b,d,g,i	e
2	1650–2050	a,c,f,g	d	a,c,f,g	f ^b	a,c,f,g	f	b,d,g,i	i
1 (bottom of reactor)	1050–1650	a,c,f,g	e ^b	a,c,f,g	e	a,c,f,g	e	b,d,g,i	f ^b

^aLoadings are indicated by letters a through i and are defined in Table 10.12.

^bBlended beds: one-year irradiations will be to a maximum dose of approximately 1.4×10^{21} neutrons/cm²·sec; two-year irradiations to a maximum dose of approximately 2.8×10^{21} neutrons/cm²·sec; three-year irradiations to a maximum dose of approximately 4.2×10^{21} neutrons/cm²·sec.

candidates; however, all fuel combinations are covered in each odd-numbered element. The six 15-in. sections of the odd-numbered elements will be quartered lengthwise to obtain one sample of each fuel type, as indicated in Fig. 10.4. Even-numbered elements will provide larger amounts of the various fuel combinations

for additional hot-cell studies as necessary or desirable. They may also be the first irradiated specimens representative of actual 1100-MW(e) reactor fuel that will become available for use in reprocessing studies in TURF.

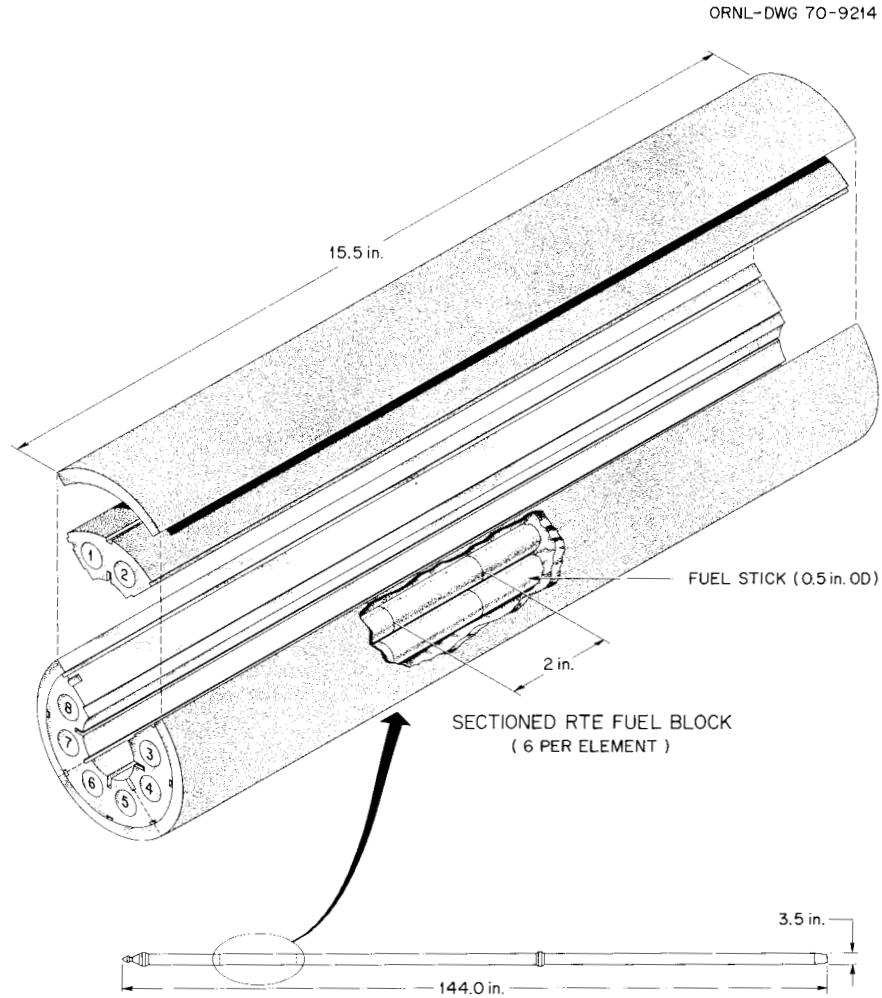


Fig. 10.4. Recycle test element.

11. Refabrication Development

J. D. Sease P. A. Haas

The equipment and processes required for refabricating fuel are being developed. Refabrication starts with the ^{233}U -nitrate solution from the solvent extraction process and ends with a completed fuel element ready for shipment to the reactor. Included are sol preparation; microsphere forming, drying, and firing; particle handling and particle coating; fuel stick fabrication; fuel element assembly; and all the inspections involved in each production step. In addition to development of equipment and processes for these operations, simulated HTGR recycle fuel must be provided for head-end reprocessing development and irradiation testing. Thus besides the long-term goal of developing processes and equipment for commercial-scale recycle operations, processes and equipment must be developed early in the program to provide this test material. Usually this is done by building equipment useful in both process development and in fabricating small quantities of fuel for testing.

11.1 Sol-Gel Studies and Particle Preparation

P. A. Haas	B. S. Finney
J. P. McBride	C. C. Haws
W. D. Bond	W. L. Pattison

One important application of sol-gel processes is the preparation of ThO_2 , UO_2 , and $\text{ThO}_2\text{-UO}_2$ spheres for GCR fuel elements. Currently the procedures and remotely operated equipment required for fuel preparation in the Thorium-Uranium Recycle Facility (TURF) are being developed. During the current reporting period, most of the work was on CUSP (concentrated urania sol preparation) UO_2 sols and UO_2 spheres, but the improved procedures developed for recycle of 2-ethyl-1-hexanol (2EH) for UO_2 sphere formation will

also be useful for $\text{ThO}_2\text{-UO}_3$ sphere preparation. The preparation of $\text{ThO}_2\text{-UO}_3$ sol and $\text{ThO}_2\text{-UO}_2$ spheres will be resumed during the next reporting period.

11.1.1 $\text{ThO}_2\text{-UO}_2$ microsphere preparation

The solvent-extraction sol-preparation and the CPDL sphere-preparation systems will be operated to supply $\text{ThO}_2\text{-UO}_2$ spheres for head-end reprocessing test elements. Components of both systems were borrowed or moved to meet needs of the CUSP UO_2 development studies, and replacement of these components has started. This production effort will be planned to also

1. demonstrate the improved 2EH recycle procedures (developed for CUSP UO_2 sols) for $\text{ThO}_2\text{-UO}_3$ sols,
2. demonstrate the flowsheets for the thorium-to-uranium ratio required for FSV HTGR fuel elements,
3. check some of the procedures and equipment proposed for remote operation and control of sphere-forming systems.

The exact ratio of thorium-to-uranium required for FSV HTGR fuel elements depends on calculations of nuclear requirements. While $\text{ThO}_2\text{-UO}_2$ spheres with ratios of 2.0 to 4.25 have been prepared, variations in the ratio require variations in the flowsheet conditions.

The schedule for these operations will be selected to meet the Metals and Ceramics Division's schedule for test element fabrication and to minimize interference with CUSP development studies.

11.1.2 Urania-sol preparation

The CUSP process developed at ORNL has been selected as the method for preparation of urania sols

because it is most amenable to scaleup and consistently produces good sols with desirable characteristics. The various aspects of CUSP sol preparation, including uranous nitrate feed preparation, laboratory- and engineering-scale process development, sol preparation, and equipment design and instrumentation are discussed in the following paragraphs.

Engineering development of the CUSP process for preparing UO_2 sol was continued. The spray-column equipment used for nitrate extraction was modified by adding a surge tank and appropriate valves so that 4 to 17 liters of UO_2 sol per batch (1.0 to 4.6 kg) could be prepared. A 17-liter batch is the maximum that can be reduced in the batch slurry reductor.

Operation of the modified spray column was satisfactory, but some difficulty was encountered in maintaining the position of the solvent-aqueous-phase interface during crystallization. The aqueous phase flows from the spray column to the surge tank through a jack leg that is used to control the position of the interface. The height of the jack leg is a function not only of the static height of solvent above the aqueous phase but also of the aqueous phase flow rate, which is normally about 3.25 liters/min. During crystallization and subsequent degassing, the aqueous-phase flow rate fluctuates due to partial cavitation conditions in the recirculating pump, and very careful control is required to maintain the interface at the proper level. Figure 11.1 is a schematic diagram of the equipment layout, while Fig. 11.2 shows the equipment.

Urania sol preparation runs were made in the mixer-settler and spray column equipment to evaluate the use of 0.5 M amine instead of 0.25 M amine. The more concentrated amine provides greater flexibility in operation, and the conductivity excursion due to the release of NO_3^- during crystallization can be more easily controlled. However, the use of 0.5 M amine promotes the formation of emulsions, and upon standing, an emulsified layer rises to the top of the sol products. The solvent becomes much darker and in less time than when 0.25 M amine is used. It is concluded that about 0.3 M is the maximum concentration that should be used.

It would be advantageous in terms of increased capacity and elimination of a sol concentration step to make more concentrated UO_2 sols by the CUSP process. Accordingly, attempts were made in laboratory- and engineering-scale equipment to make about 2 M U(IV) feed solutions by catalytic reduction with H_2 . The reductions were carried out with 750-ml volumes of the appropriate U(VI) solutions. Stable solutions

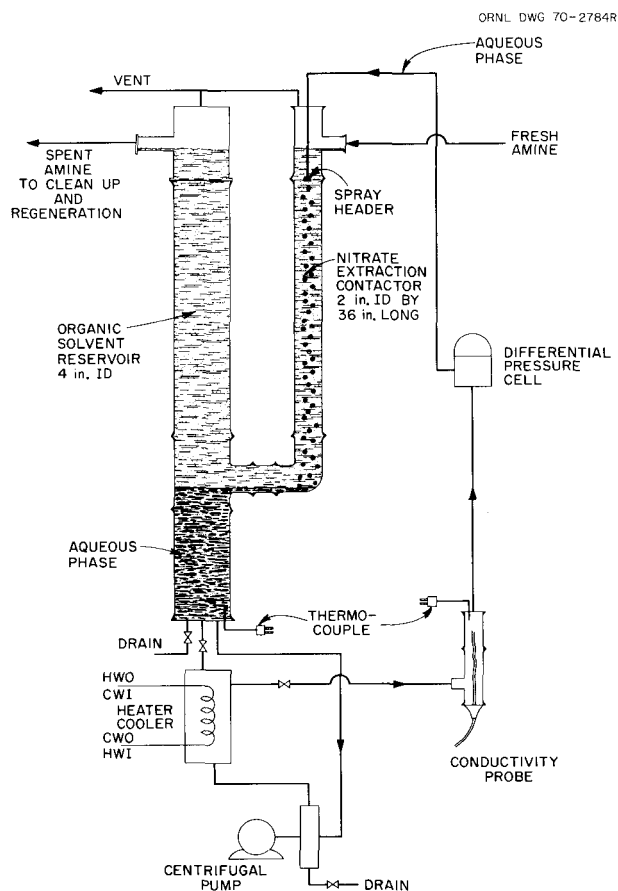


Fig. 11.1. Schematic diagram of equipment layout for pilot-plant-scale UO_2 sol preparation.

with U(IV) molar concentrations of 1.93, 2.03, and 2.09 were prepared. A small amount of green precipitate (estimated to contain less than 2% of the uranium) separated from the two higher concentration solutions on standing overnight prior to analysis. The compositions of the initial solutions and the final solutions obtained in each experiment are given in Table 11.1.

An 8-liter feed batch of 1.8 M U , 3.83 M NO_3^- , 1.08 M COOH^- , and 0.1 M urea was reduced in the batch slurry reductor in 3 hr. The analysis of the resultant U(IV) solution was as follows: 1.83 M U , 3.93 M NO_3^- , 0.63 M COOH^- , and 0.06 M urea. The solution could not be drained from the reductor through the $10\text{-}\mu$ pore stainless steel filter and was siphoned out. After standing overnight, there was a small amount of sediment in the bottom of the container. Two 4-liter batches of sol (SCSHB-46 and -47) were prepared by using this feed in the spray-column nitrate-extraction

PHOTO 101023

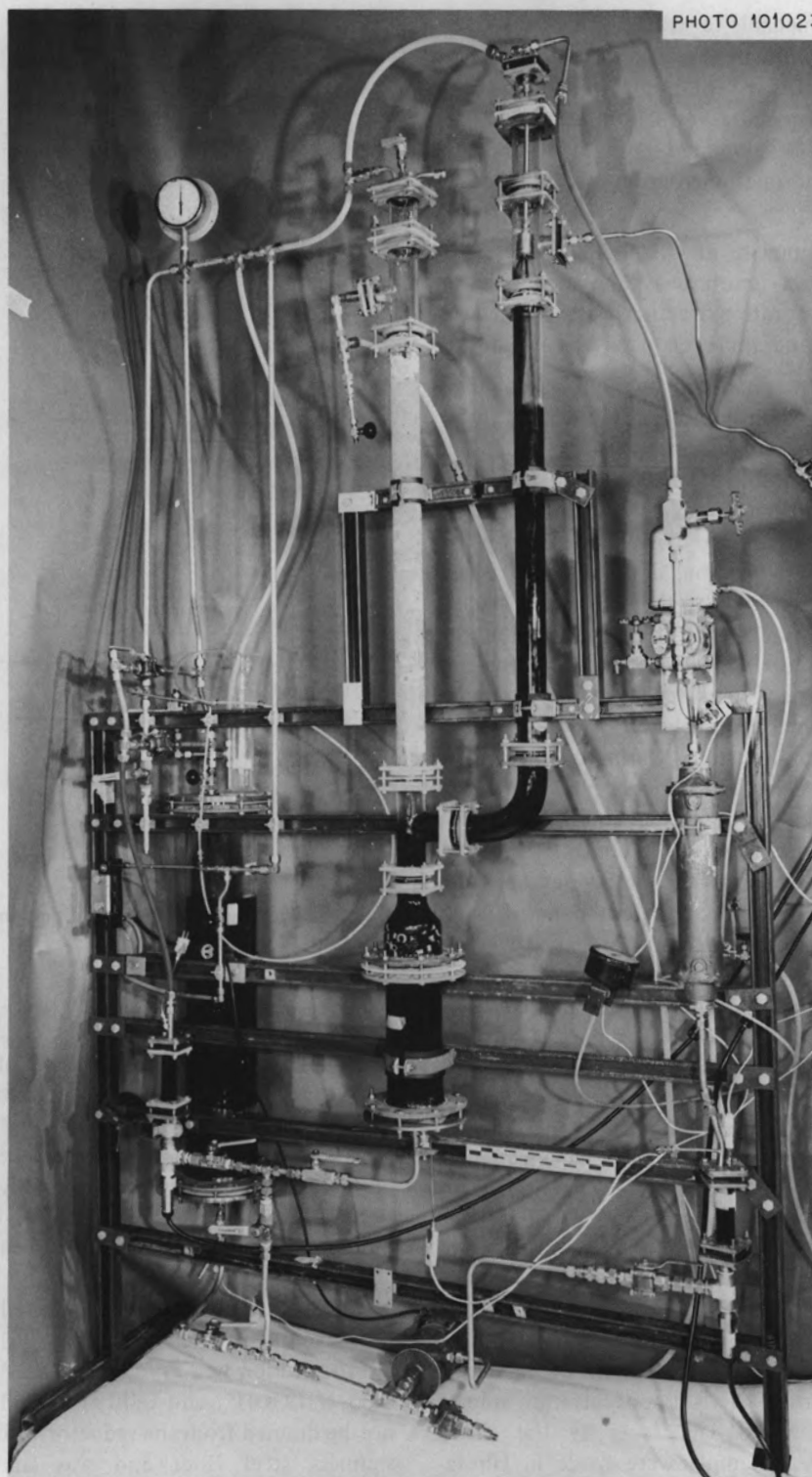


Fig. 11.2. Equipment for pilot-plant-scale preparation of UO_2 sol.

Table 11.1. Solution compositions used in attempts to make concentrated uranium feed solutions for preparation of UO_2 sol

Experiment	Concentrations (M)			
	Uranium	NO_3^-	HCOO^-	Urea
	Initial solution (nominal) ^a			
CFR-7	2.0	4.2	1.2	0.11
-8	1.8	3.8	0.9	0.11
-9	1.9	4.0	1.1	0.11
	Final solution			
CFR-7	2.09	4.56	0.59	
-8	1.93	4.13	0.52	0.10
-9	2.03	4.32	0.63	0.08

^aNot analyzed.

system with modified CUSP flowsheets. The sol products were fluid, had good appearances, and gave the following analyses:

	SCSHB-46	SCSHB-47
Conductivity at end of final (25°C) extraction, $\mu\text{mho/cm}$	5905	3830
NO_3^- -to-U ratio, mole/mole	0.18	0.117
U(IV)-to-U ratio, mole/mole	0.84	0.87

11.1.3 Sphere forming

When a specified sol feed is used to form gel spheres, the composition of the organic fluidizing medium is the principal operating variable. The successful continuous operation of a sphere-forming column requires that the alcohol composition be controlled within satisfactory ranges. This control is still based primarily on observation, and operations are controlled in three stages:

1. satisfactory initial conditions,
2. control of surfactant depletion,
3. control of excessive accumulations of surfactants, degradation products, or impurities.

Tests on the UO_2 sols from the CUSP process were continued to develop and demonstrate the stages listed above. The results obtained to date show more problems relative to sphere formation from CUSP sols than from ThO_2 or $\text{ThO}_2\text{-UO}_3$ sols.

A test program was conducted using 1 M CUSP UO_2 sols with ion-exchange treatment of the 2EH to remove

HNO_3 and HCOOH before entering the still to remove water. Most of the operation was with a sol feed of 10 cc/min or about 1 kg UO_2 per 8-hr day (allowing for startup and shutdown time). The pH of the 2EH leaving the ion-exchange column was about 6, indicating good removal of HNO_3 and HCOOH . The 2EH leaving the still did not show the yellow color produced when the ion-exchange treatment is not used; this indicates that the ion-exchange treatment prevents degradation of surfactants in the still. In order to keep the pH of the 2EH below 5, HNO_3 must be added after distillation. Span additions averaging about 30 cc/hr of still operation were necessary to control coalescence, clustering, and contact chipping. Formation of gel spheres with this recycle procedure was as good and perhaps better with recycled 2EH than with virgin 2EH. The requirements for high and variable Span 80 additions and the cracking of more than 50% of the spheres during firing were persistent problems. Drying of 2EH samples at 115°C for density measurements showed the accumulation of high-boiling, high-density fractions in the 2EH without accumulation of Span 80 on the ion-exchange resin, as initially believed. The amount of cracking after firing of UO_2 spheres from CUSP sol was plotted as a function of cumulative additions of Span 80 to the 2EH. The samples after 2.5 vol % or more Span 80 additions consistently showed 80 to 100% cracking after firing. When clustering was noticeable, the amounts of cracking were also high. Samples with little clustering and less than 1.4 vol % Span additions to the 2EH showed less than 50% cracking.

Recent results indicate that inadequate holdup times in the sphere-forming column and exposure to oxidation at the start of the firing cycle can contribute to excessive cracking of the 500- μ UO_2 spheres from CUSP sols. Small samples fired in a laboratory furnace showed less cracking than similar samples fired in the large unit-operations furnace. Small samples of gel spheres were formed with $\frac{1}{2}$ -, 1-, $1\frac{1}{2}$ -, and 2-hr average holdup times in the sphere-forming column. After drying and firing in small-scale equipment, the fired samples generally show 90 to 98% cracked spheres for the $\frac{1}{2}$ -hr column residence time and 0 to 15% cracked spheres for the 1-, $1\frac{1}{2}$ -, and 2-hr residence times, as shown in Table 11.2. Use of 2EH recovered by complete distillation gave slightly more cracking than virgin 2EH with the same sol. The first sol prepared with a higher, 1.8 M U, concentration gave 10 to 15% cracking in virgin 2EH, whereas the sols of 1 M U gave no cracking (Table 11.2). The samples formed with a 1-hr column residence time had a better appearance

Table 11.2 Cracking of fired spheres versus column residence time

Sol No.	40	40	41	46
Sol description	Standard, 1 M	Standard, 1 M	Standard, 1 M	Special, 1.8 M
2EH source	Virgin	Recycled by distillation	Virgin	Virgin
Cracked spheres, %, after firing as a function of indicated column residence time				
1/2 hr	90		98	98
1 hr	0	0	1	15, 15
1 1/2 hr	0	15	0	
2 hr	0	15	0	15, 15

than those with a 1 1/2- or 2-hr residence time, although the difference does not show up as a difference in the amount of cracking.

11.2 Fueled-Graphite Fabrication Development

J. D. Sease F. J. Furman
P. A. Haas C. B. Pollock
J. M. Robbins

The principal effort in fueled-graphite development has been the fabrication of fuel required for recycle test elements (RTE's) to be irradiated in the Peach Bottom reactor. Fuel for these elements was fabricated in a combined effort of ORNL and Gulf General Atomic (GGA). Details of the irradiation experiment are discussed in Chapter 12. Development efforts were principally on particle preparation and particle coating, although more emphasis is now being placed on fuel-stick fabrication.

11.2.1 RTE fabrication

Material for eight RTE's to be irradiated in the Peach Bottom reactor was prepared at ORNL.¹ This material included approximately 15 kg of coated particles, 2000 in. of fuel sticks, and two segments (one-sixth of an element) of loose loaded particles. The elements are described in Chapter 12. The types of fuel particles prepared are listed below:

Fuel type	Nominal kernel diameter (μ)	Designation
(Th-20% U)O ₂	350	Reference recycle particle
(Th-33% U)O ₂	350	Full-burnup particle
UO ₂	100	Alternate recycle particle
ThO ₂	400	Alternate fertile particle

The reference recycle particle is that specified in the HTGR Fuel Recycle Development Program Plan. The alternate recycle particle, besides being what the name implies, also could be an alternate for the UC₂ make-up fissile fuel particle. The ThO₂ particle is the alternate to the ThC₂ fertile particle.

Typical properties of the coated particles are listed in Table 11.3. The UO₂ particles were coated in graphite cone furnaces that have a 1 1/4- to 1 3/4-in. ID, and the other particles were coated in the prototype remotely operated coating furnace that has a 5-in. ID. Acetylene diluted with helium was used for depositing the inner buffer coating on all particles, and propylene was used for depositing the outer isotropic coating. The carrier gas was argon. Typical ThO₂, (Th,U)O₂, nonspherical (Th,U)O₂, and UO₂ particles are shown in Fig. 11.3.

For the RTE's, the particles were formed into fuel sticks having a 0.490-in. diameter and a 2.14-in. length. The particles were bonded by injecting hot pitch with filler into a bed of particles held in a mold. The matrix material was 15V coal tar from Allied Chemical Company mixed with 35% AXM graphite flour from Poco Graphite, Inc. The types of fuel sticks and the number of each type produced are listed below:

Stick type	Number produced
(Th-20% U)O ₂	180
(Th-33% U)O ₂ + ThO ₂	186
(Th-33% U)O ₂ + ThC ₂	330
UO ₂ + ThO ₂	228

1. J. M. Robbins and J. H. Coobs, "Development of Bonded Beds of Coated Particles for HTGR Fuel Elements," pp. 10-15, *Gas-Cooled Reactor Program Semiann. Progr. Rept. Mar. 31, 1970*, USAEC Report ORNL-4589, Oak Ridge National Laboratory.

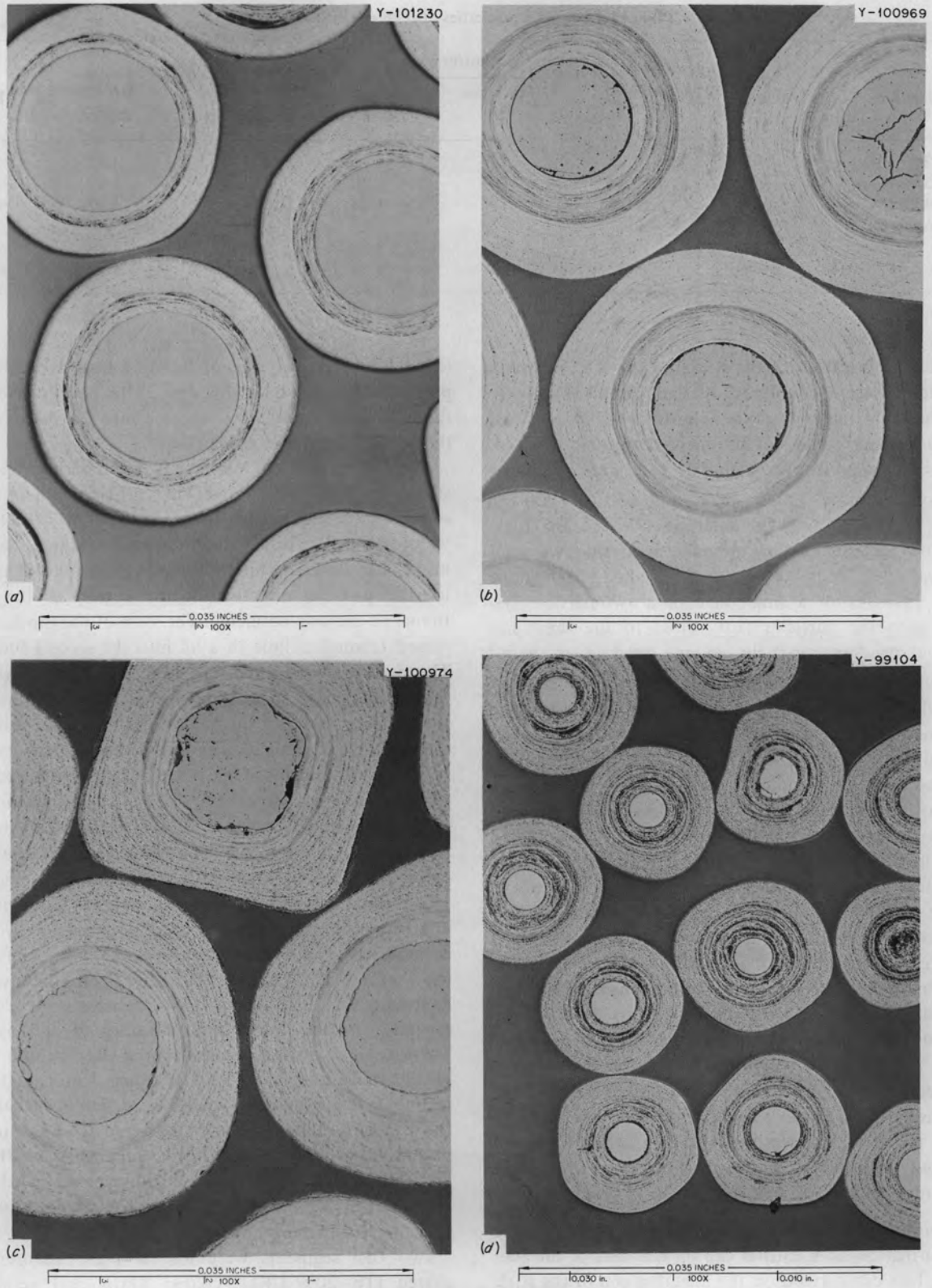


Fig. 11.3. Typical coated particles. (a) ThO_2 . (b) $(\text{Th,U})\text{O}_2$. (c) Nonspherical $(\text{Th,U})\text{O}_2$. (d) UO_2 .

Table 11.3. Typical properties of RTE coated particles

Particle type	Kernel diameter (μ)	Density (g/cm^3)	Buffer coating		Outer coating		BAF
			Thickness (μ)	Density (g/cm^3)	Thickness (μ)	Density (g/cm^3)	
(Th-20% U)O ₂	349	10.10	73	1.10	104	1.92	<1.09
(Th-33% U)O ₂	350	10.10	82	1.16	130	1.88	<1.09
(Th-33% U)O ₂ nonspherical	373	10.09	79	1.24	136	1.87	<1.09
UO ₂	111	10.06	54	1.20	68	1.89	<1.09
ThO ₂	400	9.92	54	1.30	70	1.92	<1.09

During fabrication of the sticks for the RTE's, several problems were encountered. An early problem was that the bonding material containing 40 wt % Poco AXM graphite flour could not be injected through the 2-in. fuel bed made from a blend of two sizes of coated particles (250 to 500 μm UO₂ and 600 to 1000 μm ThO₂). The reason was determined to be the high-volume particle loading obtained with the two sizes of particles. Most previous work had been done with particles of a single size or a two-particle system with the particles fairly close to the same size and a resultant particle volume loading of about 62 to 65%. With the RTE particle blend, volume loadings as high as 70% were obtained, with the value depending on the sphericity of the particles. Also it was found that a mix containing 35 wt % graphite flour instead of 40 wt % could be used.

Another problem with the bonding mix developed when the original batch of graphite flour was depleted and it was necessary to start on a new supply. An identical mix made with the new batch of filler would inject only about $\frac{1}{2}$ in. into the bed of particles. It was then determined that the original batch of filler had been ground to pass through a 325-mesh screen, and the new batch had been ground to pass through a 200-mesh screen. Therefore, even though both flours were screened through a 40- μm precision screen prior to use, more fines were in the original batch of flour than in the second batch. This problem was solved by screening and using the -27- μm particles from the new batch of filler. However, this was wasteful of graphite flour and pointed up the need for developing a filler with optimum particle size distribution.

A problem that could not be eliminated entirely was the formation of a carbon cap on one end of the fuel stick. This cap formed on the injection end of the stick when the particles settled slightly during injection and

left a thin layer, or cap, of bonding material without particles at the end of the stick. This happened even though the particles were vibrated into the molds and the bed of particles was restrained.

A blending problem was encountered in making the sticks containing UO₂ and ThO₂. This problem was solved by feeding the particles simultaneously from the vibratory feeders into a double funnel leading into the mold. The double-funnel arrangement permitted feeding the particles directly into the bottom of the top funnel to prevent bouncing. The stem of the top funnel passed through a hole in a lid into the second funnel. The particles were directed against the angled wall of the second funnel so that they were mixed by bouncing and swirling. The lid on the second funnel contained the bouncing particles and kept them from being scattered. Radiographs indicated that this method of mixing gave a consistently good blend, as shown in Fig. 11.4d. Figure 11.4a shows a fuel stick made from particles that were blended by pouring directly into a mold; the resulting swirl pattern may be seen. Figure 11.4b shows a blend formed with a momentary interruption in the feeding of the ThO₂ particles, which is indicated by the black band toward the bottom and the excess of ThO₂ at the top. Figure 11.4c shows what happened when UO₂ and ThO₂ particles were fed in separate streams down opposite sides of the mold. There is an obvious concentration of UO₂ on one side of the mold and ThO₂ on the other. Unfortunately, many of the UO₂-ThO₂ sticks were produced before this problem of blending was discovered. Consequently, several sticks were rejected, and others with less-than-ideal homogeneity were accepted to meet the schedule. The fabrication of the RTE's was completed, and all sticks were shipped in the latter part of May 1970.

Two fuel segments were loaded with mixtures of coated (Th-20% U)O₂, coated ThC₂, and graphite flour. This particle mixture is the reference recycle fuel

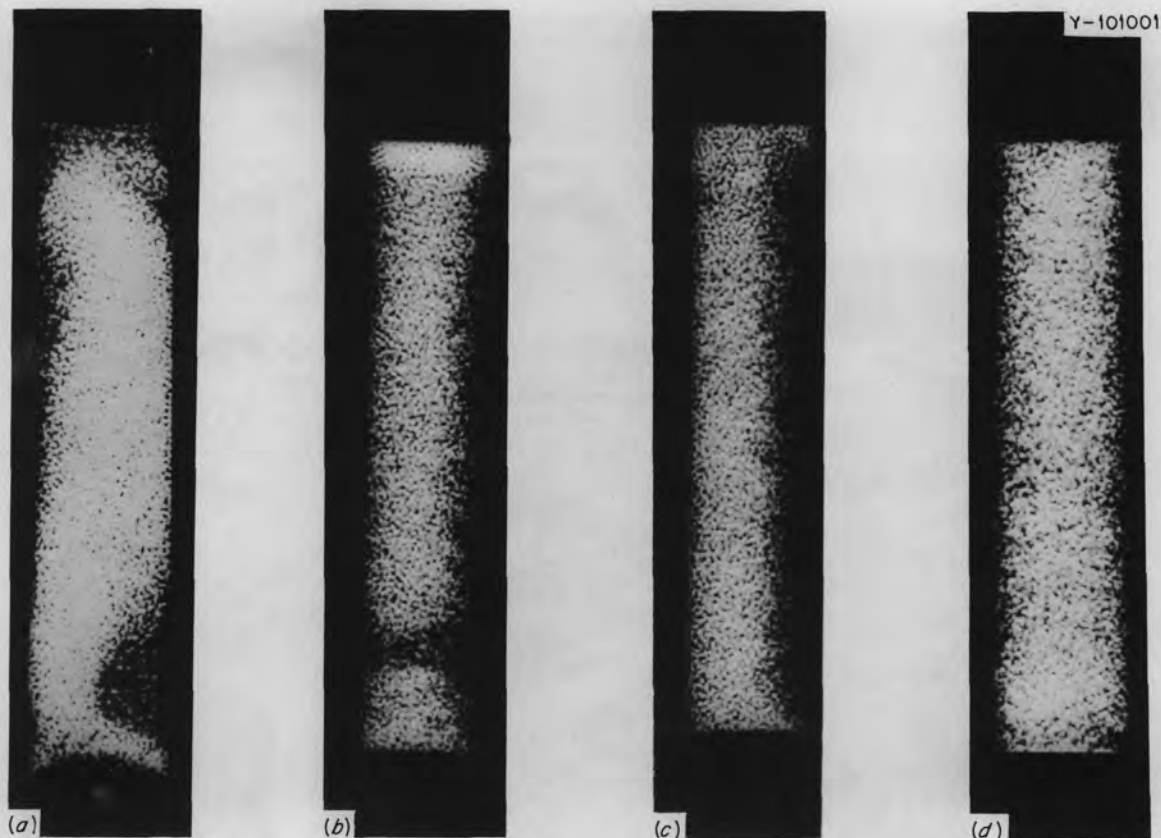


Fig. 11.4. Radiographs showing various degrees of blending obtained in HTGR fuel sticks with two sizes of coated particles. (a) Particles poured directly into mold. (b) Blend formed with momentary interruption in feeding of ThO_2 particles. (c) Particles fed in separate streams down opposite sides of mold. (d) Particles loaded with double-funnel arrangement.

mixture; however, the reference fuel is bonded together to form fuel sticks, while this fuel was loaded as loose particles. In the loading of these loose particle segments, the three types of particles were loaded concurrently from three Syntron vibrators on which were mounted V-trough feeders. The filling rate was about 1 in./min. After all eight holes of the fuel segment were loaded, 65-g steel cylinders were placed on top of each hole to hold the particle bed in place, and the segment was vibrated by a Syntron vibrator to settle the bed. The method of mounting the segment onto the vibrator is shown in Fig. 11.5. A glass dummy fuel hole was mounted on the side and filled with low-density ($\sim 2.4 \text{ g/cm}^3$) coated particles and uncoated ThO_2 . After extensive vibration, only a small area at the top of the column appeared to have partially segregated. This demonstrated the practicality of settling loose beds by vibration.

After the initial settling, additional graphite flour was added to fill the bed with graphite. (Loading all the

graphite during the initial feeding caused the bed to expand beyond the volume required for the particles.)

When the filling was completed the beds were sealed in place by adding 2 cm^3 of methyl-ethyl-ketone and 10% polystyrene. After the sealing mixture dried, the segments were checked for contamination and shipped to Gulf General Atomic for loading into Peach Bottom fuel elements. A dummy hole for each segment was filled with the same mixture as that used for the segment holes and retained at ORNL for future cold reprocessing tests prior to testing the irradiated segments.

11.2.2 Particle coating

The equipment and process for coating HTGR recycle fuel particles are currently being developed. The prototype remotely operated coating furnace, which was used successfully to coat RTE particles after only a very brief break-in period, is being modified to incorporate

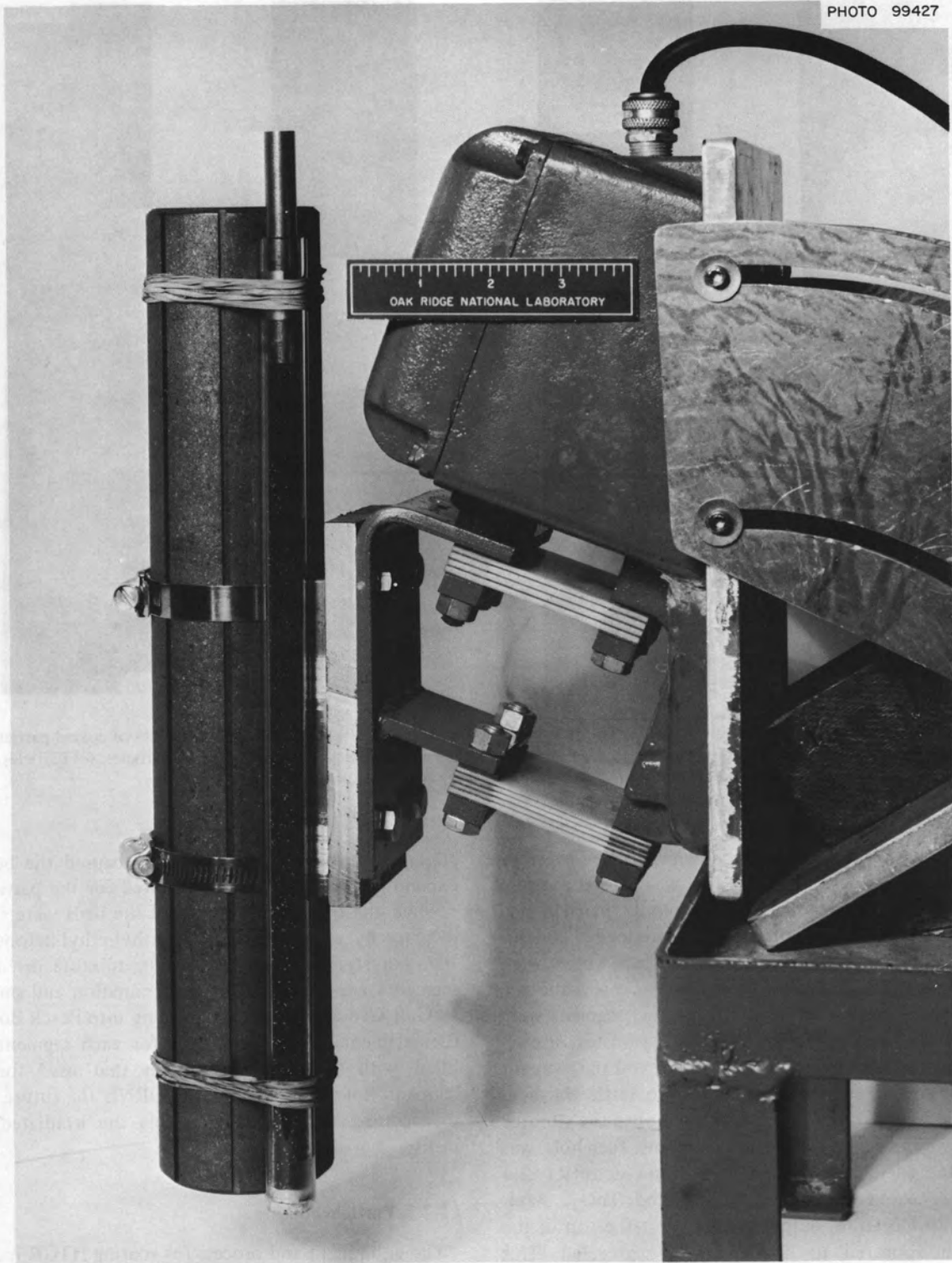


Fig. 11.5. RTE segment vibrator.

improved electrodes, unloading systems, and off-gas systems. A series of experiments is being run to determine how variation of the parameters used in coating affect the amount of faceting and soot inclusions in high-density coatings.

The coating system was not in operation during this reporting period for various reasons. First, while the RTE coating runs, in general, demonstrated the excellence of the coating system, they indicated some minor problems that would prove troublesome in later operations, and modifications were required. Second, some of the RTE material was slightly contaminated with ^{238}Pu , and therefore to allow operators to work with the prototype coater without extensive precautions, such as the wearing of gas masks, the furnace had to be completely disassembled and decontaminated. Some parts were cheaper to replace than to decontaminate. Third, extensive modifications of the laboratory in which the coater is located were made during late summer and fall, and the furnace system could not be operated.

The only modification needed on the furnace itself was a change of material on the electrodes to permit tighter clamping of the heating element assembly to minimize contact resistance. The original electrodes were made of high-phosphorus copper. The bolt which held the heating element was an integral part of the electrode. High-phosphorus copper, although having better creep resistance at high temperatures than other grades of copper, has inadequate strength for bolts. The design was modified to incorporate heat-treated beryllium-copper bolts joined mechanically and with soft solder to the electrodes. (Soft solder was used to prevent annealing of the beryllium-copper bolts and was adequate because the joint is water cooled.) Tellurium-copper bolts were used for the electrodes because the tellurium-copper alloy has high conductivity and is considerably easier to machine than most other grades of copper.

The unloading system is being modified to increase the cooling rate of the particles after coating. Originally the particles were dumped directly from the furnace into a water-cooled hopper. However, it took as long as

45 min to completely cool the particles. An argon supply is being added to the cooling hopper so that the particles can be fluidized and the rate of heat transfer improved.

An experimental soot filter is being incorporated into the exhaust line of the furnace. The original bag filter in a 55-gal drum is being replaced with a flat filter that will be critically safe regardless of fissile content. The filter, which has an effective area of 9 ft², is mounted vertically so that the soot can be shaken into a collection tube at the bottom. A piston in the tube compresses the soot and pushes it out of the filter housing.

A series of experiments was started to determine which parameters used in the deposition of high-density pyrolytic carbon affect the amount of faceting and soot inclusion in the coating. Also the effect of coating parameters on furnace cone life is being investigated. The parameters being considered include furnace temperature, furnace pressure, hydrocarbon gas flow, diluent gas flow, and furnace load. These experiments are being conducted in the 5-in. coater in the coated particle development laboratory pending completion of the modifications to the prototype coater.

11.2.3 Fuel stick fabrication

A fuel stick fabrication line with a capacity of about 400 in. of fuel stick per day is being constructed. This line will consist of a coated-particle batch blender for blending multiple batches of either fissile or fertile particles, a combination fissile-fertile particle blender and fuel-stick-mold loader, fuel-stick molds, a mold heater, a pitch injector, and a fuel-stick ejector. The line will be able to fabricate fuel sticks of various lengths and will be instrumented to provide data needed for the design of the TURF fuel-stick fabrication line. Also, other more advanced equipment and processes for stick making will be easy to incorporate and test on this line. In addition to using the line for development work, quantities of fuel sticks are to be fabricated for use in head-end processing development and irradiation testing.

12. Fuel Irradiations

T. N. Washburn A. R. Olsen
R. B. Fitts

The irradiations of the HTGR fuel recycle program have two main objectives: (1) to provide irradiated fuel for head-end processing studies and (2) to proof test recycle fuels produced in prototype equipment. The test conditions of interest include fuel temperatures between 600 and 1300°C, burnup to 20% FIMA in the (Th,U)O₂ particles, and fast-neutron fluences up to 8×10^{21} neutrons/cm² ($E > 0.18$ MeV).

The program involves capsule irradiations in research reactors, pilot-scale irradiations in the Peach Bottom reactor, and a series of tests in the Fort St. Vrain reactor (eventually including remotely fabricated recycle test elements). The first two stages of this program are currently being implemented: (1) accelerated burnup-rate capsule irradiations and (2) irradiation of recycle test elements (RTE's) in the Peach Bottom reactor.

12.1 Capsule Tests

A. R. Olsen

The accelerated burnup-rate capsule tests are designed to test the performance of coated particles processed in TURF (thorium-uranium recycle facility) prototype equipment and provide small samples for chemical processing studies. The fuel particles in these first two capsules will reach approximately full HTGR design burnup and fast-neutron dose in about six months of irradiation. The results will be available in advance of the receipt of fuel from the large-scale (RTE) irradiations. Additional capsule tests will be made as the remote reprocessing development reaches critical stages.

The fuel performance in an HTGR is a complex interaction of fuel burnup effects and the effects of fast-neutron irradiation damage to the pyrolytic-carbon coatings and to the carbonaceous bonding material. The

relative importance of the effects of burnup and fast-neutron damage is influenced by the time and temperature of irradiation and also the neutron energy spectrum. In a commercial HTGR the neutron energy spectrum is such that the thermal-neutron flux and the fast-neutron flux ($E > 1$ MeV) are essentially equal. In the J-8 position of the ETR, where these tests are to be conducted, the peak thermal-neutron flux (2200 m/sec) is reported to be 6.42×10^{14} neutrons/cm²·sec and the peak fast-neutron flux is 3.31×10^{14} neutrons/cm²·sec ($E > 1$ MeV). Therefore a capsule has been designed that incorporates thermal-neutron filter shrouds to reduce the thermal-flux to fast-flux ratio by a factor of approximately 2.6 so as to more nearly simulate the HTGR conditions.

Two capsules are being fabricated for irradiation in the ETR starting in the first quarter of 1971. The capsule design is shown schematically in Fig. 12.1. Four fissile-fertile particle combinations will be irradiated at four temperatures to fast-neutron fluences of approximately 8×10^{21} neutrons/cm² ($E > 0.18$ MeV). These four combinations are those of principal interest to the HTGR recycle program and are the combinations that receive emphasis in the RTE tests described in the following section. The loadings for the two capsules are given in Table 12.1.

The fabrication of the thermal-neutron shrouds for these capsules is in progress. The shrouds are being made from zirconium-hafnium alloys supplied by Bettis Atomic Power Laboratory, where they have been successfully employed for similar purposes.¹ The

1. R. M. Lieberman, "A System for Calculation of Fission Power in Irradiation Tests," pp. 473-490, in *National Symposium on Developments in Irradiation Testing Technology, 1969*, USAEC Report CONF-690910, 1969.

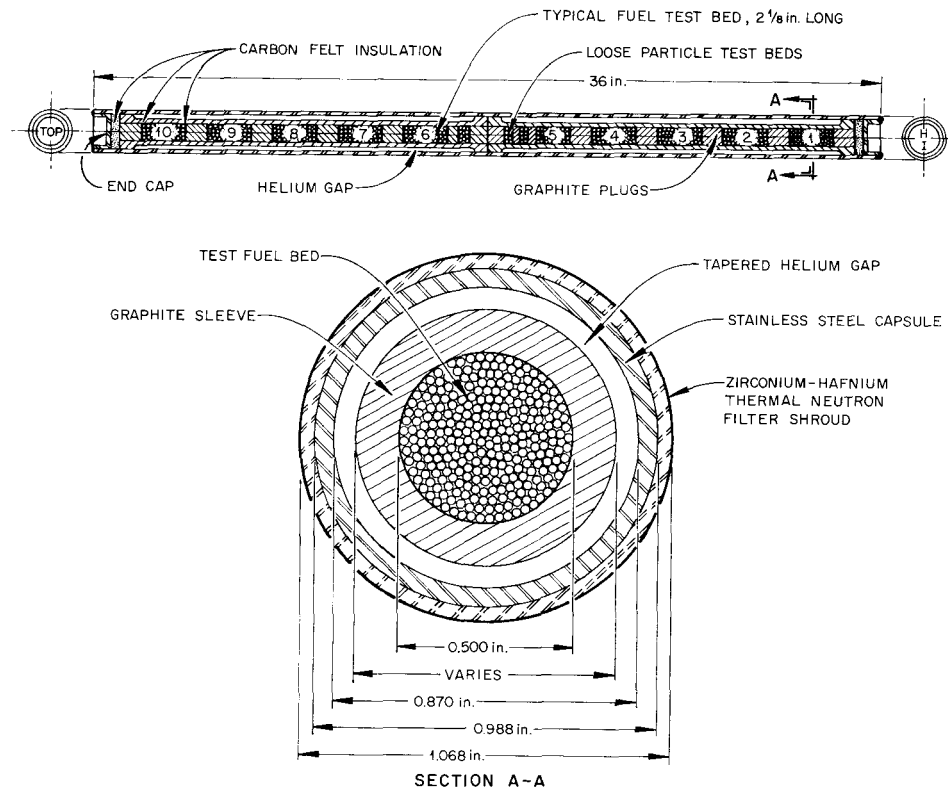


Fig. 12.1. Design of capsules to be inserted in ETR.

shrouds are formed from flat sheet stock, welded to form a tube blank, and sized to final dimensions. The thickness of these shields was based on an evaluation of the thermal-neutron shielding effectiveness of the material made with the ANISN² discrete-ordinates neutron-transport code with 36 neutron energy groups.

A mockup capsule is required for checking before any capsule can be inserted into an ETR core position. This capsule is used in the ERT critical facility to evaluate reactor core loadings. The mockup planned has an axial access hole into the fueled region to accept fission monitors. If this modification is acceptable to ETR personnel, it will be possible to measure the fission rate at three locations along the axial center line of the mockup capsule during exposure in the critical facility. These measurements will be used to normalize the fission-rate calculations, define the actual effectiveness

of the thermal-neutron shrouds, and observe effects of changes in ETR core loading at each reactor cycle.

The stainless steel and graphite components for both capsules and the nuclear mockup counterparts are fabricated. Preassembly of these components and quality-assurance inspections are about 90% complete. The fuel particles for incorporation in these capsules have all been fabricated, and characterization is 80% complete. Fabrication of these particles into fuel sticks is scheduled for the near future.

12.2 Recycle Test Elements

R. B. Fitts

Irradiation of test fuel elements known as recycle test elements (RTE's) was started in the Peach Bottom reactor in July of 1970. These elements contained fuel samples similar to recycle fuels proposed for use in 1100-MW(e) HTGR's.

Descriptions of the eight test elements and their contents are given in Fig. 12.2 and Tables 12.2 and 12.3. The plans for utilization of the RTE's after

2. W. W. Engle, Jr., *A Users Manual for ANISN*, USAEC Report K-1693, Oak Ridge Gaseous Diffusion Plant, 1967.

Table 12.1. Fuel loadings for HTGR irradiation test capsules H-1 and H-2

Position	Capsule H-1		Capsule H-2	
	Temperature (°C)	Particle mix ^a	Temperature (°C)	Particle mix ^a
1	1050	f	950	f
2	1050	g	950	g
3	1050	c	950	c
4	1050	a	950	a
5	1050	f	950	f
LP ^b	1050	a	950	a
LP ^b	1050	x	950	x
LP ^b	1300	x	750	x
6	1300	f	750	f
7	1300	a	750	a
8	1300	c	750	c
9	1300	g	750	g
10	1300	g ^c	750	g ^c

^aParticle mix: a = (4.2 Th,U)O₂ with Biso coating plus ThO₂ with Biso coating
 c = (2 Th,U)O₂ Biso plus ThO₂ Biso
 f = UC₂ Triso plus ThC₂ Biso
 g = UO₂ Biso plus ThO₂ Biso
 x = UO₂ Biso from fueled resin particles plus ThO₂ Biso

^bLP are loose particles in approximately 1-in.-long beds for extensive metallographic examination and performance analysis.

^cBlended beds; all others are bonded beds.

Table 12.2. Particle loading combinations of interest

Combination designations	Combination particles		HTGR application
	Fissile	Fertile	
a	(4.2 Th,U)O ₂	ThO ₂ ^a	Reference recycle
b	UO ₂	ThC ₂	Advanced recycle or advanced makeup
c	(2 Th,U)O ₂	ThO ₂	Alternate recycle with accelerated burnup
d	(2 Th,U)O ₂	ThC ₂	Reference recycle with accelerated burnup
e	UC ₂	ThC ₂	Alternate makeup
f	UC ₂ ^b	ThC ₂	Reference makeup
g	UO ₂	ThO ₂	Alternate makeup and alternate recycle
h	UC ₂	ThO ₂	Alternate makeup
i	UC ₂ ^b	ThC ₂ ^b	Fort St. Vrain fuel

^aThe RTE's containing (4.2 Th,U)O₂ will actually contain no ThO₂ particles in order to maximize the uranium content of the particle bed.

^bTriso coating; all others are Biso coatings.

Table 12.3. Particle combinations in RTE fuel sticks^a

Position of fuel block in element	Center-line temperature range (°F)	First discharge		Second discharge		Final discharge			
		RTE-1 all bonded (quartered)	RTE-2	RTE-3 all bonded (quartered)	RTE-4	RTE-5 all bonded (quartered)	RTE-6 all bonded	RTE-7 all bonded (quartered)	RTE-8
6 (top of reactor)	2050–1950	bdei	f	bdei	e ^b	bdei	g	acfg	f
5	2250–2050	bdeh	a ^b	bdeh	d	bdeh	f	acfg	i
4 (maximum flux)	2250–2300	acfg	e	acfg	f	acfg	f	bdeh	d
3 (maximum flux)	2050–2250	acfg	f ^b	acfg	a ^b	acfg	d	bdhi	e
2	1650–2050	acfg	d	acfg	f ^b	acfg	f	bdhi	i
1 (bottom of reactor)	1050–1650	acfg	e ^b	acfg	e	acfg	e	bdhi	f ^b

^aLoadings are indicated by letters, which are defined in Table 12.2.

^bBlended beds.

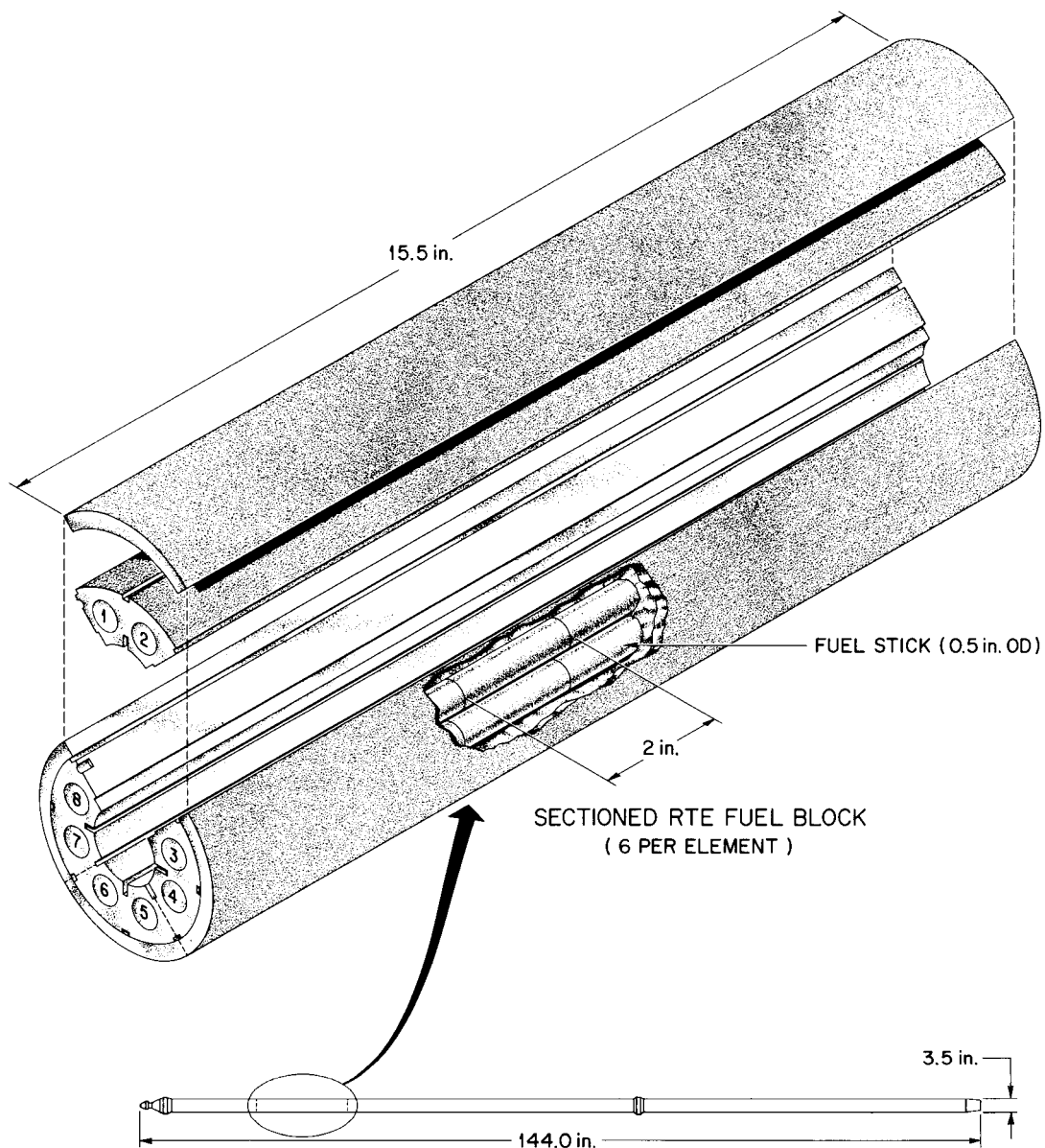


Fig. 12.2. Recycle test element.

irradiation were given previously.³ The first six of the RTE's were inserted in the Peach Bottom reactor and

3. T. N. Washburn, R. B. Fitts, and A. R. Olsen, "Recycle Test Elements," *Thorium Fuel Cycle Development Ann. Progr. Rept. Mar. 31, 1970*, USAEC Report ORNL-4629, pp. 86-91, Oak Ridge National Laboratory.

have been operating as planned since July 14, 1970. As of September 25, 1970, these elements have accumulated 73 full-power days of irradiation. This was 24% of the planned test duration for the low-burnup (1-year) elements and about 7% of that for the maximum-exposure (3-year) elements. An additional element (RTE-1) is being prepared for insertion at a shutdown scheduled for early 1971.

11

ORGANIZATION CHART
GAS-COOLED REACTOR-THORIUM UTILIZATION PROGRAMS

FEBRUARY 18, 1971

